UNIVERSITÀ DEGLI STUDI DI PADOVA

Department of Biomedical Sciences

Ph.D. COURSE IN BIOMEDICAL SCIENCES

XXXVI cycle

PROTEIN KINASE CK2 IN HUMAN DISEASES: TOO MUCH OR TOO LITTLE?

Coordinator: Ch.mo Prof. Ornella Rossetto

Supervisor: Ch.mo Prof. Maria Ruzzene

Ph.D. student: Camila Paz Quezada Meza

INDEX

INDEX ..... **III**

FIGURE INDEX ..... **VII**

TABLE INDEX ..... **IX**

ABBREVIATIONS ..... **X**

1. AMINOACIDS X
2. ACRONYMS XI
3. MEASUREMENT UNITS XVI

SUMMARY **1**

INTRODUCTION **5**

1. PROTEIN PHOSPHORYLATION 5
   - *1.1. Cellular importance of protein phosphorylation* *6*
   - *1.2. Protein kinases* *6*
     - 1.2.1. Protein kinases classification 7
     - 1.2.2. Conserved protein kinase structure 9
     - *1.2.3.* Kinase activity regulation 10
2. PROTEIN KINASE CK2 11
   - *2.1. CK2 structure* *12*
     - 2.1.1. CK2 catalytic subunits 12
     - 2.1.2. CK2 regulatory β subunit 14
     - 2.1.3. CK2 tetrameric holoenzyme 15
   - *2.2. CK2 substrate specificity* *16*
   - *2.3. CK2 "regulation"* *18*
   - *2.4. Protein kinase CK2 physiopathology* *19*
     - 2.4.1. Physiological roles of CK2 20
     - 2.4.2. CK2 in human diseases 22
       - 2.4.2.1 CK2 in cancer 26
       - 2.4.2.2 CK2 in neurodevelopmental disorders 27
   - *2.5. CK2 inhibition* *29*

MATERIALS AND METHODS **31**

1. *IN VITRO* EXPERIMENTS 31
   - *1.1. In vitro phosphorylation assay* *31*
   - *1.2. In vitro CK2 activity assays* *31*
2. CELL CULTURE AND TRANSFECTION 32

2.1. Cell lines and cell culture *32*
2.2. Stromal-CML cells co-culture model *32*
2.2.1. Cell transfection 33
2.2.2. Selection of stably transfected clones 33
3. CELL TREATMENTS AND FUNCTIONAL ASSAYS 33
3.1. CK2 pharmacological inhibition *33*
3.2. Cell viability assay *34*
3.3. FACS analyses of apoptosis *34*
3.4. Colony formation assay *35*
3.5. Protein stability assays *35*
3.6. Ubiquitin-proteasome proteolytic pathway inhibition *35*
4. PROTEIN ANALYSIS 35
4.1. Cell lysis *35*
4.2. Cell fractionation *36*
4.3. Antibodies *36*
4.4. Co-immunoprecipitation experiments *37*
4.5. Western blot analysis *37*
5. STATISTICAL ANALYSIS 38

CHAPTER I: CK2 IN FRIEDREICH'S ATAXIA 40

1. INTRODUCTION 41
1.1. Friedreich's ataxia *41*
1.1.1. Clinical features and care 41
1.1.2. Frataxin: the responsible for the pathology of Friedreich's ataxia 42
1.2. CK2 in Friedreich's ataxia *44*
2. AIM OF THE STUDY 46
3. RESULTS 48
3.1. CK2 directly phosphorylates FXN in S89 and S206 ..... *48*
3.2. Phosphorylation of S206 by CK2 regulates FXN turnover *49*
3.3. CK2 inhibition increases extra-mitochondrial FXN *50*
3.4. CK2 targeting increases endogenous FXN protein levels in HEK-293 cells *52*
3.5. CK2 targeting increases endogenous FXN protein levels in FRDA patients-derived cells *53*
4. DISCUSSION 54

CHAPTER II: CK2 IN CHRONIC MYELOID LEUKEMIA 57

1. INTRODUCTION 58
1.1. Chronic myeloid leukemia *58*
1.1.1. BRC-ABL1: the responsible of the pathology of chronic myeloid leukemia 58
1.1.2. Clinical features and care 58

1.1.3. Tyrosine Kinase Inhibitor resistance 59
1.2. CK2 in chronic myeloid leukemia 61
1.2.1. CK2 in T315I-induced TKI resistance in chronic myeloid leukemia 62
1.2.2. CK2α knockout enhance sensitivity to TKIs in T315I -resistant cells 64
2. AIM OF THE STUDY 66
3. RESULTS 68
3.1. CK2 pharmacological inhibition reduces KBM5-T315I cell viability and promotes apoptosis 68
3.2. CK2 inhibitor CX-4945 reduces BCR-ABL1 signaling in KBM5-T315I cells 69
3.3. CK2 inhibitor CX-4945 reduces KBM5-T315I cell viability and induces apoptosis even in the presence of stromal cells 71
3.4. CK2 inhibitor CX-4945 reduces KBM5-T315I cell viability under hypoxic conditions 73
3.5. CK2 inhibitor CX-4945 reduces KBM5-T315I clonogenic potential even in the presence of stromal cells 74
3.6. CK2 inhibitor CX-4945 is effective in reduce cell viability and pro-survival signaling pathways in a second T315I-resistance model 75
4. DISCUSSION 78
CHAPTER III: CK2 IN POIRIER–BIENVENU NEURODEVELOPMENTAL SYNDROME 80
1. INTRODUCTION 81
1.1. Poirier–Bienvenu neurodevelopmental syndrome 81
1.1.1. Clinical features and care 81
1.1.2. CK2β: the responsible of the pathology of POBINDS 81
2. AIM 83
3. RESULTS 84
3.1. Establishment of the cellular model for the POBINDS mutant biochemical analysis 84
3.2. POBINDS CK2β mutants display differential protein expression 85
3.3. Reduced protein levels of POBINDS CK2β mutants is due to increased proteasome-dependent degradation 86
3.4. POBINDS CK2β mutants display different CK2 activity 87
4. DISCUSSION 90
CHAPTER IV: CK2 INTERACTION WITH SARS-COV-2 NUCLEOCAPSID PROTEIN 96
1. INTRODUCTION 97
1.1. Severe Acute Respiratory Syndrome Coronavirus 2 (SARS-CoV-2) 97
1.1.1. SARS-CoV-2 Nucleocapsid protein 99
1.2. CK2 activity stimulation upon viral infection 100
2. AIM 102
3. RESULTS 103

3.1. CK2 phosphorylates the SARS-CoV-2 N protein 103

3.2. SARS-CoV-2 N protein strongly activates CK2 in vitro 103

3.3. N-protein physically associates to CK2 106

3.4. SARS-CoV-2 N protein enhances the phosphorylation level of CK2 substrates in cells 107

4. DISCUSSION 109

GENERAL CONCLUSION 111

RELATED PROJECTS AND PUBLICATIONS 113

1. PROTEIN KINASE CK2 AND SARS-COV-2 REVIEW 114
2. ROLE OF CK2 IN CONTROLLING ER-PHAGY 125
3. ROLE OF CK2 IN THE GLYCOLYTIC PHENOTYPE OF TUMOR CELLS 143

REFERENCES 160

ACKNOWLEDGMENTS 187

FIGURE INDEX

Figure 1. Schematic representation of protein phosphorylation. 5
Figure 2. Protein phosphorylation as molecular switch mechanism. 7
Figure 3. Human kinases classification. 9
Figure 4. Conserved structural features of eukaryotic protein kinases catalytic domain. 10
Figure 5. CK2α displays ePKs conserved motives. 13
Figure 6. CK2 β-β dimer. 15
Figure 7. CK2 holoenzyme "butterfly"-shaped structure. 16
Figure 8. Web logo analysis of CK2-validated phospho-sites. 17
Figure 9. CK2 role in pro-survival pathways. 22
Figure 10. CK2 is involved in different human pathologies. 25
Figure 11. Human FXN sequence displays putative CK2 phosphorylation sites. 45
Figure 12. CK2 phosphorylates FXN in S89 and S206. 48
Figure 13. Phosphorylation of S206 by CK2 regulates FXN turnover. 50
Figure 14. CK2 inhibition increases extra-mitochondrial FXN. 51
Figure 15. CK2 targeting increases endogenous FXN protein levels in HEK-293 cells. 52
Figure 16. CK2 inhibition with CX-4945 increases endogenous FXN protein levels in FRDA patients-derived cell lines. 53
Figure 17. CK2 is overexpressed and involved in pathological signaling in T315I resistant cells. 63
Figure 18. CK2α genetic ablation enhances sensitivity to TKIs in T315I -resistant cells. 65
Figure 19. CK2 pharmacological inhibition reduces KBM5-T315I cell viability and promotes apoptosis. 69
Figure 20. CK2 inhibitor CX-4945 reduces pro-survival signaling pathways in KBM5-T315I cells. 70
Figure 21. CK2 inhibitor CX-4945 reduces KBM5-T315I cell viability and induces apoptosis even in the presence of stromal cells. 72
Figure 22. CK2 inhibitor CX-4945 reduces KBM5-T315I cell viability under

hypoxic conditions. 73
Figure 23. CK2 inhibitor CX-4945 reduces KBM5-T315I clonogenic potential. 74
Figure 24. CK2 pharmacological inhibition reduces K562-T315I cell viability and promotes apoptosis. 76
Figure 25. Selected POBINDS CK2β mutants. 83
Figure 26. Cellular model for the study of POBINDS CK2β mutants. 84
Figure 27. POBINDS CK2β mutants display differential protein expression. ... 85
Figure 28. POBINDS CK2β mutants display differential protein stability. 86
Figure 29. POBINDS CK2β mutants display different CK2 activity. 88
Figure 30. The reduced activity of POBINDS C137F and H165R CK2β mutants depends on their reduced protein levels. 89
Figure 31. Structural representation of the of the SARS-CoV-2 N protein. 99
Figure 32. CK2 phosphorylates the SARS-CoV-2 N protein. 103
Figure 33. SARS-CoV-2 N protein increases CK2 activity towards a model peptide substrate. 104
Figure 34. SARS-CoV-2 N protein increases CK2 activity towards model protein substrate. 106
Figure 35. SARS-CoV-2 N protein physically interacts with CK2 in cells. 106
Figure 36. N protein enhances the phosphorylation level of CK2 cellular substrates. 108

TABLE INDEX

Table I. Examples of protein-protein interactions that activate CK2 19
Table II. Classification of CK2 inhibitors 30
Table III. FXN cellular functions 43
Table IV. Symptomatology of POBINDS patients carrying the selected *CSNK2B* variants 93
Table V. Symptomatology of POBINDS familiar cases 95

ABBREVIATIONS

1. AMINOACIDS

Ala	Alanine	A
Arg	Arginine	R
Asn	Asparagine	N
Asp	Aspartic Acid	D
Cys	Cysteine	C
Gln	Glutamine	Q
Glu	Glutamic acid	E
Gly	Glycine	G
His	Histidine	H
Ile	Isoleucine	I
Leu	Leucine	L
Lys	Lysine	K
Met	Methionine	M
Phe	Phenylalanine	F
Pro	Proline	P
Ser	Serine	S
Thr	Threonine	T
Trp	Tryptophan	W
Tyr	Tyrosine	Y
Val	Valine	V

2. ACRONYMS

+ssRNA	Positive-Sense Single-Stranded RNA
7-AAD	7-aminoactinomycin D
ABL1	Abelson murine leukemia 1 kinase
ADP	Adenosine di-phosphate
AGC	Calcium-phospholipid-dependent kinases
AML	Acute myeloid leukemia
AMPPNP	Adenylyl-imidodiphosphate
AP	Accelerated phase
ATP	Adenosine triphosphate
AUTS2	Autism susceptibility candidate
B-ALL	B-cell acute lymphoblastic leukemia
BCR	Breakpoint cluster region protein
BCR-ABL1	Quimeric BCR-ABL1 fusion kinase
BMM	Bone marrow microenvironment
BP	Blast phase
BRCA1	Breast cancer gene 1 tumor suppressor
BSA	Bovine serum albumin
BSA	Bovine serum albumin
CAMK	Ca2+/calmodulin-regulated kinases
cAMP	Cyclic adenosine monophosphate
Cas9	CRISPR-associated protein 9
CDKs	Cyclin-dependent kinases
CK1	Casein kinase 1
CK2	Casein kinase 2
CK2a	CK2 kinase subunit α
CK2β	CK2 kinase subunit β
CLL	Chronic lymphocytic leukemia
CMGC	CDKs, MAPKs, GSK, HIPKs and CK2 kinase group
CML	chronic myeloid leukemia
COVID-19	Coronavirus disease 2019
CoVs	Coronaviruses

CP	Chronic phase
CRISPR	Clustered regularly interspaced short palindromic repeats
CRKL	Crk-like protein
CSNK2	CK2 kinase
C-spine	Catalytic spine
CTD	C-terminal domain
C-terminal	Protein carboxyl-terminus
DD	Developmental delay
DEMEM	Dulbecco's Modified Eagle Medium
DMSO	Dimethyl sulfoxide
Dvl	Dishevelled
EDTA	Ethylenediamine tetraacetic acid
EGTA	Ethylene glycol tetraacetic acid
ePK	Eukaryotic protein kinase
ER	Endoplasmic reticulum
ERGIC	ER-to-Golgi intermediate compartment
ERK	Extracellular signal-regulated kinases
FBS	Fetal bovine serum
FGF-1	Fibroblast growth factor 1
FMRP	Fragile X mental retardation protein
FRDA	Friedrich’s ataxia
FXN	Frataxin
G-CK	Genuine casein kinase
GSK	Glycogen synthase kinase
GTP	Guanosine triphosphate
H1N1	Influenza A virus subtype H1N1
HCl	Hydrogen chloride
HCV	hepatitis C virus
HEPES	Piperazineethanesulfonic acid
HIPKs	Homeodomain-interacting protein kinases
HIV-1	Human immunodeficiency virus
HRP	Horseradish peroxidase

Hsp90	Heat shock protein 90
HSV-1	Herpes simplex virus type 1
IBV	Avian infectious bronchitis coronavirus
ID	Intellectual disability
IDCS	Intellectual disability-craniodigital syndrome
IKK	IκB kinase
IL-6	Interleukin 6
IM	Imatinib
ISC	Iron-sulfur clusters
ISCU	Iron-sulfur cluster assembly enzyme
IκB	Inhibitor of NF-κB
JAK2	Janus kinase 2
KCl	Potassium chloride
KD	Kinase domain
KH_2PO_4	Potassium dihydrogen phosphate
KO	Knock-out
Lyn	Lck/Yes novel tyrosine kinase
MAPKs	Mitogen-activated protein kinases
MEK	Mitogen-activated protein kinase kinase
MERS-CoV	Middle East respiratory syndrome
mRNA	Messenger RNA
mTOR	Mammalian target of rapamycin
MTT	Thiazolyl blue tetrazolium bromide
Mw	Molecular weight
N protein	SARS-CoV-2 nucleocapsid protein
$Na_2HPO_4 \cdot 2H_2O$	Di-Sodium hydrogen phosphate dihydrate
NaCl	Sodium chloride
NCCN	National Comprehensive Cancer Network
NF-κB	Nuclear factor-κb
Nrf2	Nuclear factor erythroid 2-related factor 2
NTD	N-terminal domain
N-terminal	Protein amino-terminus
OCNDS	Okur-Chung neurodevelopmental syndrome

ORF	Open reading frame
PAGE	polyacrylamide gel electrophoresis
PARP	Poly ADP-ribose polymerases
PBS	Phosphate buffered saline
Ph	Potential of hydrogen
pH	Potential of hydrogen
PhK	Phosphorylase kinase
PI3K	Phosphoinositide 3-kinase
Pin1	Peptidyl-prolyl isomerase
PIP3	Phosphatidylinositol (3,4,5)-trisphosphate
PK	Protein kinase
POBINDS	Poirier–Bienvenu Neurodevelopmental Syndrome
polyQ	Polyglutamine expansion
POMs	Polyoxometalates
PP2A	Protein phosphatase 2A
PRC	Polycomb repressive complex
PTEN	Phosphatase and tensin homolog
PTM	Post-translational modification
PVDF	Polyvinylidene fluoride
RBD	RNA-binding domain
RGC	Receptor guanylate cyclase kinases
RNA	Ribonucleic acid
ROS	Reactive oxygen species
RPMI	Roswell Park Memorial Institute
R-spine	Regulatory spine
S6RP	S6 ribosomal protein
SAG	Sensitive to Apoptosis Gene protein
SARS-CoV	Severe Acute Respiratory Syndrome Coronavirus
SARS-CoV-2	Severe Acute Respiratory Syndrome Coronavirus 2
SDS	Sodium Dodecyl Sulfate
siRNA	Short interfering RNA
SLITRK1	SLIT and NTRK-like family, member 1
SNARE	Soluble NSF Attachment Protein Receptor

STAT	Signal Transducer and Activator of Transcription
STE	Sterile kinases
T1DM	Type 1 diabetes mellitus
T2DM	Type 2 diabetes mellitus
T-ALL	T-cell acute lymphoblastic leukemia
TBB	4,5,6,7-tetrabromobenzotriazole
TCF/LEF	T-cell factor/lymphoid enhancer factor
TDB	Tetrabromo-deoxyribofuranosyl-benzimidazole
Th	T helper cells
TIF-1α	Tripartite Motif protein 24
TK	Tyrosine kinases
TKI	Tyrosine kinase inhibitors
TKL	Tyrosine kinase-like
TMPRSS2	Transmembrane protease, serine 2
Tris	Tris (hydroxymethyl) aminomethane
TTBS	Tris buffered saline plus Tween 20
Tween 20	Polysorbate 20
WT	Wild type
XRCC	X-ray cross complementing protein

3. MEASUREMENT UNITS

bp	Base pair
h	Hour
°C	Celsius
µM	Micromolar
M	Molar
mA	Milliampere
mg	Milligram
min	Minute
mL	Milliliter
mM	Millimolar
mm	Millimeter
ng	Nanogram
nM	Nanomolar
nm	Nanometer
rpm	Revolutions per minute
V	Volt
v/v	Volume per volume
w/v	Weight per volume
µg	Microgram

SUMMARY

CK2 is a protein kinase composed by two catalytic subunits α or α′, that can be active also as monomers, and two regulatory subunits β. CK2 is constitutively active and, by phosphorylating hundreds of substrates, is involved in different signaling pathways, as the PI3K/Akt, the IKK/NF-κB, the JAK2/STAT3 and the Wnt/β-catenin pathways. CK2 is also implicated in several human diseases; among them, its role in cancer is the most widely studied, but its pathological functions have been also reported in diabetes, obesity, atherosclerosis, cardiovascular diseases, neurologic disorders, and viral infections.

The main aim of this work was the investigation of the role of CK2 in four non-related human diseases, namely Friedrich's ataxia (FRDA), chronic myeloid leukemia (CML), Poirier-Bienvenu Neurodevelopmental Syndrome (POBINDS) and coronavirus disease 2019 (COVID-19).

CK2 and Friedrich's ataxia

Friedreich's ataxia (FRDA) is a rare autosomal-recessive cardio- and neuro-degenerative disease, caused by mutations in the *FXN* gene, which leads to a significant reduction in the expression of frataxin (FXN), a mitochondrial protein that plays a key role in iron sulfur clusters assembly. Thus, any attempt to increase FXN levels is encouraged from a therapeutic perspective. Previous studies have shown that FXN proteasome-mediate degradation can be promoted by phosphorylation and since the FXN sequence contains five potential consensus sites for CK2, we investigated whether this kinase also plays a role in regulating FXN turnover. Our research revealed that frataxin can be phosphorylated at S206 by CK2 kinase, and this phosphorylation promotes frataxin turnover, significantly reducing its protein expression. Moreover, we found that CK2 acts mainly over extra-mitochondrial FXN, and that CK2 targeting, by pharmacological inhibition with its clinal grade inhibitor CX-4945 or by genetic ablation, increases frataxin expression in human cells. More importantly, CK2 inhibition by CX-4945 in FRDA patients-derived cells promoted frataxin accumulation. These encouraging *in vitro* and *ex vivo* results suggest CK2 as a valuable target in FRDA and pave the way for future *in vivo* studies.

CK2 in chronic myeloid leukemia

Chronic myeloid leukemia (CML) is a myeloproliferative neoplasia caused by the fusion tyrosine kinase BCR-ABL1, which is constitutively active and sufficient to maintain the leukemia phenotype of CML. The current standard of care for CML is the use of tyrosine kinase inhibitors (TKIs), as imatinib, however around 25% of the patients develop resistance. One of the worst types of resistance is the one caused by the mutation T315I in BCR-ABL1, since patients bearing this mutation are only responsive to ponatinib, a TKI with strong side effects, thus eagerly waiting for additional or alternative therapies. CK2 is overexpress and contributes to aberrant signaling in T315I-cells, thus the aim of this work was to evaluate the potential of CK2 as a pharmacological target for this kind of CML drug-resistance. We found that T315I imatinib-resistant cells are highly sensitive to several CK2 inhibitors. We mainly focused on the clinical grade inhibitor CX-4945, finding that it induced apoptosis and reduced survival pathways, as BCR-ABL1, STAT-3, STAT-5, and Lyn, that are specifically hyperactivated in T315I imatinib-resistant cells. Most effects were mirrored by genetic targeting of the CK2α catalytic subunit by siRNA downregulation or CRISPR/Cas9 knockout, which also induced increased sensitivity towards TKIs. The effects of CX-4945 were exerted even in the presence of bone marrow microenvironment-mimicking conditions, and under hypoxic conditions, where the action of most drugs was significantly reduced. Our results, mainly obtained in the most common cellular model T315I-KBM5, but with the key findings reproduced also in a second newly developed line, T315I-K562, allow to conclude that CK2 targeting is a promising strategy to counteract this aggressive kind of drug resistance in CML.

CK2 in Poirier-Bienvenu Neurodevelopmental Syndrome

The Poirier–Bienvenu neurodevelopmental syndrome (POBINDS) is a rare and newly discovered neurologic disorder with early onset epilepsy, intellectual disability, and developmental delay as main traits. POBINDS is caused by mutations in the *CSNK2B* gene coding for the regulatory β subunit of CK2, and to date 91 cases have been reported being mostly *CSNK2B de novo* variants. The biochemical characteristics of the CK2β mutants remain largely unknown. Therefore, with this project we aimed to establish a cellular model for the characterization of POBINDS mutants and to biochemically analyse some of

them, chosen because found in Italian patients, as a first step of a further analysis in patients-derived cells and animal models. As model, we started from HEK-293AD CK2β knockout (KO) cell clones, that present reduced CK2 activity. These cells were stably transfected with CK2β wild type (WT), which restored CK2 activity, thus validating the model. We therefore stably expressed POBINDS mutants into the CK2β KO cells, to analyse their expression and CK2 activity. We found reduced protein expression of three out of the five analysed POBINDS mutants. Moreover, protein stability assays showed that, in comparison to the WT, two of the mutants were less stable, presumably due to an increased cleavage by a proteasome-dependent mechanism. These two mutants also showed defective CK2 activity compared to the WT. Altogether, our results show that some POBINDS CK2β mutants present defective CK2 activity and decreased protein stability. However, not all the analysed mutants displayed differences compared to WT CK2β. Moreover, we did not observe a clear-cut correlation between the biochemical features of a certain mutant and the phenotypes of the patients harbouring that mutation. Although several speculations can be done to explain these discrepancies, a more extended biochemical characterization will help in better understanding the biochemical features/phenotype correlation. In particular, we are now collecting cells derived from patients, that will directly clarify if their properties are consistent with their clinical presentation.

CK2 and COVID-19

It has been reported that, in cells infected by Severe Acute Respiratory Syndrome Corona Virus 2 (SARS-CoV-2), the virus responsible for the COVID-19 pandemic, different CK2-dependent phospho-sites are upregulated, suggesting an enhanced CK2 activity of the host cells upon SARS-CoV-2 infection. Moreover, CK2 was found at the actin filopodial protrusions induced by the infection, colocalized with the SARS-CoV-2 nucleocapsid (N) protein, pointing this protein as a putative candidate for the effects on CK2 activity. The main aim of this project was therefore to understand if and how the SARS-CoV-2 N protein can modulate the activity of CK2. Our results showed a weak phosphorylation of the N protein by CK2, but, more importantly, the experiments revealed that the N protein strongly stimulated CK2 activity (up to 5-fold) in a time- and dose-dependent

manner, towards both peptide and protein substrates. Interestingly, this increase in activity was mainly observed with the monomeric CK2α, with a more modest stimulation produced on the tetrameric CK2 and the monomeric isoform CK2α'. Using HEK-293AD and HEK-293AD CK2β knockout cell clones stably transfected with the SARS-CoV-2 N protein we confirmed the interaction of CK2 with the N protein and observed N protein-dependent activation of CK2, especially in the CK2β KO cells. We are now designing short peptides to identify the exact region of N protein responsible for the activating effects. Therefore, our results not only shed light on the mechanisms by which CK2 is implicated in COVID-19, but also provide hypothesis for the development of a CK2 activator. Since no compound able to activate CK2 is currently available, it could turn to be useful in all those conditions were a CK2 defective function is observed.

In summary, this thesis adds evidence to the concept that CK2 is a valuable target for diverse human diseases. Moreover, in addition to the historical view of this enzyme as a “too much” thing, with a pathological role which requires inhibition, here we highlight that also the “too low” condition exists for CK2 as disease-driving molecule. For the physiological functionality of CK2, a balance, the “right level”, is necessary, that, when lost, could require either inhibition or activation.

INTRODUCTION

1. Protein phosphorylation

Protein phosphorylation is one of the most frequent post-translational modifications (PTMs). To date it is estimated that more than one-third of the human proteome is phosphorylated (Ardito et al., 2017; Ramazi & Zahiri, 2021). This type of modification is reversible and corresponds to the covalent addition of a phosphate group (PO_4), normally obtained from the purine nucleotide triphosphate (ATP or GTP) γ-phosphoryl (PO_3^{2-}) group, to the hydroxyl group of a protein substrates, as illustrated in Figure 1. The phosphorylation reaction is catalyzed by enzymes known as protein kinases (also referred as phosphotransferases) and the phosphate group transfer is commonly facilitated by magnesium (Mg^{2+}) or manganese ions (Mn^{2+}), which chelate the phosphate groups of ATP. In cells, almost all of the phosphorylation events occur either in serine, threonine, or tyrosine residues, with serine as the most common and tyrosine the least common residues to be phosphorylated. The phosphorylation of this three residues is considered as the canonical phosphorylation, however, less often other amino acids, as aspartate, lysine, histidine and arginine, can be phosphorylated in what is called noncanonical phosphorylation (Mascher et al., 2006). The reverse process or dephosphorylation, that implies the removal of the phosphoryl group from the protein substrate, is catalyzed by enzymes known as phosphatases.

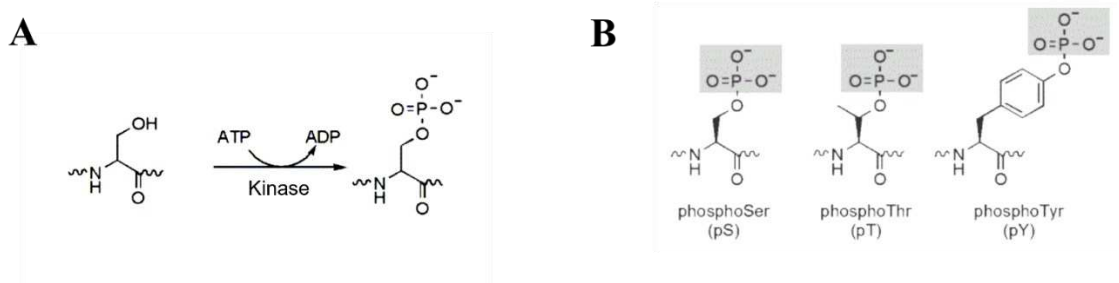

Figure 1. Schematic representation of protein phosphorylation.

(A) The protein kinase transfers the phosphate group of a molecule of ATP to the hydroxyl group of a serine residue to form phosphotyrosine and ADP. (B) Structure of phospho-threonine, phospho-threonine, and phospho-tyrosine residues (modified from Walsh et al., 2005).

1.1. Cellular importance of protein phosphorylation

In cells, the phosphorylation/dephosphorylation modifications act as molecular switches of a big variety of proteins, having a pivotal role in cellular regulation and signal transduction of essential processes, as metabolism, cell proliferation, cell differentiation, apoptosis, cytoskeletal dynamics, and gene expression (Ardito et al., 2017). The phosphorylation process modifies its targets due to three intrinsic characteristics of the addition of a phosphoryl-group. First, as this group has three hydrogen bond acceptors, the phosphorylated protein would have the potential to create new bonds. Secondly, the phosphoryl-group has two negative charges, implying that its addition can modify the electrostatics of the substrate, thus having the potential to modify binding and catalytic properties. And thirdly, adding the phosphoryl-group can alter the shape and size of the substrate, modifying its surface and creating new binding sites (Ellis & Kobe, 2013). Schematically represented in Figure 2, these changes in the substrate can have different functional consequences, as to induce the active or the inactive conformation (Cole et al., 2003), favor protein-protein interactions (Nishi et al., 2011), generate changes in the subcellular location (Kuwahara et al., 2008), and promote the formation or removal of a second PTM (Hunter, 2007). Moreover, a single kinase may simultaneously phosphorylate several substrates, acting in numerous cell signaling pathways and leading to amplification of the signaling, thus turning the phosphorylation process extremely regulated and complex (Humphrey et al., 2015).

1.2. Protein kinases

The discovery of protein phosphorylation started in 1906 with the identification of phosphate in the protein vitellin by Phoebus Levene (Levene & Alsberg, 1906), however, it is not until mid-1950s that things started to heat up when groups working on glycogen metabolism discovered the first protein kinase, the phosphorylase kinase (PhK), an enzyme responsible of glycogen breakdown (Fischer & Krebs, 1955). In 1968, Krebs and colleagues purified the second

kinase to be discovered: the cAMP-dependent protein kinase (PKA), which a few years later would lead to the concept of kinase cascade and to underline the importance of the protein phosphorylation in different cell processes (Taylor et al., 1990; Walsh et al., 1968). To date, it is known that around 2% percent of the human genome encodes protein kinases, containing more than 500 protein kinases (PKs), which constitute one of the largest protein families.

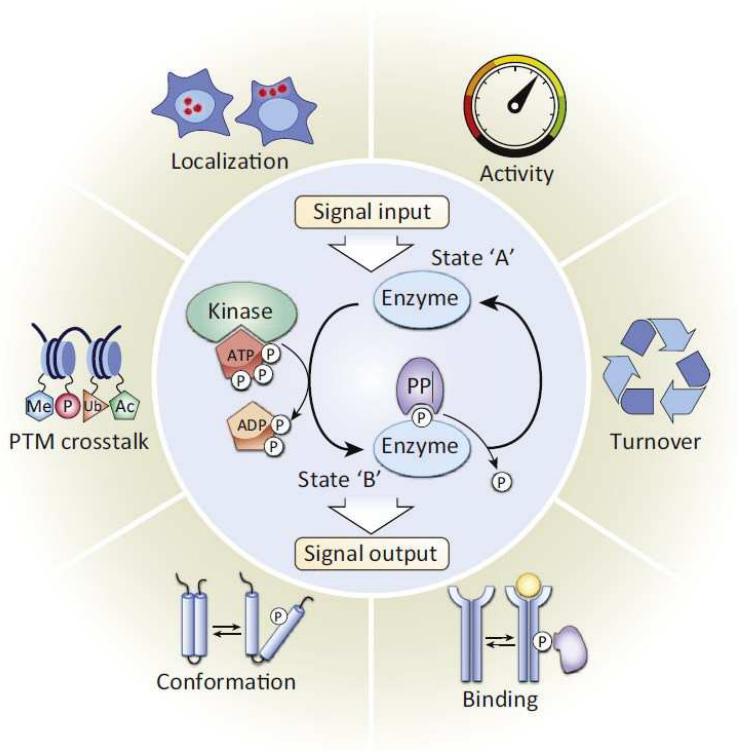

Figure 2. Protein phosphorylation as molecular switch mechanism.

Schematic representation of a reversible protein phosphorylation where the addition of a phosphate group is mediated by a kinase and the removal by a phosphatase (PP). In eukaryotic cells, the phosphorylation/dephosphorylation modulation can regulate activity, turnover, localization, binding properties, conformation, and post translational modifications (PTM) of the substrate protein, acting as molecular switches. Ac, acetylation; Me, methylation, P, phosphorylation; Ub, ubiquitination. (Humphrey et al., 2015)

1.2.1. Protein kinases classification

The most frequent classification for protein kinases divides them into two subfamilies depending on the residue they phosphorylate: serine/threonine (S/T)

kinases, which target either serine or threonine, and tyrosine kinases, which have tyrosine as substrate. Serine residues are the most frequently phosphorylated followed by threonine and tyrosine, with 86.4%, 11.8% and 1.8% of the phosphorylating events respectively. This classification can present difficulties due to the dual-specificity protein kinases that can phosphorylate both serine/threonine and tyrosine residues, and additionally the protein kinases that phosphorylate histidine or aspartate residues, although this phosphorylation is less stable than the canonical type (Schwartz & Murray, 2011).

As represented in Figure 3, a second type of classification subdivide the human kinases into 497 eukaryotic protein kinases (ePKs) and 58 atypical kinases, which include the lipid kinases (Kanev et al., 2019; Manning et al., 2002). The eukaryotic protein kinases can be further subdivided into: cyclic nucleotide- and calcium-phospholipid-dependent kinases (AGC) (comprising the PKA, PKG and PKC families), the Ca2+/calmodulin-regulated kinases (CAMK), the casein kinase 1 family (CK1), the CMGC group (which includes the cyclin-dependent kinases (CDKs), mitogen-activated protein kinases (MAPKs), glycogen synthase kinase (GSK), homeodomain-interacting protein kinases (HIPKs) and casein kinase 2 (CK2)), the receptor guanylate cyclase kinases (RGC), the homologs of yeast Sterile 7, Sterile 11, Sterile 20 kinases (STE), the tyrosine kinase-like (TKL) and tyrosine kinases (TK) (including receptor and non-receptor types). This subdivision gives rise to the “human kinome” (see Fig. 3)

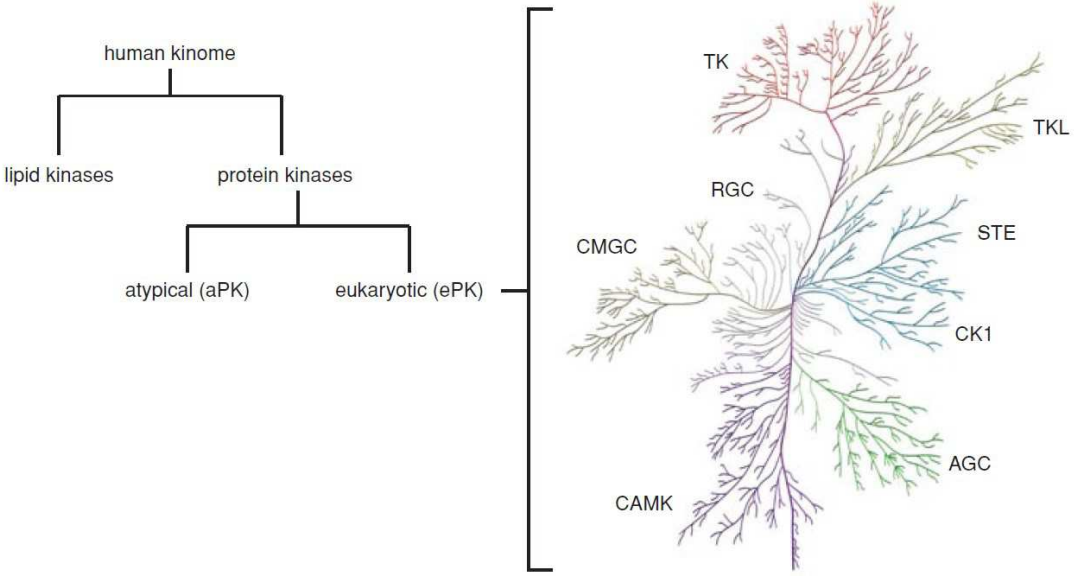

Figure 3. Human kinases classification.

The human kinome is composed by lipid and protein kinases. Protein kinases can be classified as atypical or eukaryotic, which in turn can be classified into subgroups based on their sequence similarity. For kinase group abbreviations see the text (modified from Duong-Ly & Peterson, 2013; based in Manning et al., 2002).

1.2.2. Conserved protein kinase structure

The understanding of the kinase structure can unveil the substrate recognition mechanism of a kinase, shedding light on important information that can be used with therapeutic purposes, as for example the design of inhibitors or activators. Although *in-silico* analysis using only the sequence of kinases has been proved adequate to define conserved motifs of protein kinases, it is the sum of this information and the crystallographic structure that can give precise information regarding the architecture of a kinase. Despite the diversity that can be found between protein kinase families, the sequence and structure of the catalytic core of the protein kinase has been found to be highly conserved among them.

It is possible to distinguish two separated lobes conserved on the structure of the catalytic domain of protein kinases: the N-lobe and the C-lobe (Taylor & Kornev, 2011). The N-lobe is the smaller one and mainly comprises the N-terminal sequence disposed as a β-sheet with five strands and a helical subdomain named αC-helix, which is spatially positioned between the two lobes. The N-lobe also presents conserved motifs as the Glycine-rich Loop (GxGxxG), which is the most flexible part of the lobe and responsible for the donor phosphates orientation for catalysis, and the AxK motif, in which a conserved lysine is present, responsible to couple the phosphates of the ATP to the αC-helix. The C-lobe is the larger lobe, reported as highly stable and composed mainly by α-helices plus a β-sheet, forms the kinase core presenting the catalytic loop that helps with the orientation of the substrate protein and directs the catalytic event (Figure 4). In addition to the N- and the C-lobes, there are two conserved hydrophobic motifs comprising residues from both lobes, named “spines”. The regulatory spine (R-spine) is an spatial motif observed only in active kinases, while the catalytic spine (C-spine) is completed by the binding of the ATP, contributing to its positioning towards the C-lobe (Kornev et al., 2006).

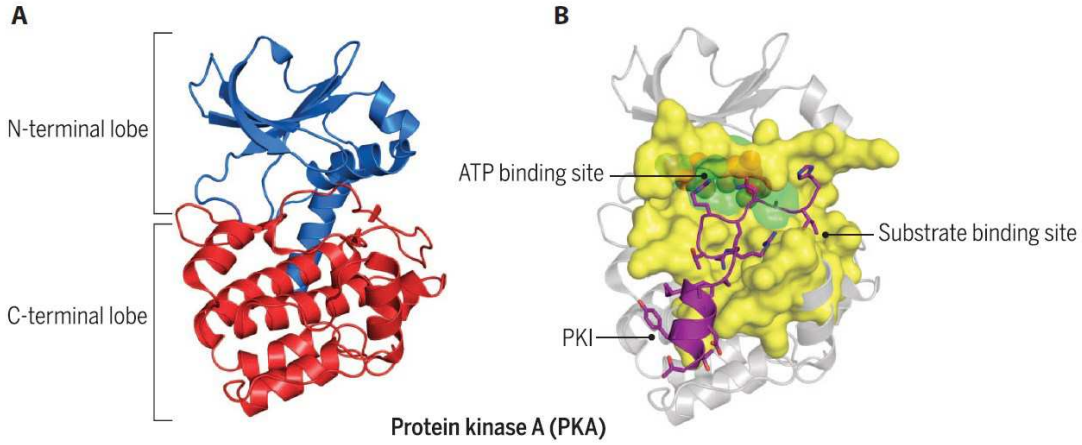

Figure 4. Conserved structural features of eukaryotic protein kinases catalytic domain.

Ribbon representation of the archetypal protein kinase A (PKA) catalytic domain. (A) the bilobed catalytic domain with the N-terminal lobe (blue) mainly composed by b-strands and the C-lobe mostly helical (colored red). (B) A more detailed view of the catalytic domain shows the substrate binding site (yellow) interacting with the substrate (purple) and the ATP binding site (green) in the cleft between the lobes. PKI, protein kinase inhibitor (de Oliveira et al., 2016)

1.2.3. Kinase activity regulation

Eukaryotic PKs, distinguishing from most metabolic enzymes, have evolved to be highly regulated and most of the times only transiently activated (Johnson & Lewis, 2001). The regulatory mechanism follows a differential conformation between the active and inactive states, this way, kinases ready to execute their catalytic function present a specific active conformation where key regulatory and catalytic residues are aligned. One of the hallmarks of the active state is the presence of the R-spine, and a second hallmark of this state is the stabilization of the so called Activation-loop (A-loop), typically mediated by phosphorylation and/or protein–protein interactions (Arter et al., 2022). It has been described that while the sequential steps to place the key residues of the active site in their proper positions, thus activating the kinase, are well conserved among kinases, the inactive states show a diverse range of conformations from rotated into suboptimal positions for the catalysis to quite disordered conformations in some of the cases (Taylor & Kornev, 2011). Moreover, the dynamics between the “on” and “off” conformations are in accordance with the kinase functions, being reported that most of the proteins are inactive in basal conditions, switching to

their active state upon specific signals. However, there are exceptions to this concept, as is the case of the object of this thesis, the constitutively active kinase CK2, to which the following paragraphs are dedicated.

2. Protein kinase CK2

CK2 (previously known as CKII and frequently referred to as CSNK2, from the gene name), is a highly conserved S/T protein kinase present in all eukaryotic organisms. The acronym CK2 comes from the term “casein kinase 2” given after Burnett and Kennedy isolated from liver two distinct enzymes (namely casein kinase 1 and casein kinase 2) that were able to phosphorylate casein *in vitro* (Burnett & Kennedy, 1954). However, and as they first hypothesized, in physiological conditions casein is phosphorylated by another kinase, identified several years later as G-CK or genuine casein kinase, and not by CK2 (Venerando et al., 2014). From the discover of Burnett and Kennedy, the study of CK2 has progressively continued over the years followed by the deciphering of its subunits primary structures in 1987 (Saxena et al., 1987), and their tridimentional structures in 1998 and 2001 (Chantalat et al., 1999; Niefind et al., 2001). Moreover, several works have compared the properties of the “casein kinases” CK1 and CK2 as well as the specifical CK2 properties (Hathaway & Traugh, 1982; Venerando et al., 2014).

To date, a vast number of studies have shown that CK2 is ubiquitously expressed and localized mainly in nucleus and cytoplasm but also possible to be found in other subcellular compartments, as plasma membrane and mitochondria (Filhol & Cochet, 2009). CK2 is constitutively active, thus not requires any phosphorylation event or signaling to be activated, however its functions are mainly regulated by changes in protein expression and in subcellular localization, substrate availability/accessibility, protein interaction/binding and ratio of its subunits/isoforms (Borgo et al., 2021b; Litchfield, 2003; St-Denis & Litchfield, 2009).

As it phosphorylates hundreds of substrates, CK2 is considered extraordinarily pleotropic, accounting for up to 25% of the phosphoproteome (Venerando et al.,

2014). Indeed, CK2 has been described to be involved in virtually all cellular processes, as for example cell proliferation, cell survival, apoptosis, and cell cycle regulation, moreover, has also been described to regulate several transcription factors, thus controlling protein synthesis. This way, it is not surprising that CK2 is involved in several human diseases, extensively described in cancer but also implicated in inflammatory diseases, neurologic disorders and viral infections, as it will be described in the next paragraphs.

2.1. CK2 structure

In cells, CK2 is usually present as an heterotetrameric holoenzyme composed by two catalytic, α and/or α', and two regulatory subunits β (Hathaway & Traugh, 1979), where the tetrameric conformations can be $CK2\alpha_2/CK2\beta_2$, CK2αα'/CK2β, or $CK2\alpha'_2/CK2\beta_2$ complexes. In the following paragraphs, the characteristics of the monomeric subunits as well as of the tetrameric enzyme will be described.

2.1.1. CK2 catalytic subunits

CK2 has two catalytic subunits isoforms, α and α', which are highly homologous, with a global sequence identity of approximately 75% between them. Interestingly, they only differ in their C-terminal domain, which is highly conserved among species. The catalytic subunits are coded by two different genes: *CSNK2A1* (found on chromosome 20p13) encodes the 391 aminoacids long subunit α (Mw 45 kDa) and *CSNK2A2* (found on chromosome 16p21) encodes the 350 aminoacids long subunit α' (Mw 41 kDa) (Wirkner et al., 1995). Moreover, CK2α can suffer C-terminal proteolysis and be present at a molecular weight of 38 kDa (Faust et al., 1999), although the physiological relevance of this cleavage is not known.

From a structural point of view, the CK2 catalytic subunits are part of the eucaryotic kinase CMGC subfamily and, as pointed in Figure 5, and they present the canonical kinase structural motifs: the N- and C- lobes, αC helix, the glycine-rich loop, the substrate binding site, the catalytic loop, and the activation loop. However, the CK2 catalytic subunits present some particular features in their

catalytic domain, as a reduced and more hydrophobic ATP-binding pocket due to the presence of the hydrophobic residues V66 and M163 that in most ePKs are conserved as alanine and leucine residues, respectively (Niefind et al., 1998). Moreover, in contrast to most CMGC and S/T kinases, the activation loop of the catalytic subunits does not possess a regulatory phosphorylation site, as their N-terminal region is constantly in an active conformation. Furthermore, the CK2 glycine-rich loop correspond to a “GxGxxS” motive, which differs in a glycine residue compared to the classically denoted “GxGxxG” motive (Sarno et al., 1997).

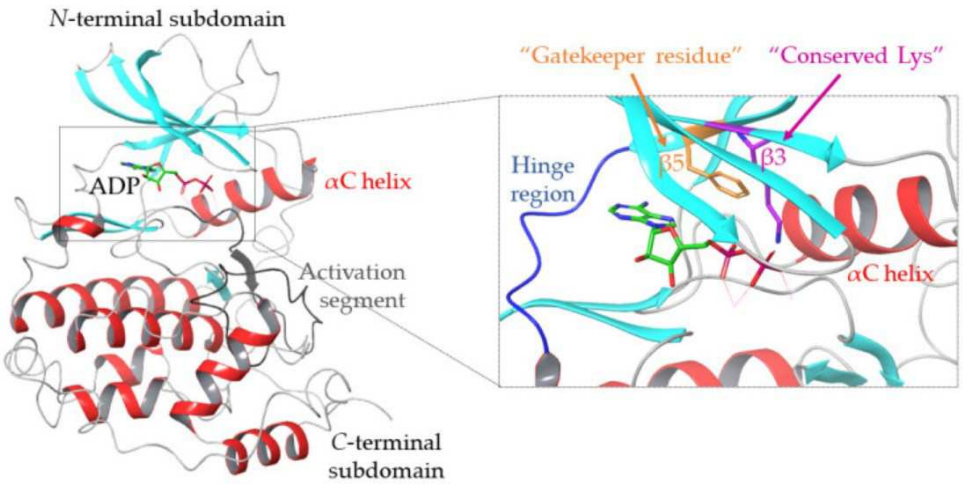

Figure 5. CK2α displays ePKs conserved motives.

Ribbon representation of the crystal structure of CK2α catalytic domain bound to ADP where it is possible to identify the N- and C- lobes, the activation loop (dark grey) and the hinge region (blue). Moreover, α-helices are in red, including the αC helix; β-strands are in cyan; and the conserved sites K68 and F113, necessary for the catalytic activity of all the kinases are in magenta and orange, respectively. (PDB:6YPN) (modified from Atkinson et al., 2021)

CK2 α and α' display similar enzymatic properties *in vitro* (Bodenbach et al., 1994), however there is evidence that suggest differential cellular roles. In mice, whereas CK2α knockout is lethal at early embryological stages, CK2α’ knockout is viable, displaying however round-headed infertile spermatozoa in male mice (Buchou et al., 2003; Dominguez et al., 2011). Additionally, there are isoform-specific protein interactions reported, as is the case of the phosphatase PP2A and the peptidyl-prolyl isomerase Pin1 that only interact with the α subunit (Hériché et al., 1997; Messenger et al., 2002)

2.1.2. CK2 regulatory β subunit

The CK2β regulatory subunit has the most conserved amino acid sequence between species among the CK2 subunits, is composed by 215 aminoacids (Mw 28 kDa) and is coded by the *CSNK2B* gene (found on chromosome 6p21) (Pyerin & Ackermann, 2001).

CK2β presents structural and biochemical particularities, as the presence of autophosphorylation sites at S2, S3 and potentially at S4 in its N-terminal sequence that increase the kinase activity (Bodenbach et al., 1994). Moreover, while an acidic region comprising the residues in position 55 to 64 in the CK2β N-terminal region presents autoinhibitory effects (Meggio et al., 1994), the region comprising the residues in position 181 to 203 in the C-terminal acts as a positive regulatory domain of CK2 activity (Pinna & Meggio, 1997). In addition, CK2β contains a sequence that resembles the “destruction box” responsible of mitosis-specific degradation of cyclin B (Glotzer et al., 1991), however in this case its role is the regulation of the stability of the tetrameric enzyme as well its own (Allende & Allende, 1995; Zhang et al., 2002).

As shown in Figure 6, the C-terminal of CK2β presents a zinc finger motif containing four cysteine residues, C109, C114, C137, and C140, involved in the β-β dimerization. The abundance of β-sheets that characterizes this area and its elevated hydrophobicity contribute to form hydrophobic interactions between monomers, in fact, it has been reported that the disruption of the zinc finger by mutations in C109 and C114 prevents CK2β dimerization as well as the interaction between β and alpha subunits (Chantalat et al., 1999). It has been suggested that β-β dimerization is a crucial prerequisite for establishing a stable complex with the catalytic subunits, as CK2β mutants unable to form dimers exhibit deficient holoenzyme formation.

Several evidence suggests that the noncatalytic CK2β subunit is crucial in the formation of the tetrameric CK2, as well as in the regulation of its catalytic activity and stability, in its substrate selectivity and serves as a docking platform for recruitment of substrates or potential regulators (Canton et al., 2001; Graham & Litchfield, 2000; Marin, Meggio, & Pinna, 1999; Meggio et al., 1992a). Moreover, based on the presence of CK2β in different cellular compartments to the ones

with CK2α presence, it has been suggested that CK2β may operate also as an independent entity (Krek et al., 1992). In fact, CK2β has been reported to interact independently with the protein kinases c-Mos and A-Raf, acting as negative and positive regulator of kinase activity, respectively (Chen et al., 1997). Additional studies have implicated CK2β in interactions with the superoxide radical production enzyme p47-phox (Kim et al., 2001), the tumor suppressor BRCA1 (O'Brien et al., 1999), and the traffic regulator LYST (Tchernev et al., 2002).

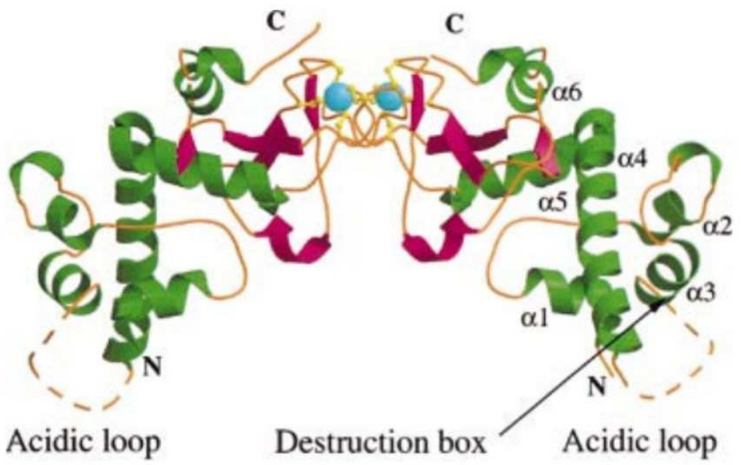

Figure 6. CK2 β-β dimer.

Ribbon representation of the crystal structure of CK2 β-β dimer where the zinc atoms and cysteine ligands are in blue and yellow, respectively. β-strands are in pink and α-helices in green (modified from Chantalat et al., 1999).

2.1.3. CK2 tetrameric holoenzyme

As shown in Figure 6, the CK2 holoenzyme presents a "butterfly"-shaped structure where the catalytic subunits (α and/or α') are linked to the β-β dimer through the C-terminal domain of the regulatory subunits (Niefind et al., 2001), resulting in a structure more stable and usually with higher catalytic activity than the monomeric catalytic subunits by themselves.

Different evidence has suggested the existence of higher levels structures of the CK2 holoenzyme. For example, the ring-shaped structures detected in Drosophila cells, later replicated *in vitro*, are composed by four tetramers able to

dissociate into $\alpha_2\beta_2$ tetramers in high salt concentration conditions (Glover, 1986; Valero et al., 1995). Trimeric aggregates of human CK2 tetramers have also been described *in vitro*, in which the CK2β N-terminal domain of a first tetramer interacts with the catalytic α subunit of a second tetramer (Lolli et al., 2014; Lolli, Pinna, & Battistutta, 2012). In this model, the autophosphorylation of CK2β at S2 would represent an autoinhibitory mechanism of regulation. Nevertheless, the presence of this structure in living organisms is yet to be confirmed.

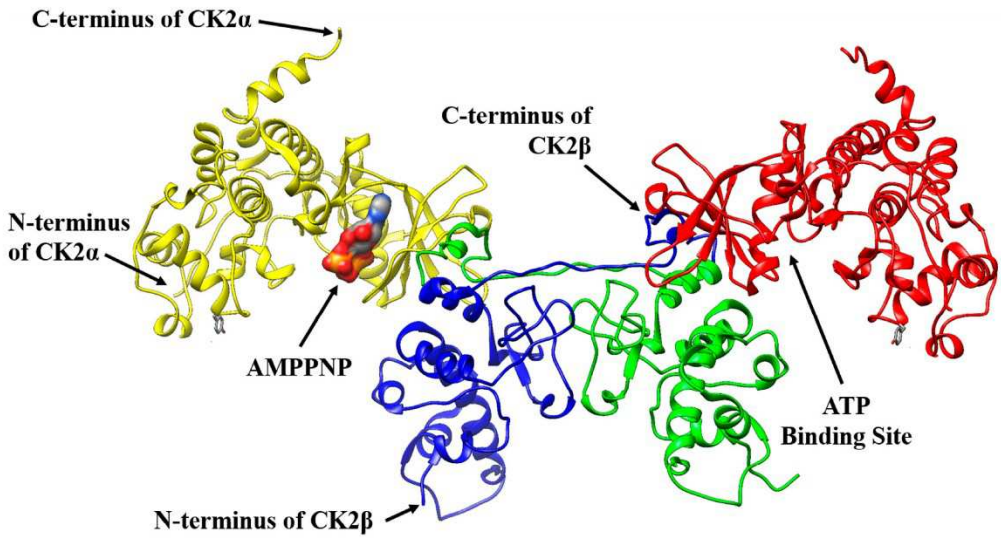

Figure 7. CK2 holoenzyme "butterfly"-shaped structure.

Ribbon representation of the crystal structure of heterotetrameric CK2, where the α subunits (in yellow and red) bind to the regulatory C-terminal of the β subunit (in blue and green). AMPPNP, a non-hydrolysable ATP analogue, is bound in one catalytic α-subunit ATP binding pocket (PDB: 1JWH) (Nienberg et al., 2016).

2.2. CK2 substrate specificity

CK2 is an acidophilic kinase that phosphorylates sites surrounded by acidic residues. The CK2 consensus recognition sequence has been extensively studied, and to date, it stands out as one of the most specific and precisely defined among ePKs (Meggio, Marin, & Pinna, 1994; Salvi et al., 2009). The CK2 minimal consensus sequence is denoted by the sequence S/TxxD/E/pS/pY: the amino acid to be phosphorylated (position 0) is a serine or a threonine, and the

minimal requirement is the presence of an acidic residue (thus a glutamic or aspartic acid, or a previously phosphorylated serine (pS) or tyrosine (pT)) at position n+3 from the target site, as shown in Figure 8. Different bioinformatic analyses using CK2 *bona fide* substrates (533 phospho-sites) have revealed that besides this minimal requirement the presence of additional acidic residues between n-7 and n+7 increases the probability of phosphorylation by CK2, whereas the presence of basic residues in the proximity of the target site have a negative influence. Moreover, the presence of a proline residue at position +1 is detrimental (Meggio & Pinna, 2003; Salvi et al., 2009). Although CK2 is definitely a S/T kinase, it can also phosphorylate tyrosine residues, but this is unusual and not yet proven *in vivo* (Marin et al., 1999b).

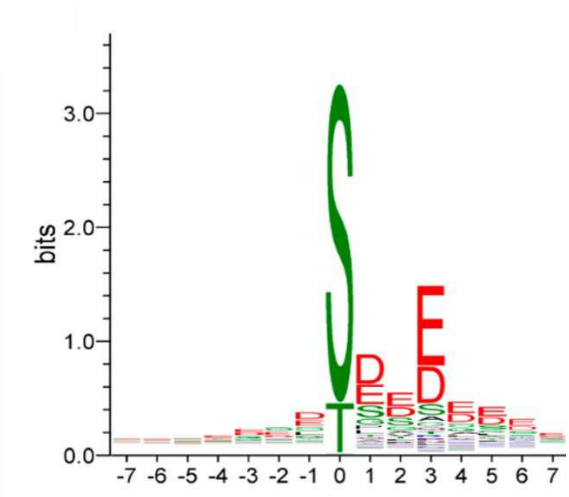

Figure 8. Web logo analysis of CK2-validated phospho-sites.

The sequence has been produced from the analysis of 767 non-redundant CK2-validated phospho-sites collected from the PhosphoSitePlus database. The font height corresponds to the frequency of the presence of a certain residue at that specific position (modified from Cesaro et al., 2023).

Although the presence of the consensus sequence is almost mandatory for a site to be phosphorylated by CK2, the regulatory β subunit has a key role in determining CK2 substrate specificity. For example, the presence of the β subunit severely prevents the phosphorylation of calmodulin, a reported CK2 *in vivo* substrate (Meggio, et al., 1992b), while the CK2 phosphorylation of the protein HIV-REV60 (Marin et al., 2000) and the translation factor eiF2β (Salvi et al., 2006), both CK2 *in vivo* substrates, occurs only in presence of the β subunit. This

way, substrates can be classified in 3 groups based on their requirement of β subunit to be phosphorylated: substrates that can be phosphorylated either in the presence or the absence of CK2β are consider as class I substrates, substrates where CK2β affects negatively their phosphorylation are consider class II substrates, while substrates where CK2β is essential in their phosphorylation are class III substrates (Pinna, 2002). However, this classification is based on *in vitro* experiments and since *in vivo* CK2 has been mainly found in its tetrameric form, the physiological consequences of this classification are not yet completely understood.

2.3. CK2 "regulation"

Despite the "locked" constitutive conformation of CK2 described above, different possibilities of modulating its activity have been proposed (Borgo et al., 2021b). As expected for a constitutive enzyme, the first regulation tool is represented by changes in the expression levels; indeed, as it will be described below, for example in tumor cells the frequently observed higher CK2 activity is usually associated with higher expression levels of its subunits. However, other mechanisms have been proposed, ranging from subcellular translocations to partner interactions.

Also, post translational modification has been analyzed. The CK2β S2 autophosphorylation site was reported to result in increased kinase activity (Zhang et al., 2002). Phosphorylation of CK2α at T13 by AKT and T360 and S362 by ERK2 are proposed to increase the CK2-mediated phosphorylation of TIF-1α and α-catenin, respectively (Ji et al., 2009; Nguyen & Mitchell, 2013). Phosphorylation of CK2α at Y255 by Lyn and c-Fgr kinases results in an up to three-fold increased activity (Donella-Deana et al., 2003).

Another putative regulation mechanism is represented by the interactions between CK2 and specific protein partners. Table I shows the list of the proteins proposed to activate CK2. It has to be noted, however, that the effective *in vivo* relevance of this findings is often still to be proven.

Table I. Examples of protein-protein interactions that activate CK2

Interactor	Affected CK2 Substrate(s)	Biological Function	References
AT2	Cav1.2	Cardiovascular Regulation	(Kashihara et al.,2014)
CaMKII	GluN2B	Glutamate Signalling	(Sanz-Clementeet al.,2013)
CD163	AKT	Cell Proliferation	(di Masi et al., 2020)
CD5	N/A	Adaptive Immunity	(Raman et al.,1998)
CKIP-1	PAK1	Cell Morphology	(Kim et al.,2015)
FACT	p53	DNA Damage Response	(Keller et al., 2001)
FGF-1	CK2β	Cell Proliferation	(Skjerpen et al.,2002)
FGF-2	Nucleolin	Cell Proliferation	(Bonnet et al., 1996)
HSP90	N/A	Stress Response	(Miyata et al., 1995)
L1CAM	PTEN; p53	Neuritogenesis	(Wang et al., 2015)
MEK	ERK	Cell Proliferation	(Plotnikov et al., 2019)
NELFE	N/A	Cell Proliferation	(Yu et al., 2021)
p21	HDAC2	Cell Proliferation	(Jia et al., 2016)
p38β	SET	Stress Response	(Arriazu et al.,2020)
Pin1	N/A	Cell Cycle	(St-Denis et al., 2011)

CK2 activity is also known to be stimulated *in vitro* by polyamines, organic polycationic alkylamines that indeed can be found in mammalian cells (Park, 2006; Sagar et al., 2021), but the physiological occurrence of this mechanism is not confirmed. From *in vitro* studies, spermine resulted to be the most effective polyamine in increase CK2 activity (Leroy et al., 1997), probably by a mechanism that involves its binding to CK2β at T72 (Leroy et al., 1995). This binding would affect the substrate recognition function of CK2β (Boldyreff et al., 1994; Marin et al., 1997). Moreover, increased CK2α and CK2β expression and activity where found upon overexpression of ornithine decarboxylase, the enzyme responsible for catalyze the first step of the spermine biosynthesis (Shore et al., 1997).

2.4. Protein kinase CK2 physiopathology

In signal transduction, CK2 has been defined as a “lateral player”, following a different mechanism of action compared to most protein kinases that usually react to external stimuli by transmitting the information to the nucleus through a hierarchical mechanism in a figurative “vertical” direction (Ruzzene & Pinna, 2010). CK2 acts in a “horizontal” direction, acting at the same time over different pathways and over different components within them. This can be achieved since

CK2 is a constitutively active kinase, thus not requiring external stimuli to enter in an active state, and therefore always ready to act in cells.
CK2 has been described as an extraordinarily pleiotropic enzyme, with more than 700 human *bona fide* phospho-site substrates identified to date, according to the PhosphoSitePlus (Cesaro et al., 2023), and many of them confirmed *in vivo*. For this reason, it acts in virtually all cellular processes, mostly related in cell survival and maintenance, thus it is not surprising that it is also involved in different human diseases.

2.4.1. Physiological roles of CK2

CK2 acts in different pathways, mainly favoring pro-survival and antiapoptotic signals. Some of the most studies pathways in which CK2 is involved are presented in Figure 9 and listed below:

PI3K (phosphoinositide 3-kinase)/Akt pathway: in this pathway, that operates as a pro-survival signaling cascade, CK2 stabilizes and simultaneously reduces the activity of the tumor suppressor lipid phosphatase PTEN, which plays a crucial inhibitory role dephosphorylating PIP3 and thus suppressing pro-survival signaling (Torres & Pulido, 2001). Moreover, CK2 directly phosphorylates Akt at S129, contributing to its complete activation together with the canonical T308 and S73 activation phosphosites (Di Maira et al., 2009). To date, phospho-S129 Akt is considered one of the most reliable probes for CK2 activity, especially useful to monitor CK2 activity in response to inhibitors. Furthermore, CK2 promotes the pathway activity by promoting the binding of Akt to the chaperone Hsp90, which results in the protection of the T308 phospho-residue from the activity of phosphatases (Di Maira et al., 2009).
IKK (IκB kinase)/NF-κB pathway: the transcription factor NF-κB acts over anti-apoptotic and pro-proliferation genes, with a key role in cell development. The NF-κB functions are controlled by IκB, inhibitor of NF-κB that retains it in the cytosol blocking its translocation to the nucleus, and by IKK, which upon the adequate stimuli phosphorylates IκB promoting its degradation. CK2 has been shown to directly phosphorylate IκBα and to activate IKK (Eddy et al., 2005;

McElhinny et al., 1996), both resulting in IκB degradation and the consequent NF-κB release. Moreover, CK2 phosphorylates the NF-κB p65 subunit at S529, enhancing NF-κB p65 transcriptional activity (Wang et al., 2000).

JAK/STAT pathway: JAK-STAT signaling plays a key role in the regulation of cell survival, proliferation, and differentiation. In normal cells, cytokines and growth factors temporarily activate JAK tyrosine kinases to execute their function. CK2 has been reported to phosphorylate the kinase JAK2 and the transcription factor STAT3 (Manni et al., 2013; Zheng et al., 2011), resulting in amplification of downstream signaling, including immune system transient signaling initiated by interleukins (ILs), such as IL-6 (Seif et al., 2017).

The Wnt/β-catenin pathway: The canonical Wnt pathway controls cell proliferation, mainly in embryonic development, and tissue self-renewal. In this pathway, Dvl inhibits GSK-3β activity, which in its active state phosphorylates the transcription factor β-catenin promoting its proteasome-mediated degradation. CK2 has been described to phosphorylate and consequently stabilize Dvl and β-catenin (Song et al., 2003; Willert et al., 1997), as well as to promote binding in the nucleus of the transcription factor TCF/LEF.

DNA repair pathways: Throughout the different stages of the cell cycle, it is possible to identify at least five major ways of DNA repair: mismatch repair, base excision repair, homologous recombination, nucleotide excision repair, and non-homologous end joining. CK2 phosphorylates different proteins in the repair pathways generally increasing their association to DNA (Rabalski et al., 2016), as in the case of XRCC1 (Loizou et al., 2004) and XRCC4 (Koch et al., 2004), proteins crucial for the DNA double-strand break repair.

Many other interactions of CK2 have been reported across several signaling pathways, such as tyrosine-kinase receptors (de Gooijer et al., 2018), Notch1 (Zhang et al., 2013), mTOR (Di Lorenzo et al., 2022; Gowda et al., 2017), Erk1/2 (Plotnikov et al., 2019) and Hedgehog (Jia et al., 2010). It is important to note that, the influence of CK2 over the different pathways obviously dependent on its activity, and because this is constitutive, its expression level is crucial, becoming the effect more evident in pathological conditions where it is overexpressed.

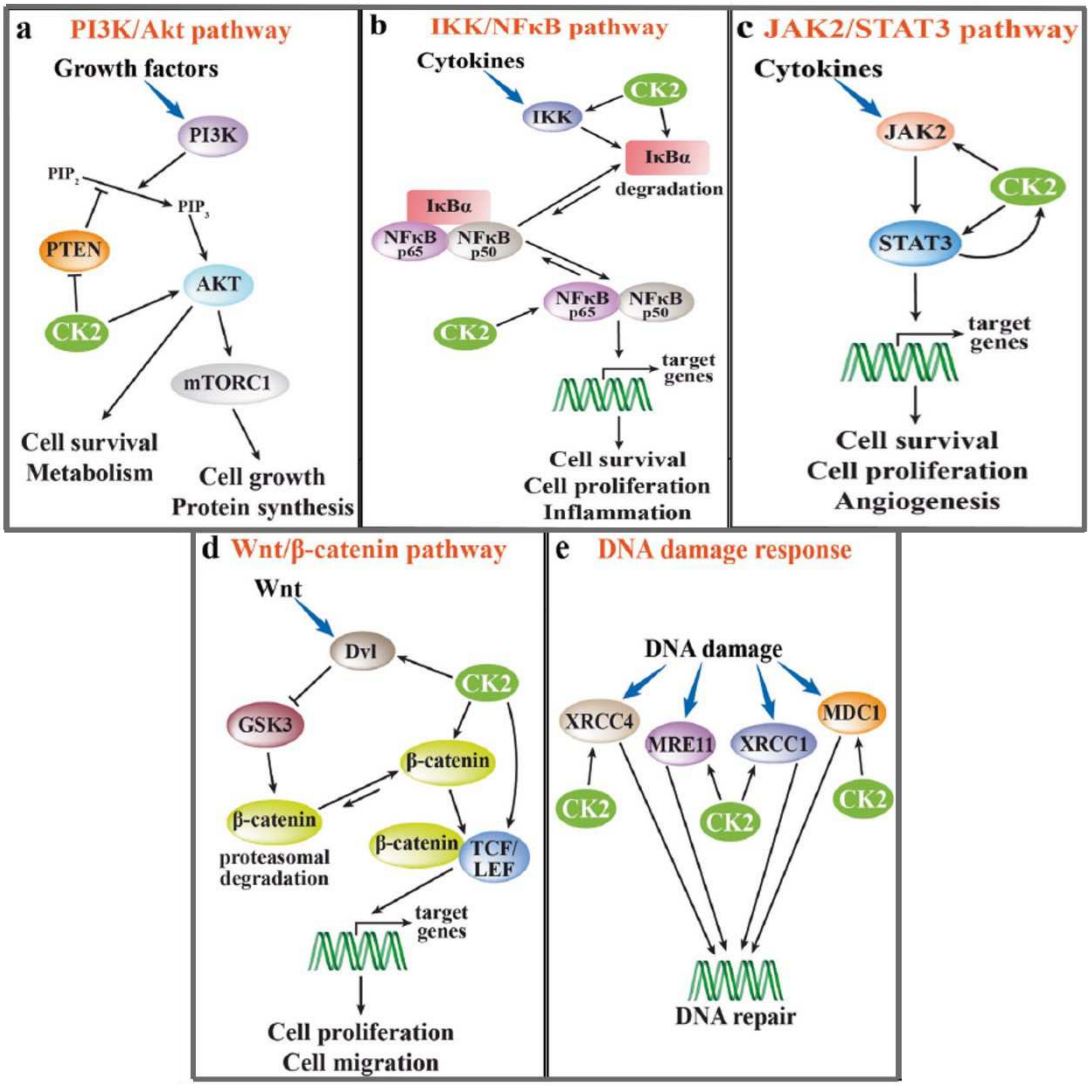

Figure 9. CK2 role in pro-survival pathways.

Schematic representation of the role of CK2 in: (A) PI3K/Akt pathway, (B) IKK/NF-κB pathway, (C) JAK2/STAT3 pathway, (D) Wnt/β-catenin pathway and (E) DNA damage response (modified from Borgo et al., 2021a).

2.4.2. CK2 in human diseases

As expected, given its pleiotropic nature and its constitutively active conformation, CK2 has been associated to several diseases, as shown in Figure 10, and listed below:

Viral infections: CK2 has been reported to phosphorylate several viral proteins, with over 40 cases documented (Meggio & Pinna, 2003). Between them, there are the HIV-1 Rev protein (Meggio et al., 1996), the hepatitis C NS5A and

hepatitis B La proteins (Dal Pero et al., 2007; Schwartz et al., 2004), the leader L protein of the encephalomyocarditis virus (Basta et al., 2014), the matrix M protein of human respiratory syncytial virus (Bajorek et al., 2014), the Kaposi's sarcoma-associated herpesvirus ORF57 (Majerciak et al., 2015), the nucleocapsid protein of the Hantaan virus (Yoon et al., 2015) and the NSP1 of rotavirus (Davis et al., 2017). Interestingly, the human papillomavirus E7 protein, one of the first reported cases (Firzlaff et al., 1989), is the target of clinical-grade anticancer drug CIGB-300 (Perea et al., 2008). Moreover several viruses have been reported to exploit the activity of CK2 for their infective cycles and propagation, as the Human Cytomegalovirus (St-Denis & Litchfield, 2009), the Epstein-Barr Virus (Montenarh et al., 2023), and several coronaviruses, including the SARS-CoV-2 responsible of the COVID-19 pandemic. In fact, the CK2 inhibitor CX-4945 is in clinical trials to test its efficacy over SARS-CoV-2 infection (University of Arizona, 2023).

Neurodegenerative Diseases: CK2 has been described in several neurodegenerative diseases, as in Parkinson's disease where it phosphorylates α-synuclein, promoting its aggregation in Lewis bodies (Okochi et al., 2000). In Alzheimer's disease CK2 indirectly induces the α-secretase activity, which led to reduction of amyloid β-peptide production (Lenzken et al., 2010). However, CK2 also induces tau hyperphosphorylation and hippocampal CK2 overexpression in mouse models produces cognitive impairments (Zhang et al., 2018). In Huntington's disease, CK2 reduces cellular toxicity by directly and indirectly increasing the phosphorylation levels of Huntingtin protein (Atwal et al., 2011; Fan et al., 2008), which is hypo-phosphorylated in the polyQ-HTT disease-related mutants. CK2 has also been described as involved in amyotrophic lateral sclerosis, where the expression of the α subunit reduced TDP-43 aggregates, probably due to CK2-mediated phosphorylation (Yamashita et al., 2016).

Inflammation: CK2 has been suggested a therapeutical target for diseases where IL-6 is instrumental, as rheumatoid arthritis, where CK2 inhibition suppresses the secretion of IL-6 (Drygin et al., 2011; Singh & Ramji, 2008). Moreover, CK2-dependent activation of NF-κB signaling has been found essential in chronic intestinal inflammation (Parhar et al., 2007), as well as in diabetic renal fibrosis, which is ameliorated in induced diabetic animals upon CK2 targeting (Huang et al., 2017). CK2 has also been linked to renal injury due to

glomerulonephritis, a progressive inflammatory disease which is primary cause of chronic renal failure (Yamada et al., 2005). Recent studies has also shown the involvement of CK2 in immune response and in autoimmune disorders (Gibson & Benveniste, 2018), in fact, CK2 showed to promote $CD4^+$ T-cell proliferation and Th1 and Th17 responses, crucial in the contribution of this kinase in Crohn's disease (Yang et al., 2020). Moreover, CK2 inhibition attenuates chronic immune-mediated colitis progression in claudin-2-dependent manner (Raju et al., 2020).

Bacterial and parasite infections: CK2 is relevant in infections produced by bacteria such as Helicobacter pylori (Lee et al., 2014) and Listeria monocytogenes (Chong et al., 2009), and by parasites as the ones induced by Theileria (ole-MoiYoi, 1995) and Toxoplasma gondii (Delorme et al., 2003).

Diabetes and Obesity: The role of CK2 in diabetes and obesity is still not fully clear. A reduction of CK2 catalytic subunits levels in pancreatic islets from nonobese diabetic (NOD) mice, compared to healthy samples, has been reported (Sacco et al., 2016). In contrast, hearts of type 1 diabetes mellitus (T1DM) rats showed increased levels of CK2α in the sarco(endo)plasmic reticulum and reduced levels in the nuclei when compared to normal rats (Bitirim et al., 2018). Moreover, our group have found overexpression and upregulation of CK2 in the adipose tissue of obese and obese type 2 diabetes mellitus (T2DM) mice when compared with their controls (Borgo et al., 2017). Similarly, higher CK2 levels were found in adipose tissue from different obese human subjects when compared to normal-weight controls, independently of the presence of T2DM, and these CK2 alterations were reverted upon significant weight loss, suggesting that aberrant CK2 signaling might be related to obesity rather than T2DM (Borgo et al., 2017). Additionally, different works have demonstrated that CK2 phosphorylates components related to the insulin metabolism, suppressing insulin expression/release (Lupp et al., 2014; Meng et al., 2010; Rossi et al., 2015). Consequently its inhibition was suggested to promote insulin secretion (Doliba et al., 2017; Servas et al., 2017).

Cardiovascular Diseases: CK2 has been associated with the pathogenesis of cardiac ischemia–reperfusion injury (Zhou et al., 2018). In fact, reduction of the accumulation of vascular smooth muscle cells within the neointimal compartment, a cause of accelerated atherosclerosis, was observed upon CK2 inhibition

(Wadey et al., 2017). However, CK2 has been found necessary for the physiologic hypertrophy of heart (Abdul-Ghani et al., 2017), and its downregulation was associated with cardiac hypertrophy (Murtaza et al., 2008). Moreover, its interrupted interaction with the SK2 potassium channel has been related to heart failure (Yang et al., 2015).

The involvement of CK2 in cancer and neurodevelopmental diseases, being particularly relevant for this thesis, will be described in more detail in the next paragraphs.

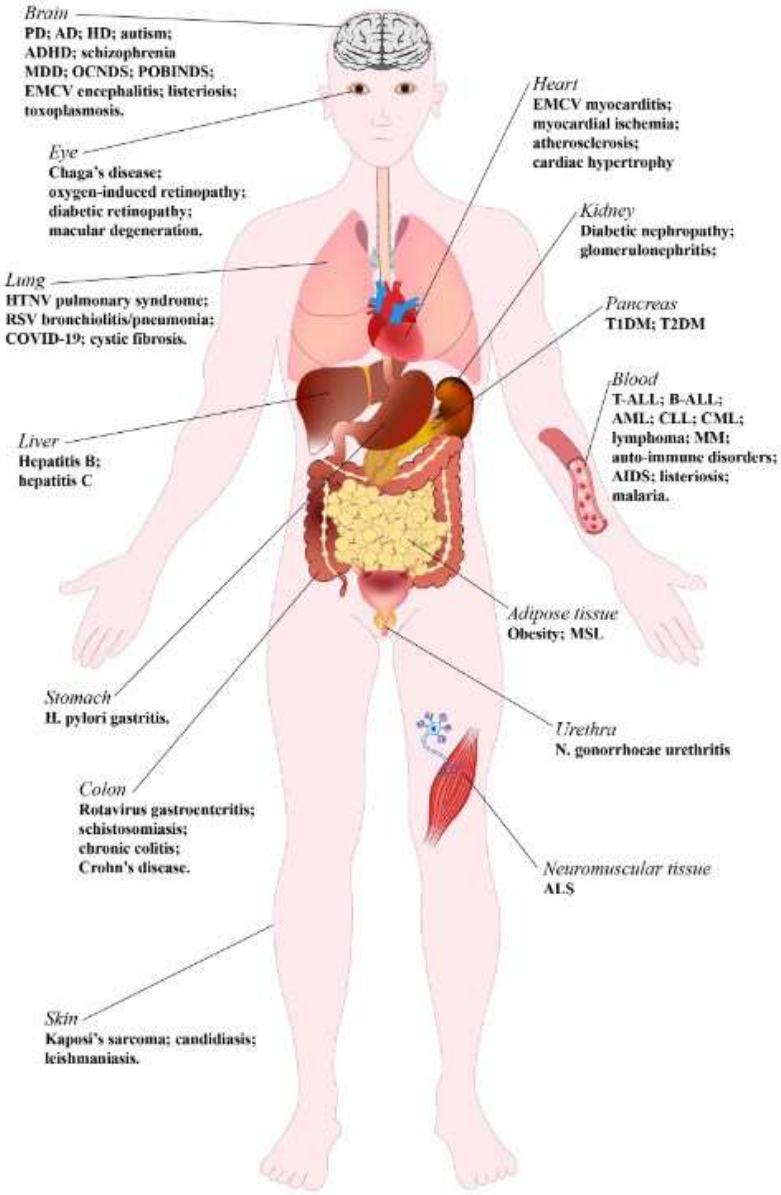

Figure 10. CK2 is involved in different human pathologies.

Schematic representation of the tissues/organs interested by human diseases where the involvement of CK2 has been reported. Solid tumors have not been included (modified from Borgo et al., 2021a).

2.4.2.1 CK2 in cancer

The role of CK2 in cancer is the best documented. CK2 relevant participation has been described in several leukemias, where its overexpression and/or pro-oncogenic role have been extensively studied, such as T-cell acute lymphoblastic leukemia (T-ALL) (Silva et al., 2010), B-cell acute lymphoblastic leukemia (B-ALL) (Gomes et al., 2014; Mishra et al., 2007), acute myeloid leukemia (AML) (Quotti Tubi et al., 2013), chronic lymphocytic leukemia (CLL) (Martins et al., 2010), chronic myeloid leukemia (CML) (Borgo et al., 2013), in lymphomas (Landesman-Bollag et al., 1998) and multiple myeloma (Piazza et al., 2006). Among solid tumors, CK2 important roles and/or overexpression have been reported in ovarian cancers (Kwon et al., 2022), breast cancers (Filhol et al., 2015), cervical cancers (Tugizov et al., 2005), prostate cancers (Trembley et al., 2019), bladder cancers (Jia et al., 2016), renal cell carcinoma (Rabjerg et al., 2017), pancreatic cancers (Venkat et al., 2020), glioblastoma (de Gooijer et al., 2018), medulloblastoma (Nitta et al., 2019), head and neck squamous cell cancers (Su et al., 2023), lung cancers (Pérez et al., 2022), melanoma (Zhou et al., 2016), cholangiocarcinoma (Di Maira et al., 2019), esophageal cancers (Yoo et al., 2012), gastric cancers (Jiang et al., 2019), hepatocellular carcinoma (Zhang et al., 2015) and mesothelioma (Zhang et al., 2014), as reviewed in Trembley et al., 2023 and in Borgo et al., 2021a.

The promotion of tumor progression by CK2 has been explained by its involvement in all the hallmarks of cancer. It provides selective advantage in growth and proliferation (Yde et al., 2008), facilitates altered stress response and supports overall survival (Wang et al., 2005; Weng et al., 2001), is involved in genome instability and mutation (Montenarh, 2016), promotes invasion and metastasis (Deshiere et al., 2013), favors metabolic rewiring (Silva-Pavez & Tapia, 2020; Zonta et al., 2021), induces angiogenesis and vascularization (Montenarh, 2014), supports the tumor microenvironment (Rodriguez et al., 2008), and contributes to immune escape (Kim et al., 2008). Of course, not necessarily CK2 exerts all these actions at the same time, and, consistently with its “lateral player” function mentioned before, its roles are mainly achieved through the modulation of other oncogenic signaling pathways, which are crucially hyperactive in each specific cancer (Firnau & Brieger, 2022; Hanahan,

2022; Trembley et al., 2023).
CK2 levels are usually higher in cancer cells than in normal counterpart tissues (Ruzzene Pinna 2010). Although isolated evidence for CK2 gene amplification has been reported (Gray et al., 2014), to date, no CK2 gain of function mutation has never been found, and the increased CK2 activity observed in different cancer cells is mainly due to an increased protein amount (Di Maira et al., 2007). Moreover, tumor cells have been proposed to be “addicted” to CK2 (Ruzzene & Pinna, 2010), as they seem to depend more on CK2 than normal cells, probably as a consequence of the higher and constant requirement of activation of pro-survival and anti-apoptotic pathways not observed in healthy cells. However, this “addiction” of tumor cells to CK2 has a positive implication, as in turn they are also more sensitive to CK2 inhibition than normal cells, and this has prompted the investigation of CK2 inhibitors as possible chemotherapeutics (Borgo & Ruzzene, 2021; Cozza et al., 2013; Strum et al., 2022; Venerando et al., 2014).

2.4.2.2 CK2 in neurodevelopmental disorders

The investigation of the role of CK2 in neurodevelopmental disorders is more recent compared to the study of its role in other diseases, however in the last ten years the evidence linking CK2 to several disorders has increased, as described below:

CK2 has been linked to Tourette syndrome, as it phosphorylates SLITRK1, a transmembrane protein that regulates synapse formation and that has been described mutated in subjects with the syndrome. Phosphorylation of SLITRK1 on the CK2 site produced SLITRK1-enhanced neurite outgrowth (Kajiwara et al., 2009).
CK2 has also been described involved in Schizophrenia. The first evidence reported reduction in the activity and protein levels of CK2 in frontal cortex extracts from schizophrenic patients compared to normal brains (Aksenova et al., 1991). A subsequent work showed the reduction of CK2α protein levels in prefrontal cortex from 15 schizophrenia patients, confirming the previous results (Castillo et al., 2010). This work also pointed that the decrease of the CK2-dependent phosphorylation of syntaxin-1 contributes to the pathophysiology of

schizophrenia by altering the release of neurotransmitters as a consequence of reduced ability of syntaxin-1 to form SNARE complexes.

Major depressive disorder is a common disorder by itself and as comorbidity in many others neurodevelopmental disorders. While the phosphorylation of syntaxin-1 by CK2 was not as important in this disorder as in schizophrenia patients (Castillo et al., 2010), a recent work has showed the implication of CK2 in the negative transcriptional and posttranscriptional regulation of the 5-HT_4 receptor, a serotonin receptor with therapeutic target potential (Castello et al., 2018). In this work, CK2α knockout mice presented antidepressed-like phenotype associated to the 5-HT_4 receptor overexpression in the prefrontal cortex.

The role of CK2 in autism has been mainly linked to its interaction with the nuclear protein AUTS2 (Gao et al., 2014), often altered in autism. This produces modifications in the normal transcriptional programs, as one of AUTS2 interaction partners is the Polycomb repressive complex 1 (PRC1) which has a major transcriptional regulation role through epigenetic mechanisms. AUTS2 exerts its functions as a member of the PRC1.5 complex, and its interaction with CK2 modulated its ability to interact with other components of the complex. CK2 has also been proposed to be responsible for the phosphorylation of the fragile X mental retardation protein (FMRP). Mutations in *FMRP* gene, located on the X chromosome, cause the Fragile X syndrome, the most common genetic cause of autism. CK2 is suggested to phosphorylate a site that regulates the FMRP functions as mRNA-binding protein, with relevance related to neuroplasticity processes (Bartley et al., 2016).

As evident from what has been described so far, the role of CK2 in neurodevelopmental and psychiatric disorders is quite complex, implying different mechanisms of action depending on the disease, and having no genetic bases. However, in the recent years two different, nonetheless symptomatically similar, neurodevelopmental disorders, named Okur-Chung neurodevelopmental syndrome (OCNDS) and Poirier-Bienvenu neurodevelopmental syndrome (POBINDS), have been associated to variants of the CK2α catalytic subunit (*CSNK2A1* gene) and the CK2β regulatory subunits (*CSNK2B* gene), respectively (Okur et al., 2016; Poirier et al., 2017). Both disorders are characterized by different degrees of intellectual disability, behavioral problems, developmental delay, hypotonia, and motricity deficits. Moreover, one of the main

features of POBINDS is the early-onset seizures, also presents in some OCNDS patients, although with a reduced rate (Ballardin et al., 2022). Both syndromes are considered rare disorder, with so far only 160 diagnosed cases of OCNDS (*CSNK2A1 Foundation)* and 91 cases reported of POBINDS (Li et al., 2023).
The Poirier-Bienvenu neurodevelopmental syndrome will be described later in more detail, being one of the topics of this work.

2.5. CK2 inhibition

Given its involvement in several human diseases, CK2 is a prominent drug target. To date, there is a wide spectrum of available CK2 inhibitors, as shown in Table II. Most of the CK2 inhibitors are ATP competitive, which could be supposed a disadvantage, as the catalytic site is highly conserved among PKs (as mentioned in INTRODUCTION.1.2.2), thus resulting in not specific inhibition. However, CK2 presents distinct features in its catalytic site, as a smaller ATP-binding site due to the presence of bulky hydrophobic residues (V66 and I174) not observed in others PKs (Niefind et al., 1998). This particular characteristic makes CK2 more sensitive to relatively small inhibitors as compared to enzymes with a larger site, in where the interaction with the inhibitors results less favored (Battistutta et al., 2001; Cozza et al., 2013). On the contrary, a smaller catalytic site makes CK2 less responsive to bigger inhibitors, as in the case of staurosporine, which is effective in most PKs but not on CK2 (Meggio et al., 1995).
Given the CK2 particularities, the ATP competitive CK2 inhibitors share some common properties: they are hydrophobic and planar heterocyclic scaffolds with hydrophilic portions aimed to target the residues V66 and I174. These inhibitors can be categorized based on their chemical structures, as shown in Table II. Among them, it is possible to identify several subclasses. They range from several natural compounds, as apigenin, myricetin, and quercetin (Lolli, et al., 2012), to multitarget inhibitors as TDB, which inhibits CK2 and Pim-1 (Cozza et al., 2014) to the promising clinical grade inhibitor CX-4945 (Pierre et al., 2011).
Even though most CK2 inhibitors are ATP-competitive, non-competitive inhibitors have also been developed, as the allosteric inhibitors Pc, that acts between the α and β subunits (Laudet et al., 2007), and POMs, a class of inhibitor whose mechanism of action is not fully understood (Fabbian et al., 2022; Prudent et al.,

2008). Bi-substrate inhibitors, as ARCs (Viht et al., 2015) or K137-E4 (Cozza et al., 2015), have shown increased specificity as they compete with the phosphate acceptor peptide and the phosphate donor nucleotide. Moreover, peptide inhibitors, designed to block specific CK2-dependent phosphorylation sites, are showing promising results, as the clinical grade peptide CIGB-325, that targets the phosphoreceptor domain of the papillomavirus E7 protein (Perea et al., 2018).

Table II. Classification of CK2 inhibitors

Class of inhibitor	Subclass	Representative compounds	References
ATP competitive inhibitors	Polyhalogenated benzimidazoles and benzotriazoles	TBB	(Sarno et al., 2001)
		TDB	(Cozza et al., 2014)
		DMAT	(Pagano et al., 2008)
	Flavonoids	Quercetin	(Sarno et al., 2003)
	Coumarins	Ellagic acid	(Cozza et al., 2011)
	Anthraquinones	Quinalizarin	(Cozza et al., 2015)
	Pyrazolotriazines	Compound 9e	(Nie et al., 2007)
	SRPIN803 derivatives	Compound 4	(Dalle Vedove et al., 2020)
	Carboxyl acid derivatives	TBCA	(Cozza et al., 2009)
		IQA	(Sarno et al., 2003)
			(Pierre et al., 2011)
		CX-4945 CX-5011	(Battistutta et al., 2011)
	Triazol bromoguaiacol derivatives	GO289	(Oshima et al., 2019)
Peptide competitive inhibitors	-	CIGB-325	(Perea et al., 2018)
Allosteric inhibitors	α/β interface targeting	Pc	(Laudet et al., 2007)
	-	POMs	(Prudent et al., 2008)
Bi-substrate inhibitors	-	K137-E	(Cozza et al., 2015)
		ARCs	(Viht et al., 2015)

Currently, only two CK2 inhibitors have entered the clinical stage: CX-4945 (Silmitasertib) in trials as a chemotherapeutic (Pediatric Brain Tumor Consortium, 2023; Senhwa Biosciences, Inc., 2021, 2023a, 2023b; University Hospital, Grenoble, 2020) and as treatment for COVID-19 (Recknor, 2022; University of Arizona, 2023), and CIGB-325 also as a chemotherapeutic (Laboratorio Elea Phoenix S.A., 2015, 2016).

MATERIALS AND METHODS

1. *In vitro* experiments

1.1. *In vitro* phosphorylation assay

In vitro phosphorylation assays of recombinant FXN (Abcam) or recombinant SARS-CoV-2 N protein (BioVendor) were performed using 5 ng of purified recombinant tetrameric CK2 (α2β2) or 100 ng of CK2α (kindly provided by Dr. Andrea Venerando, University of Udine, Italy). The reactions were performed in a radioactive mix of 50 mM Tris-HCl pH 7.5, 10 mM $MgCl_2$, 0.1 M NaCl and 10 μM [γ-^{33}P-ATP] (1000-2000 c.p.m/pmol) when tetrameric CK2 was used or 50 mM Tris-HCl pH 7.5, 10 mM $MgCl_2$ and 10 μM [γ-^{33}P-ATP] (1000-2000 c.p.m/pmol) with the monomeric CK2. The reactions were incubated at 30°C for 20 min and stopped by the addition of Laemmli buffer. The proteins then were separated in SDS-PAGE, stained with Coomassie blue, and analyzed by digital autoradiography (CyclonePlus Storage Phosphor System, PerkinElmer).

1.2. *In vitro* CK2 activity assays

In vitro CK2 activity assays were performed using 5 ng of purified recombinant tetrameric CK2 ($\alpha_2\beta_2$) or 100 ng of CK2 α or α' subunits (kindly provided by Dr. Andrea Venerando, University of Udine, Italy). The CK2 model peptide substrate "CK2-tide" (RRRADDSDDDDD) (kindly provided by Prof. Oriano Marin, University of Padova, Italy) or casein were used as CK2 substrates. The selected CK2 substrate and different concentrations of recombinant SARS-CoV-2 nucleocapsid protein (BioVendor) were incubated in a radioactive mix of 50 mM Tris-HCl pH 7.5, 10 mM $MgCl_2$, 0.1 M NaCl and 10 μM [γ-^{33}P-ATP] (1000-2000 c.p.m/pmol) for the tetrameric CK2, or 50 mM Tris-HCl pH 7.5, 10 mM $MgCl_2$ and 10 μM [γ-^{33}P-ATP] (1000-2000 c.p.m/pmol) for the monomeric CK2. The reactions were incubated at 30°C for 20 min and stopped by sample absorption on phospho-cellulose P81 papers, which were then immediately washed three times with 75 mM phosphoric acid to elute unincorporated [γ-^{33}P-ATP]. The washed phospho-cellulose P81 papers were immersed in scintillation liquid and then radioactivity was read in a scintillation counter (Perkin Elmer).

2. Cell culture and transfection

2.1. Cell lines and cell culture

The human cell lines HEK-239T and CK2α knockout HEK-239T cells, and the HEK-293AD and CK2β knockout HEK-293AD cells (kindly provided by Prof. Mauro Salvi and Dr. Christian Borgo, University of Padova, Italy) were grown in D-MEM (Sigma) supplemented with 10% (v/v) Fetal Bovine Serum (FBS) and PSG 1X (100 U/mL penicillin, 100 mg/mL streptomycin, 2 mM L-glutamine) (Sigma). The FRDA patient-derived cell lines FRDA50, FRDA203 and FRDA214 were cultured in DMEM/F12 media supplemented with 10% (v/v) FBS and PSG 1X (in collaboration with Prof. Malisan's group, University of Rome Tor Vergata, Italy).

Human CML cell lines KBM5, KBM5-T315I (He et al., 2020), K562 and K562-T315I (kindly donated by Jong-Won Kim (Sungkyunkwan University, Korea) and Dennis Dong Hwan Kim (University Health Network, Canada) (Jang et al., 2021)), and the murine stromal cell line MS-5 (kindly donated by Prof. Sandra Marmiroli, University of Modena and Reggio Emilia, Italy), were grown in RPMI 1640 supplemented with 10% (v/v) FBS and PSG 1X, in the absence (KBM5, K562 and MS-5) or presence (KBM5-T315I and K562-T315I) of 1 μM imatinib. Imatinib was removed before experiments, followed by a wash-out period of 2–3 days.

All cells were maintained at 37°C in a humidified atmosphere with 21% O_2, 5% CO_2 (normoxia). Hypoxia (1% O_2, 5% CO_2) was obtained using either a Hypoxia Chamber (StemCell Technologies) or the $INVIVO_{200}$ hypoxia workstation (Ruskinn Technology Ltd., UK).

2.2. Stromal-CML cells co-culture model

4 x 10^4 MS-5 cells/well were seeded in 12-well plates 16 hours prior to the seeding of 2.8 x 10^5 KBM5-T315I cells/well. Mono-cultured KBM5-T315I cells were used as control. After 48 hours of co-culture, the cells were treated for the times and conditions indicated under the specific result. After treatments, the co-cultured and mono-cultured KBM5-T315I cells were carefully collected from the well, centrifugated for 5 min at 2400 rpm and washed with sterile PBS (Sigma)

before their use for functional assays.

2.2.1. Cell transfection

Transient frataxin expression: HEK-293T cells were transiently transfected with the construct pcDNA3.1-Frataxin1-210 coding for the human frataxin cDNA or the selected phosphomimetic (S89D, S206D) or non-phosphorylatable (S89A, S206A) frataxin mutants (GenScript).

Stable expression of CK2β POBINDS mutants: CK2β knockout HEK-293AD cells were transfected with the construct pcDNA3.1-HA-CK2β, carrying hygromycin resistance, and coding for the human CK2β cDNA or the CK2β POBINDS mutants (E61del, R111H, R111P, C137F and H165R) (GenScript).

Stable expression of SARS-CoV-2 nucleocapsid protein: HEK-293AD and CK2β knockout HEK-293AD cells were transfected with the pTwist_CMV_6-HA-SARS-CoV-2 nucleocapsid protein, carrying puromycin resistance, and coding for the SARS-CoV-2 nucleocapsid protein (Addgene).

All the transfections were performed with the jetOPTIMUS kit ® (Polyplus), following the manufacturer instructions. The media was changed 4 hours after transfection, and for transient transfection, treatments or lysis were done after 36- or 48 hours post-transfection.

2.2.2. Selection of stably transfected clones

To obtain stably transfected cells, the CK2β-transfected CK2β knockout HEK-293AD cells were treated with hygromycin 200 µg/mL for three weeks. Similarly, the SARS-CoV-2 N protein-transfected HEK-293AD and CK2β knockout HEK-293AD cells were treated with increasing concentration of puromycin (2, 3 and 4 µg/mL) for three weeks. The expression of CK2β or SARS-CoV-2 N protein was analyzed by Western blot after this period to confirm the stably transfection.

3. Cell treatments and functional assays

3.1. CK2 pharmacological inhibition

For frataxin protein expression levels analysis, 5 x 10^5 HEK-293T, frataxin-

transfected HEK-293T and the FRDA50, FRDA203 and FRDA214 cells (in collaboration with Prof. Malisan's group, University of Rome Tor Vergata, Italy) were treated with 1 µM and 5 µM CX-4945 (MedChemExpress).

For viability assays, 3 x 10^4 KBM5-T315I or K562-T315I cells were seeded in triplicate in 96-well plates 16 hours prior treatments with escalated concentrations (1, 3, 5, 10 and 20 µM) of the CK2 inhibitors CX-4945, GO289 or SGC-CX-1 (all of them MedChemExpress). Cells were treated for 24, 48 and 72 hours as indicated. Treatment with 1 µM imatinib mesylate (Cayman Chemical) was used as control of resistance. For signaling pathways analysis, 6 x 10^6 cells were seeded in 100 mm dishes 16 hours prior 24 hours treatment with escalated concentrations of CX-4945, or 1 µM imatinib mesylate or 2 nM ponatinib. For the stromal-CML cells co-culture model, 24- or 48 hours treatment with CX-4945 were performed after 48 hours from the seeding of the KBM5-T325I cells.

All the inhibitors were dissolved in DMSO, which was added to the controls of the treatments.

3.2. Cell viability assay

Cell viability in response to treatments was measured by MTT assays (Sigma-Aldrich), according to manufacturer's protocol. For KBM5-T315I and K562-T315I cells, 3 x 10^4 cells were seeded in triplicate in 96-well plates 16 hours prior treatments of 24, 48 or 72 hours with the CK2 inhibitors, and after this period MTT was added at a final concentration of 0.45 mg/mL. For KBM5-T315I cells obtained from the co-culture, 3 x 10^4 cells were seeded in triplicate in 96-well plates and MTT was added at a final concentration of 0.45 mg/mL.

After adding the MTT, the cells were incubated for two hours at 37°C in a humidified atmosphere with 21% O_2, 5% CO_2 and the reaction was stopped by addition of 0.1N HCl in isopropyl alcohol. Plates were read at λ 540 nm absorbance, in a Tecan spectrophotometer (Lifesciences).

3.3. FACS analyses of apoptosis

Apoptosis of KBM5-T325I cells was quantified using the eBioscience™ Annexin V Apoptosis Detection Kit (Invitrogen™), following manufacturer instructions. PE conjugated Annexin V and 7-AAD staining were quantified using FACS Calibflow

cytometry.

3.4. Colony formation assay

4.5 × 10^3 KBM5-T325I cells were suspended in 1 mL of RPMI medium with 0.3 % (w/v) agar (Sigma, USA) and then seeded over a 1 mL base layer of RPMI medium with 0.6 % (w/v) agar in 12-well plates. Cells were incubated for 14 days, adding fresh RPMI medium to the semi-solid base every 3 days. After this period, the liquid media was removed and MTT at a final concentration of 0.45 mg/mL was added to the wells to count active colonies.

3.5. Protein stability assays

To evaluate CK2β protein stability, 3 x 10^5 CK2β-transfected CK2β knockout HEK-293AD cells/well were seeded in 6-well plates and, once reached 70% of confluence, treated with 100 µg/mL cycloheximide (MedChemExpress, dissolved in DMSO) for 2, 4 and 8 hours. DMSO was used for the control. After treatments, cells were lysed, and proteins analyzed by Western blot.

3.6. Ubiquitin-proteasome proteolytic pathway inhibition

8 x 10^5 CK2β-transfected CK2β knockout HEK-293AD cells were seeded in 60 mm dishes and treated with 10 µM MG-132 or 100 nM TAK-243 (both from MedChemExpress) overnight (16 hours) once reached 70% of confluence. DMSO was used was used for the control. After the treatments, the cells were lysed, and proteins analyzed by Western blot.

4. Protein analysis

4.1. Cell lysis

Cells were collected by centrifugation at 1200 rpm for 5 min, washed twice with cold PBS pH 7.4 (1.37 M NaCl, 27 mM KCl, 100 mM $Na_2HPO_4 \cdot 2H_2O$, 18 mM KH_2PO_4), resuspended in a lysis buffer (20 mM Tris-HCl pH 8, 150 mM NaCl, 1

mM EDTA, 1% (v/v) Triton X-100, 10% (v/v) glycerol) supplemented with protease inhibitor cocktail (Merck), and phosphatase inhibitor cocktails 2 and 3 (Merck), and incubated 30min on ice. Then, lysates were centrifuged at 15000 rpm for 15 min at 4°C and the supernatants, containing the cell-soluble fraction, were collected for their quantification of protein concentration by the Bradford method.

4.2. Cell fractionation

For cell fractionation, cells were washed twice with PBS and then resuspended in ice-cold hypotonic buffer (10 mM Hepes pH 7.9, 10 mM KCl, 0.9 mM EDTA, 0.9 Mm EGTA) supplemented with protease inhibitor cocktail (Merck), and phosphatase inhibitor cocktails 2 and 3 (Merck). Cells were incubated on ice for 30 min, then passed 80 times through a 21G needle using a 1mL syringe. Samples were centrifuged at 500 rpm for 5 min at 4ºC, the supernatants were collected and centrifugated at 1000 rpm for 5 min at 4ºC to discard possible non-lysed cells. The supernatants were again collected and centrifugated at 3000 rpm for 10 min at 4°C. The resulting pellets, corresponding to the nuclear fraction, were collected and resuspended in lysis buffer while the supernatants were centrifugated at 15000 rpm for 20 minutes at 4°C. The resulting pellets, corresponding to the mitochondrial fraction, were collected and resuspended in lysis buffer while to the supernatant, corresponding to the cytosolic fraction, was added lysis buffer to obtain same volume as the other fractions. Protein concentration of each subcellular fraction was determined by the Bradford method.

4.3. Antibodies

The primary antibodies used in this work were: anti-frataxin (Abcam, mouse), anti- anti-ABL1 (Calbiochem, mouse), anti-pY245-ABL (Cell Signaling, rabbit), anti-STAT5 (Cell Signaling, rabbit), anti-pY694-STAT5 (Abcam, rabbit), anti-STAT3 (Cell Signaling, rabbit), anti-pY705-STAT3 (Cell Signaling, rabbit), anti-Lyn (Epitomics, rabbit), anti-p-Y396-LYN (Epitomics, rabbit), anti-CRKL (Epitomics, rabbit), anti-Py207CRKL (Epitomics, rabbit), anti-PARP (Roche, rabbit), anti-CASP3 (Epitomics, rabbit), anti-LDH (Santa Cruz Biotechnology,

rabbit), anti-TOM20 (Santa Cruz Biotechnology, rabbit), anti-HA (Santa Cruz Biotechnology, mouse), anti-CK2β (Abcam, rabbit), anti-CK2α N-terminal (Biorad, mouse), anti-AKT1 (Sigma, mouse), anti-pS129-AKT1 (Abcam, rabbit), anti-EIF2β (Santa Cruz, mouse), anti-pS2EIF2β (Signalway antibody, rabbit), anti-NF-kB (Santa Cruz, mouse), anti-pS529NF-kB(Santa Cruz, rabbit) and anti-CK2 phospho-substrates (Cell Signaling, rabbit). All these antibodies were used at 1:1000 dilution. Anti-actin (Abcam, mouse) and anti-tubulin (Sigma-Aldrich, mouse) were used as loading control antibodies and used at 1:4000 dilution.
Anti-mouse IgG (PerkinElmer) and anti-rabbit IgG (PerkinElmer) were used as HRP-conjugated secondary antibodies, diluted 1:4000 and 1:5000 respectively.
All the antibodies were diluted in TTBS (50 mM Tris-HCl pH 7.5, 50 mM NaCl, 0.1% (v/v) Tween 20) plus 1% (w/v) BSA.

4.4. Co-immunoprecipitation experiments

Co-immunoprecipitations were performed by incubating 200 µg of cell lysates protein with the anti-HA or anti-CK2α antibodies, overnight at 4°C. Then, protein A-Sepharose (Sigma-Aldrich) was added and incubated for 30 min at 4°C. Immunoprecipitates were obtained by centrifugation at 2000 rpm for 2 min at room temperature, washed twice with 50 mM Tris-HCl pH 7.5 and centrifugated at 3000 rpm for 4 min. The immunocomplexes were resuspended in 5 mM Tris-HCl pH 7.5, solubilized in Laemmli buffer and analyzed by Western blot.

4.5. Western blot analysis

For Frataxin detection, 50 µg of HEK-293T cells lysates or 10 µg FXN-transfected HEK-293T cells lysate were solubilized in Laemmli buffer and loaded on 15% SDS-PAGE gel. The run was performed at 30 mA per gel for 1h at 4°C, using a Running Buffer containing 25 mM Tris, 192 mM Glycine and 0.1% (v/v) SDS. Proteins were then blotted onto nitrocellulose blotting membranes (Amersham™ Protran®), using the Lightning Blotter™ semi-dry transfer system (PerkinElmer) at 24 V, 700 mA for 10 min at room temperature. After blotting, the nitrocellulose membranes were blocked with TTBS plus 5% (w/v) BSA for 1h and then washed three times with TTBS. The membranes were incubated with the corresponding primary antibody overnight at 4°C.

For BCR-ABL1 detection, 50 µg proteins from total lysate were solubilized in Laemmli buffer, loaded on 7.5% SDS-PAGE gel. The run was performed at 30 mA per gel for 1h at 4°C, using a Running Buffer containing 25 mM Tris, 192 mM Glycine and 0.1% (v/v) SDS. Proteins were then blotted onto polyvinylidene fluoride (PVDF) membranes (Immobilon-P Millipore), using Hoefer™ TE22 Mini Tank Blotting Unit (Hoefer™) at 60 V, 400 mA for 2.3 h at 4°C. Dried PVDF membranes were then washed with TTBS and then incubated overnight at 4°C with the corresponding primary antibody.

For the rest of the proteins to be detected, 20 µg of total lysate were solubilized in Laemmli buffer, loaded on 11% SDS-PAGE gel. The run was performed at 30mA per gel for 1h at 4°C, using a Running Buffer containing 25mM Tris, 192mM Glycine and 0.1% (v/v) SDS. Proteins were then blotted onto PVDF membranes using the Lightning Blotter™ semi-dry transfer system (PerkinElmer) at 24 V, 700 mA for 20 min at room temperature. Dried PVDF membranes were then washed with TTBS and then incubated overnight at 4°C with the corresponding primary antibody solution.

For both types of blotting membranes, after 16 hours of incubation, the primary antibodies were removed and the membranes were washed three times with TTBS. The membranes were then incubated with the corresponding HRP-conjugated secondary antibody solution for 30 min at room temperature. After this time, the secondary antibodies were removed from the membranes, followed by three washes of the membranes TTBS. The signals were developed using a chemiluminescence solution composed by 2.25 mL H_2O, 250 µL 1 M Tris pH 9.35, 1 µL H_2O_2 and 2.5 mL of a luminol solution (prepared with 78 mg luminol and 95 mg p-iodophenol dissolved in 100 mL 0.1 M Tris pH 9.35) plus 30% (w/v) BSA. Immuno-stained bands were detected with chemiluminescence on ImageQuant LAS 500 and analyzed with Carestream Molecular Imaging software.

5. Statistical analysis

Data were analyzed using Prism Software (GraphPad). Data were expressed as mean ± Standard Deviation (SD). The statistical analysis was performed using one-way or two-way ANOVA and/or multiple comparison test with Dunnett's post

test depending on the type of experiment/data. For the analysis, at least 2 independent experiments were performed. ns no significant, *P < 0.05, **P < 0.01, ***P <0.005, ****P < 0.001.

CHAPTER I: CK2 IN FRIEDREICH'S ATAXIA

1. Introduction

1.1. Friedreich's ataxia

Friedreich's ataxia (FRDA) is a rare hereditary autosomal recessive disease that accounts for the most common type of inherited ataxia, affecting around 1 in 50,000 person in Europe and in the USA (Lynch et al., 2021). FRDA is caused by mutations in the frataxin (FXN) gene, more specifically by a guanine–adenine–adenine (GAA) trinucleotide repeat expansion in the gene located on chromosome 9q13 (Koeppen, 2011). While normal alleles present no more than 33 GAA repeats, around 96% of FRDA patients present homozygotic GAA expansions of 66 to 1500 repeats. The left 4% of patients present heterozygotic expanded GAA repeat plus a point or insertion/deletion mutation in the other allele of the FXN gene (Koeppen, 2011; Lynch et al., 2021).

1.1.1. Clinical features and care

FRDA clinical onset is typically before adulthood with only a 15% of patients showing the firsts manifestations past 25 years of age. Traditionally, FRDA has been classified as a neurodegenerative disease with ataxia as the main feature, but lately has been suggested to be considered and approached as a multisystemic disorder since, together with the neurological dysfunctions, patients with FRDA often develop diabetes and cardiomyopathies. Interestingly, the onset and the severity of the neurological features of FRDA patients have been correlated with the number of GAA-triplet repeats (Filla et al., 1996; Indelicato et al., 2020; Reetz et al., 2015).

Regarding the neurological features, limb and gait ataxia are the most common presentations. However, other neurological conditions are present as dysarthria (motor speech disorder), spasticity, loss of proprioceptive sensation, lower extremity weakness, absent reflexes, and loss of vibration and proprioception sensation and sensory nerve loss, that among others can cause urinary urgency and neuropathic pain (Corben et al., 2010; Harding et al., 2020; M. Patel

et al., 2016; Reetz et al., 2015) . Moreover, FRDA patients can present a broad spectrum of visual and auditory alterations leading to vision and hearing loss in advanced ages (Rance et al., 2010; Seyer et al., 2013). Cardiac dysfunction is the cause of death of about 60% of FRDA patients (Koeppen et al., 2015). Cardiac abnormalities are usually present in individuals with FRDA as for example hypertrophic cardiomyopathy, observed in up to two thirds of them, which in some cases also leads to cardiac fibrosis (Mottram et al., 2011; Schadt et al., 2012). Other common comorbidities are scoliosis and dysphagia, both present in up to 90% of patients (Rummey et al., 2021; Vogel et al., 2014), diabetes mellitus type 1 and type 2 occurs in up to 30% of patients (Tamaroff et al., 2022), reduced bone density (Eigentler et al., 2014), sleep apnea (Corben et al., 2010), depression & mental illness (Costabile et al., 2018).
To date, providing care to FRDA patients still remains a challenge, as there are no cures for the disease, and for years patients have been treated symptomatically, for example with agents for spasticity (tizanidine, baclofen) or neuropathic pain (gabapentin, duloxetine). In early 2023, the Food and Drug Administration (FDA) approved omaveloxolone as the first therapeutic for the management of FRDA in patients aged 16 years and older (FDA, 2023). Currently, due to the lack of cures for FRDA, any strategy aimed at increasing the FXN protein levels is considered relevant from a therapeutic point of view.

1.1.2. Frataxin: the responsible for the pathology of Friedreich's ataxia

The primary consequence of the repeated GAA-triplet expansions in the FXN gene is the drastic reduction of FXN mRNA and protein expression. In fact, FRDA patients' peripheral tissues express less than 10% of the FXN levels observed in healthy subjects (Campuzano et al., 1996, 1997; Jiralerspong et al., 1997). In physiological conditions, FXN mRNA is expressed in heart, pancreas, skeletal muscle, liver, and spinal cord, which are the most affected tissues in FRDA patients (Campuzano et al., 1996). Interestingly, FXN expression levels are correlated with the number of GAA-triplet repeats, suggesting that the levels of expressed FXN are linked to the severity of the neurological features of FRDA

patients (Lazaropoulos et al., 2015).

As FRDA patients cardiac tissue and mouse models have shown increased mitochondrial iron, reduced iron-sulfur clusters (ISC) and heme synthesis, and elevated mitochondrial reactive oxygen species (ROS), FXN was first proposed to be an iron storage protein, with the role of providing iron for ISC cluster and heme biosynthesis (Bradley et al., 2000; Delatycki et al., 1999; Lamarche et al., 1980; Miranda et al., 2002; Wong et al., 1999). However, now it is known that FXN is mainly involved in ISC biosynthesis, a crucial process in eukaryotes due to the function of ISCs as prosthetic groups to several proteins, including DNA repair enzymes and electron transport proteins, thus involving FXN in several cellular processes, as shown in Table III.

Table III. FXN cellular functions

Cellular process	Function	References
Fe–S biogenesis.	FXN interacts with components of the iron sulphur assembly complex ISCU, NFS1 and ISD11.	(Schmucker et al., 2011)
Krebs cycle	FXN acts in the activation of Aconitase enzyme through facilitation and stabilization of Fe group transfer.	(Bulteau et al., 2004)
Heme biosynthesis	FXN mediates iron delivery to Ferrochelatase in heme synthesis.	(Yoon & Cowan, 2004)
Electron transport and metabolism	FXN interacts with electron transport chain Complex II. Consistently, reduction in FXN expression is correlated with ATP reduction.	(Lodi et al., 1999; Vázquez-Manrique et al., 2006)
Antioxidant response	FXN deficiency reduces expression of Nrf2, a transcription factor that regulates antioxidant response.	(Kobayashi et al., 2004; Shan et al., 2013)
Iron homeostasis	Frataxin deficiency reduces ferroportin1 expression and increases transferrin receptor 1 and mitochondrial iron importer mitoferrin-2 expression, contributing to mitochondrial iron accumulation.	(Koeppen et al., 2007; Navarro et al., 2015)

Human frataxin is translated in the cytosol as a full-length protein precursor FXN^{210} (Mw 23 kDa) and targeted to mitochondria through an N-terminal mitochondrial localization sequence. Upon import into mitochondria, the precursor undergoes a two-step proteolytic cleavage by the mitochondria

processing peptidase, resulting in an intermediate form $FXN^{42–210}$ (Mw 18 kDa), that is subsequently cleaved to the mature form $FXN^{81–210}$ (Mw 14 kDa) (Condò et al., 2007; Koutnikova et al., 1998; Schmucker et al., 2008). In human, two isoforms with extra-mitochondrial location have been characterized: FXN II ($FXN^{76–210}$, Mw 15 kDa) and FXN III ($FXN^{1–5,53–210}$, Mw 18 kDa) (Guo et al., 2018; Xia et al., 2012). These isoforms present a different tissue distribution compared to the canonical FXN, as the highest mRNA levels of FXN II were found in the cerebellum, while the ones of FXN in heart. In FRDA patients' hearts, the canonical FXN is the predominant form, however in healthy condition and other tissues the ratio among the different isoforms has not been determined (Weng et al., 2020).

Little is known about the regulation of FXN protein expression levels. The C-terminal region (CTR) has been pointed as crucial to the protein stability and dynamics (Faraj et al., 2014). Moreover, a few studies have pointed the importance of post-translational modifications in the turnover of the protein, which seems to be proteasome-dependent. FXN-transfected HEK-293 cells treated with proteasome inhibitors, such as MG-132, showed precursor accumulation and a consequent increase of the mature form of up to of 2.5 fold (Benini et al., 2017; Rufini et al., 2011). The results were attributed to the ubiquitination on K147 of the FXN precursor by the RING E3 ligase RNF 126, moreover ubiquitin-competing molecules promoted FXN accumulation (Benini et al., 2017; Rufini et al., 2015). A second post-translational modification was linked to FXN degradation: the phosphorylation of Y118 by Src kinase increases FXN ubiquitination, which was confirmed by systematic point mutations of eight tyrosine residues (Y74, Y95, Y118, Y123, Y143, Y166, Y175 and Y205) to phenylalanine residues, observing that the Y118F mutant totally abrogated FXN ubiquitination, decreasing degradation of the protein (Cherubini et al., 2015). Moreover, FXN-transfected HEK-293 cells treated with different Src inhibitors promoted FXN accumulation in a dose-dependent form.

1.2. CK2 in Friedreich's ataxia

Despite its involvement in several diseases, including different

neurodegenerative diseases, to date there is no evidence of CK2 implication in FRDA or in frataxin modulation. However, as shown in Figure 11, according to the CK2 minimal consensus sequence (see INTRODUCTION 2.2), seven residues within the FXN sequence can be identified as putative CK2 phosphorylation sites.

```
  1 MWTLGRRAVA GLLASPSPAQ AQTLTRVPRP AELAPLCGRR GLRTDIDATC TPRRASSNQR
 61 GLNQIWNVKK QSVYLMNLRK SGTLGHPGSL DETTYERLAE ETLDSLAEFF EDLADKPYTF
121 EDYDVSFGSG VLTVKLGGDL GTYVINKQTP NKQIWLSSPS SGPKRYDWTG KNWVYSHDGV
181 SLHELLAAEL TKALKTKLDL SSLAYSGKDA
```

Figure 11. Human FXN sequence displays putative CK2 phosphorylation sites.

Aminoacidic sequence of human FXN is shown. Serine and threonine residues that fulfil the CK2 consensus are in red and bold, those in red but not bold fulfil the minimal requirement but display also detrimental features (basic residues in the vicinity). The tyrosine phosphorylated by Src (Y118) and the K147 ubiquitinated by the RING E3 ligase RNF 126, both residues relevant in FXN turnover, are shown in blue and green, respectively.

2. Aim of the study

As explained in the Introduction, there is no cure for FRDA, and, despite the recent approval of omaveloxolone, the restoration of the frataxin levels still remains the main focus for therapeutics strategies. Therefore, any hypothesis aimed at increasing the FXN protein levels is considered relevant from a therapeutic point of view. CK2 has never been described in FRDA or in frataxin modulation. However, due to the observation that FXN sequence displays seven putative CK2-phosphorylation sites, and the evidence from Prof. Malisan's group that phosphorylation by Src kinase can regulate the FXN protein levels by affecting its ubiquitination (Cherubini et al., 2015), we hypothesized that also CK2 has the potential to regulate FXN levels through its phosphorylation.

To test this hypothesis, our aims were:

i. To evaluate the direct phosphorylation of FXN by CK2

To evaluate if CK2 can directly phosphorylate FXN, we performed several *in vitro* phosphorylation assays using recombinant CK2 and FXN, together with mass spectrometry analysis to identify possible phosphorylation sites.

ii. To investigate the importance of the CK2-dependent phosphorylation in FXN protein levels

To understand whether CK2 phosphorylation might regulate the FXN protein levels, we exploited non-phosphorylatable and phospho-mimetic FXN mutants in HEK-293T cells.

iii. To evaluate if CK2 targeting can increase FXN levels in human cells

To this aim, we first evaluated the involvement of CK2 in mitochondrial and extra-mitochondrial FXN through CK2 pharmacological inhibition. Then we evaluated the FXN levels in HEK-293T cells after CK2 targeting by pharmacological inhibition, taking advantage of the availability of a clinical grade CK2 inhibitor (CX-4945), and by CK2 subunit ablation, exploiting HEK-293T CK2α knockout (KO

CK2α) and CK2α' knockout (KO CK2α´) cell clones. Moreover, to corroborate the results, CK2 pharmacological inhibition in FRDA patient-derived cells was performed.

3. Results

3.1. CK2 directly phosphorylates FXN in S89 and S206

The first aim was to evaluate whether CK2 phosphorylates FXN, and to this purpose we performed *in vitro* radioactive phosphorylation assays using recombinant CK2 and the recombinant FXN precursor, thus the full-length FXN (210 aa). As shown in Figure 12A, the phosphorylation assays revealed that FXN is susceptible to CK2 phosphorylation, either by the tetrameric form as well as by the monomer α.

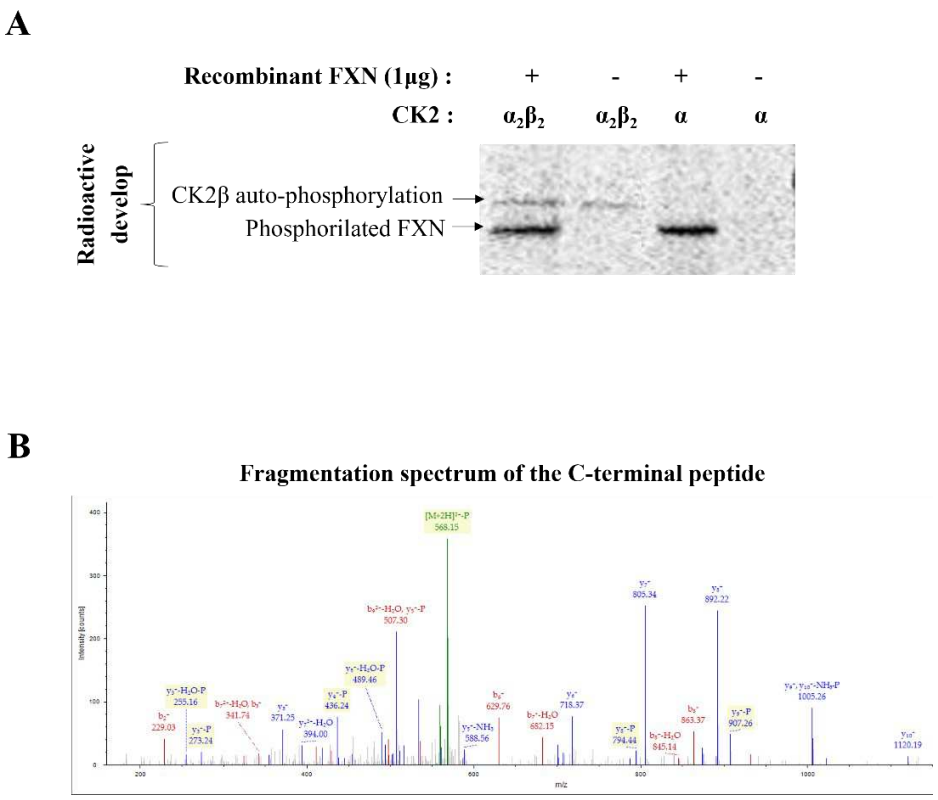

Figure 12. CK2 phosphorylates FXN in S89 and S206.

(A) *In vitro* FXN protein phosphorylation by CK2. For the assay, 1µg of recombinant FXN was incubated for 20 min at 30°C with 5ng of recombinant tetrameric CK2 ($\alpha_2\beta_2$) or 100ng of CK2α in the presence of a radioactive phosphorylation mixture. The activity of these amounts of the two CK2 isoforms (tetrameric and monomeric) was similar towards the model peptide casein (not shown). Phosphorylation was detected upon SDS-PAGE separation and digital autoradiography (Cyclone plus). (B) Fragmentation spectrum of the C-terminal peptide by mass spectrometry analysis.

After confirming that CK2 does phosphorylate FXN and having in consideration that the FXN sequence presents seven putative CK2-phosphorylation sites, we wondered which were the actual phosphorylation sites. To give an answer to this question, in collaboration with Dr. Arrigoni (University of Padova, Italy), by mass spectrometry analysis we identified the serine 206 (S206) as the main phosphorylation site, along with a small amount of phospho-serine 89 (S89) (Figure 12B).

3.2. Phosphorylation of S206 by CK2 regulates FXN turnover

Confirmed the phosphorylation of FXN by CK2 and the sites, we decided to evaluate if the phosphorylation by CK2 have an effect in the FXN protein levels. To this purpose, we exploited non-phosphorylatable (S89A and S206A) and phospho-mimetic (S89D and S206D) FXN mutants. After transfection of these mutants in HEK-293T cells, and as shown in Figure 13A, we were able to detect all three FXN forms: precursor (P, Mw 23 kDa), intermediate (I, Mw 18 kDa) and mature (M, Mw 14 kDa). Interestingly, for unknown reasons, the S89D mutant migrated at apparently higher molecular weight, however, no significant differences in the FNX levels were observed between the S89A and the S89D mutants, or compared to the transfected wild type protein (WT), suggesting that the phosphorylation of this residue is not involved in the modulation of the FXN amount. On the contrary and very interestingly, the S206A mutant displayed a significant increase of the mature FXN form compared to the WT, while the opposite was observed for the S206D mutant, which presented a strong reduction of all the FXN forms (Fig. 13A).

To exclude that the reduced levels of the S206D mutant were due to a transfection problem, we evaluated different transfection times. Although the results are preliminary, they showed that the S206 mutant, compared to the WT, displayed similar levels in the expression of all the FXN bands at the shortest transfection time (12h), suggesting that no transfection problem has to be associated to this mutant (Fig 13B). After 36 hours post transfection, the mature and intermediate bands are still similar to those of the WT protein, while the

reduction in the precursor band starts to be evident. Altogether, these results suggest that the lower amounts of the S206A mutant, as well visible in Fig 13A, are indeed due to the mutation (and not to a transfection problem with this plasmid).

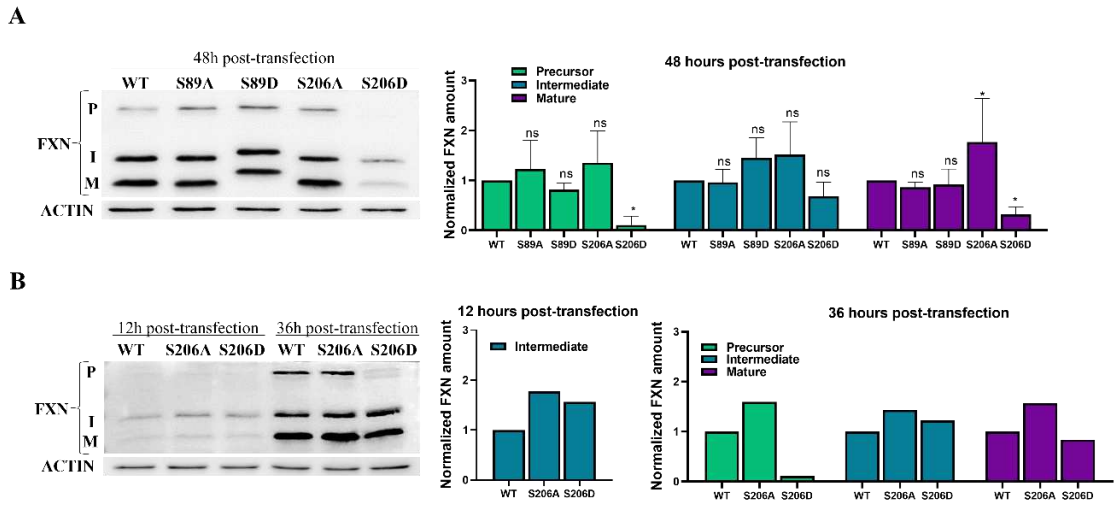

Figure 13. Phosphorylation of S206 by CK2 regulates FXN turnover.

HEK-293T cells transfected with the non-phosphorylatable (S89A and S206A) and phospho-mimetic (S89D and S206D) FXN mutants. (A) Lysates were obtained 48 hours post-transfection. (B) Lysates of HEK-293T cells transfected with S206A and S206D FXN were obtained 12- and 36 hours post-transfection. Representative images of Western blot from (A) 3 and (B) 1 independent experiments are shown, where 10 µg of proteins were loaded (left). Quantification upon normalization to the loading control (actin) is shown on the right, with data presented as mean ± SD. Statistical analysis was performed with two-way ANOVA with Dunnett 's post test. ns no significant, *P < 0.05, **P < 0.01, ***P <0.005, ****P < 0.001. In (B), data are results from one independent experiment.

3.3. CK2 inhibition increases extra-mitochondrial FXN

As the results shown so far suggested a role of CK2 in the modulation of FXN levels, we wondered which is the underlying mechanism. CK2 is mostly located in nucleus and cytoplasm, however with evidence of its presence also in mitochondria (Damuni & Reed, 1988; Sarrouilhe & Baudry, 1996). FXN is mainly a mitochondrial protein, but with a minimal fraction present as extra-mitochondrial (Guo et al., 2018; Xia et al., 2012). We wanted to evaluate if the modulation of

the FXN levels by CK2 were restricted to mitochondria, thus we performed subcellular fractionation of FXN-transfected HEK-293T cells upon CK2 inhibition by the clinical grade CK2 inhibitor CX-4945, which is currently in clinical trials against COVID-19 and cholangiocarcinoma.

As the FXN intermediate and precursor levels were extremely low to detect after the fractionation process, in these experiments we evaluated the mature FXN form. As shown in Figure 14A, CK2 inhibition induced a slight increase of the total FXN levels after 24 hours of treatment.

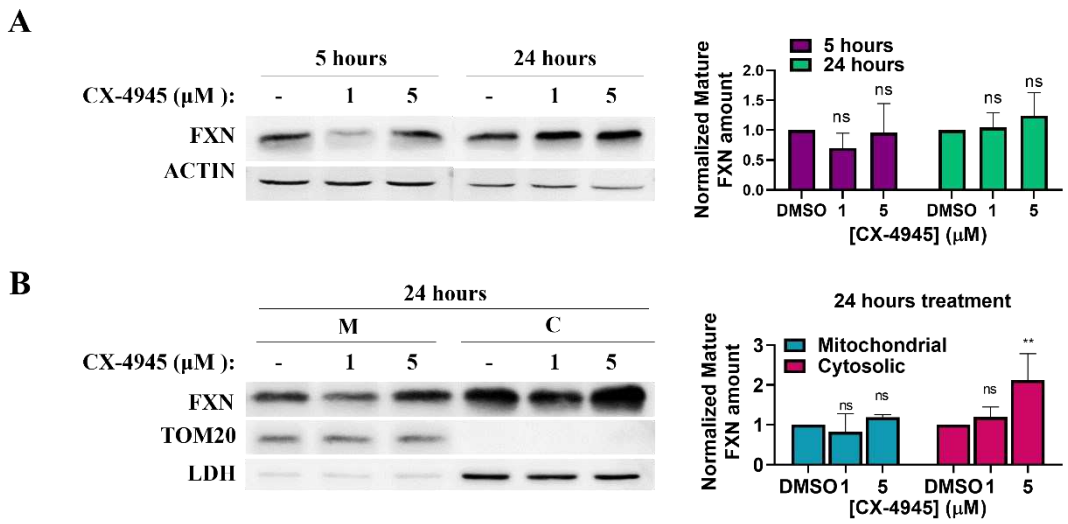

Figure 14. CK2 inhibition increases extra-mitochondrial FXN.

FXN-transfected HEK 293T cells treated with 1 μM and 5 μM CX-4945. (A) Mature FXN in the total cell lysate after 5- and 24 hours treatment with CX-4945. Actin was used as a loading control. (B) Mature FXN in the mitochondrial and cytosolic fractions after 24 hours treatment with CX-4945. TOM20 and LDH were used as loading controls of the mitochondrial and cytosolic fractions, respectively. In (A) and (B), representative images of Western blot from 3 independent experiments are shown, where 10 μg of proteins were loaded (left). Quantification upon normalization to the loading control is shown on the right, with data presented as mean ± SD. Statistical analysis was performed with two-way ANOVA with Dunnett 's post test. ns no significant, *P < 0.05, **P < 0.01, ***P <0.005, ****P < 0.001.

After standardization of the fractionation protocol, we obtained two different subcellular fractions: the mitochondrial (M) and the cytosolic (C), both with reliable degrees of purity as judged by the expected presence of TOM20 and LDH, used as mitochondrial and cytosolic markers respectively (Figure 14B left). The analysis of the FXN levels in the subcellular fractions in response to CK2 inhibition showed interesting results: a significant increase of the of extra-

mitochondrial mature FXN levels was induced by 5 μM CX-4945 treatment, while no significant changes were observed in the mitochondrial FXN levels (Figure 14B).

3.4. CK2 targeting increases endogenous FXN protein levels in HEK-293 cells

Given the observed increase of the FXN levels upon treatment with the CK2 inhibitor CX-4945 in FXN-transfected HEK 293T cells, we decided to evaluate the effect of CK2 targeting on the endogenous FXN levels. In HEK-293T cells, the endogenous precursor and intermediate forms of FXN were not detectable. However, the mature FXN band, as shown in Fig. 15A, was visible, and the cell treatment with CX-4945 induced its increase. Additionally, we exploited a different approach to target CK2, namely the use of HEK-293T CK2α knockout (KO CK2α) and CK2α' knockout (KO CK2α´) cell clones. The ablation of either one or the other of the two CK2 catalytic subunits reduces the global cellular activity of the enzyme of around 40-60% (not shown). Interestingly, this produced an increase of about 2-fold of the total FXN levels, compared to FXN levels of control cells (Figure 15B).

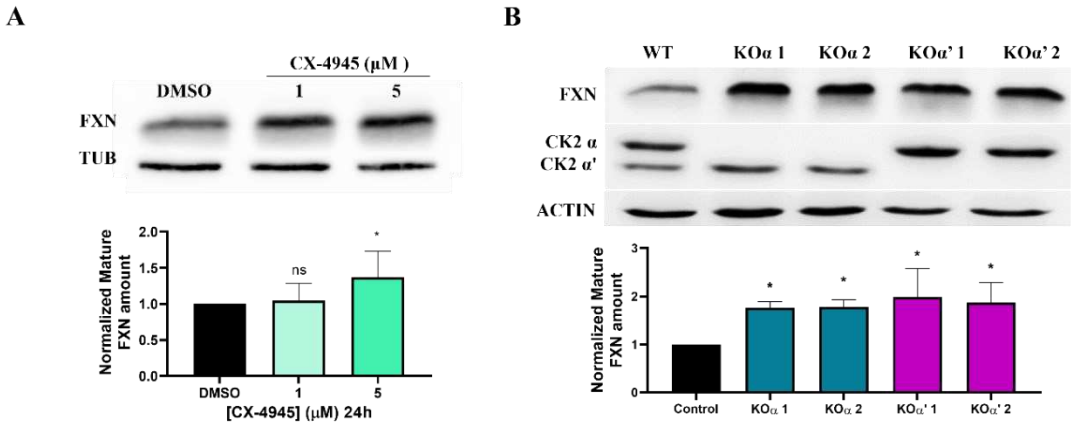

Figure 15. CK2 targeting increases endogenous FXN protein levels in HEK-293 cells.

(A) Endogenous mature FXN levels of HEK-293T cells treated for 48 hours with the CK2 inhibitor CX-4945 (1 μM and 5 μM). The results were normalized by the loading control (tubulin); and the (B) endogenous mature FXN levels of two HEK-293T CK2α knockout cells clones (KO CK2α 1

and KO CK2α 2) and two CK2α' knockout cells clones (KO CK2α' 1 and KO CK2α' 2). The results were normalized by the loading control (actin). Representative images of Western blot from 3 independent experiments are shown, where 50 µg of proteins were loaded (left). Quantification upon normalization to the loading control is shown on the right, with data presented as mean ± SD. Statistical analysis was performed with one-way ANOVA with Dunnett's post test. ns no significant, *P < 0.05, **P < 0.01, ***P <0.005, ****P < 0.001.

3.5. CK2 targeting increases endogenous FXN protein levels in FRDA patients-derived cells

The encouraging results obtained by CK2 targeting in HEK-293T cells prompted us to analyze the effect in FRDA patients-derived cells. To this purpose, in collaboration with Prof. Malisan's group (University of Rome Tor Vergata,Italy), we inhibited CK2 by treatments with CX-4945 in three FRDA patient-derived cell lines, named FRDA50, FRDA203 and FRDA214. As shown in Figure 16, CK2 inhibition slightly but significantly increased the mature FXN levels in all the analyzed cells.

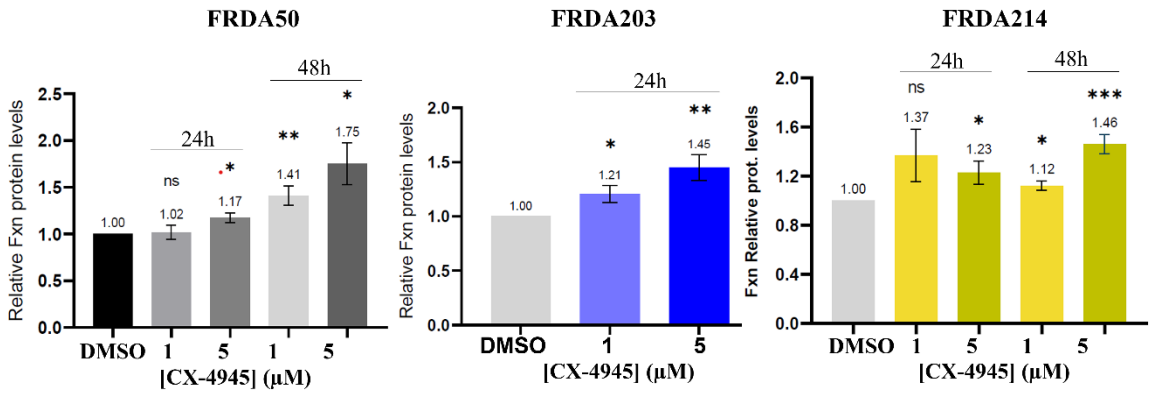

Figure 16. CK2 inhibition with CX-4945 increases endogenous FXN protein levels in FRDA patients-derived cell lines.

FRDA patients-derived cell lines FRDA50, FRDA203 and FRDA214 were treated for 24- or 48 hours with 1 µM and 5 µM CX-4945, as indicated. Cells were then lysed, 40 µg of proteins were analyzed by Western blot for FXN, and the quantification of the FXN mature bands is shown in the graphs, upon normalization on actin, used as loading control. Results from 3 independent experiments are presented as mean ± SD. Statistical analysis was performed with one-way ANOVA with Dunnett's post test. ns no significant, *P < 0.05, **P < 0.01, ***P <0.005, ****P < 0.001.

4. Discussion

This study shows for the first time that frataxin can be phosphorylated by CK2, and that this promotes reduction of its protein levels. Moreover, here we found that CK2 acts mainly over extra-mitochondrial FXN and that CK2 targeting increases frataxin expression in human cells, and more importantly, in FRDA patients-derived cells, where the clinical grade CK2 inhibitor CX-4945 promoted frataxin accumulation.

Our demonstration that CK2 actually phosphorylates FXN at S206, and barely at S89, requires some important comments and considerations. First, since we used full length frataxin in the *in vitro* phosphorylation assays we can conclude that CK2 is able to phosphorylate the FXN precursor, but we cannot exclude that the phosphorylation occurs also on FXN already cleaved to the intermediate and/or the mature form. Secondly, not all the expected sites, based on the consensus sequence, are phosphorylated by CK2. Obviously, this can be the consequence of the protein structure, as some residues might be protected and not accessible for phosphorylation. But, for example, we expected that one site could be T119, since this region of the protein should be exposed, as this residue follows the Y118 found to be affected by Src kinase (Cherubini et al., 2015), and since the previous intervention of Src, by introducing further acidity, could in theory facilitate the subsequent phosphorylation by CK2. At present, we do not have an explanation for the lack of phosphorylation of the T119 residue by CK2. However, preliminary *in silico* analysis of the region structure (Cesaro L., personal communication) suggests that T119 is not as exposed as Y118.

Protein kinases can modulate different properties of their targets through phosphorylation, such as activity, localization, protein interactions and turnover. Indeed, FXN phosphorylation by Src kinase on Y118 was found to increase its ubiquitination and consequently its proteasomal-dependent degradation (Cherubini et al., 2015). Our results suggest that also CK2, by phosphorylating frataxin at S206, might regulate the turnover of the protein, however, the mechanism underlying this regulation is yet to be investigated. Based on the available information, two mechanisms can be proposed: the first is that the CK2 phosphorylation affect the frataxin stability via a structural and/or electrostatic

change of the protein, since the S206 resides within the C-terminal region (CTR) of the protein, a segment constituted by the residues from 196 to 210 that lacks periodic structure. This segment has been reported to be important for the protein stability, as the absence or mutations of the CTR produce reduced stability, and changes in the structural dynamics and function of the protein (Castro et al., 2019; Faraj et al., 2014). It is therefore conceivable that the S206 phosphorylation alters the CTR structure and prevents its stabilizing function. The second possibility is that CK2 phosphorylation promotes FXN ubiquitination, which is not an isolated event as CK2, a constitutively active kinase, has been described to regulate the turnover of several proteins, as for example with the pancreatic duodenal homeobox 1 protein (PDX-1) (Klein et al., 2017) and the Sensitive to Apoptosis Gene protein (SAG) (He et al., 2007), of which CK2 negatively regulates the stability in a proteasome-dependent manner. However, our preliminary results (not shown) did not highlighted any changes in the ubiquitylation levels of FXN in response to CK2 inhibition, but further experiments will be necessary before completely excluding this hypothesis.

Interestingly, our subcellular fractionation experiments suggest that CK2 would affect more the extra-mitochondrial, in particular cytosolic, than mitochondrial frataxin. It has to be reminded that FXN is generated as a precursor protein in the cytosol, and then processed through a double cleavage, which occurs in the mitochondria. Therefore, it is possible that CK2 phosphorylates FXN in the cytosol, and this prevents its translocation to the mitochondria.

Despite the recent approval of the first drug for FRDA treatment, from a therapeutic perspective any attempt to increase FXN levels is encouraged. In this view, since we observed an increase of the FXN level upon CK2 targeting in HEK-293T cell, and more importantly, in three FRDA patient-derived cell lines, our work suggests that CK2 might be a promising target candidate, also considering the wide spectrum of CK2 inhibitors available, some already of clinical grade (CX-4945 and CIGB-300). As the increase of frataxin, even at low levels, can be helpful in the amelioration of the damage generated by its strong reduction in FRDA patients, our results, although preliminary, are encouraging. Naturally, further studies will be necessary, especially to understand if the increase of frataxin produced by CK2 inhibition can protect the cells from the stress-induced mitochondrial damage associated to the low level of frataxin in FRDA cells. This

will pave the way for further studies, also *in vivo* FRDA models. Moreover, our work highlights the possible relevance of the cytosolic FXN, an isoform of which not much has been reported so far and whose functions probably deserve further attention.

CHAPTER II: CK2 IN CHRONIC MYELOID LEUKEMIA

1. Introduction

1.1. Chronic myeloid leukemia

Chronic myeloid leukemia (CML) is a myeloproliferative neoplasm, characterized by the uncontrolled growth of myeloid cells at different stages of maturation, that accounts for approximately 15% of new cases of leukemia in adults, with an estimated incidence of 2 cases per 100.000 adults (Jabbour & Kantarjian, 2018).

1.1.1. BRC-ABL1: the responsible of the pathology of chronic myeloid leukemia

The main cause of the CML pathogenesis is the *BCR-ABL1* fusion gene, resulted from the juxtaposition of the Abelson murine leukemia (*ABL1*) gene on chromosome 9 with the breakpoint cluster region (*BCR*) gene on chromosome 22, after the chromosomal translocation t(9;22)(q34;q11) between the long arms of their respective chromosomes (Rowley, 1973). This translocation results in the expression of the oncoprotein BCR-ABL1, a constitutively active tyrosine kinase that promotes aberrant activation of different signaling pathways, leading to and supporting leukemia (Daley et al., 1990). It has been described that the main signaling pathways affected by the constitutive activation of BCR-ABL1 are Src family kinases, JAK/STAT, Ras/MAPK and PI3K/AKT pathways, whose functions and interactions promote cell growth and survival, as well as inhibition of cell death (Chai et al., 1997; Chu et al., 2007; Zhao et al., 2006).

1.1.2. Clinical features and care

CML can be classified into three phases based on the amount of immature white blood cells (blasts) present in bone marrow and peripheral blood: a chronic phase (CP), followed by an accelerated phase (AP) and an aggressive blast phase (BP). About 90% of patients are diagnosed in chronic phase, progressing to AP and then to BP within 3 to 5 years when untreated (Clarke & Holyoake, 2017). Moreover, the American Cancer Society reports that the average age of diagnosis

is around 64 years in Western countries, while in other countries the average has been reported lower (Mishra et al., 2013); and that half of the patients on CP are asymptomatic. When symptoms are present, these may include fatigue, fever, weight loss, and left upper quadrant pain that is often a result from anemia and splenomegaly. Among AP warning signals are worsened anemia and splenomegaly and organ infiltration, while CML-BP presents more aggressive symptoms such as severe bleeding, fever and infections.

The first line treatment for CML is the use of tyrosine kinase inhibitors (TKIs) which have noticeably improved patient survival since 2001, with the approval of imatinib mesylate (IM) for the treatment of CML patients (Druker et al., 2001; Efficace et al., 2011). As IM is now available generic and worldwide, it has become an effective and also cost-effective initial therapy. However, it is estimated that about 25% of patients will develop intolerance or resistance to TKI therapy, facilitating the progression to accelerated phase or blast crisis (Osman & Deininger, 2021; Steegmann et al., 2016). Due to this reason, after IM, second- and third-generation TKIs have been developed and some of them even approved for the treatment of CML patients, as nilotinib, dasatinib, bosutinib and ponatinib (Bradeen et al., 2006; Deguchi et al., 2008; Haddad et al., 2022; Morita & Sasaki, 2021; Puttini et al., 2006).

1.1.3. Tyrosine Kinase Inhibitor resistance

According to the National Comprehensive Cancer Network (NCCN) guidelines, patients with more than a 10% of *BCR-ABL*1 transcript levels (following the qPCR International Scale) at ≥6 months and those with *BCR-ABL1* transcript levels above 1% after 15 months of treatment are considered to have TKI-resistant disease (Radich et al., 2018). Different mechanisms have been described to produce TKI resistance, being *BCR-ABL1* genomic amplification and point mutations in the ABL1 kinase domain the better defined.

The first mechanism involves the overexpression of BCR-ABL1 due to gene amplification, that might allow the persistent kinase activity despite the TKIs treatment, enabling cell survival of the tumor cells (Gadzicki et al., 2005; Gorre et al., 2001). On the other hand, point mutations in ABL1 kinase domain (KD) are the most common mechanism of TKI resistance, moreover, KD mutations were

found more frequently in blastic phase patients compared to chronic phase patients, suggesting that the rescue of BCR-ABL1 signaling is critical in the progression of the disease (Branford et al., 2003; Soverini et al., 2006).

The degree of resistance to different TKIs varies across the mutants, plus the complexity of having multiple mutations changes the patients outcome as well as the response to the frontline TKI used (Radich et al., 2018). More than 50 different KD mutations have been reported; 12 residues can be considered hotspots as they account for most of the mutations: M244, G250, Q252, Y253, E255, V299, F311, T315,F317, M351, F359, and H396 (Zabriskie et al., 2014). Most of these mutations reduce the accessibility of the TKIs to the ABL1 drug binding site. However, the degree of resistance to the different TKIs widely varies, as for example the mutations M351T or F311L can be managed with dose escalation, while a notable opposite case is the T315I mutation, which is resistant to almost all TKIs (Soverini et al., 2018).

The ABL1 T315I is particularly interesting, due to its high prevalence among the point mutations as well as for its extremely resistant phonotype. The T315I mutation has been described as a “gatekeeper” mutation that through the substitution of the threonine with a bulkier hydrophobic isoleucine residue causes a steric clash, preventing the access of IM to the ATP-binding pocket (Patel et al., 2017). Moreover, this mutation is also resistant to second- generation TKIs, that have been described to be effective over most of the point mutations, as dasatinib and nilotinib, due to the need of these inhibitors to establish a high-affinity binding to BCR-ABL1 through a hydrogen bond with the residue T315 (Eide & O’Hare, 2015; O’Hare et al., 2007). To date, the treatment of patients with this mutation is restricted to the use of ponatinib, a third-generation TKI, that does not require the formation of the critical hydrogen bond with the residue T315 to exert high-affinity binding to BCR-ABL1 (O’Hare et al., 2009; Redaelli et al., 2009). However, despite to be the only inhibitor effective against the ABL1 mutation T315I, ponatinib showed to produce serious arterial occlusive events, as cardiovascular and cerebrovascular occlusion, in 31% of patients and other secondary effects (Cortes et al., 2018), making alternative therapies urgently necessary.

1.2. CK2 in chronic myeloid leukemia

As described in the main introduction, CK2 is a constitutively active S/T kinase involved in several physiological processes, mainly regulating positively proliferative pathways. CK2 has also been described involved in numerous diseases (Borgo et al., 2021a), particularly in cancer, where it is frequently overexpressed and contributes to the malignant phenotype by multiple mechanisms (Chua et al., 2017).

The first evidence of the involvement of CK2 in CML dates from 1985, when increased expression of CK2 was found in CML-blast crisis patients, compared to healthy blood mononuclear cells (Phan-Dinh-Tuy et al., 1985). Thirteen years later, the physical interaction between CKα and BCR-ABL1, via the ABL1 portion, was demonstrated in CML K562 cells (Hériché & Chambaz, 1998). Results from our group in LAMA84 CML cells resistant to imatinib, due to BCR-ABL1 gene amplification, showed upregulation of CK2 protein and activity levels when compared to imatinib-sensitive cells. In the imatinib resistant cells, co-localization of CK2 with BCR-ABL1 was found in cytoplasm (Borgo et al., 2013). This work also showed that the CK2 inhibitor CX-4945 was able to counteract the CK2/BCR-ABL1 interaction and induce apoptosis, while in combination with imatinib reduced the viability of the imatinib resistant LAMA84 cells. Moreover, CK2α knockdown, by siRNA, restored the sensitivity to low imatinib concentrations in imatinib resistant LAMA84 cells as well as in other resistant CML cell lines. A second study of our group, revealed that CK2 targeting, either by the inhibitor CX-5011 (a CX-4945 derivative) or by RNA interference, caused a dramatic dephosphorylation of S6 ribosomal protein (S6RP) at S235/236 and the consequent reduction in protein translation, in imatinib-resistant CML cell lines (Salizzato et al., 2016). This work also showed the synergistic action of CX-5011 with either imatinib or the MEK-inhibitor U0126 in reducing the viability of imatinib-resistant CML cells.

It has also been described that BCR-ABL1 induces the inactivation of PTEN by CK2 phosphorylation in CML cells, and CK2 inhibition, by the inhibitor TBB, promoted PTEN reactivation and apoptosis induction (Morotti et al., 2015). Additionally, this study links for the first time CK2 with the BCR-ABL1 T315I

mutation, as CK2 inhibition by TBB induced apoptosis of BCR-ABL1 T315I CML primary cells from a bone marrow sample. Recently, the work of Mitrovský and colleagues (Mitrovský et al., 2023), confirmed our previous findings (Borgo et al., 2013), as they found higher CK2 activity in six novel imatinib- and dasatinib-resistant CML cell lines, compared to sensitive cells. Interestingly, among their novel lines, JURL-MK1 cells with the T315I mutation were also present. Although a detailed analysis of them was not performed, this work shed light on a possible involvement of CK2 also in T315-induced CML TKI resistance.

1.2.1. CK2 in T315I-induced TKI resistance in chronic myeloid leukemia

Our group had already started to investigate the role of CK2 in the T315I-dependent imatinib resistance of CML, before this PhD thesis work started. Two variants of the CML cell line KBM5 were exploited: the wild type KBM5 cells harboring wild type BCR-ABL1 and normally sensitive to imatinib (here often referred to as S, from “sensitive”), and KBM5-T315I imatinib-resistant cells, harboring the BCR-ABL1 T315I mutation. Important to notice, these cells were the only cell model of this resistance available at the beginning of the study.
As shown in Figure 17, the KBM5-T315I cells displayed higher levels of the CK2 catalytic subunits CK2α and CK2α’ compared to imatinib-sensitive cells (Figure 17A). CK2 activity was evaluated through the phosphorylation of two of its substrates, Akt1 at S129 (Di Maira et al., 2005, 2009) and NF-kB p65 subunit at S529 (Wang et al., 2000). Compared to imatinib-sensitive cells, the KBM5-T315I cells displayed increased phosphorylation of the two CK2 activity reporters (Figure 17A). As reported in Figure 17B, in KBM5-T315I cells, BCR-ABL1 is not only mutated, but also overexpressed and hyperactivated, as indicated by its autophosphorylation site Y245. Moreover, regarding BCR-ABL1 downstream pro-survival pathways, in KBM5-T315I cells, Akt is hyper-activated, as judged by the activation site S473, as well as increased Akt total protein and phosphorylated levels of Akt downstream-target rpS6. KBM5-T315I cells displayed similar ERK1/2 activation level, compared to the imatinib-sensitive cells, despite this pathway should be dependent on BCR-ABL1 (Amarante-Mendes et al., 2022).

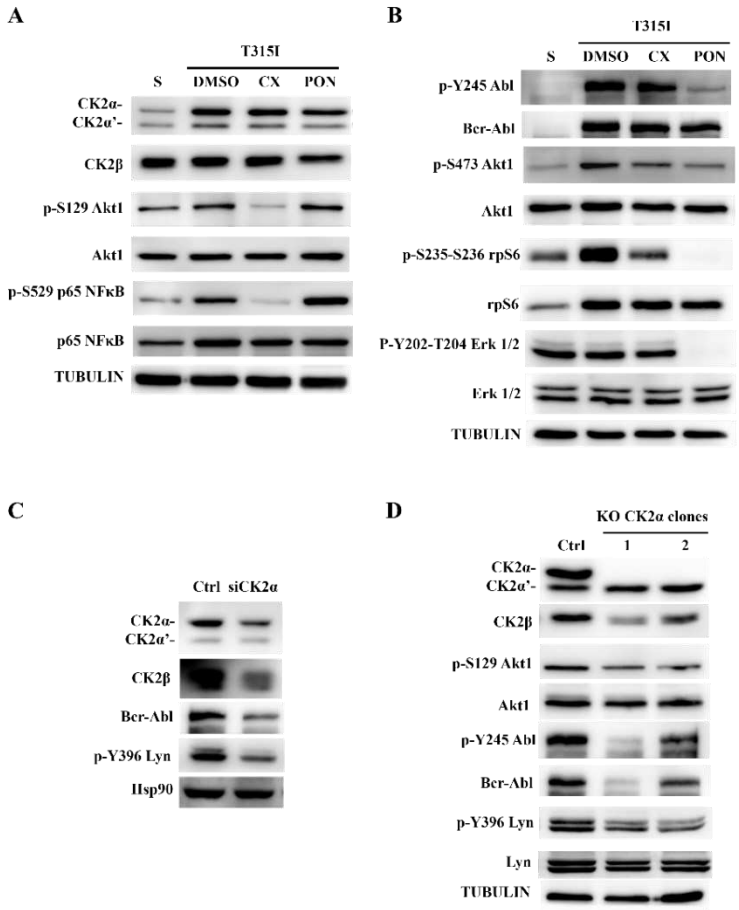

Figure 17. CK2 is overexpressed and involved in pathological signaling in T315I resistant cells.

Representative images of Western blot to control (A) CK2 expression levels and activity and (B) BCR-ABL1 expression levels and downstream signaling in KBM5 cells sensitive to imatinib (S) and in KBM5-T315I imatinib-resistant cells (T315I), treated with 3 μM CX-4945 (CX) or 2 nM ponatinib (PON) for 5 hours. CK2 targeting by (C) transient CK2α siRNA knockdown and (D) CK2α knockout (KO CK2α 1 and KO CK2α 2). (Unpublish data from Dr. Salizzato)

Then KBM5-T315I cells were treated with the clinical grade CK2 inhibitor CX-4945, to evaluate the effects of CK2 inhibition on these signals, and compare them with those induced by ponatinib, the only TKI active also against T315I-BCR-ABL1 (Kantarjian et al., 2022). As expected, ponatinib almost abrogated the BCR-ABL1 and ERK1/2 activation, and reduced the Akt and rpS6 signaling pathways, without affecting the CK2 protein-amount and its activity towards its specific targets (Figure 17A and B). CX-4945, as expected, produced a strong reduction in the phosphorylation of the CK2-dependent sites (Figure 17A); alongside with a not so expected and encouraging reduction of the increased signaling in KBM5-T315I cells compared to the imatinib-sensitive cells (Figure

17B). Interestingly, the ERK1/2 activity state, which was not increased in the KBM5-T315I compared to sensitive cells, was not affected by the CK2 inhibitor.
To further confirm the results obtained with CX-4945, supporting the CK2 involvement in the imatinib-resistance of KBM5-T315I cells, CK2 was targeted by CK2α siRNA knockdown and by CK2α genetic ablation (Figure 17C and D). CK2α transient knockdown, which is accompanied by the expected CK2β reduction due to its instability when not associated with the catalytic subunits (Borgo et al., 2019; Lüscher & Litchfield, 1994), decreased BCR-ABL1 protein level, confirming the close interaction between CK2 and BCR-ABL1 in these T315I-induced imatinib resistant cells (Figure 17C). Also in the two CK2α knockout (KOα) cell clones, a significant down-regulation of the CK2β regulatory subunit was observed, as expected (Borgo et al., 2019; Lüscher & Litchfield, 1994), without any alteration of the catalytic isoform CK2α' levels. As shown in Figure 17D, the KOα cells presented reduced CK2 activity, as reported by the phosphorylation levels of its targets Akt1 S129 and p65 NF-kB S529. CK2α ablation produced a reduction of BCR-ABL1 and interestingly, of the activation levels of Lyn, a Src kinase overexpressed in imatinib resistant cells (Donato et al., 2003).

1.2.2. CK2α knockout enhance sensitivity to TKIs in T315I -resistant cells.

Additionally, as showed in Figure 18, when cell viability was measured in response to TKIs, in comparison to the parental KBM5-T315I cells normally expressing CK2, the KBM5-T315I CK2 knockout (KOα) cell clones showed enhanced sensitivity to ponatinib (third-generation TKI) (Fig 18A) and also to bosutinib (Fig. 18B), a second-generation TKI, ineffective in overcoming the TKI resistance associated to the BCR-ABL1 T315I mutation *in vivo* (Remsing Rix et al., 2009).

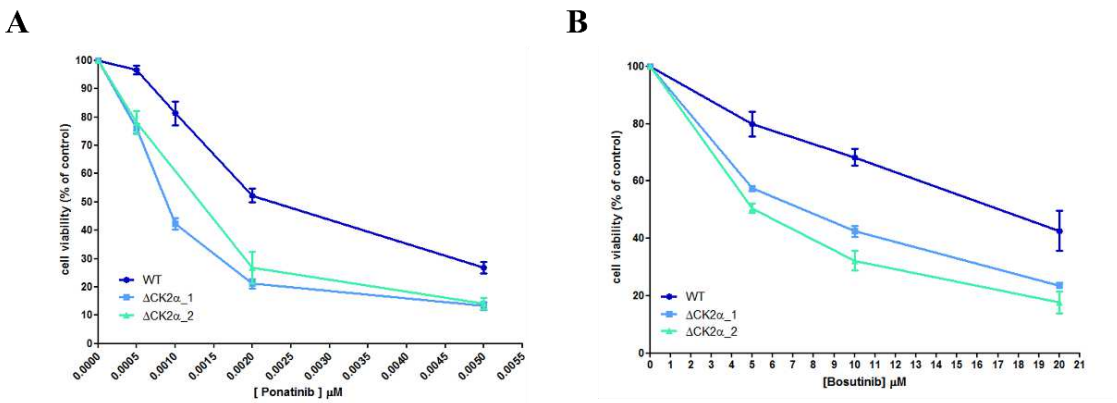

Figure 18. CK2α genetic ablation enhances sensitivity to TKIs in T315I -resistant cells.

Cell viability of KBM5-T315I CK2α knockout cell clones (KO CK2α 1 and KO CK2α 2) after treatment with the TKIs (A) ponatinib and (B) bosutinib. (Unpublish data from Dr. Salizzato).

2. Aim of the study

CK2 is a constitutively active kinase involved in several human diseases, especially described in cancer. CK2 has been proven to support the CML phenotype, however, its relevance in BCR-ABL1 T315I-induced TKI resistance, suggested by a few studies, has never been investigated. Data from our group, have recently reveal that CK2 contributes to the aberrant and overexpressed signaling pathways in T315I-cells. Moreover, CK2 pharmacological or genetic targeting dampened those signals, additionally sensitizing T315I-cells towards TKIs. Altogether, these results let us hypothesize that CK2 is a valuable target and its inhibition by the clinical grade inhibitor CX-4945 a possible therapeutical strategy for imatinib-resistance of CML cells bearing the BCR-ABL1 T315I mutation.

To test this hypothesis, our aims were:

i. **To characterize the effect of CK2 pharmacologic inhibitors over malignant features in T315I-resistant cells**

To reach this aim, we evaluated the effect of CK2 pharmacologic inhibitors over the cell viability and apoptosis by using KBM5-T315I cell as a model of T315I-resistant cells. Moreover, we investigated the mechanism by which the CK2 inhibitor CX-4945 dampens the tumorigenic phenotype.

ii. **To evaluate the efficacy of CX-4945 on T315I-resistant cells in the presence of stromal cells**

To understand if the effect of CX-4945 was reduced by the bone marrow microenvironment (BMM) protection of the leukemia cells, we performed different cell functional assays to evaluate cell viability, apoptosis and clonogenic potential of T315I-resistant cells in the presence of stromal cells. Additionally, we evaluated CX-4945 efficacy under hypoxic conditions.

iii. **To corroborate the results in a second T315I -resistant model**

To this aim, we evaluated some of the effects of CX-4945 in a second T315I -

resistant cellular model, in the meantime developed by a Korean group.

3. Results

3.1. CK2 pharmacological inhibition reduces KBM5-T315I cell viability and promotes apoptosis

As previous results from our group have revealed that CK2 supports important signaling pathways in KBM5 cells bearing the BCR-ABL1 T3151 mutation (KBM5-T315), thus promoting the resistant phenotype (see CHAPTER II.1.2), we decided to characterize the effect of CK2 pharmacological inhibition over the malignant phenotype in views of a therapeutic strategy. As it has been extensively described that CK2 promotes proliferation and anti-apoptotic signaling in tumoral cells (Ruzzene & Pinna, 2010), including CML cells (Borgo et al., 2013), we decided to first evaluate whether different CK2 inhibitors were able to reduce cell viability of KBM5-T315I. To this purpose, we performed MTT viability assay of KBM5-T315I cells with the ATP-competitive CK2 inhibitors CX-4945 (Siddiqui-Jain et al., 2010), GO289 (Oshima et al., 2019) and SGC-CK2-1 (Wells et al., 2021), using imatinib as a control of resistance. As shown in Figure 19A, the three inhibitors significantly reduced KBM-T315I cell viability even at low micromolar concentrations, in contrast to imatinib that, as expected, was found to be ineffective even at concentrations considerably higher than those used for sensitive cells.

As the three inhibitors tested displayed similar efficacy in reducing viability, we selected CX-4945 to continue our work, as it is already in ongoing clinical trials as chemotherapeutic (Pediatric Brain Tumor Consortium, 2023; Senhwa Biosciences, Inc., 2021, 2023a, 2023b; University Hospital, Grenoble, 2020). We then evaluated if the effect of CX-4945 on KBM-T315I cells is time-depended, and we confirmed a concentration- and time-dependent effect, observing significant reduction even after 24 hours treatment, as shown in Figure 19B. Additionally, we evaluated if the reduction of viability promoted by CX-4945 in KBM-T315I cells was due to apoptosis, and indeed we found that the treatment induced a dose-dependent cleavage of the apoptosis-associated proteins PARP and caspase-3 (Figure 19C), suggesting that the CX-4945 induces cell death by apoptosis, as further confirmed by FACS analysis (see below, Figure 21C).

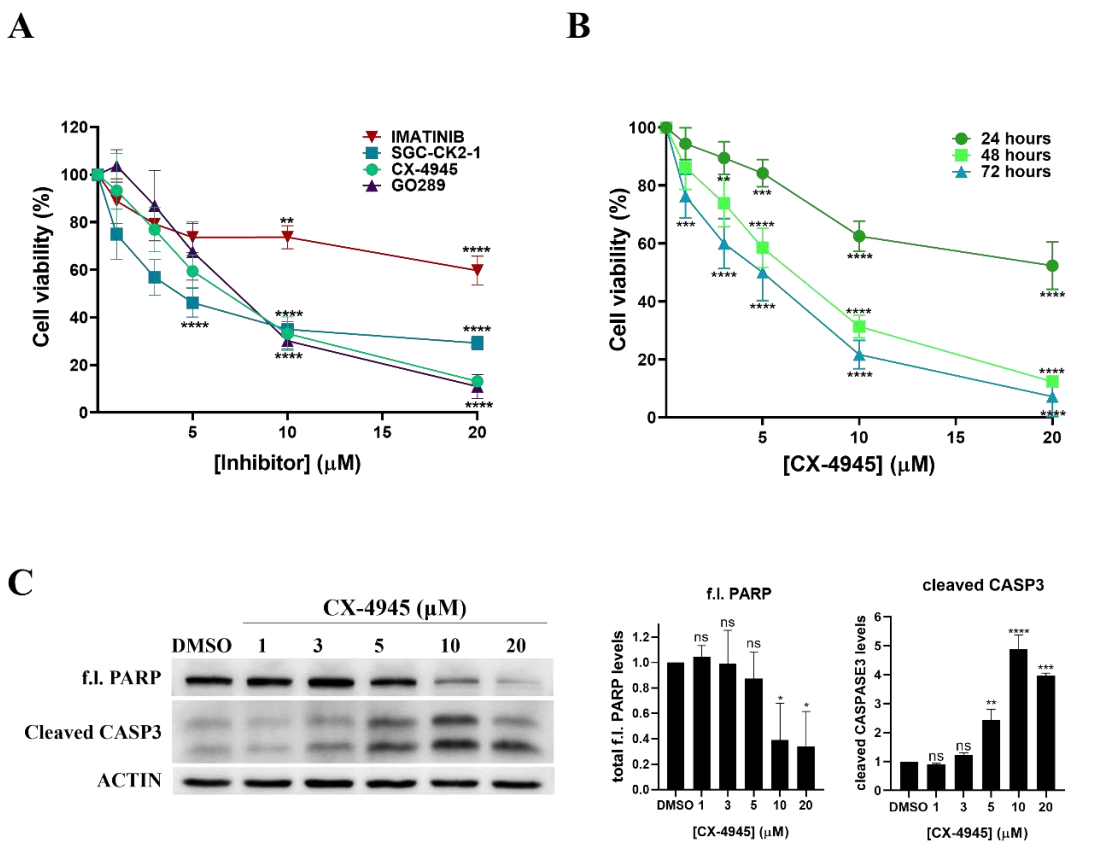

Figure 19. CK2 pharmacological inhibition reduces KBM5-T315I cell viability and promotes apoptosis.

(A) Cell viability of KBM5-T315I cells after 48h treatment with the ATP-competitive CK2 inhibitors CX-4945, GO289 and SGC-CK2-1 at 1, 3, 5, 10 and 20 μM. (B) KBM5-T315I cell viability after treatment with 1, 3, 5, 10 and 20 μM CX-4945 for 24, 48 or 72 hours. (C) Apoptosis-associated proteins PARP (f.l.: full-length) and caspase 3 (CASP3). Representative images of Western blot from 3 independent experiments are shown, where 20 μg of proteins were loaded (left). Quantification upon normalization to the loading control (actin) is shown on the right, with data presented as mean ± SD. In (A) and (B), data from 3 independent experiments is presented as mean ± SD. Statistical analysis was performed with two-way ANOVA (A and B) or one-way ANOVA (C) with Dunnett's post test. ns no significant, *P < 0.05, **P < 0.01, ***P <0.005, ****P < 0.001.

3.2. CK2 inhibitor CX-4945 reduces BCR-ABL1 signaling in KBM5-T315I cells

We then went into further detail about the different signaling pathways affected by CX-4945 in these cells. As shown in Figure 20, CX-4945, as expected, almost completely abrogates CK2 activity even at the lowest concentration, as reported

by its substrate Akt1 at S129 (Di Maira et al., 2005, 2009). Interestingly, CX-4945 showed to be also effective, even at the lowest concentrations, in significantly reducing the activation levels of BCR-ABL1 (as judged by its phosphorylation at Y245 (Hantschel & Superti-Furga, 2004)), and of the oncogenic transcription factor STAT3 (Wingelhofer et al., 2018) (as judged by its phosphorylation at Y705 (Johnson et al., 2018)). At higher concentrations, CX-4945 was also effective in reducing the protein expression of STAT5, a transcription factor that is a BCR-ABL1 substrate and supports survival in CML (Schafranek et al., 2015; Shuai et al., 1996). Moreover, CX-4945 treatment reduced Src- kinase Lyn signaling (a regulator of BCR-ABL phosphorylation commonly overexpressed in imatinib resistant cells (Donato et al., 2003; Wu et al., 2008)), affecting both Lyn protein level and Lyn activation, as reported by its phosphorylation at Y396 (Donella-Deana et al., 1998). The BCR-ABL1 substrate CRKL did not show any alteration, neither in the total levels or at the BCR-ABL1 phosphorylation site Y207(de Jong et al., 1997), upon CK2 inhibition.

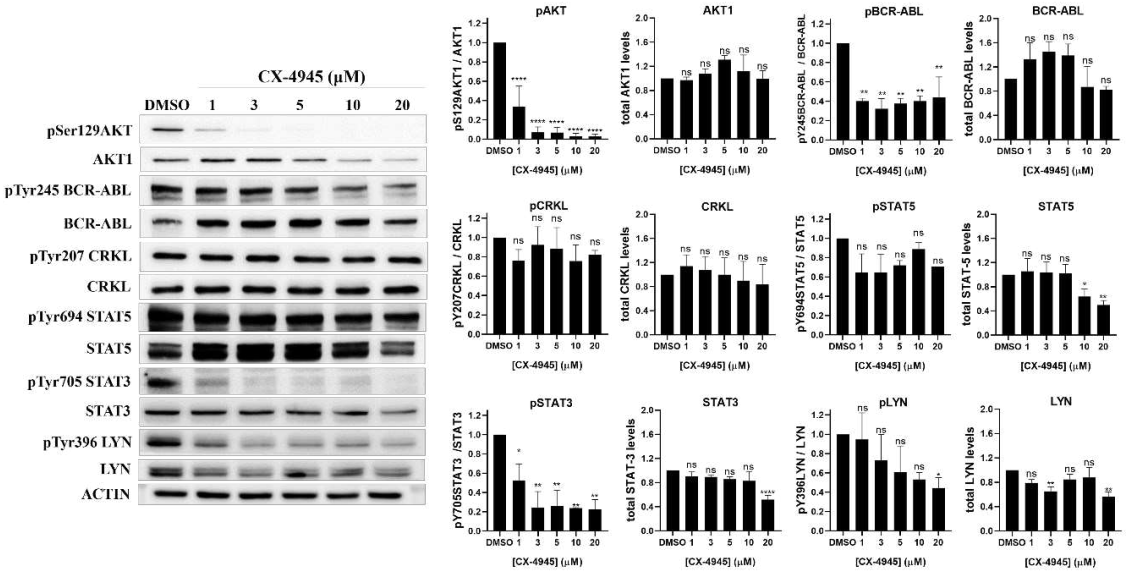

Figure 20. CK2 inhibitor CX-4945 reduces pro-survival signaling pathways in KBM5-T315I cells.

Pro-survival signaling proteins from KBM5-T315I cells treated for 24 hours with 1, 3, 5, 10 and 20 μM CX-4945. Representative images of Western blot from 3 independent experiments are shown, where 50 µg or 20 µg of proteins were loaded (left). Quantification upon normalization to the loading control (actin), and to the total proteins in the case of phospho-antibodies, is shown on the right, with data presented as mean ± SD. Statistical analysis was performed with one-way ANOVA with Dunnett's post test. ns no significant, *P < 0.05, **P < 0.01, ***P <0.005, ****P < 0.001.

3.3. CK2 inhibitor CX-4945 reduces KBM5-T315I cell viability and induces apoptosis even in the presence of stromal cells

The potential of the bone marrow microenvironment (BMM) to provide protection to the leukemia cells through multidimensional interactions, can drive or sustain therapy resistance in different types of leukemia, including CML (Patterson & Copland, 2023). Therefore, to characterize the effect of CX-4945 also for this aspect, we decided to evaluate its efficacy in co-cultures of the KBM5-T315I cells with MS-5 stromal cells, kindly donated by Prof. Marmiroli's group (University of Modena and Reggio Emilia, Italy), a model that partially mimics the protective effects of the BMM. The two cell lines were co-cultured for 48 hours pre-treatment, then, CX-4945 treatment was performed for further 48 hours, and after this time the KBM5-T315I cells were collected from the co-culture and analyzed, as described in Figure 21A.

First, we performed MTT assays to measure the cell viability of the KBM5-T315I cells, that were easily collected from the co-culture due to their growth in suspension, differently to the MS-5 cells, which, growing in adhesion, were left on the bottom of the culture flask. As shown in Figure 21B, CX-4945 was as effective in reducing KBM5-T315I cell viability in co-culture with stromal cells, as in the mono-culture. This was a first indication that the inhibitor can overcome the stromal cell protection. To be completely sure to exclude MS-5 cells from our viability analysis, and to go further in details on the type of death induced by the inhibitor, we performed flow cytometry analysis (FACS) of the KBM5-T315I collected from the co-culture after labeling with Annexin V, which due to its high affinity for phosphatidylserine enables the recognition of early-stage cell apoptosis, and 7-aminoactinomycin D (7-AAD) for the recognition of necrotic cells. Preliminary analysis (in collaboration with Prof. Marmiroli's group, University of Modena and Reggio Emilia, Italy) had shown that the cells collected from the co-culture were exclusively KBM5-T315I (not shown). The results of our FACS analysis for the apoptotic marker confirmed that CX-4945 induced apoptosis in KBM5-T315I cells in a dose-dependent manner (Figure 21C, quadrants Q1 and Q2). Moreover, in the presence of the MS-5 cells, the

percentage of apoptotic cells induced by each CX-4945 concentration was quite similar to that observed in the corresponding mono-culture condition, with only a slight reduction at 20 μM (Figure 21D).

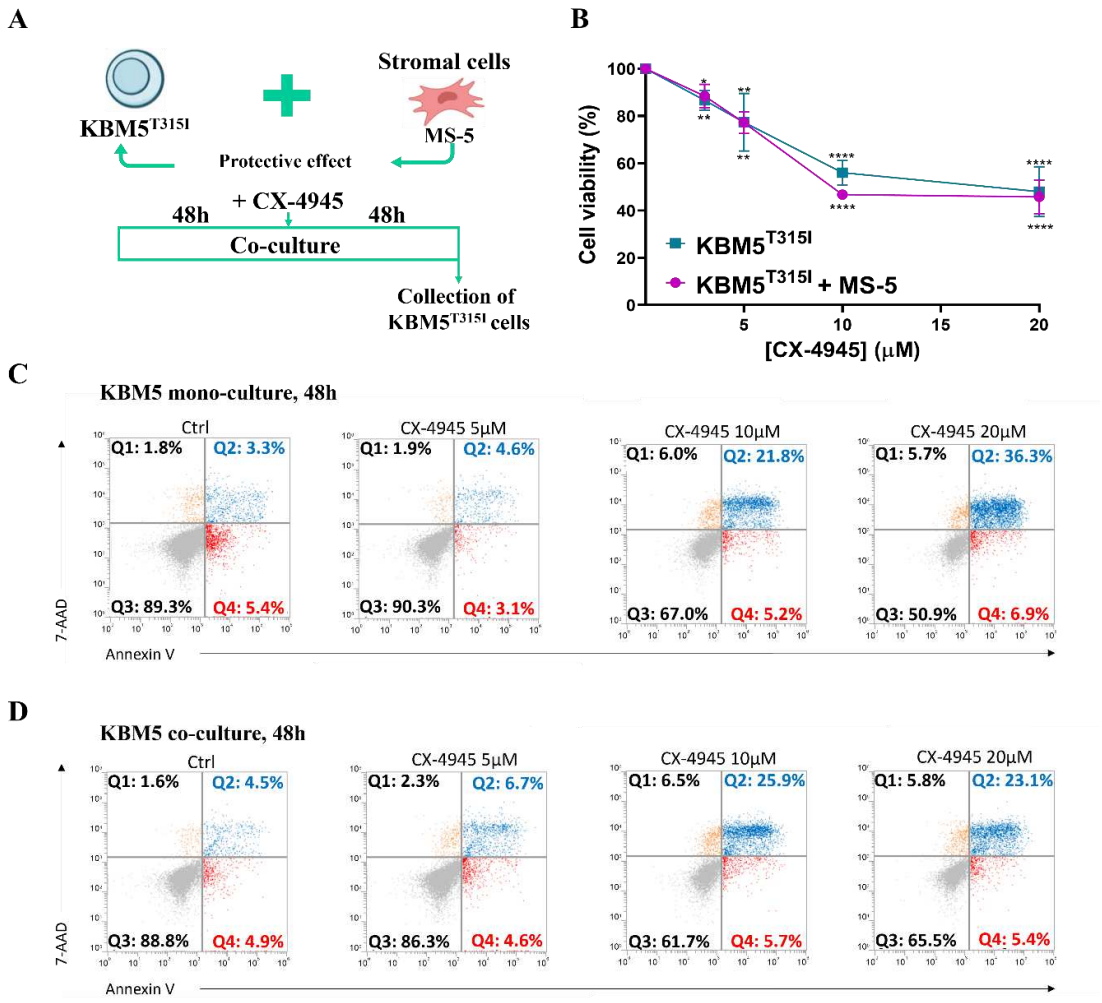

Figure 21. CK2 inhibitor CX-4945 reduces KBM5-T315I cell viability and induces apoptosis even in the presence of stromal cells.

(A) Schematic representation of the co-culture model, where the KBM5-T315I cells were co-cultured with MS-5 stromal cells 48 hours pre-treatment. After this time, 48 hours CX-4945 treatments were performed and later the KBM5-T315I cells were collected from the co-culture and analyzed. Mono-cultured KBM5-T315I cells were used as control. (B) Cell viability ofS mono- and co-cultured KBM5-T315I cells after treatment with 1, 3, 5, 10 and 20 μM CX-4945. Cell apoptosis, quantified using Annexin V/7-AAD assay by flow cytometry, of (C) mono-cultured and (D) co-cultured KBM5-T315I cells after 5, 10 and 20 μM CX-4945 treatments. In (B), data from 3 independent experiments are presented as mean ± SD, and statistical analysis was performed with two-way ANOVA with Dunnett's post test. ns no significant, *P < 0.05, **P < 0.01, ***P <0.005, ****P < 0.001.

3.4. CK2 inhibitor CX-4945 reduces KBM5-T315I cell viability under hypoxic conditions

Since the bone marrow microenvironment exerts its protection over leukemia cells especially under hypoxic conditions (Houshmand et al., 2019), which also support leukemia stem cells persistence (Ng et al., 2014), thus promoting the TKI-resistant phenotype of CML cells (Copland et al., 2006), we decided to assess the efficacy of CX-4945 under hypoxic conditions and in presence of stromal cells. To this purpose, in collaboration with Prof. Marmiroli's group, we established a model where KBM5-T315I cells were co-cultured in normoxia with MS-5 stromal cells for 48 hours, then treated with CX-4945 under hypoxia (1% O2, 5% CO2) or normoxia (21% O2, 5% CO2) for comparison. After preliminary experiments, we determined that, in this case, the convenient treatment time was 24 hours; in fact, the 48 hours treatment applied to the experiments shown so far was found to induce death under these hypoxic conditions, as well as in untreated cells. Our experimental model is depicted in Figure 22A. Using this model, we found that CX-4945 reduced the cell viability of KBM5-T315I cells in hypoxic conditions to a similar extent to the normoxia condition, and, more importantly, also similarly either in the absence or in the presence of stromal cells (22B).
Altogether, our results of co-culture experiments suggest that CX-4945 is probably able to overcome the BMM protective effect.

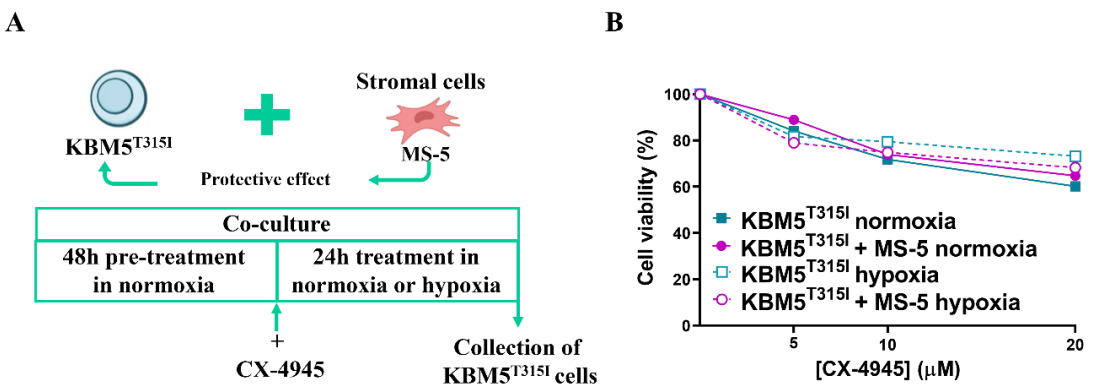

Figure 22. CK2 inhibitor CX-4945 reduces KBM5-T315I cell viability under hypoxic conditions.

(A) Schematic representation of the model, where KBM5-T315I cells were co-cultured in normoxia with MS-5 stromal cells 48 hours pre-treatment. After this time, 24 hours CX-4945 treatments

were performed under hypoxia (1% O2, 5% CO2) or normoxia (21% O2, 5% CO2) and later the KBM5-T315I cells were collected from the co-culture and analyzed. Mono-cultured KBM5-T315I cells and CX-4945 treatment in normoxia were used as controls. (B) Cell viability of mono- and co-cultured KBM5-T315I cells after 1, 3, 5, 10 and 20 μM CX-4945 treatments, in normoxia and hypoxic conditions. Statistical analysis was not performed since the results derive from a single experiment.

3.5. CK2 inhibitor CX-4945 reduces KBM5-T315I clonogenic potential even in the presence of stromal cells

Given the encouraging results, we further exploited our established co-culture model (Figure 21A) by performing soft-agar clonogenic assays. This approach, which evaluates the formation of colonies, can reveal the clonogenic potential/proliferative ability of the cells in a more stringent and reliable way than survival or growth assays (Li, 2004; Simanovsky et al., 2008), thus allowing to better understand the potency of a putative drug. As showed in Figure 23, we found that CX-4945 strongly reduced the clonogenic potential of mono-cultured KBM5-T315I cells. In co-culture, the effect was partially reduced by the protective action of the stromal cells, but only at the lowest CX-4945 concentrations, while, at the highest ones, there were almost no colonies, both in mono- and co-cultured conditions.

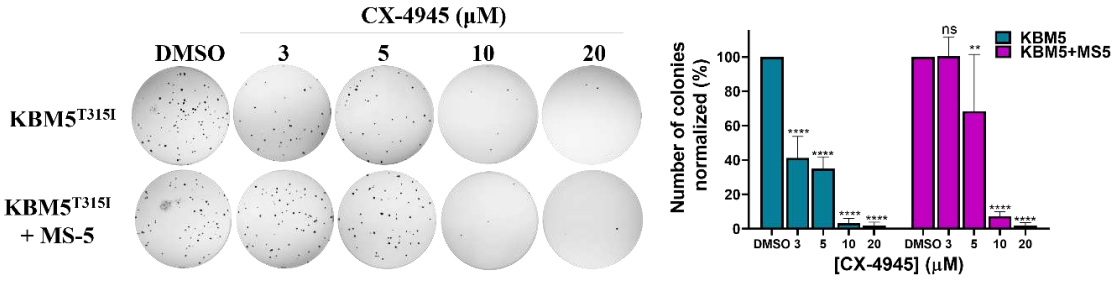

Figure 23. CK2 inhibitor CX-4945 reduces KBM5-T315I clonogenic potential.

Soft-agar colony assay of mono- and co-culture KBM5-T315I cells. The KBM5-T315I cells were cultured alone or with MS-5 stromal cells 48 hours pre-treatment. After this time, 48 hours CX-4945 treatments were performe, and later the KBM5-T315I cells were collected and seeded in semi-solid soft agar. The cells were cultured for 14 days and then treated with MTT to count live

colonies. Representative images from 2 independent experiments are shown (left). Quantification is shown on the right, with data presented as mean ± SD. Statistical analysis was performed with two-way ANOVA with Dunnett's post test. ns no significant, *P < 0.05, **P < 0.01, ***P <0.005, ****P < 0.001.

3.6. CK2 inhibitor CX-4945 is effective in reduce cell viability and pro-survival signaling pathways in a second T315I-resistance model

Despite the interest in the T315I-induced resistance, for years the KBM5-T315I cells were the only cellular model available. However, in the last couple years, a few new models have been established. We were able to obtain a K562-T315I cell line, kindly donated by Dr. Jong-Won Kim (Sungkyunkwan University, Korea) and Dr. Dennis Dong Hwan Kim (University Health Network, Canada) (Jang et al., 2021), that we used to corroborate the results obtained with the KBM5-T315I cells.

We first evaluated whether different CK2 inhibitors were able to reduce cell viability of K562-T315I cells. To this purpose, we performed MTT cell viability assays after 48 hours treatment with the ATP-competitive CK2 inhibitors CX-4945, GO289 and SGC-CK2-1, using imatinib as a control of resistance. As shown in Figure 24A, similarly to what observed in KBM5-T315I cells, the three inhibitors significantly reduced K562-T315I cell viability even at low micromolar concentrations, in contrast to imatinib that, as expected, was found to be ineffective even at concentrations considerably higher than those used for sensitive cells. The apoptotic nature of the cell death induced by CX-4945, as in KBM5 cells, was confirmed by the cleavage of the apoptotic marker PARP (Fig 24B).

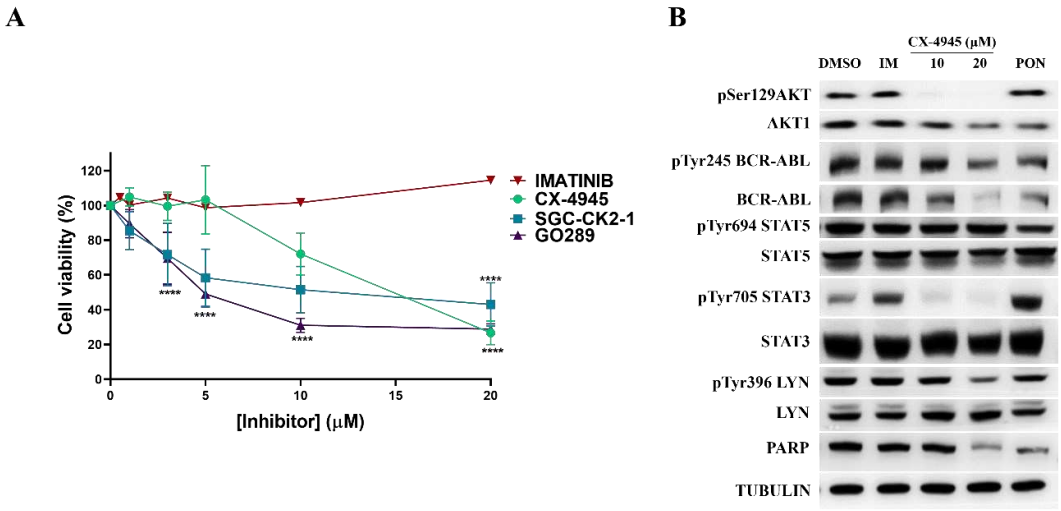

Figure 24. CK2 pharmacological inhibition reduces K562-T315I cell viability and promotes apoptosis.

(A) Cell viability of K562-T315I cells after 48 hours treatment with the ATP-competitive CK2 inhibitors CX-4945, GO289 and SGC-CK2-1 at 1, 3, 5, 10 and 20 μM, or imatinib as negative control. (B) Pro-survival signaling proteins in K562-T315I cells after 24 hours 10 and 20 μM CX-4945 treatments. Treatments with 1 μM imatinib (IM) and 2 nM ponatinib (PON) were used as control. 50 µg or 20 µg of proteins were loaded. In (A), data from 3 independent experiments are presented as mean ± SD, and statistical analysis was performed with two-way ANOVA (A) with Dunnett's post test. ns no significant, *P < 0.05, **P < 0.01, ***P <0.005, ****P < 0.001. In (B), statistical analysis was not performed since the results derive from a single experiment.

As shown in Figure 24.B, a 24 hours treatment with CX-4945 (10 and 20 μM), as expected, almost completely abrogated CK2 activity (as judge by the reporter substrate Akt1 at S129 (Di Maira et al., 2005, 2009)). Interestingly, as in KBM5-T315I cells, a number of pro-survival signaling proteins are also affected by CX-4945: it reduces the BCR-ABL1 levels, the activation levels of the oncogenic transcription factor STAT3 (Wingelhofer et al., 2018), and the activation levels of the Src- kinase Lyn (as reported by its phosphorylation at Y396 (Donella-Deana et al., 1998)). In contrast, in this case the BCR-ABL1 substrate STAT5 did not show any alteration. As expected, the treatment with imatinib did not reduce any of the analyzed signaling, while ponatinib was effective in reducing BCR-ABL1 and inducing PARP cleavage, however the effects were modest compared to those observed with CX-4945.

In summary, although preliminary due to the recent availability of this cell model,

our results with K562-T315I cells confirm the sensitivity to CK2 targeting in this kind of TKI resistance.

4. Discussion

The connection between CK2 and BCR-ABL1, the disease-driving molecule of CML, had already been investigated in our laboratory (Borgo et al., 2013). Here, we extend the study to a particularly interesting case of TKI resistance of CML, the one caused by the BCR-ABL1 T315I-mutation. We showed that the activation of BCR-ABL1 is sustained by CK2 in T315I cell lines. We found that CK2 supports their malignant phenotype by the enhancement of some of the main signaling pathways associated to CML tumor progression and TKI-resistance, such as Akt (Singh et al., 2021), NF-kB (Morotti et al., 2015), Lyn (Wu et al., 2008), STAT3 (Nair et al., 2012) and STAT5 (Ye et al., 2006). Importantly, our work also demonstrates that CK2 targeting induces apoptosis and reduces the clonogenic potential of the T315I CML cells. Moreover, a potential synergistic effect between CK2 targeting and TKIs is observed, opening new perspectives of possible combined therapies based on CK2 inhibitors and TKIs.

As CK2 inhibitor, we mainly focused on CX-4945, given its clinical grade, but when we used different inhibitors, we observed similar effects. Moreover, beside the pharmacological inhibition by ATP-competitive inhibitors, we also applied other approaches to reduce CK2 signaling, including the CK2 genetic targeting, either by CK2α knockout by CRISPR-Cas9 or knockdown by siRNA. Most of the effects were similar, thus confirming the particularly high specificity of the CK2 inhibitors. However, in the case of the BCR-ABL1 protein levels, we found that only CK2 genetic targeting but not CX-4945 reduced it in KBM5-T315I cells. This interesting observation suggest that the physical presence of CK2, and not merely its activity, is necessary for this effect on BCR-ABL1, as it has been suggested before due to its co-localization (Borgo et al., 2013). However, in K562-T315I cells, the effect of reducing the BCR-ABL1 protein levels is induced also by CX-4945. Currently, we have no explanation for this discrepancy, and further investigation will be needed to understand the complex interaction between CK2 and BCR-ABL1.

Our data also suggest that the inhibition of CK2 would be exerted even in the presence of bone marrow microenvironment and under hypoxic conditions, where the action of most drugs is significantly reduced (Aggoune et al., 2014;

Cambria et al., 2023; Le et al., 2020; Zhou et al., 2016). Of course, further studies will be necessary to confirm this finding *in vivo*. Although we performed our experiments mainly with KBM5 cells, the only T135I cell model available at the beginning of this study, at the end we could replicate some experiments with a newly developed cell model, K562 cells (Jang et al., 2021). The preliminary results obtained so far suggest that the effects of CK2 targeting can be generalized for this kind of TKIs resistance in CML.

Indeed, CK2 has been extensively described as a valuable drug target in cancer, and the concept of “CK2 addiction” (Ruzzene & Pinna, 2010), that refers to the higher dependence on CK2 displayed by cancer cells compared to healthy cells, offers important therapeutic advantages: targeting only one protein, CK2, produces the down-regulation of many signaling pathways, which are characteristic of cancer cells, thus reducing the risk of damaging healthy cells. The availability of several CK2 inhibitors, including two already in clinical trials: CIGB-300 (Laboratorio Elea Phoenix S.A., 2015, 2016) and CX-4945 (Pediatric Brain Tumor Consortium, 2023; Senhwa Biosciences, Inc., 2021, 2023a, 2023b; University Hospital, Grenoble, 2020), complete the view of the actual relevance of our findings. Although our results are only *in vitro*, we think they are promising, and important to pave the way for future studies in higher models of this TKI resistance, as in patient-derived cells or in one of the few and newly developed mouse models (Mian et al., 2021).

CHAPTER III: CK2 IN POIRIER–BIENVENU NEURODEVELOPMENTAL SYNDROME

1. Introduction

1.1. Poirier–Bienvenu neurodevelopmental syndrome

Poirier–Bienvenu neurodevelopmental syndrome (POBINDS) is a rare autosomal-dominant disorder caused by a heterozygous variant of *CSNK2B,* the gene coding for the regulatory β subunit of CK2. The disorder was discovered in 2017 by Poirier and collaborators (Poirier et al., 2017), and to date 91 patients have been reported (Li et al., 2023; Trivisano et al., 2023).

1.1.1. Clinical features and care

POBINDS patients have shown highly heterogeneous clinical phenotypes, with early onset epilepsy, different degrees of intellectual disability (ID), developmental delay (DD) and hypotonia as the main features (Di Stazio et al., 2023; Orsini et al., 2022). In fact, analysis of the symptomatology of 81 patients reported that 66 had seizures under the age of 3 years, 60 displayed varying degrees of ID and 72 of DD (Li et al., 2023). Less frequently, patients also present autism and language, behavioral, mental and/or motor disorders (Di Stazio et al., 2023).

Most of the patients have been treated symptomatically with anti-epileptic drugs (as levetiracetam and sodium valproate) as there is no actual cure or specific treatment, however the efficacy of this antiepileptic drugs varies from patient to patient as it depends on the type and severity of the seizures (Yang et al., 2021).

1.1.2. CK2β: the responsible of the pathology of POBINDS

CK2β is the regulatory subunit of the tetrameric kinase CK2, which plays key functions in the formation of the tetrameric CK2, as well as in the regulation of the holoenzyme stability, in its substrate selectivity and serving as a docking platform for recruitment of substrates or potential regulators (Canton et al., 2001;

Graham & Litchfield, 2000; Marin, Meggio, & Pinna, 1999; Meggio et al., 1992a) (see INTRODUCTION 2.1.2).

CSNK2B is on chromosome 6 (6p21.33), has a genomic size of 3988 bp and contains seven exons that encode the 215 amino acids protein CK2β. From the 91 POBINDS cases reported, 88 carry a *de novo* mutation, while only 3 cases have been reported to be inherited from an affected parent (Trivisano et al., 2023). Moreover, in an analysis with the data of 81 cases, approximately 60 *CSNK2B* variants were found associated with the disease, of them 19 are missense, 15 frameshift, 14 non-sense and 12 splicing mutations (Li et al., 2023). The data shows that POBINDS-linked variants can be found across the exonic and intronic sequences, thus found along the whole CK2β protein sequence with no clear variant hotspots identified.

Due to the recent discovery of this syndrome, very few studies are available, and a link between genotype and phenotype of POBINDS patients is still not clear (Bonanni et al., 2021; Di Stazio et al., 2023; Li et al., 2023; Orsini et al., 2022; Yang et al., 2022). Attempts have been performed also by *in-silico* analyses, based on the available structural/functional information on CK2β (see INTRODUCTION 2.1.2), suggesting a more severe phenotype for some CK2β mutants (Ballardin et al., 2022; Unni et al., 2022). For example, the variants that affect the zinc finger (C109, C114, C137, and C140) have been suggested to hypothetically reduce the CK2 activity and increment seizures. Nakashima and collaborators (Nakashima et al., 2019), have shown a reduced expression of the CK2β p.T37Yfs*5 mutant, and the inability to interact with CK2α of the CK2β p.P179Yfs*49 mutant. However, the biochemical implications of most CK2β mutants in the CK2 activity/functions, and the subsequent cellular effects, are still largely unknown and need to be investigated.

2. Aim

The main aim of this work was to perform a biochemical characterization of five POBINDS CK2β mutants selected among those found in Italian patients (Orsini et al., 2022). As shown in Figure 25, the selected variants were: E61del, R111H, R111P, C137F and H165R. We chose these variants because we plan first to characterize them in a cellular model, and then move to *ex vivo* experiments, exploiting our collaboration with Dr. Orsini (Azienda Ospedaliero Universitaria Pisana, Italy), who can provide us with patients-derived cells.

To our purposes, we therefore wanted to establish a reliable cellular model using HEK-293AD CK2β knockout (KO) cell clones and stably transfecting them with WT *CSNK2B* or the selected *CSNK2B* variants. In our cellular model, we evaluated protein expression, activity, and stability of each selected CK2β mutant.

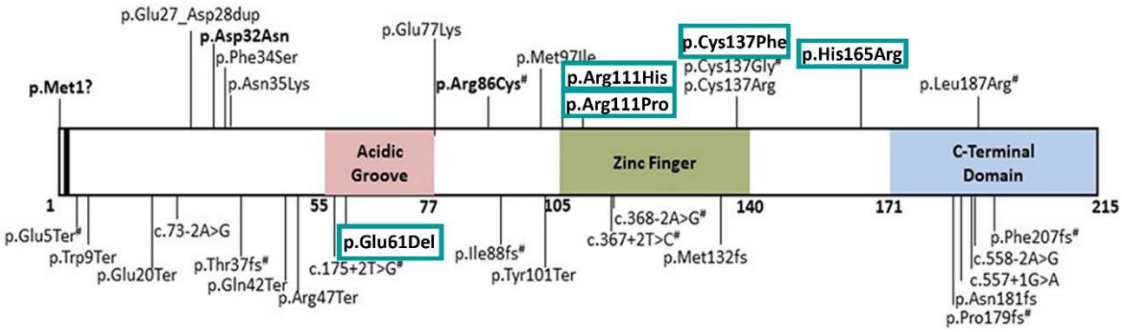

Figure 25. Selected POBINDS CK2β mutants.

Schematic representation of the protein sequence of CK2β and some of its domains. POBINDS-associated mutations are represented over the CK2β sequence, and the ones selected for this work are highlighted by blue rectangles (modified from Ernst et al., 2021)

3. Results

3.1. Establishment of the cellular model for the POBINDS mutant biochemical analysis

For the characterization of the selected mutants, we exploited HEK-293AD CK2β knockout (KO) cell clones. As shown in Figure 26A, these cells, lacking the CK2β subunit, displayed reduced CK2 activity towards different substrates (as shown by the phosphorylation of Akt at S129) in comparison to wild type cells. Moreover, as expected (Borgo et al., 2019), they also display reduced CK2α' expression level.

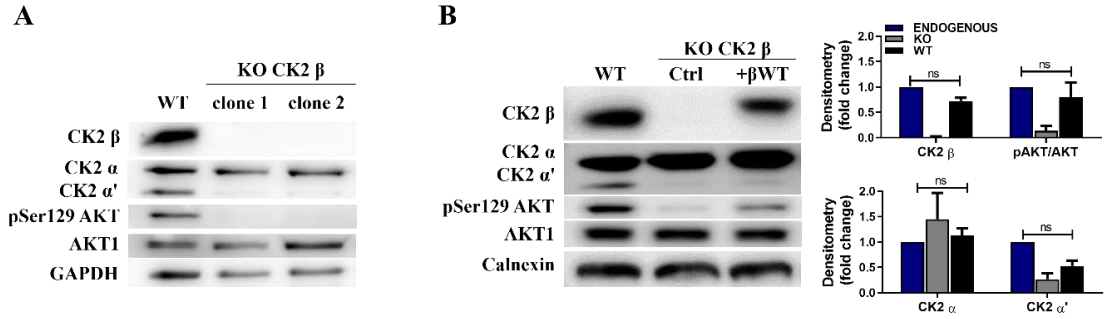

Figure 26. Cellular model for the study of POBINDS CK2β mutants.

Protein levels of CK2β, α and α' subunits, and phospho-S129 Akt, as reporter of CK2 activity. (A) Lysates from two HEK-293AD CK2β knockout (KO) cells clones (clone 1 and 2) are shown in comparison to wild type (WT) cells. (B) HEK-293AD CK2β KO cells were transfected with the empty vector (Ctrl) or CK2β WT, as indicated, and compared to WT HEK-293AD cells. Representative images of Western blot from 3 independent experiments are shown, where 20 µg of proteins were loaded (left). Quantification upon normalization to the loading control (calnexin) is shown on the right, with data presented as mean ± SD. Statistical analysis was performed with one-way ANOVA with Dunnett's post test. ns no significant, *P < 0.05, **P < 0.01, ***P <0.005, ****P < 0.001.

To establish a reliable model, we stably transfected the HEK-293AD CK2β KO cells with CK2β wild type (WT) and evaluated the extent of its expression. As shown in Figure 26B, the transfection of WT CK2β in the KO cells recovered an appreciable level of CK2β. Moreover, this was accompanied by a partial rescue of the CK2α' expression, and the CK2 catalytic activity (see phospho-S129 Akt).

As visible from the quantification of the bands of Fig 26B, the transfected cells did not display significant differences compared to the WT cells, thus confirming the model as an effective tool to study the CK2β POBINDS mutants. Therefore, we stably transfected each one of the five selected POBINDS variants (E61del, R111H, R111P, C137F and H165R) into the HEK-293AD CK2β KO cells, and performed the characterization described below, using the CK2β WT–transfected HEK-293AD CK2β KO cells as a control.

3.2. POBINDS CK2β mutants display differential protein expression

We first evaluated the CK2β protein levels in the stably transfected HEK-293AD CK2β KO cells described above. As shown in Figure 27, our results revealed differences in CK2β expression among the mutants. In fact, while the CK2β R111H and E61del mutants displayed expression levels similar to WT CK2β, the R111P, H165R and C137F mutants showed significantly reduced protein levels. Moreover, the CK2β mutants H165R and C137F did not recovered the CKα' levels, reportedly reduced in HEK-293AD CK2β knockout (KO) cells.

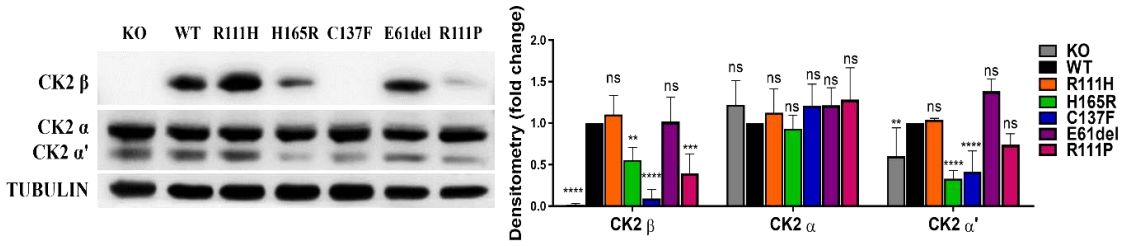

Figure 27. POBINDS CK2β mutants display differential protein expression.

CK2β and CK2 catalytic subunits α and α' expression levels in HEK-293AD CK2β knockout (KO) cells stably transfected with the five selected POBINDS variants (E61del, R111H, R111P, C137F and H165R). CK2β WT–transfected HEK-293AD CK2β KO cells were used as control. Representative images of Western blot from 3 independent experiments are shown, where 20 µg of proteins were loaded (left). Quantification upon normalization to the loading control (tubulin) is shown on the right, with data presented as mean ± SD. Statistical analysis was performed with one-way ANOVA with Dunnett's post test. ns no significant, *P < 0.05, **P < 0.01, ***P <0.005, ****P < 0.001.

3.3. Reduced protein levels of POBINDS CK2β mutants is due to increased proteasome-dependent degradation

To understand the reason behind the difference in the CK2β levels displayed by the mutants, we performed protein stability assays by treating the stably transfected cells with the protein synthesis inhibitor cycloheximide (McKeehan & Hardesty, 1969) for different lengths of time. This allows to follow how the amounts of a certain protein changes along the time, and therefore to evaluate its stability and turnover. As shown in Figure 28A, compared to CK2β WT, the H165R and C137F mutants showed significantly reduced protein stability, while the E61del, R111H and R111P mutants did not displayed significant differences compared to the control.

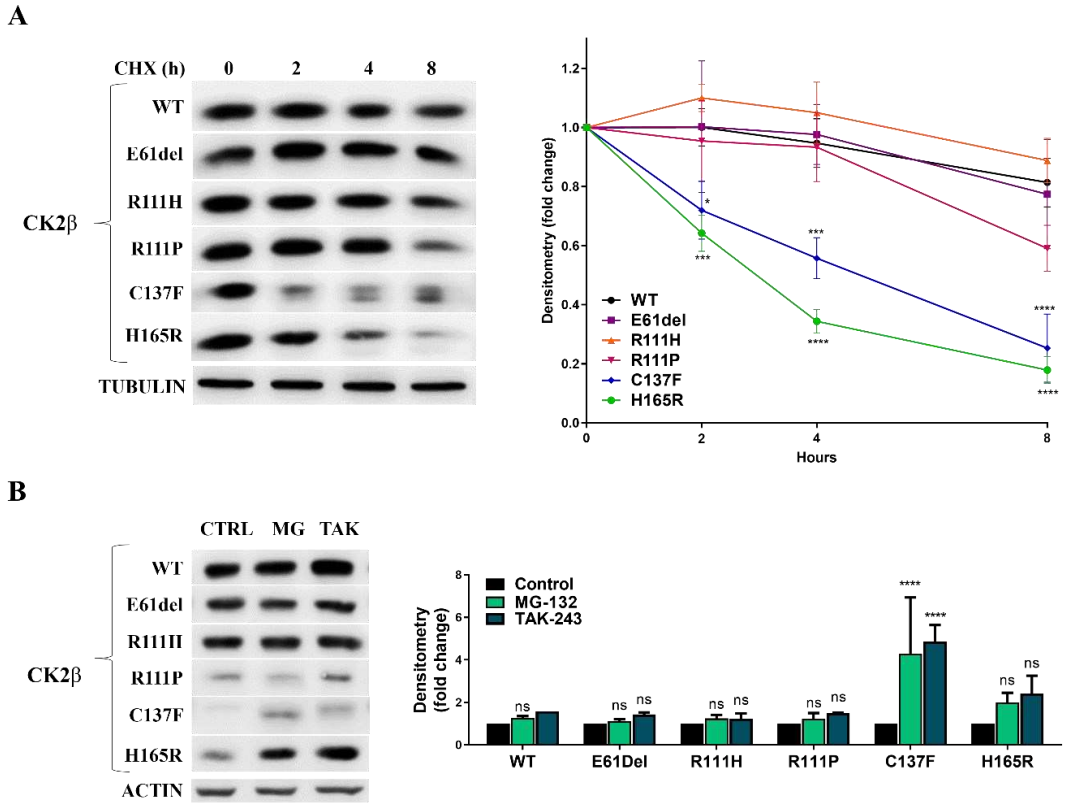

Figure 28. POBINDS CK2β mutants display differential protein stability.

CK2β expression levels of HEK-293AD CK2β knockout (KO) cells stably transfected with the selected POBINDS variants (E61del, R111H, R111P, C137F and H165R) after (A) treatment with cycloheximide (CHX) 100 µg/mL for 2, 4 or 8 hours and (B) treatment with 10 µM MG-132 or 100

nM TAK-243 for 16 hours. CK2β WT–transfected HEK-293AD CK2β KO cells were used as control. The results are normalized by the loading control (tubulin or actin). Representative images of Western blot from (A) 3 and (B) 2 independent experiments are shown, where 20 µg of proteins were loaded (left). Quantification upon normalization to the loading control (tubulin or actin) is shown on the right, with data presented as mean ± SD. Statistical analysis was performed with two-way ANOVA (A) or one-way ANOVA (B) with Dunnett's post test. ns no significant, *P < 0.05, **P < 0.01, ***P <0.005, ****P < 0.001. Data with no statistical analysis are results from one independent experiment.

This reduced stability of some mutants suggested that their lower cellular levels were due to increased degradation of the protein. Little is known about the regulation of the CK2β subunit turnover; however, it has been demonstrated that CK2β is prone to ubiquitination and consequent proteasome-degradation (French et al., 2007). Therefore, we decided to check if the reduced stability displayed by the CK2β C137F and H165R mutants was due to proteasome-dependent degradation. To this purpose, we analyzed the CK2β levels of the stably transfected cells after treatments with the proteasome inhibitor MG-132 (Holecek et al., 2006), or the inhibitor of the ubiquitin activating enzyme (UAE) TAK-243 (Hyer et al., 2018). As shown in Figure 28B, treatments with both compounds strongly increased the protein amounts of CK2β C137F mutant and slightly increased the levels of the CK2β H165R mutant, thus suggesting that their reduced cellular levels (see Figure 27) are mainly due to an abnormally high proteasome-dependent degradation.

3.4. POBINDS CK2β mutants display different CK2 activity

Since CK2β plays an important role in the regulation of the catalytic activity, stability and substrate specificity of the tetrameric CK2 (see INTRODUCTION 2.1.2), to understand whether the *CSNK2B* variants affect cellular CK2 functions, we analyzed the phosphorylation levels of three CK2 substrates: Akt1 at S129 (Di Maira et al., 2005, 2009), NF-kB at S529 (Wang et al., 2000) and EIF2β at S2 (Llorens et al., 2006), and used them to evaluate the functionality of the selected CK2β mutants. As shown in Figure 29, the transfection of the CK2β R111P, C137F and H165R mutants did not recover CK2 activity, as they displayed

strongly reduced phosphorylation levels of the Akt, NF-kB and EIF2β sites, similarly to those observed in not transfected KO cells. On the contrary, the CK2β E61del and R111H mutants recovered CK2 activity to an extent similar to the WT-transfected cells. Interestingly, the E61del mutant showed a reduction of the phosphorylation levels of EIF2β but not of the Akt and NF-kB sites, suggesting that the effect of this mutant might be substrate-dependent.

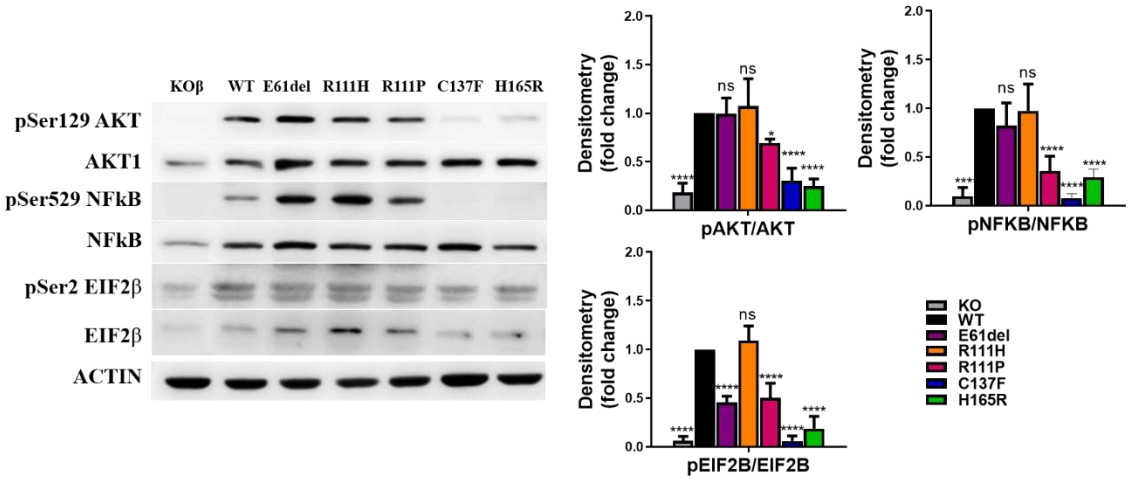

Figure 29. POBINDS CK2β mutants display different CK2 activity.

CK2 activity, analyzed by the phosphorylation levels of three substrates: pS129 Akt1, pS529 NF-kB and pS2 EIF2β, of HEK-293AD CK2β knockout cells stably transfected with the selected POBINDS variants (E61del, R111H, R111P, C137F and H165R) or CK2β WT as control. Representative images of Western blot from 3 independent experiments are shown, where 20 µg of proteins were loaded (left). Quantification upon normalization to the loading control (actin) is shown on the right, with data presented as mean ± SD. Statistical analysis was performed with one-way ANOVA with Dunnett's post test. ns no significant, *P < 0.05, **P < 0.01, ***P <0.005, ****P < 0.001.

To evaluate whether the reduction of the CK2 activity displayed by the CK2β H165R and C137F mutants was intrinsically related to the mutations or due to the reduced protein amount (see Figure 27 and 28A), we increased their CK2β levels by treatment with MG-132 or TAK-243 (see Figure 28B) and evaluated CK2 activity by checking the phosphorylation level of Akt at S129 and EIF2β at S2. As shown in Figure 30, the increase of both CK2β C137F and H165R mutant protein levels after TAK-243 treatment, resulted in a slight increase of the Akt phospho-S129 and EIF2β phospho-S2. These results, although preliminary, would suggest that the reduction of the CK2 activity displayed by these two mutants is at least

in part due to the loss of stability.

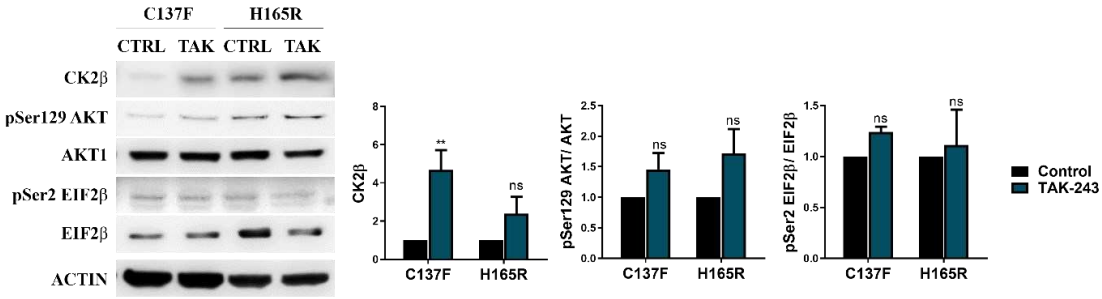

Figure 30. The reduced activity of POBINDS C137F and H165R CK2β mutants depends on their reduced protein levels.

CK2β and CK2 substrates pS129 Akt1 and pS2 EIF2β levels of C137F-transfected and H165R-transfected HEK-293AD CK2β knockout cells after treatment with 10 μM MG-132 or 100 nM TAK-243 for 16 hours, to increase CK2β protein amount. CK2β WT–transfected HEK-293AD CK2β KO cells were used as control. Representative images of Western blot from 2 independent experiments are shown, where 20 μg of proteins were loaded (left). Quantification upon normalization to the loading control (actin) is shown on the right, with data presented as mean ± SD. Statistical analysis was performed with one-way ANOVA with Dunnett's post test. ns no significant, *P < 0.05, **P < 0.01, ***P <0.005, ****P < 0.001.

4. Discussion

Our study is the first biochemical characterization of POBINDS *CSNK2B* variants. We focused our research on a group of five mutants that were identified in Italian POBINDS patients. We found that, when we transfected them in the established cellular model, three of them, namely R111P, C137F and H165R, displayed reduced expression. We demonstrated that these three mutants showed impaired CK2 activity, but, at least for the H165R and C137F mutants, this is a consequence of a reduced protein stability due to increased proteasome-dependent degradation. Instead, in the case of the CK2β mutants E61del and R111H, that were expressed at levels similar to the CK2β WT, no obvious alterations in the biochemical characteristics analyzed so far was found for the R111H, while the E61del mutant showed hampered phosphorylation of only one of the analyzed CK2 substrates, suggesting that this mutation does not globally reduce the activity but probably affects the substrate selection.

To go in more detail, we can analyze our results in comparison of the effects expected from the literature and the *in silico* hypothesis. Concerning the C137F mutant, our results were somehow expected. In fact, using six functional prediction programs, Unni and collaborators had predicted that this mutation should strongly impact on the enzyme functionality (Unni et al., 2022), since the C137 is one of the four conserved cysteine residues located within the CK2β zinc-finger region (aa 105–146) that coordinate Zn^{2+} ions. This process is essential for the β-β subunit dimerization, which in turn, is necessary for the CK2 holoenzyme formation (Canton et al., 2001). Mutations in any of these cysteine residues have a high probability of interfering with the zinc finger structure. Moreover, the replacement of the cysteine with a phenylalanine can cause steric clash with the neighboring residues due to the benzene ring (Unni et al., 2022). Our results are consistent with these predictions, since this mutant is the one with the strongest biochemical alterations among the five studied mutants, with a very reduced stability and an almost complete abrogation of CK2 activity.

Compared to the C137F mutant, the H165R mutant displayed a milder alteration in its stability, with a less reduced protein expression. The residue H165 is buried inside the α-helix structure forming part of the hydrophobic cluster of the CK2β dimerization interface, and its mutation to arginine, that may induce steric

hindrance, has been predicted to produce a local structural change due to the rupture of the hydrogen bond with its neighbor residue G162 (Niefind et al., 2001; Yang et al., 2021). Interestingly, despite the higher protein level compared to the C137F mutant, the H165R mutant almost completely abrogated the CK2 activity, consistently with the *in silico* prediction by Unni and collaborators (Unni et al., 2022).

The R111P and R111H mutants are particularly interesting, as R111 is a buried residue also located within the CK2β zinc-finger region, and the mutation to proline has been suggested to produce a structural rearrangement, thus affecting the coordination of the Zn^{2+} ions (Lolli, Pinna, & Battistutta, 2012; Niefind et al., 2001; Unni et al., 2022). Interestingly, the R111P mutation, that through *in silico* analysis has been predicted to produce functional impact (Unni et al., 2022), showed reduction of the protein level, that seems not sensitive to the inhibitors of the proteasome system, and a reduced CK2 activity. Instead, when we analyzed the mutation of this arginine to histidine (R111H), intriguingly, our results indicated that this mutation did not induce any significant difference in the expression, stability, and activity, compared to the WT.

Another mutant that did not show obvious differences to the CK2β WT is CK2β E61del. The residue E61 is located in the CK2β acidic loop (aa 55–64), a domain that can bind to the CK2α basic cluster and down-regulate CK2 activity by impeding the access of negatively charged substrates to the active site (Boldyreff et al., 1994; Marin et al., 1997). On this basis, changes at this site could be expected to prevent the formation of the tetrameric holoenzyme and alter CK2 activity. In contrast, from the results obtained so far, we can say that the expression and stability of the protein is not affected by this mutation, suggesting a normal assembly of the holoenzyme. However, this mutant showed reduced phosphorylation of one of the CK2 substrates analyzed, indicating that this mutation might affect the CK2 activity in a substrate dependent manner.

An important line of considerations that can be done with our results involves the correlation between the biochemical properties displayed by the CK2β mutants and the clinical phenotype of the patients that carry them. In the case of the CK2β H165R mutant, a certain correlation occurs: we found a strong reduction of the protein levels, stability and especially of the CK2 activity. This is in agreement with the phenotype of the 4 reported patients with this mutation (Table IV,

modified from Li et al., 2023), who display similar clinical features, which include an extremely early onset of seizures (days/newborn), profound intellectual disability (ID), severe developmental disability (DD), different facial deformities among other symptoms. However, and similar to what described in previous works (Bonanni et al., 2021; Di Stazio et al., 2023; Li et al., 2023; Orsini et al., 2022; Yang et al., 2022), in general, we did not find a clear correlation between the biochemical features of the studied CK2β mutants and the reported symptomatology of the patients carrying the respective *CSNK2B* variants, showed in Table IV (modified from Li et al., 2023). The clearest example is the CK2β R111H mutant: our work did not highlight alteration neither in protein expression and stability nor in CK2 activity compared to the CK2β WT, while the patient with this variant presents a severe phenotype with generalized tonic–clonic seizure, profound ID and DD.

The difficulty in finding a correlation between clinical phenotype and the biochemical properties of the CK2β mutants might have different explanations. First of all, data obtained so far are only a preliminary characterization of the mutants, and several other biochemical properties will require deeper investigation. We plan to investigate the ability of the mutants to form the β-β dimer, to bind the CK2 catalytic subunits α and α', and to interact and/or form complexes with other proteins. It is also worth to notice that the function of CK2β on CK2 activity is mainly in the selection of substrates. Therefore, it is possible that the effect of a mutation is exerted on a certain substrate and not on the global activity of the enzyme. Our evaluation was performed using the most common CK2 substrates, but it does not necessarily reveal the whole panorama, and a god idea might be, if not a phospho-proteome analysis of the transfected cells, at least to focus on pathways associated to embryogenesis and neural development, where the detrimental effects of POBINDS mutants may be exerted. For example, there has been recently reported two *CSNK2B* variants linked to a new intellectual disability-craniodigital syndrome (IDCS), different from POBINDS, in which the missense mutations D32H and D32N downregulated the Wnt-signaling, which is involved in animal developmental (Asif et al., 2022; Hayat et al., 2022).

Table IV. Symptomatology of POBINDS patients carrying the selected *CSNK2B* variants (modified from Li et al., 2023).

Variant	Gender	Age	Seizure/ Onset time	Epilepsy types	EEG	MRI	DD	ID	Hypotonia	Autism	Facial deformities	Speech impediment	Impairment of psychomotor development	Other	Reference
E61del	F	18 years	8 months	febrile seizures	/	+	+	+ (profound)	+	/	depressed and receding forehead, hypertelorism, prominent glabella, low-placed ears, short filter, small, teeth diastasis and retrognathia	speech delay	motor delay (profound)	lymphedema, severe scoliosis, long tapered fingers, and cardiac anomalies	Orsini et al, 2022
R111H	F	16 months	16 months	GTC	+	+	+ (profound)	+ (profound)	-	/	high palatal arch and microcephaly	speech delay	motor delay (profound)	infantile spasms, spastic hypertonus (profound)	Orsini et al, 2022
R111P	M	5+ years	13 months	myoclonic epilepsy, GTC	+	+	+ (mild)	+ (moderate)	/	/	/	speaking only several words	/	/	Yang et al , 2022
	M	9+ years	/	/	/	-	-	-	/	/	/	-	/	growth retardation, LD	Yang et al , 2022
	M	2 years	5 months	GTC	-	-	+(mild)	+(mild)	-	/	-	speech delay	motor delay	-	Li et al, 2019
	F	16 months	5 months	GTC	-	-	+(mild)	+(mild)	-	/	-	speech delay	motor delay	-	Li et al, 2019
C137F	F	7 months	5 months	tonic–clonic	-	-	+(mild)	+(mild)	-	-	-	-	hyperactive, difficult to concentrate, motor delay	-	Yang et al, 2021
	F	2 years	6 months	GTC	+	-	-	-	-	/	-	-	-	-	Li et al 2019
H165R	F	7 months	Newborn	focal motor seizures, myoclonic spasms	-	-	+ (Profound)	+ (profound)	+	/	simultaneous apnea, bilateral strabismus, tongue protrusion, dysplastic ears (overfolded helix)	+	gross motor development delay	myoclonic movements, obstructive laryngomalacia	Wilke et al, 2022
	M	7 days	7 days	focal-clonic seizure	+	+	+	+ (profound)	+	+	a triangular-shaped face, small nose, horizontal eye rims, and small and round ears	/	poor motor skills	distal dystonia, laryngomalacia, hypoacusia, and growth restriction	Orsini et al 2022
	M	8 months	5 days	myoclonic	+	-	+ (profound)	+ (profound)	-	-	-	monosyllabic	motor delay	-	Yang et al, 2021
	M	7 years	3 days	focal seizures	/	+	+ (bedridden)	+ (Profound)	-	-	inverted mouth shape	speech delay, not able speak any meaningful words	+	acute gastroenteritis, frequent acute pneumonia, GERD	Nakashima et al, 2019

F: Female. **M:** Male. **+**: Positive. **-**: Negatives. **+/-**: Boundary. **/**: Not available
GTC: Generalized tonic-clonic. **ID**: Intellectual disability. **DD:** Developmental delay. **LD:** learning disability. **ADHD:** Attention deficit hyperactivity disorder. **GERD:** Gastroesophageal reflux disease.. **EEG:** electroencephalogram.

Another possible cause of the difficulty to find correlations between the biochemical characteristics and the clinical phenotype is that, as often observed in genetic syndromes, the mechanisms underlying the POBINDS phenotype are much more complex than what apparently expected, being dependent on the specific patient “environment” where a *CSNK2B* variant is expressed. This can be exemplified by two recently described familiar cases (Trivisano et al., 2023), in which the patients present the same *CSNK2B* variant but quite different symptomatology. This is especially clear among the three cases of the Family 2, as reported in Table V (modified from Trivisano et al., 2023). Of course, we can only speculate on this, imagining, for example, that a certain CK2 substrate, whose phosphorylation is hampered by a mutation, could be by chance particularly highly expressed in the cells of a certain patient. In this case, even a partial phosphorylation could provide enough phospho-molecules to ensure the proper function of that protein. This hypothetical patient would have a milder phenotype than a patient with the same mutation, but lower amount of the specific CK2 protein substrate.

As mentioned above, this is only the first step of our biochemical/biological characterization, since, while we will continue working with the cellular model in here presented, we are now also close to evaluate patients’ samples and to establish animal models for further studies.

Table V. Symptomatology of POBINDS familiar cases (modified from Trivisano et al., 2023)

	Family 1		Family 2		
	Case 1	Case 2	Case 1	Case 2	Case 3
Age at study	9 y	34 y	17 y	11 y	42 y
Gender	M	M	F	F	F
CSNK2B variant	NM_001320: c.175 + 1G > C; p.?	NM_001320: c.175 + 1G > C; p.?	NM_001320: c.142C > T; p. Gln48Ter	NM_001320: c.142C > T; p. Gln48Ter	NM_001320: c.142C > T; p. Gln48Ter
Previously reported variant	no	no	no	no	No
Inheritance	Inherited	n.a.	Inherited	Inherited	n.a.
Age at walking	4 y	n.a.	4 y	18 m	n.a.
Age at first words	4 y 6 m	n.a.	n.a., language delay	12 m	n.a.
Cognitive disability (age)	Moderate ID (IQ n.a.) (9 y)	Mild disability FIQ = 61; VCI = 61; PRI = 75; WMI = 75; PSI = 72 (33 y)	Mild disability IQ = 62 (17 y)	No disability IQ = 90 (11 y)	Mild disability (IQ n.a.) (42 y)
Behavioral problems	Disruptive behavior disorder	no	no	Attention deficit	Not collaborative and maladaptive behaviour
Epilepsy	yes	yes	yes	yes	yes
Age at epilepsy onset	3 m	3 y	2 y	10 y	9 m
Seizure type at onset	focal to bilateral seizures characterized by right eye deviation, sialorrhea, cyanosis, clonic jerks of four limbs	febrile seizures	febrile generalized tonic-clonic seizures	focal seizures characterized by loss of consciousness, sialorrhea, hypertonia, oral cyanosis	generalized
Seizure frequency at onset	daily	sporadic	sporadic	monthly	unknown
Other types of seizures during FU (age)	tonic-clonic generalized seizures (7 y)	no	seizures characterized by scream, eye deviation, diffuse hypertonia and bilateral clonic jerks (9 y), absence seizures (9 y)	absence seizures (10 y)	No
Drug resistance	yes	no	no	no	No
Seizure persistence at FU (frequency)	yes, monthly	no	yes, monthly	yes, sporadic	Yes, sporadic
Current ASMs	LTG, VPA, CLB	none	ETS	ETS, LEV	VPA
Previous ASMs	PB	none	ETS	LEV	VPA
EEG (age)	Normal BA, sporadic diffuse epileptiform abnormalities (7 y 5 m);Slow BA, no epileptic abnormalities (9 y 5 m)	Normal (33 y)	Slow BA, generalized epileptic abnormalities (12 y);Normal BA, bilateral T epileptic abnormalities (17 y)	Normal BA, multifocal and generalized epileptic abnormalities (10 y 9 m); Slow BA, Multifocal epileptiform abnormalities during awake and diffuse during sleep (11 y 4 m)	n.a.
Other electrophysiological test	VEP and SEP normal	no	no	no	no
Other Neurological signs	ataxia	no	no	no	no
Brain MR	normal	n.a.	pineal gland abnormalities	n.a.	n.a.
Dysmorphisms	Arched upper lip with dental diastema and large central upper incisors, elongated face, prognathism, open mouth, with downturned corners	Elongated face, dental abnormalities, prognathism	Elongated face, ptosis, strabismus, bulbous nose, dental diastema, large central incisors	Bulbous nose, prominence of upper dental arch, extroverted lower lip	Elongated face, large superior incisors, prognathism
Other comorbidities	Aortic root dilatation (Z-score 2, 4)	Growth retardation in infancy	no	no	no

n.a.: not available; **y**: years; **m:** months; **M:** male; **F:** female; **EEG:** electroencephalography; **MRI:** magnetic resonance; **VEP:** visual evoked potentials; **SEP:** somatosensory evoked potential; **DQ:** Developmental Quotient; **IQ:** Intellectual Quotient; **FIQ:** Full Intellectual Quotient; **VCI:** Verbal Comprehension Index; **PRI:** Perceptual Reasoning Index; **WMI:** Working Memory Index; **PSI:** Processing Speed Index; **LEV:** levetiracetam; **VPA:** valproate; **CBZ:** carbamazepine; **ETS:** ethosuximide; **CLB:** clobazam; **PB:** phenobarbital; **MDZ:** midazolam; **FU:** follow-up; **ASMs**: anti-seizure medications; **BA:** background activity; **F:** frontal; **C:** central; **T:** temporal; **P:** parietal; **O:** occipital; **Fam** = Family; **ACMG:** American College of Medical Genetics and Genomics; **P:** pathogenic; **LP:** likely pathogenic

CHAPTER IV: CK2 INTERACTION WITH SARS-COV-2 NUCLEOCAPSID PROTEIN

1. Introduction

1.1. Severe Acute Respiratory Syndrome Coronavirus 2 (SARS-CoV-2)

Coronaviruses (CoVs) (family *Coronaviridae*) are subdivided into four genera: α, β, γ, and δ; meanwhile α and β coronaviruses infect mammals, γ and δ principally infect birds. Most of the known human coronaviruses produce common cold symptoms in the infected subjects. However, three zoonotic β coronaviruses have been reported to cause severe symptoms in humans: the Severe Acute Respiratory Syndrome Coronavirus (SARS-CoV) (Drosten et al., 2003), the Middle East Respiratory Syndrome-Related Coronavirus (MERS-CoV) (Zaki et al., 2012), and the Severe Acute Respiratory Syndrome Coronavirus 2 (SARS-CoV-2) (Zhu et al., 2020). SARS-CoV-2 is the causative of COVID-19, and it was first detected in late 2019 in patients with pneumonia in Wuhan, China.

The SARS-CoV-2 virus encodes four structural proteins, namely membrane (M) protein, nucleocapsid (N) protein, envelope (E) protein and spike (S) glycoprotein, that form an envelope virion. In addition, the virus encodes the non-structural proteins, that mostly compose the viral replication and transcription complex, and the accessory proteins that usually exert immunoevasive roles. SARS-CoV-2 virus has a positive-sense single-stranded RNA genome (+ssRNA), which is encapsidated by the N protein. During the virion assembly process, the M and E proteins ensure the incorporation of the RNA genome into the viral particle, while the S protein trimers provide specificity for cellular entry receptors. The general life cycle of the coronavirus virion involves the attachment of the S protein S1 domain to the host cell receptor ACE2, which allows the cleavage of the S protein by the cell surface serine protease TMPRSS2, promoting viral uptake and fusion at the cellular membrane. After the release and uncoating of the viral RNA, the polyproteins pp1a and pp1ab are further processed into individual non-structural proteins, as the RNA replicase–transcriptase complex (RdRp), which in turn, is responsible for the replication of the structural protein. After translation of the structural protein, the N protein remains in the cytoplasm, where encapsidates the viral RNA, while the S, E and M proteins translocate into

the host endoplasmic reticulum (ER) to then translocate to the ER-to-Golgi intermediate compartment (ERGIC). Is in the ERGIC where all the structural proteins and the encapsidated RNA interact to start the budding process towards the final secretion of the virions from the infected cells by exocytosis (Lamers & Haagmans, 2022; V'kovski et al., 2021).

To promote the infection and its replication, SARS-CoV-2, similarly to others viruses, modulate complex crosstalk between different signaling pathways, activating several host cell kinases (Chatterjee & Thakur, 2022). As early as the beginning of COVID-19 pandemic, different works suggested CK2 to be among the host protein kinases exploited by SARS-CoV-2, thus representing a prominent druggable candidate (Bouhaddou et al., 2020; Gordon et al., 2020a, 2020b). In particular, in an affinity-purification/mass spectrometry analysis, Gordon and collaborators (Gordon et al., 2020a) identified CK2 among the human proteins that physically associate with SARS-CoV-2 proteins. CK2 involvement was suggested to be important in stress granule regulation; consistently, its pharmacological inhibition disrupted stress granules in SARS-CoV-2 infected cells. The global phosphorylation landscape of SARS-CoV-2 infection (Bouhaddou et al., 2020) reported upregulation of several CK2-dependent phospho-sites of viral and host cell proteins in SARS-CoV-2 infected Vero E6 cells, suggesting enhanced CK2 activity upon SARS-CoV-2 infection. Moreover, this work revealed CK2 co-localization with the viral N protein in infection-induced filopodia protrusions with budding viral particles in Caco-2 cells. This results were supported by a second study of Gordon and collaborators (Gordon et al., 2020b), that found interaction of both CK2 catalytic subunits, α and α', and the CK2β regulatory subunit with the viral N protein after affinity-purification/mass spectrometry analysis of SARS-CoV-2 infected cells. Moreover, among the suggested 22 sites reported to be phosphorylated in N protein, two of them are predicted to be CK2 target (Bouhaddou et al., 2020; Davidson et al., 2020). Additionally, transcriptome and computational analyses of SARS-CoV-2 infected Calu-3 cells showed activation of CK2 (Shaath & Alajez, 2020), and Fatoki and coworkers described CK2 as one of the key players in the SARS-CoV-2 lifecycle (Fatoki et al., 2021).

1.1.1. SARS-CoV-2 Nucleocapsid protein

The SARS-CoV-2 N protein, composed of 419 amino acids, is encoded by the open reading frame ORF9 of the virus and its fundamental function is the packaging of the viral genome into a long helical ribonucleocapsid complex. As shown in Figure 31A, five domains have been described in the N protein: a N-terminal domain (NTD), a RNA-binding domain (RBD), a predicted disordered central linker (LINK), a dimerization domain, and a C-terminal domain (CTD) (Cubuk et al., 2021). Although the structure of the full-length N protein is not yet available, some structural features are known, as for example that the NTD folds into six antiparallel β-sheets with a protruding positively charged β-hairpin that forms a basic finger, while the CTD assembles into a cuboid shape composed of homologous dimers (Yan et al., 2022). The RNA binding sites reside between the NTD protruding β-hairpin and the core structure (Yan et al., 2022), as shown in Figure 31B.

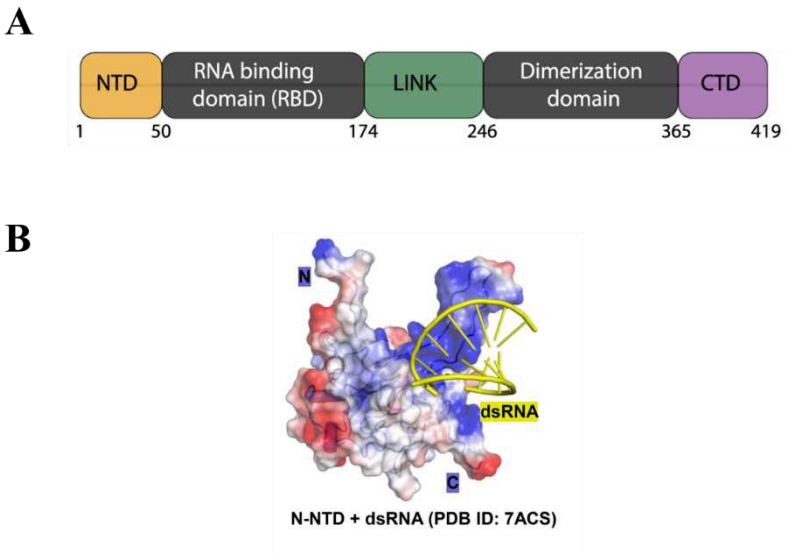

Figure 31. Structural representation of the of the SARS-CoV-2 N protein.

(A) Schematic representation of the SARS-CoV-2 N protein domains. (B) SARS-CoV-2 N protein N-terminal domain in complex with double strand RNA. Positive charge potential is presented in blue, while negative charge potential is presented in red. N-terminal domain (NTD), RNA-binding domain (RBD), central linker (LINK), C-terminal domain (CTD), double strand RNA (dsRNA) (modified from (A) Cubuk et al., 2021; (B) Yan et al., 2022).

In other coronaviruses, the N protein has also regulatory roles in the viral life cycle, controlling the host cellular machinery (Kopecky-Bromberg et al., 2007; Surjit et al., 2006). This seems also probable for the SARS-CoV-2 N-protein, since, among CoVs, the N protein sequence is highly conserved, and it represents one of the most abundant structural proteins in virus-infected cells (He et al., 2004).

Interestingly, the SARS-CoV-2 N-protein is not the only N protein that has been suggested to interact with CK2, as there is evidence of biological important relationships between N protein and CK2 in different CoVs. For example, in Avian infectious bronchitis coronavirus (IBV), a lower affinity for random RNA by the N protein was linked to the phosphorylation of four predicted CK2 sites (Chen et al., 2005). Later, it was demonstrated that two of these sites were phosphorylated by a different kinase activated during IBV replication (ataxia-telangiectasia mutated and Rad3-related, ATR) (Fang et al., 2013). CK2 has also been suggested to be one of the kinases that, by phosphorylating SARS-CoV N protein, allows its binding to 14-3-3 proteins allowing its translocation to the cytoplasm (Surjit et al., 2006). Gordon and coworkers found association of SARS-CoV and MERS N protein with all the three CK2 subunits, although the consequences were not elucidated by the authors (Gordon et al., 2020b).

In summary, the N proteins/CK2 connections seem to be a common feature of CoVs-infected cells.

1.2. CK2 activity stimulation upon viral infection

As described in the introduction (see INTRODUCTION 1.2.3), most of the kinases are in an inactive conformation and their activation in response to specific stimuli usually requires a phosphorylation event and/or binding to a specific effector (Endicott et al., 2012). However, this is not true for all kinases, and specifically CK2 has been described as a constitutively active enzyme, structurally “locked” in an active conformation, thus not needing any phosphorylation event or a second messenger to be catalytically competent. Despite this permanent active state, it is known that CK2 can undergo a sort of regulation in different cellular conditions (see INTRODUCTION 2.3), for example by binding to other molecules (Borgo et al., 2021b).

Several examples have been reported of protein interactions suggested to increase the activity of CK2. The activation is often exerted towards a specific substrate, as for the binding of CK2α and CK2β to FGF-1 during cell proliferation, reported to stimulate the autophosphorylation of CK2β (Skjerpen et al., 2002). Many other cases are known, as shown in Table I (see INTRODUCTION 2.3), although the effective *in vivo* relevance of these findings is often still to be proven. Several viruses exploit CK2 to complete their replication and life cycle, thus it is not surprising that CK2 activity stimulation has been observed also upon virus infection. One of the first observations was in human cytomegalovirus transformed cells, which, compared to normal cells, displayed an increment of CK2 activity due to increased CK2 protein levels (Muganda et al., 1995). Similarly, transgenic mice expressing the hepatitis C virus (HCV) core and F proteins reveled increased CK2β protein levels (Hu et al., 2013), and transfection of the HCV core protein in hepatoma cells produced stimulation of CK2 expression and CK2 activity (Foka et al., 2014).

While in all these cases the increased CK2 activity was due to higher protein expression levels, in the case of the influenza A virus (H1N1), CK2 activity was higher in infected cells without changes in its protein level (Hui & Nayak, 2002). Similarly, increased CK2 activity without increased CK2 levels was observed in cells infected by the herpes simplex virus type 1 (HSV-1), and this was interpreted as due to interaction with the ICP27 viral protein (Koffa et al., 2003). Another example is the Epstein-Barr Nuclear Antigen 1 (EBNA1) viral protein that, through its binding to CK2β, increases CK2 association and consequent phosphorylation of the promyelocytic leukemia protein (PML) (Sivachandran et al., 2010). Virus-dependent CK2 stimulation was also observed by the Rev protein of the immunodeficiency virus type-1 (HIV-1); in this case the protein is both a CK2 substrate (Meggio et al., 1996) and a potent activator of CK2 (Ohtsuki et al., 1998), however these data were produced only *in vitro.*

2. Aim

Although there is strong evidence supporting a connection between SARS-CoV-2 and CK2 in infected cells, the direct evidence of CK2 activation by the viral proteins and the actual phosphorylation of N protein by CK2 have not been demonstrated. Our work hypothesizes that SARS-CoV-2 N protein is phosphorylated by CK2 and that the activation of CK2 observed in SARS-CoV-2 infected cells is mediated by its interaction with the N protein.
To test this hypothesis, our aims were:

i. To evaluate the direct phosphorylation of SARS-CoV-2 N protein by CK2

To evaluate if CK2 can directly phosphorylate SARS-CoV-2 N protein, we performed several *in vitro* phosphorylation assays using recombinant CK2 and N protein.

ii. To assess the effect of SARS-CoV-2 N protein on CK2 activity

To understand whether SARS-CoV-2 N protein can increase CK2 activity, we performed several *in vitro* phosphorylation assays to evaluate the activity of recombinant CK2 towards model peptide and protein substrates, in the presence of recombinant N protein.

iii. To assess the interaction of SARS-CoV-2 N protein and CK2 in cells

To evaluate if CK2 and SARS-CoV-2 N protein interact in cells, following an increase of the CK2 activity, we established a cellular model using HEK-293AD and HEK-293AD CK2β knockout (KO) cell clones stably transfected with the N-protein.

3. Results

3.1. CK2 phosphorylates the SARS-CoV-2 N protein

To evaluate if CK2 can directly phosphorylate SARS-CoV-2 N protein, we performed *in vitro* radioactive phosphorylation assays using recombinant CK2 and recombinant SARS-CoV-2 N protein as substrate. As shown in Figure 32, the phosphorylation assays revealed that N protein is phosphorylated either by the tetrameric CK2 (Figure 32A) as well as by the monomeric subunit CK2α (Figure 32B). However, a stoichiometric analysis and a comparison between the level of phosphorylation of the N protein and of other known CK2 substrates (not shown), revealed that the level of phosphorylation of N protein was very low.

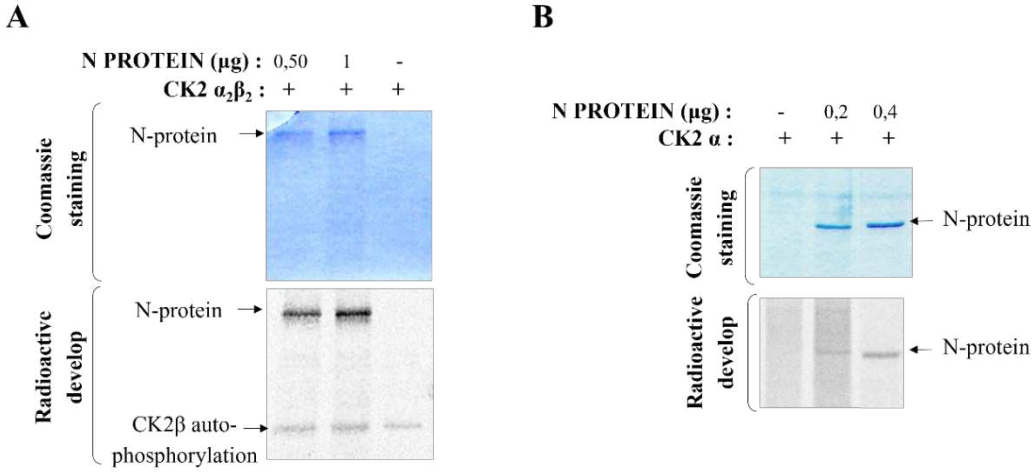

Figure 32. CK2 phosphorylates the SARS-CoV-2 N protein.

In vitro SARS-CoV-2 N protein phosphorylation using (A) 0.5 µg and 1 µg of recombinant N protein and 5 ng of recombinant tetrameric CK2 ($\alpha_2\beta_2$) or (B) 0.2 µg and 0.4 µg of recombinant N protein and 100 ng of monomeric CK2α. The proteins were incubated for 20 min at 30°C in the presence of a radioactive phosphorylation mixture. Phosphorylation was detected upon SDS-PAGE separation and digital autoradiography (Cyclone plus). Data are results from one independent experiment.

3.2. SARS-CoV-2 N protein strongly activates CK2 *in vitro*

To understand whether the SARS-CoV-2 N protein can increase CK2 activity, we

performed *in vitro* phosphorylation assays to evaluate the activity of recombinant tetrameric CK2 and the monomeric subunits CK2α and CK2α' towards the model peptide substrate CK2-tide, in the presence of increasing concentrations of recombinant N protein. As shown in Figure 33A, we found significantly increased activity of the tetrameric CK2 α2β2 as well as both catalytic subunits, upon the addition of N protein. This increase was dose-dependent, and it showed to be much more pronounced on CK2α, arriving up to a 5-fold increase, while CK2α' and tetrameric CK2 presented a more modest effect, of almost 2-fold increase. Therefore, we decided to investigate more in detail the effect of N protein on CK2 activity using CK2α. We evaluated the dose- and time-dependance of this strong activation. We observed that significant stimulatory effect starts at 100 ng of N protein and increases in a dose dependent manner, arriving to a plateau at 1000ng of N protein (Figure 33B). Moreover, at constant concentration of N protein, the effect over CK2α activity increases during the incubation time, at least up to 20 min (Figure 33C).

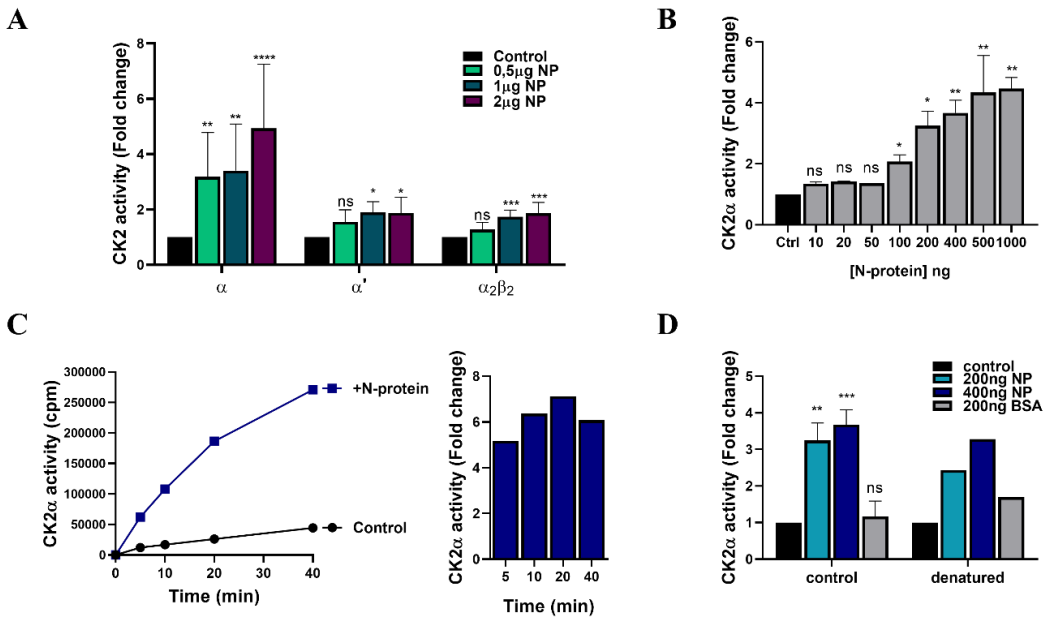

Figure 33. SARS-CoV-2 N protein increases CK2 activity towards a model peptide substrate.

In vitro CK2 activity towards CK2-tide peptide was measure using (A) CK2 α2β2 as well as both monomeric subunits CK2α and CK2α' in presence of 0.5, 1 and 2 µg of recombinant N protein. The proteins were incubated for 20 min at 30°C in the presence of a radioactive phosphorylation mixture; (B) CK2α in presence of increasing concentrations of recombinant N protein (10, 20, 50,100, 200, 400, 500 and 1000 ng). The proteins were incubated for 20 min at 30°C in the presence of a radioactive phosphorylation mixture; (C) CK2α in presence of 250 ng of recombinant N protein. The proteins were incubated for 5, 10, 20 and 40 min at 30°C in the

presence of a radioactive phosphorylation mixture; (D) CK2α in presence of 200 and 400 ng of native (control) or thermal denatured recombinant N protein. 200 ng of native and denatured bovine serum albumin (BSA) was used as control. The proteins were incubated for 20 min at 30°C in the presence of a radioactive phosphorylation mixture. Data from 2 independent experiments are presented as mean ± SD. Statistical analysis was performed with two-way ANOVA (A) or one-way ANOVA (B) with Dunnett's post test. ns no significant, *P < 0.05, **P < 0.01, ***P <0.005, ****P < 0.001. Data with no statistical analysis are results from one independent experiment.

Then, to assess whether the stimulation of CK2α activity requires N protein's tridimensional structure, we compared the effects of N protein in its native structure or after thermal treatment, expected to produce at least partial denaturation. Surprisingly, as shown in Figure 32.D, the activation of CK2α was also observed by using thermal denatured N-protein, suggesting that the stimulation does not require higher structure elements and that probably the responsible for the activation is a short element not affected by the denaturation. Figure 33D also shows that the stimulation of CK2α specifically requires the N-protein, pointing that unspecific proteins, as bovine serum albumin, neither native nor denatured, produce this increase of CK2α activity.

Additionally, we evaluated the effect of the SARS-CoV-2 N protein on the CK2α activity using one of its model protein substrates, casein. As shown in Figure 34, the N protein activated CK2α activity towards casein, however to a lower extent, compared to what observed towards the peptide substrate, reaching a maximum of 2.5-fold increase. This might be due to a possible steric hindrance that the N protein can produce, thus limiting accessibility to the catalytic site to bigger substrates when compared to small peptides.

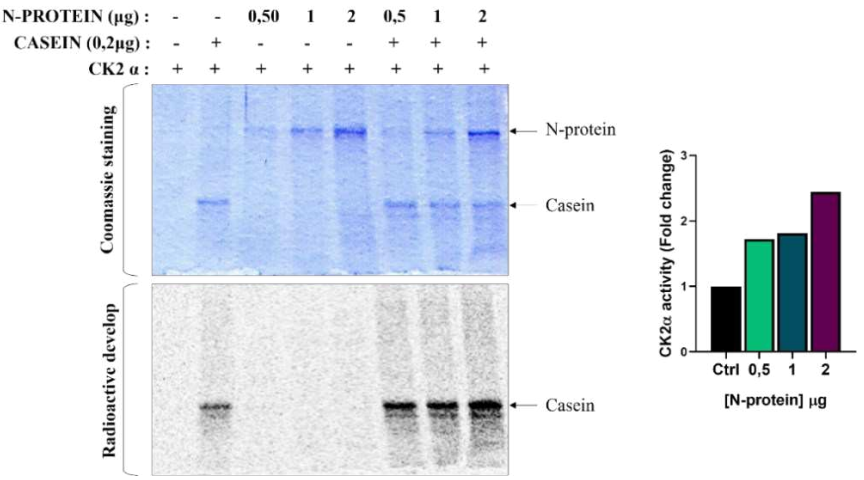

Figure 34. SARS-CoV-2 N protein increases CK2 activity towards model protein substrate.

In vitro CK2 activity towards casein was measure using CK2α in presence of 0.5, 1 and 2 µg of recombinant N protein. The proteins were incubated for 20 min at 30°C in the presence of a radioactive phosphorylation mixture. Phosphorylation was detected upon SDS-PAGE separation and digital autoradiography (Cyclone plus). Data are results from one independent experiment.

3.3. N-protein physically associates to CK2

We moved our investigation to the evaluation of the stimulatory effect of the SARS-CoV-2 N protein over CK2 activity in cells, and to this purpose we used HEK-293AD and HEK-293AD CK2β knockout (β KO) cell clones and stably transfected them with the HA-tagged N protein. In these cells, we first assessed the physical association between CK2 and N protein by co-immunoprecipitation experiments. As shown in Figure 35, we found co-precipitation of N protein with CK2α, and also the opposite, since CK2α co-precipitates with the precipitated HA-N protein. The association was observed both in HEK-293AD WT and β KO cells, suggesting that N protein interacts with CK2α independently of CK2β.

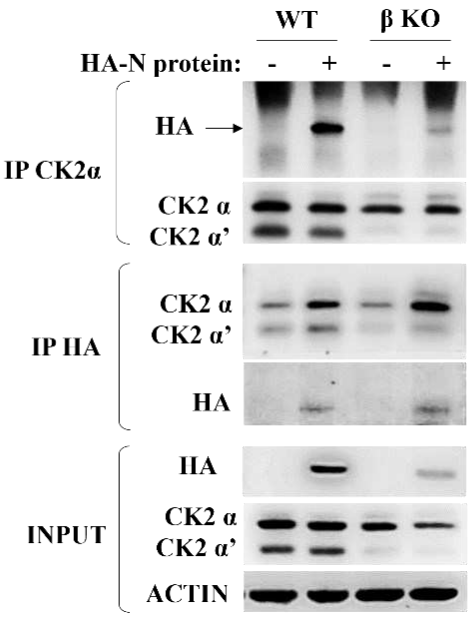

Figure 35. SARS-CoV-2 N protein physically interacts with CK2 in cells.

Immunoprecipitation of CK2α and HA-tagged N protein from protein lysates of HEK-293AD (WT) and HEK-293AD CK2β knockout (β KO) cells stably transfected with the HA-tagged N protein. Not-transfected cells (thus not expressing N-protein) were used as control (first and third lanes). Data are results from one independent experiment.

3.4. SARS-CoV-2 N protein enhances the phosphorylation level of CK2 substrates in cells

To evaluate if the activation of CK2 activity by the N protein also occurred in cells, we continue working with the HEK-293AD (WT) and HEK-293AD CK2β knockout (β KO) cell clones stably transfected with the HA-tagged N protein. Figure 36 shows different lysates of WT or βKO cells (two different clones) with increasing levels of N-protein expression (revealed by anti-HA antibody) due to increasing concentrations of puromycin, the antibiotic drug used to select the N-protein expressing cells. By exploiting a CK2 phospho-substrate antibody, that recognizes the consensus sequence for CK2 phosphorylation, we analyzed the cellular CK2-dependent phosphorylation levels by Western Blot in these lysates. As visible in fig 36, in the WT cells the expression of the N-protein did not produce significant increase of the bands recognized by the CK2 phospho-substrate antibody, when compared to the non-transfected WT cells. On the contrary, in β KO cells the presence of N protein is accompanied by an increase of some of the bands recognized by the CK2 phospho-substrate antibody, which are marked by the solid arrows in Figure 36. Interestingly, this increase is, at least in part, proportional to the N protein expression levels, and the phospho-bands affected by the expression of the N protein appear to be bands mainly reduced by lack of the CK2β subunit, as in the HEK-293T β KO are strongly reduced compared to WT cells.

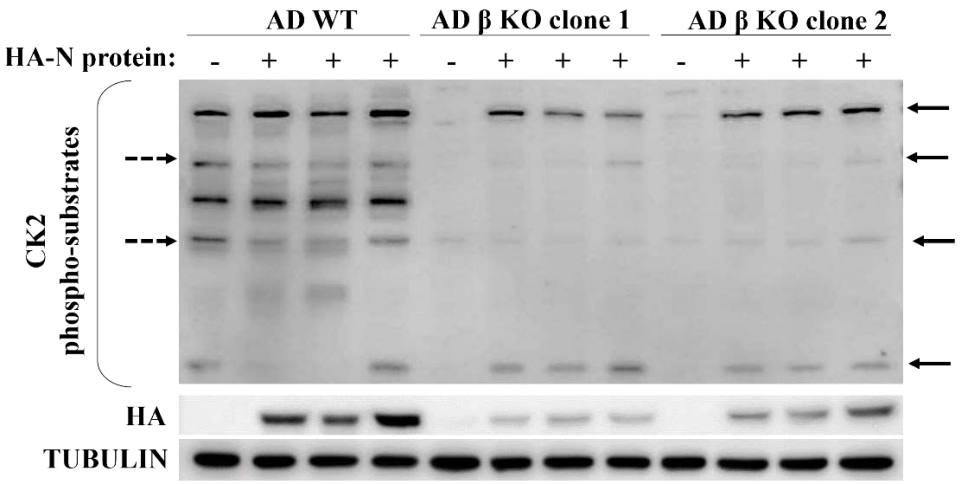

Figure 36. N protein enhances the phosphorylation level of CK2 cellular substrates.

Western blot of HEK-293AD (WT) and HEK-293AD CK2β knockout (β KO clone 1 and 2) cells stably expressing different levels of HA-tagged N protein. CK2-dependent phosphorylation levels detected by a CK2 phospho-substrate antibody that recognizes the consensus sequence for CK2 phosphorylation. Solid arrows mark the bands with a positive effect on CK2 activity by the N protein, while dashed arrows show bands with an inhibitory effect on CK2 activity by the N protein. Data are results from one independent experiment.

As probably expected, not all the phospho-bands recognized by the CK2 phospho-substrate antibody are affected by the presence of the N protein in the HEK-293T β KO cells. On this regard, it should be kept in mind that CK2 is also active as a monomer, and that one of the roles of CK2β is driving the substrate selection, a characteristic that probably cannot be fulfilled by the N protein. Moreover, as shown by the dashed arrows in Figure 35, we observed that in WT cells some of the phospho-bands recognized by the CK2 phospho-substrate are reduced upon transfection of the N protein, which might be associated to a possible competition with CK2β.

4. Discussion

Our results demonstrate that SARS-CoV-2 N protein is a lousy *in vitro* substrate of CK2 holoenzyme and CK2α. More strikingly, our results show that the SARS-CoV-2 N protein increases CK2 activity *in vitro* and in cells. Although *in vitro* the activation by the N protein was observed in CK2 holoenzyme, CK2α' and CK2α, the last one presented the stronger increase. Activation of CK2α by denatured N protein suggest that, rather than the tertiary structure, a short sequence region of the N protein might be the responsible of the effect observed on CK2α. Preliminary results obtained by an *in silico* analysis, in collaboration with Dr. Leonardi (University of Padova, Italy), allow to hypothesize that a relevant could be the [89-106] sequence of the N-protein. We are now producing the corresponding synthetic peptide to analyze its effect on CK2 activity, and, if the results are promising, we will conjugate the peptide to a cell-penetrating sequence to check its effects in cells.

As far as the CK2 side is concerned, our results suggest that the interaction with the N protein might be in a region of CK2α that is less accessible in the CK2 holoenzyme and probably less conserved in CK2α'.

The results that we obtained in cells allow interesting considerations. First, the strongest effects were observed in β KO cells, where the predominant catalytic subunit is CK2α, obviously not combined in the tetrameric holoenzyme. This is consistent with what observed *in vitro*, with the α monomeric form as the most sensitive to the activation, and with our co-precipitation experiments, that suggest a direct association to α, independent of the presence of β. Moreover, it is worth notice that N protein did not stimulate all the visible CK2-dependent phospho-bands, interestingly, the bands stimulated were mainly CK2 β-dependent bands, being strongly reduced in the KO cells. However, not all these bands were affected by the N protein expression. This is in line with the hypothesis that the N protein, by interacting with CK2α, can somehow mimic the effect of CK2β, not activating generically the enzyme but instead being involved in the substrate specificity. In this view, the inhibitory effect induced by the N protein on some of the CK2-dependent phospho-bands would not necessarily be a negative characteristic, as it could be similar to the negative regulation of CK2 activity by the β subunit (Pinna, 2002).

Since CK2 is mostly present in cells as the tetrameric holoenzyme, the fact that the strongest activation by the N protein is towards the catalytic monomer could put in doubt the relevance of our results. However, the holoenzyme presents dynamic properties and it has been suggested that monomeric CK2 could be transiently or locally present (Deshiere et al., 2013). It has also been suggested that CK2α could bind partners different from CK2β (Filhol et al., 2015; Filhol & Cochet, 2009). Additionally, from a therapeutic perspective our result can be interesting: to date, there are several CK2 inhibitors, including CX-4945 (Pierre et al., 2011) currently in clinical trials against COVID-19, but there are no CK2 activators available. Despite there is evidence of possible mechanisms of activation of CK2, a therapeutic activator has never been considered necessary, since in most diseases where CK2 is involved, it is overexpressed/upregulated. However, the recently discovered neurodevelopmental disorders caused by mutations in the genes for CK2 α and β (Ballardin et al., 2022) have highlighted the importance to develop also CK2 activators. In this context, our results represent an initial step for the development of a CK2 activator.

GENERAL CONCLUSION

This thesis evaluated different aspects of the involvement of CK2 in four non–related diseases: Friedrich ataxia (FRDA), chronic myeloid leukemia (CML), Poirier–Bienvenu neurodevelopmental syndrome (POBINDS) and COVID-19.
The involvement of CK2 in several diseases has been known for many years, and, since it is a constitutively active enzyme, essential in virtually all cellular processes, one can be induced to think that the problem in these diseases is associated to its loss of function. Instead, in most of the pathological conditions where its involvement has been described, CK2 was found to be “too much”. Despite the mechanisms underlying this “too much” condition can extensively vary between diseases, the usage of CK2 inhibitors has been suggested as a valuable strategy for different pathologies, especially, but not only, several types of cancer. It has been also demonstrated that targeting CK2 is not a problem for healthy cells, since cancer cells, which are addicted to CK2, are much more sensitive to its inhibition, therefore normal cells survive to inhibitor doses that are sufficient to induce cancer cell death. In this thesis, we confirm this historical view of CK2 as a therapeutic target to be inhibited, adding further evidence of conditions where this strategy can be pursued.
In fact:

1. in FRDA, we showed the involvement of CK2 in the turnover of the frataxin, the protein responsible for the pathology in this disease, and we provided initial evidence that CK2 inhibition in FRDA patient cells is able to increase frataxin levels and can therefore be interesting from a therapeutic point of view.
2. in CML, where CK2 was already known to be involved, we found encouraging results on the effects of CK2 inhibition in cells that are resistant to the first line CML therapy (the tyrosine kinase inhibitors, TKIs) due to the T315I mutation of BCR-ABL1. The patients harboring this mutation display one of the most severe CML phenotypes, and for them only third-generation TKI therapy is available, with unfortunately frequent and important side effects. Therefore, our finding of inhibitors that

efficiently induce apoptosis in these cells represent a promising alternative to be further investigated, either as monotherapy or in combination with TKIs (thus allowing to reduce the TKI effective doses).

3. in COVID-19, CK2 has already been proposed as a target, with the CK2 inhibitor CX-4945 in clinical trial for this disease. Here, we studied in detail the connection between the SARS-CoV-2 N protein and CK2, finding results that strongly support the value of CK2 inhibition in COVID-19. But our investigation on the CK2 activation by SARS-CoV-2 N protein has other important implications. Indeed, our study intends to arrive at the design of a CK2 activator.

Why should a CK2 activator be important?

The answer to this question refers to the fourth disease that we investigated in this thesis, POBINDS, and other similar conditions. In fact, only recently new conditions where CK2 was supposed to be “too low” have been discovered, the genetic diseases POBINDS and Okur-Chung (OCNDS). Here, we characterized for the first time some of the POBINDS mutants, founding that, at least for some of them, CK2 activity is indeed hampered, and a CK2 activator would be probably necessary. Our results showing the ability of the SARS-CoV-2 N protein to strongly activate CK2 are a first step for the potential development of a therapeutic CK2 activator: we are now identifying short peptides within the N protein sequence with the ability to activate CK2α, and, once this is confirmed, we aim at producing cell-permeable derivatives that will be tested as activators of CK2 in cells. The cellular model that we established for the analysis of the effects of the POBINDS mutations will be a valuable tool to initiate this analysis.

In summary, we can conclude that CK2 is a key molecule that, to maintain its physiological functionality, should be kept at the “right level”: if the “too much” condition, known for several years, has to be obviously avoided, we now know that also the “too low” condition exists with pathological implications. Our study provides evidence of the need for the right balance, and also preliminary suggests strategies to correct possible unbalanced conditions.

RELATED PROJECTS AND PUBLICATIONS

1. PROTEIN KINASE CK2 AND SARS-COV-2 REVIEW

CK2 has already been proposed as a target in COVID-19, with the CK2 inhibitor CX-4945 in clinical trial for this disease. Although the main aim of my work was the study of the connection between the SARS-CoV-2 N protein and CK2, I contributed to the review titled “Protein Kinase CK2 and SARS-CoV-2: An Expected Interplay Story” published in the journal *Kinases and Phosphatases*, which explore the relationship between CK2 and SARS-CoV-2 as well as with other viruses of the coronavirus family, highlighting also possible therapeutic strategies (Quezada Meza & Ruzzene, 2023).

kinases and phosphatases

MDPI

Review

Protein Kinase CK2 and SARS-CoV-2: An Expected Interplay Story

Camila Paz Quezada Meza and Maria Ruzzene *

Department of Biomedical Sciences, University of Padova, 35121 Padova, Italy; camilapaz.quezadameza@studenti.unipd.it
* Correspondence: maria.ruzzene@unipd.it

Abstract: Protein kinase CK2 is a Ser/Thr protein kinase that phosphorylates hundreds of substrates mainly related to survival and proliferation pathways. It has long been considered an anti-cancer drug target. However, during the recent COVID-19 pandemic, CK2 inhibitors have been repurposed as anti-SARS-CoV-2 drugs. This was based on the initial finding of CK2 among the proteins of the host cell that interact with the viral proteins and modulate the infection. Since then, several studies have deepened our understanding of the CK2/COVID-19 connection, and we deem it is time to review all the findings. Interestingly, other coronaviruses cross-talk with CK2 as well, with similarities and differences compared to the SARS-CoV-2 case. Therefore, we believe that the analysis of the effects obtained by targeting CK2 in case of coronavirus infections, both at the molecular and phenomenological level, will help in extrapolating information that could be useful not only for COVID-19 (whose pandemic emergency is hopefully turning off) but also for other infections.

Keywords: protein kinase CK2; CSNK2A1; CSNK2A2; CSNK2B; coronaviruses; COVID-19; SARS-CoV-2

check for updates

Citation: Quezada Meza, C.P.; Ruzzene, M. Protein Kinase CK2 and SARS-CoV-2: An Expected Interplay Story. *Kinases Phosphatases* **2023**, *1*, 141–150. https://doi.org/10.3390/kinasesphosphatases1020009

Academic Editor: Veerle Janssens

Received: 9 May 2023
Revised: 1 June 2023
Accepted: 13 June 2023
Published: 16 June 2023

Copyright: © 2023 by the authors. Licensee MDPI, Basel, Switzerland. This article is an open access article distributed under the terms and conditions of the Creative Commons Attribution (CC BY) license (https://creativecommons.org/licenses/by/4.0/).

1. Introduction

1.1. CK2 General Features, Structure, and Regulation

Protein kinase CK2 is a Ser/Thr kinase expressed in all eukaryotic cells and involved in all cellular processes. It localizes mainly in the nucleus and cytoplasm, but also other sub-cellular compartments [1], such as mitochondria and plasma membrane, where it can be exported to the external side and is therefore considered an ecto-kinase [2]. The acronym CK2 originates from the term "casein kinase 2" since this protein kinase was initially regarded as responsible for the phosphorylation of milk casein [3]. However, it was later clear that casein is physiologically phosphorylated by another kinase (G-CK, or genuine casein kinase, recently identified with Fam20C [3]). At the same time, it is not a physiological substrate of CK2, which in turn phosphorylates hundreds of substrates [4] and is involved in virtually all cellular processes. It is ubiquitously expressed and essential for embryonal development [5], and its levels are particularly high in physiologically and pathologically rapidly proliferating cells [6–8]. Indeed, cancer cells are known to be addicted to CK2 [9], which plays essential roles in potentiating cancer hallmarks and tumorigenic signals [10–12]. Therefore, CK2 is presently considered a cancer drug target [13–17].

CK2 is constitutively active, meaning that it does not require signaling by second messengers or phosphorylation events to be activated, and its functions are roughly regulated by changes in protein expression. However, several mechanisms have been proposed that might contribute to modulating the activity of this enigmatic kinase, ranging from changes in subcellular localization, substrate availability/accessibility, association to other proteins, composition in subunits/isoforms, and supramolecular polymerization of the kinase holoenzyme [18,19].

From a structural point of view, mammalian CK2 is a tetrameric holoenzyme: it is composed of two catalytic subunits (α or α', coded by two different genes, *CSNK2A1* and *CSNK2A2*, respectively) and two regulatory subunits β, coded by the *CSNK2B* gene. Different holoenzyme combinations are possible ($\alpha_2\ \beta_2$, $\alpha'_2\ \beta_2$, and $\alpha\alpha'\beta_2$). However,

the catalytic subunits are also active as monomers, and the regulatory functions of β are mainly to preserve the enzyme stability and drive the selection of substrates [20]. The actual existence of the isolated CK2 subunits in cells is still uncertain: several pieces of evidence (reviewed in [18]) suggest a role of the monomeric catalytic subunits, not combined with the regulatory ones, in specific pathological conditions, especially in cancer cells. Nevertheless, a direct demonstration of the isolated α or α′ subunits in cells has never been provided.

The two isoforms of the catalytic subunit, α and α′, are supposed to be mainly overlapping in their functions, but a few differential roles have also been reported: they differ mainly for their C-terminal sequences, through which they can bind different partner proteins, what is hypothesized to allow them exerting some isoform-specific functions [21].

1.2. CK2 in Diseases

CK2 activity is implicated in a plethora of diverse human diseases, as recently reviewed [22]. As mentioned above, its pathological functions are mainly documented in cancer. The first connection between CK2 and mammalian tumorigenesis dates back to the late 80s, when Ole-MoiYoi and coworkers, by studying bovine theileriosis (a cattle parasite disease that represents a naturally occurring animal model), provided the earliest evidence of a molecular causative link between CK2 and mammalian lymphoid oncogenesis (as reviewed in [23]). Subsequently, a huge amount of data was collected supporting a tumorigenic role for CK2 in different types of human hematological malignancies and solid cancers, where it is often found overexpressed compared to normal tissues [24,25]. Given the close relationship frequently occurring between viral infections and tumorigenesis, this profound engagement of CK2 in cancer has particular relevance for the topic of this review, as will be discussed below.

For a detailed description of the many other diseases where CK2 has been found involved, we refer the readers to another recent review [22]. Here we can just briefly list the CK2 implication in inflammation and autoimmune disorders [26], diabetes and obesity [27], diverse ophthalmic pathologies [28,29], cardiovascular diseases, such as cardiac ischemia–reperfusion injury, atherosclerosis, and cardiac hypertrophy [30–32]. CK2 is also considered an emerging target for neurological and psychiatric disorders [33] and possibly for cystic fibrosis [34]. Moreover, recently, psychiatric disorders and syndromes due to mutations of the genes for the CK2 subunits have been identified [35]. Specifically, they are called Okur-Chung Neurodevelopmental Syndrome or OC-NDS (mutations of the *CSNK2A1* gene, coding for CK2 α) and Poirier-Benvenu Neurodevelopmental Syndrome or POBINDS (mutations of the *CSNK2B* gene, coding for CK2 β).

Notably, other well-known functions of CK2 are in human infections; given the relevance of the topic of this review, they will be dealt with separately in the next paragraph.

1.3. CK2 in Viral Infections

Protein phosphorylation is a widespread and effective way to modulate protein functions, which even viruses exploit for their replication and life cycle. However, they depend on host protein kinases for the catalysis of this process; consistently, the activation of specific cellular kinases in response to the infection has been frequently observed, with the consequent phosphorylation of viral proteins, but also increased phosphorylation level of host cell proteins [36]. CK2 is among the most pleiotropic kinases, with 25 % of the phospho-proteome depending on its activity [3]. Therefore it makes sense that it could also be crucial for viruses. Indeed, its involvement in the phosphorylation of viral proteins has been known for many years, with 40 cases documented in 2003 [4]. One of the first reported cases is the human papillomavirus E7 protein; interestingly, this is the target of CIGB-300, a clinical-grade drug displaying promising anticancer properties [37,38]. Other notable examples (recently reviewed [8,22]) are the HIV-1 Rev protein, hepatitis C and B virus proteins, NSP1 of rotavirus, the nucleocapsid protein of the Hantaan virus, the matrix M protein of the human respiratory syncytial virus, the leader L protein of the encephalomyocarditis virus, the Kaposi's sarcoma-associated herpesvirus ORF57. Other viruses reported

to exploit the activity of CK2 for their infection and propagation are Epstein-Barr Virus (EBV) [39], Herpes Simplex Viruses (HSV), Human Cytomegalovirus (CMV) [8], and the list is continuously increasing, now also including coronaviruses, as described below in more details. In many cases, the infection preludes tumor transformation; therefore, the involvement of CK2, a pro-tumor kinase, is not so unexpected.

The mechanisms by which the phosphorylation by CK2 of viral proteins contributes to the infection are largely unknown. In some cases, the classical antiapoptotic mechanism that CK2 exerts by phosphorylating sites near a caspase site and preventing cleavage [40] might also apply to viral proteins, as reported in the case of ORF57 [41]. For the human papillomavirus E1 protein, it has been demonstrated that the phosphorylation by CK2 stabilizes ATP-dependent DNA helicase activity, which is essential for viral replication [42].

Regardless of the phosphorylated protein and the effect produced, it is worth noting that CK2 targeting has been proposed to stimulate host defence against virus infection by increasing IFN-α and IFN-β response, possibly by regulating the RIG-1 dependent signaling pathway [43,44]. This mechanism would not be limited to a specific viral infection.

2. CK2 and Coronaviruses

Coronaviruses are viruses known for many years, named after the Latin word for crown "corona" due to their peculiar glycoprotein spikes on the virus's surface, visible by electron microscopy, that resemble the solar corona. They are subdivided into four genera, namely α, β, γ, and δ. α and β coronaviruses (β-CoV) infect mammals, while γ and δ primarily infect birds. Until the SARS-CoV outbreak in 2003, coronaviruses were not given much attention by scientists since the ones known to infect humans caused minor symptoms. Presently, three human coronaviruses are known that can produce severe symptoms, all belonging to the β genus: the Severe Acute Respiratory Syndrome Coronavirus (SARS-CoV, identified in 2003), the Middle East Respiratory Syndrome-Related Coronavirus (MERS-CoV, identified in 2012), and the Severe Acute Respiratory Syndrome Coronavirus 2 (SARS-CoV-2, recognised in 2019). They cause diseases called SARS, MERS, and COVID-19, respectively.

The CK2 involvement in coronavirus infection is supported by several observations, as summarized in Figure 1. Firstly, the human β-CoV receptor on the host cell is ACE2 (angiotensin-converting enzyme 2), a known CK2 target [45]. As early as 2010, Chen and coworkers found that the CK2-dependent phosphorylation of ACE2 at the specific site Ser787 is increased upon binding of SARS-CoV; this activates downstream signal transduction pathways, namely ERK1/2 and AP-1, upregulating the fibrosis-associated CCL2 (chemokine C-C motif ligand 2) which mediates lung inflammation and lung fibrosis and facilitates viral invasion into the host cell. Consistently, the dysregulated production of inflammatory cytokines in response to SARS-CoV is reduced by the inhibition of CK2 [46].

The essential role of CK2 in β-CoV replication has been recently demonstrated [47] by developing a β-CoV reporter assay based on mouse hepatitis virus (MHV), a member of the β-CoV genus, frequently used as a model to study the virulence of other β-CoVs, since it does not require restrictive safety facilities. The β-CoV binding to the ACE2 receptor occurs through the spike protein (S protein) present on the surface of the virus [48] and is followed by clathrin-mediated endocytosis [49]. Yang and coworkers used a chemogenomic approach to demonstrate that CK2 inhibitors suppress murine, bat, and human β-CoV replication. They further confirmed the results by the genetic knockdown of the individual CK2 subunits and provided evidence that the effects are due to the reduced endocytosis of the spike protein [47].

A β-coronavirus bovine (BCoV) model was instead exploited by Perea's group [50] to investigate the efficacy of the anti-CK2 peptide CIGB-300 (in ref [50] called CIGB-325) in inhibiting the viral infection. The authors found that CIGB-300 has an antiviral effect in cell-based assays and reduced M (membrane) and N (nucleocapsid) viral protein levels. CIGB-300 is designed to act at the substrate level: it binds to the phospho-acceptor domain and prevents CK2-dependent phosphorylation [51]. Interestingly, in pull-down assays,

CIGB-300 was found to physically interact not only with several cellular CK2 substrates, as expected, but also with the BCoV N protein. The observed CIGB-300/N protein association allows us to speculate that BCoV N protein is a putative CK2 substrate; however, further experiments will be necessary to exclude an indirect binding mediated by other proteins. The results by Perea and coworkers are particularly interesting since BCoV, despite sharing pathogenic properties with other coronaviruses, does not enter host cells by binding to the ACE2 receptor but attaches to N-acetyl-9-O-acetylneuraminic acid (Neu5, 9Ac2) through HE (haemagglutinin esterase) and S proteins [52]. The finding that CK2 targeting reduces the BCoV infection is an additional indication that ACE2 is not the only crossing point between CK2 and coronaviruses and that there are several levels by which CK2 may impact the virus life cycle.

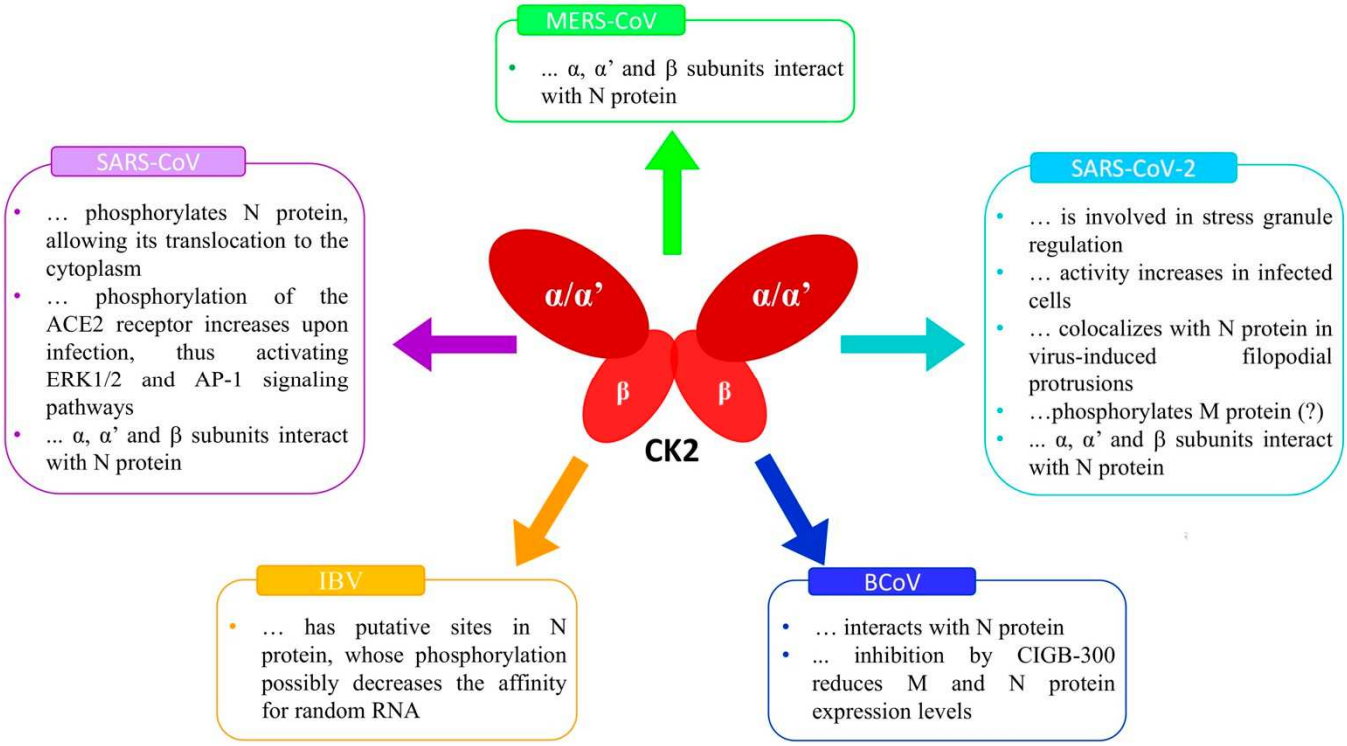

Figure 1. Connections between CK2 and β-CoVs. CK2 is depicted with the typical "butterfly" structure of the tetrameric holoenzyme. The boxes summarise the connections of CK2 to each β-CoV (see the text for references). The question mark (?) indicates still speculative finding.

Indeed, the N protein seems crucial in the CK2 regulation of coronavirus biology. N protein of the Avian infectious bronchitis coronavirus (IBV) was found to display a lower affinity for random RNA, and four phospho-sites were predicted as CK2 sites [53]. However, later it was demonstrated that at least two of these sites are not direct targets of CK2 but phosphorylated by ataxia-telangiectasia mutated and Rad3-related (ATR), a kinase activated during IBV replication [54]. In any case, CK2 can be relevant since it can be indirectly stabilized by ATR [55], thus suggesting that phosphorylation of N protein is most likely a dynamic and timely regulated process during the infection cycle.

N protein of SARS-CoV is also regulated by CK2 [56,57]: it was suggested that CK2 is among the multiple kinases that, by phosphorylating SARS-CoV N protein, allow its binding to 14-3-3 proteins and its translocation to the cytoplasm. The functional consequences of this process were not elucidated, but the authors postulated that nuclear localization of the N phosphoprotein might interfere with the cellular machinery and trigger apoptosis; other hypotheses are that phosphorylation may increase the protein stability, or promote its self-association, an essential step for viral assembly, or regulate downstream signaling pathways.

N protein has also been found to be associated with CK2 in MERS and SARS-CoV-2 infection [56], thus pointing to N proteins as a general element exploited by CK2 in β-CoVs-infected cells. The multiple levels of connection between CK2 and SARS-CoV-2 will be described in detail in the following paragraph.

3. CK2 and SARS-CoV-2

SARS-CoV-2, like the other β-CoVs, exploits the ACE receptor, a CK2 substrate [45], raising the interest in CK2 as an anti-COVID-19 target. But regardless of ACE, as early as the first year of the COVID-19 pandemic, two important papers were published that directly correlated CK2 to SARS-CoV-2 infection. Gordon et al. [58] applied an affinity-purification/mass spectrometry approach to identify host proteins exploited by the virus and already targeted by existing drugs. Among the human druggable proteins that physically associate with SARS-CoV-2 proteins, they identified CK2, which was supposed to be involved in stress granule regulation. Consistently, CK2 inhibitors disrupt stress granules. All the CK2 subunits (the α (CSNK2A1) and α′ (CSNK2A2) catalytic isoforms and the β regulatory subunit (CSNK2B)) were found to bind to the N protein [56].

The global phosphorylation landscape of SARS-CoV-2 infection was also published in 2020 [59], reporting that some CK2-dependent phospho-sites (belonging to both viral and host cell proteins) are upregulated in SARS-CoV-2 infected cells. This suggested that SARS-CoV-2 would enhance CK2 activity. They found that CK2 localizes with N protein in filopodia protrusions possessing budding viral particles markedly induced by the infection. Also, employing transcriptome and computational analyses, Shaath and Alajez [60] observed activation of CK2 in Calu-3 infected cells, and Fatoki and coworkers described CK2 as one of the key players in the SARS-CoV-2 lifecycle [61]. As reviewed by Chatterjee and Thakur [36], some of the CK2-dependent phospho-sites found in SARS-CoV-2 infected cells belong to the viral M protein, but the consequences of the phosphorylation remain unknown.

SARS-CoV-2 activates several host cell kinases [36], with the final effect of complex crosstalk between different signaling pathways globally contributing to virus infection and replication. An example of great relevance for this review is the case of the PI3K/Akt pathway: it is deeply interconnected with CK2, which potentiates it by acting at several levels [62]. Since this pathway is instrumental to SARS-CoV-2 biology [63,64], CK2 also contributes to virus replication by boosting it. Another example of the intricate network by which CK2 might sustain the SARS-CoV-2 infection is the ERK1/2 and AP-1 signaling pathway (previously mentioned also for SARS-CoV), in which PAK1, an activator of this pathway and a substrate of CK2, can promote the activation of the transcription nuclear factor-κB (NF-κB) and STAT3 pathways [65]. Both NF-κB and STAT3 are CK2 substrates, involved in the induction of inflammatory cytokine expressions and polarization of M2 macrophages promoting lung fibrosis in response to SARS-CoV-2 infection, respectively [66,67]. An additional crossing point between CK2 and SARS-CoV-2 is the Wnt/β-catenin signaling pathway, which CK2 regulates [68,69] and is crucial in SARS-CoV-2 infection since the treatment of SARS-Cov-2 infected cells with iCRT14t, a specific inhibitor of Wnt/β-catenin, decreased the cytopathic effect (changes in cell morphology caused by the virus) and reduced SARS-CoV-2 N protein level [36].

The multiple levels of connections between CK2 and SARS-CoV-2 are summarized in Figure 2.

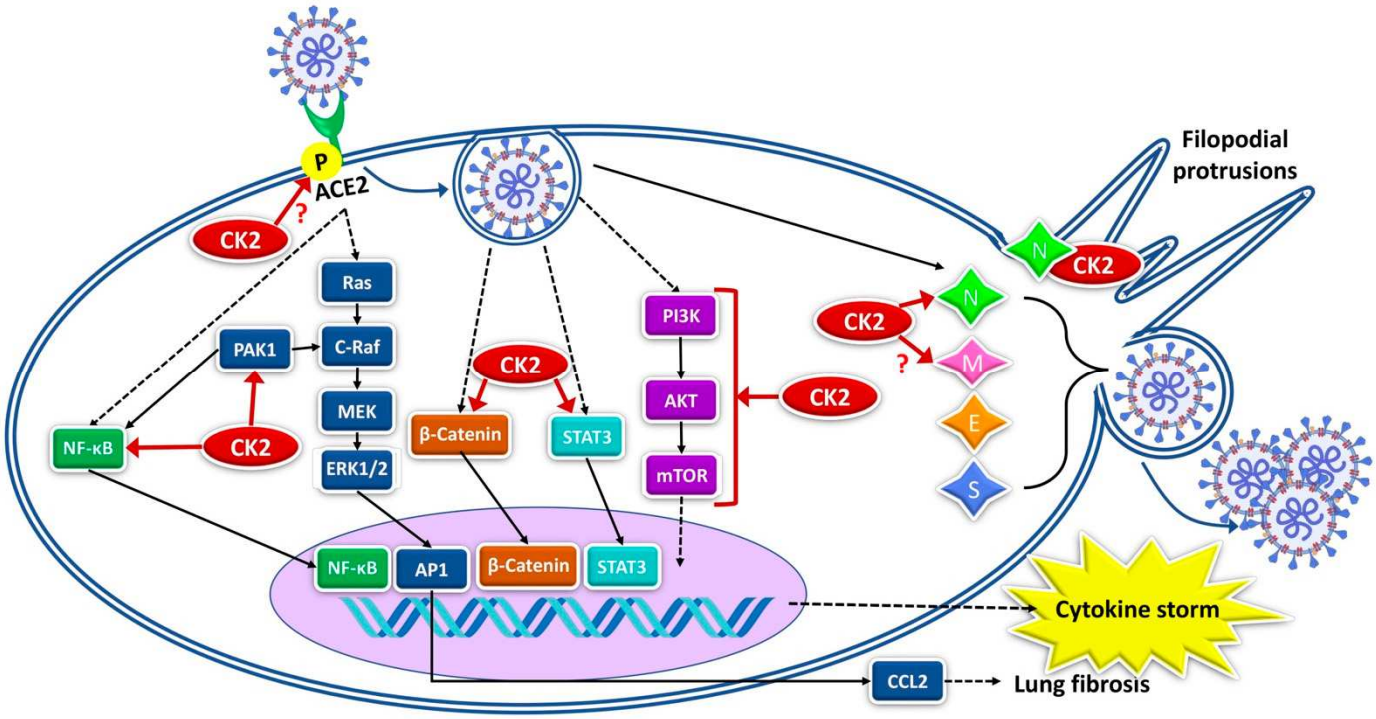

Figure 2. Different levels of CK2 involvement in SARS-CoV-2 infection. CK2 actions are indicated by the red arrows, with a question mark where data are still speculative, or the effects of the phosphorylation are not known. Dashed arrows refer to signaling pathways not defined. See the text for references.

4. CK2 Targeting as Anti-COVID-19 Strategy

The above-described involvement of CK2 in the SARS-CoV-2 biology, its druggability, and the existence of CK2 inhibitors already in human clinical trials as anticancer drugs (CX-4945 or silmitasertib (https://clinicaltrials.gov/ct2/results?cond=&term=CX-4945&cntry=&state=&city=&dist=) (accessed on 15 June 2023) and CIGB-300 (https://clinicaltrials.gov/ct2/results?cond=&term=cigb-300&cntry=&state=&city=&dist=) (accessed on 15 June 2023) have promptly sparked interest in CK2 as a possible target for COVID-19 as well, and the repurposing of the compounds.

Apart from the already quoted study on bovine coronaviruses [50], by a computational biology analysis [70], CIGB-300 has been proposed to interfere with the SARS-CoV-2 life cycle in infected human cells: it might affect the immune response to the infection and perturb the virus hijacking of RNA splicing machinery. An exploratory clinical study with CIGB-300 (now called CIGB-325) has been performed to investigate its safety and putative clinical benefit in COVID-19 patients with pneumonia [71]. Despite the small sample size (twenty patients), and the preliminary level of the study, the results were encouraging since CIGB-300 significantly reduced the median number of pulmonary lesions with mild and/or moderate adverse events.

The CX-4945 repurposing was proposed since the beginning [58] when CK2 was found to interact with SARS-CoV-2 N protein and influence stress granule regulation. CX-4945 is presently in a clinical trial for COVID-19 and coronavirus, besides cancer https://clinicaltrials.gov/ct2/show/NCT04668209?term=CX-4945&draw=2&rank=1 (accessed on 15 June 2023). Other compounds have been investigated as potential anti-COVID-19 drugs. By studying the network of genes expressed in COVID-19-infected patients, Fatoki et al. [61] tried to predict the drug compounds that could interfere with pathologic signaling pathways. They identified CK2 (along with DNA-PK) as playing a crucial role in the SARS-CoV-2 lifecycle, and, by investigating phytochemicals that could represent

therapeutic modulators, suggested emodin, ellagic acid, quercetin, and others as CK2 targeting compounds. They are indeed among the already-known inhibitors of CK2 [13].

5. Conclusions

Protein phosphorylation, elicited from the host kinases, is a well-known mechanism viruses exploit for survival. SARS-CoV-2 is no exception: the viral proteins N, M, S, 3a, and 9b were phosphorylated in about 70 different sites, corresponding to the consensus sequences of several kinases. Moreover, in SARS-CoV-2 infected cells, the phosphorylation of many host cell proteins increases (more than 15,000 phosphorylation sites identified) [36,59], and, at least in part, this is achieved through the activation of host kinases induced by the virus. Despite its constitutive activity, CK2 is among the activated enzymes. This could seem counterintuitive: what is the advantage of activating a kinase that is already catalytically competent? However, while the conformation structure of CK2 perfectly explains its constitutive activity [72], this does not exclude regulation events that can further enhance the phosphorylation of its substrates [18]. Since CK2 is very pleiotropic, being responsible for up to 25% of the phosphoproteome [3], its involvement in phosphorylating substrates instrumental for the virus life cycle is not unexpected. Moreover, its peculiar consensus sequence (S/T-x-x-E/D/pX) [73] is very common and present in several virus proteins.

As the Figure 2 summarises, CK2 and SARS-CoV-2 biology signals have several connecting points. Among them, it is worth pointing out the virus receptor ACE2, which is a substrate of CK2. Although the effects of the ACE2 phosphorylation on SARS-CoV-2 infection have never been described, by similarity with what was observed in the case of SARS-CoV [46], they are expected to be essential for the receptor functions. Other crucial levels of SARS-CoV-2/CK2 integration are the several signaling pathways strongly implicated in the infection and regulated by CK2 at multiple levels, such as PI3K/Akt, NF-κB, STAT3, Wnt/β-catenin, ERK1/2, and AP-1. However, the most significant connection is probably represented by the N protein, which can physically interact with each of the CK2 subunits and stimulate its catalytic activity. Indeed, N proteins of different coronaviruses are crucial for the functions played by CK2 in the infected cells (see Figure 1). Future studies will hopefully define the N protein/CK2 interaction at the molecular level, with exciting implications for our knowledge of CK2 biology, and ideally providing hypotheses on possible interventions to regulate its activity.

Although the COVID-19 outbreak is now less scary, it is important to highlight that identifying new antiviral therapies is still desirable to face the continued virus evolution with the possible emergence of new variants. Inevitably, selective pressure can generate drug-resistant mutants: this is frequent with direct antiviral agents, while cellular proteins exploited by the virus are less likely to be circumvented by viral escape mutants [74]. Also, considering the potential emergence of new β-CoVs, a broad-spectrum drug with activity against a wide range of viruses would be advantageous to prevent rapid viral spread. In this view, data reported so far provide strong evidence for CK2 as an ideal target. The wide availability of CK2 inhibitors and the clinical level of some of them complete the rationale for considering this kinase as a valuable target.

Author Contributions: M.R. conceptualized the manuscript. C.P.Q.M. and M.R. contributed to researching the content for the review, discussing the content, and writing the review. C.P.Q.M. perceived and designed the figures. M.R. critically reviewed the manuscript. C.P.Q.M. edited the manuscript before submission. All authors have read and agreed to the published version of the manuscript.

Funding: The work performed in the Authors' laboratory was supported by Institutional Funding (DOR and SID) to MR.

Institutional Review Board Statement: Not applicable.

Informed Consent Statement: Not applicable.

Data Availability Statement: Not applicable.

Acknowledgments: The Authors thank all the members of their laboratory for the helpful discussion.

Conflicts of Interest: The authors declare no conflict of interest.

References

1. Filhol, O.; Cochet, C. Protein Kinase CK2 in Health and Disease: Cellular Functions of Protein Ki-nase CK2: A Dynamic Affair. *Cell. Mol. Life Sci. CMLS* **2009**, *66*, 1830–1839. [CrossRef] [PubMed]
2. Rodríguez, F.; Allende, C.C.; Allende, J.E. Protein Kinase Casein Kinase 2 Holoenzyme Produced Ectopi-cally in Human Cells Can Be Exported to the External Side of the Cellular Membrane. *Proc. Natl. Acad. Sci. USA* **2005**, *102*, 4718–4723. [CrossRef] [PubMed]
3. Venerando, A.; Ruzzene, M.; Pinna, L.A. Casein Kinase: The Triple Meaning of a Misnomer. *Biochem. J.* **2014**, *460*, 141–156. [CrossRef]
4. Meggio, F.; Pinna, L.A. One-Thousand-and-One Substrates of Protein Kinase CK2? *FASEB J. Off. Publ. Fed. Am. Soc. Exp. Biol.* **2003**, *17*, 349–368. [CrossRef]
5. Dominguez, I.; Degano, I.R.; Chea, K.; Cha, J.; Toselli, P.; Seldin, D.C. CK2α Is Essential for Embryonic Morphogenesis. *Mol. Cell. Biochem.* **2011**, *356*, 209–216. [CrossRef]
6. Guerra, B.; Issinger, O.G. Protein Kinase CK2 and Its Role in Cellular Proliferation, Development and Pathology. *Electrophoresis* **1999**, *20*, 391–408. [CrossRef]
7. Issinger, O.G. Casein Kinases: Pleiotropic Mediators of Cellular Regulation. *Pharmacol. Ther.* **1993**, *59*, 1–30. [CrossRef]
8. St-Denis, N.A.; Litchfield, D.W. Protein Kinase CK2 in Health and Disease: From Birth to Death: The Role of Protein Kinase CK2 in the Regulation of Cell Proliferation and Survival. *Cell. Mol. Life Sci. CMLS* **2009**, *66*, 1817–1829. [CrossRef]
9. Ruzzene, M.; Pinna, L.A. Addiction to Protein Kinase CK2: A Common Denominator of Diverse Cancer Cells? *Biochim. Biophys. Acta* **2010**, *1804*, 499–504. [CrossRef] [PubMed]
10. Firnau, M.-B.; Brieger, A. CK2 and the Hallmarks of Cancer. *Biomedicines* **2022**, *10*, 1987. [CrossRef] [PubMed]
11. Strum, S.W.; Gyenis, L.; Litchfield, D.W. CSNK2 in Cancer: Pathophysiology and Translational Applications. *Br. J. Cancer* **2022**, *126*, 994–1003. [CrossRef] [PubMed]
12. Trembley, J.H.; Kren, B.T.; Afzal, M.; Scaria, G.A.; Klein, M.A.; Ahmed, K. Protein Kinase CK2—Diverse Roles in Cancer Cell Biology and Therapeutic Promise. *Mol. Cell. Biochem.* **2022**, *478*, 899–926. [CrossRef]
13. Borgo, C.; Ruzzene, M. Protein Kinase CK2 Inhibition as a Pharmacological Strategy. In *Advances in Protein Chemistry and Structural Biology*; Academic Press: Cambridge, MA, USA, 2021.
14. Borgo, C.; Ruzzene, M. Role of Protein Kinase CK2 in Antitumor Drug Resistance. *J. Exp. Clin. Cancer Res. CR* **2019**, *38*, 287. [CrossRef] [PubMed]
15. Buontempo, F.; McCubrey, J.A.; Orsini, E.; Ruzzene, M.; Cappellini, A.; Lonetti, A.; Evangelisti, C.; Chiarini, F.; Evangelisti, C.; Barata, J.T.; et al. Therapeutic Targeting of CK2 in Acute and Chronic Leukemias. *Leukemia* **2018**, *32*, 1–10. [CrossRef]
16. Gowda, C.; Sachdev, M.; Muthusami, S.; Kapadia, M.; Petrovic-Dovat, L.; Hartman, M.; Ding, Y.; Song, C.; Payne, J.L.; Tan, B.-H.; et al. Casein Kinase II (CK2) as a Therapeutic Target for Hematological Malignancies. *Curr. Pharm. Des.* **2017**, *23*, 95–107. [CrossRef]
17. Trembley, J.H.; Chen, Z.; Unger, G.; Slaton, J.; Kren, B.T.; Van Waes, C.; Ahmed, K. Emergence of Protein Kinase CK2 as a Key Target in Cancer Therapy. *BioFactors Oxf. Engl.* **2010**, *36*, 187–195. [CrossRef] [PubMed]
18. Borgo, C.; D'Amore, C.; Cesaro, L.; Sarno, S.; Pinna, L.A.; Ruzzene, M.; Salvi, M. How Can a Traffic Light Properly Work If It Is Always Green? The Paradox of CK2 Signaling. *Crit. Rev. Biochem. Mol. Biol.* **2021**, *56*, 321–359. [CrossRef]
19. Roffey, S.E.; Litchfield, D.W. CK2 Regulation: Perspectives in 2021. *Biomedicines* **2021**, *9*, 1361. [CrossRef]
20. Pinna, L.A. Protein Kinase CK2: A Challenge to Canons. *J. Cell Sci.* **2002**, *115*, 3873–3878. [CrossRef]
21. Litchfield, D.W.; Bosc, D.G.; Canton, D.A.; Saulnier, R.B.; Vilk, G.; Zhang, C. Functional Specialization of CK2 Isoforms and Characterization of Isoform-Specific Binding Partners. *Mol. Cell. Biochem.* **2001**, *227*, 21–29. [CrossRef]
22. Borgo, C.; D'Amore, C.; Sarno, S.; Salvi, M.; Ruzzene, M. Protein Kinase CK2: A Potential Therapeutic Target for Diverse Human Diseases. *Signal Transduct. Target. Ther.* **2021**, *6*, 183. [CrossRef]
23. ole-MoiYoi, O.K. Casein Kinase II in Theileriosis. *Science* **1995**, *267*, 834–836. [CrossRef] [PubMed]
24. Ortega, C.E.; Seidner, Y.; Dominguez, I. Mining CK2 in Cancer. *PLoS ONE* **2014**, *9*, e115609. [CrossRef]
25. Chua, M.M.J.; Lee, M.; Dominguez, I. Cancer-Type Dependent Expression of CK2 Transcripts. *PLoS ONE* **2017**, *12*, e0188854. [CrossRef]
26. Hong, H.; Benveniste, E.N. The Immune Regulatory Role of Protein Kinase CK2 and Its Implications for Treatment of Cancer. *Biomedicines* **2021**, *9*, 1932. [CrossRef] [PubMed]
27. Ampofo, E.; Nalbach, L.; Menger, M.D.; Montenarh, M.; Götz, C. Protein Kinase CK2-A Putative Target for the Therapy of Diabetes Mellitus? *Int. J. Mol. Sci.* **2019**, *20*, 4398. [CrossRef] [PubMed]
28. Ljubimov, A.V.; Caballero, S.; Aoki, A.M.; Pinna, L.A.; Grant, M.B.; Castellon, R. Involvement of Protein Kinase CK2 in Angiogenesis and Retinal Neovascularization. *Investig. Ophthalmol. Vis. Sci.* **2004**, *45*, 4583–4591. [CrossRef]

29. Morooka, S.; Hoshina, M.; Kii, I.; Okabe, T.; Kojima, H.; Inoue, N.; Okuno, Y.; Denawa, M.; Yoshida, S.; Fukuhara, J.; et al. Identification of a Dual Inhibitor of SRPK1 and CK2 That Attenuates Pathological Angiogenesis of Macular Degeneration in Mice. *Mol. Pharmacol.* **2015**, *88*, 316–325. [CrossRef]
30. Hauck, L.; Harms, C.; An, J.; Rohne, J.; Gertz, K.; Dietz, R.; Endres, M.; von Harsdorf, R. Protein Kinase CK2 Links Extracellular Growth Factor Signaling with the Control of P27 Kip1 Stability in the Heart. *Nat. Med.* **2008**, *14*, 315–324. [CrossRef]
31. Wadey, K.S.; Brown, B.A.; Sala-Newby, G.B.; Jayaraman, P.-S.; Gaston, K.; George, S.J. Protein Kinase CK2 Inhibition Suppresses Neointima Formation via a Proline-Rich Homeodomain-Dependent Mechanism. *Vascul. Pharmacol.* **2017**, *99*, 34–44. [CrossRef]
32. Zhou, H.; Zhu, P.; Wang, J.; Zhu, H.; Ren, J.; Chen, Y. Pathogenesis of Cardiac Ischemia-Reperfusion Injury Is Associated with CK2α-Disturbed Mitochondrial Homeostasis via Suppression of FUNDC1-Related Mitophagy. *Cell Death Differ.* **2018**, *25*, 1080–1093. [CrossRef] [PubMed]
33. Castello, J.; Ragnauth, A.; Friedman, E.; Rebholz, H. CK2-An Emerging Target for Neurological and Psychiatric Disorders. *Pharmaceuticals* **2017**, *10*, 7. [CrossRef]
34. Mehta, A. Cystic Fibrosis as a Bowel Cancer Syndrome, and the Potential Role of CK2. *Mol. Cell. Biochem.* **2008**, *316*, 169–175. [CrossRef]
35. Ballardin, D.; Cruz-Gamero, J.M.; Bienvenu, T.; Rebholz, H. Comparing Two Neurodevelopmental Disorders Linked to CK2: Okur-Chung Neurodevelopmental Syndrome and Poirier-Bienvenu Neurodevelopmental Syndrome-Two Sides of the Same Coin? *Front. Mol. Biosci.* **2022**, *9*, 850559. [CrossRef]
36. Chatterjee, B.; Thakur, S.S. SARS-CoV-2 Infection Triggers Phosphorylation: Potential Target for Anti-COVID-19 Therapeutics. *Front. Immunol.* **2022**, *13*, 829474. [CrossRef]
37. Gottardo, M.F.; Capobianco, C.S.; Sidabra, J.E.; Garona, J.; Perera, Y.; Perea, S.E.; Alonso, D.F.; Farina, H.G. Preclinical Efficacy of CIGB-300, an Anti-CK2 Peptide, on Breast Cancer Metastasic Colonization. *Sci. Rep.* **2020**, *10*, 14689. [CrossRef] [PubMed]
38. Perea, S.E.; Reyes, O.; Baladron, I.; Perera, Y.; Farina, H.; Gil, J.; Rodriguez, A.; Bacardi, D.; Marcelo, J.L.; Cosme, K.; et al. CIGB-300, a Novel Proapoptotic Peptide That Impairs the CK2 Phosphorylation and Exhibits Anticancer Properties Both in Vitro and Vivo. *Mol. Cell. Biochem.* **2008**, *316*, 163–167. [CrossRef]
39. Montenarh, M.; Grässer, F.A.; Götz, C. Protein Kinase CK2 and Epstein-Barr Virus. *Biomedicines* **2023**, *11*, 358. [CrossRef] [PubMed]
40. Duncan, J.S.; Turowec, J.P.; Vilk, G.; Li, S.S.C.; Gloor, G.B.; Litchfield, D.W. Regulation of Cell Proliferation and Survival: Convergence of Protein Kinases and Caspases. *Biochim. Biophys. Acta* **2010**, *1804*, 505–510. [CrossRef]
41. Majerciak, V.; Pripuzova, N.; Chan, C.; Temkin, N.; Specht, S.I.; Zheng, Z.-M. The Stability of Structured Kaposi's Sarcoma-Associated Herpesvirus ORF57 Protein Is Regulated by Protein Phosphorylation and Homodimerization. *J. Virol.* **2015**, *89*, 3256–3274. [CrossRef]
42. Piirsoo, A.; Piirsoo, M.; Kala, M.; Sankovski, E.; Lototskaja, E.; Levin, V.; Salvi, M.; Ustav, M. Activity of CK2alpha Protein Kinase Is Required for Efficient Replication of Some HPV Types. *PLoS Pathog.* **2019**, *15*, e1007788. [CrossRef]
43. Du, M.; Liu, J.; Chen, X.; Xie, Y.; Yuan, C.; Xiang, Y.; Sun, B.; Lan, K.; Chen, M.; James, S.J.; et al. Casein Kinase II Controls TBK1/IRF3 Activation in IFN Response against Viral Infection. *J. Immunol.* **2015**, *194*, 4477–4488. [CrossRef]
44. Sun, Z.; Ren, H.; Liu, Y.; Teeling, J.L.; Gu, J. Phosphorylation of RIG-I by Casein Kinase II Inhibits Its Antiviral Response. *J. Virol.* **2011**, *85*, 1036–1047. [CrossRef]
45. Kohlstedt, K.; Shoghi, F.; Müller-Esterl, W.; Busse, R.; Fleming, I. CK2 Phosphorylates the Angiotensin-Converting Enzyme and Regulates Its Retention in the Endothelial Cell Plasma Membrane. *Circ. Res.* **2002**, *91*, 749–756. [CrossRef] [PubMed]
46. Chen, I.-Y.; Chang, S.C.; Wu, H.-Y.; Yu, T.-C.; Wei, W.-C.; Lin, S.; Chien, C.-L.; Chang, M.-F. Upregulation of the Chemokine (C-C Motif) Ligand 2 via a Severe Acute Respiratory Syndrome Coronavirus Spike-ACE2 Signaling Pathway. *J. Virol.* **2010**, *84*, 7703–7712. [CrossRef] [PubMed]
47. Yang, X.; Dickmander, R.J.; Bayati, A.; Taft-Benz, S.A.; Smith, J.L.; Wells, C.I.; Madden, E.A.; Brown, J.W.; Lenarcic, E.M.; Yount, B.L.; et al. Host Kinase CSNK2 Is a Target for Inhibition of Pathogenic SARS-like β-Coronaviruses. *ACS Chem. Biol.* **2022**, *17*, 1937–1950. [CrossRef] [PubMed]
48. Lan, J.; Ge, J.; Yu, J.; Shan, S.; Zhou, H.; Fan, S.; Zhang, Q.; Shi, X.; Wang, Q.; Zhang, L.; et al. Structure of the SARS-CoV-2 Spike Receptor-Binding Domain Bound to the ACE2 Receptor. *Nature* **2020**, *581*, 215–220. [CrossRef]
49. Burkard, C.; Verheije, M.H.; Wicht, O.; van Kasteren, S.I.; van Kuppeveld, F.J.; Haagmans, B.L.; Pelkmans, L.; Rottier, P.J.M.; Bosch, B.J.; Haan, C.A.M. de Coronavirus Cell Entry Occurs through the Endo-/Lysosomal Pathway in a Proteolysis-Dependent Manner. *PLoS Pathog.* **2014**, *10*, e1004502. [CrossRef]
50. Ramón, A.C.; Pérez, G.V.; Caballero, E.; Rosales, M.; Aguilar, D.; Vázquez-Blomquist, D.; Ramos, Y.; Rodríguez-Ulloa, A.; Falcón, V.; Rodríguez-Moltó, M.P.; et al. Targeting of Protein Kinase CK2 Elicits Antiviral Activity on Bovine Coronavirus Infection. *Viruses* **2022**, *14*, 552. [CrossRef]
51. Perea, S.E.; Reyes, O.; Puchades, Y.; Mendoza, O.; Vispo, N.S.; Torrens, I.; Santos, A.; Silva, R.; Acevedo, B.; López, E.; et al. Antitumor Effect of a Novel Proapoptotic Peptide That Impairs the Phosphorylation by the Protein Kinase 2 (Casein Kinase 2). *Cancer Res.* **2004**, *64*, 7127–7129. [CrossRef]
52. Vlasova, A.N.; Saif, L.J. Bovine Coronavirus and the Associated Diseases. *Front. Vet. Sci.* **2021**, *8*, 643220. [CrossRef] [PubMed]
53. Chen, H.; Gill, A.; Dove, B.K.; Emmett, S.R.; Kemp, C.F.; Ritchie, M.A.; Dee, M.; Hiscox, J.A. Mass Spectroscopic Characterization of the Coronavirus Infectious Bronchitis Virus Nucleoprotein and Elucidation of the Role of Phosphorylation in RNA Binding by Using Surface Plasmon Resonance. *J. Virol.* **2005**, *79*, 1164–1179. [CrossRef] [PubMed]

54. Fang, S.; Xu, L.; Huang, M.; Qisheng Li, F.; Liu, D.X. Identification of Two ATR-Dependent Phosphorylation Sites on Coronavirus Nucleocapsid Protein with Nonessential Functions in Viral Replication and Infectivity in Cultured Cells. *Virology* **2013**, *444*, 225–232. [CrossRef] [PubMed]
55. Martin, S.A.; Ouchi, T. Cellular Commitment to Reentry into the Cell Cycle after Stalled DNA Is Determined by Site-Specific Phosphorylation of Chk1 and PTEN. *Mol. Cancer Ther.* **2008**, *7*, 2509–2516. [CrossRef]
56. Gordon, D.E.; Hiatt, J.; Bouhaddou, M.; Rezelj, V.V.; Ulferts, S.; Braberg, H.; Jureka, A.S.; Obernier, K.; Guo, J.Z.; Batra, J.; et al. Comparative Host-Coronavirus Protein Interaction Networks Reveal Pan-Viral Disease Mechanisms. *Science* **2020**, *370*, eabe9403. [CrossRef]
57. Surjit, M.; Kumar, R.; Mishra, R.N.; Reddy, M.K.; Chow, V.T.K.; Lal, S.K. The Severe Acute Respiratory Syndrome Coronavirus Nucleocapsid Protein Is Phosphorylated and Localizes in the Cytoplasm by 14-3-3-Mediated Translocation. *J. Virol.* **2005**, *79*, 11476–11486. [CrossRef]
58. Gordon, D.E.; Jang, G.M.; Bouhaddou, M.; Xu, J.; Obernier, K.; White, K.M.; O'Meara, M.J.; Rezelj, V.V.; Guo, J.Z.; Swaney, D.L.; et al. A SARS-CoV-2 Protein Interaction Map Reveals Targets for Drug Repurposing. *Nature* **2020**, *583*, 459–468. [CrossRef] [PubMed]
59. Bouhaddou, M.; Memon, D.; Meyer, B.; White, K.M.; Rezelj, V.V.; Correa Marrero, M.; Polacco, B.J.; Melnyk, J.E.; Ulferts, S.; Kaake, R.M.; et al. The Global Phosphorylation Landscape of SARS-CoV-2 Infection. *Cell* **2020**, *182*, 685–712.e19. [CrossRef]
60. Shaath, H.; Alajez, N.M. Computational and Transcriptome Analyses Revealed Preferential Induction of Chemotaxis and Lipid Synthesis by SARS-CoV-2. *Biology* **2020**, *9*, 260. [CrossRef]
61. Fatoki, T.H.; Ibraheem, O.; Ogunyemi, I.O.; Akinmoladun, A.C.; Ugboko, H.U.; Adeseko, C.J.; Awofisayo, O.A.; Olusegun, S.J.; Enibukun, J.M. Network Analysis, Sequence and Structure Dynamics of Key Proteins of Coronavirus and Human Host, and Molecular Docking of Selected Phytochemicals of Nine Medicinal Plants. *J. Biomol. Struct. Dyn.* **2020**, *39*, 6195–6217. [CrossRef]
62. Ruzzene, M.; Bertacchini, J.; Toker, A.; Marmiroli, S. Cross-Talk between the CK2 and AKT Signaling Pathways in Cancer. *Adv. Biol. Regul.* **2017**, *64*, 1–8. [CrossRef]
63. Basile, M.S.; Cavalli, E.; McCubrey, J.; Hernández-Bello, J.; Muñoz-Valle, J.F.; Fagone, P.; Nicoletti, F. The PI3K/Akt/mTOR Pathway: A Potential Pharmacological Target in COVID-19. *Drug Discov. Today* **2022**, *27*, 848–856. [CrossRef] [PubMed]
64. Klann, K.; Bojkova, D.; Tascher, G.; Ciesek, S.; Münch, C.; Cinatl, J. Growth Factor Receptor Signaling Inhibition Prevents SARS-CoV-2 Replication. *Mol. Cell* **2020**, *80*, 164–174.e4. [CrossRef] [PubMed]
65. Berretta, A.A.; Silveira, M.A.D.; Cóndor Captcha, J.M.; De Jong, D. Propolis and Its Potential against SARS-CoV-2 Infection Mechanisms and COVID-19 Disease: Running Title: Propolis against SARS-CoV-2 Infection and COVID-19. *Biomed. Pharmacother.* **2020**, *131*, 110622. [CrossRef]
66. Su, C.-M.; Wang, L.; Yoo, D. Activation of NF-KB and Induction of Proinflammatory Cytokines Expressions Mediated by ORF7a Protein of SARS-CoV-2. *Sci. Rep.* **2021**, *11*, 13464. [CrossRef] [PubMed]
67. Jafarzadeh, A.; Nemati, M.; Jafarzadeh, S. Contribution of STAT3 to the Pathogenesis of COVID-19. *Microb. Pathog.* **2021**, *154*, 104836. [CrossRef]
68. Ponce, D.P.; Yefi, R.; Cabello, P.; Maturana, J.L.; Niechi, I.; Silva, E.; Galindo, M.; Antonelli, M.; Marcelain, K.; Armisen, R.; et al. CK2 Functionally Interacts with AKT/PKB to Promote the β-Catenin-Dependent Expression of Survivin and Enhance Cell Survival. *Mol. Cell. Biochem.* **2011**, *356*, 127–132. [CrossRef] [PubMed]
69. Song, D.H.; Sussman, D.J.; Seldin, D.C. Endogenous Protein Kinase CK2 Participates in Wnt Signaling in Mammary Epithelial Cells. *J. Biol. Chem.* **2000**, *275*, 23790–23797. [CrossRef]
70. Miranda, J.; Bringas, R.; Fernandez-de-Cossio, J.; Perera-Negrin, Y. Targeting CK2 Mediated Signaling to Impair/Tackle SARS-CoV-2 Infection: A Computational Biology Approach. *Mol. Med.* **2021**, *27*, 161. [CrossRef]
71. Cruz, L.R.; Baladrón, I.; Rittoles, A.; Díaz, P.A.; Valenzuela, C.; Santana, R.; Vázquez, M.M.; García, A.; Chacón, D.; Thompson, D.; et al. Treatment with an Anti-CK2 Synthetic Peptide Improves Clinical Response in COVID-19 Patients with Pneumonia. A Randomized and Controlled Clinical Trial. *ACS Pharmacol. Transl. Sci.* **2021**, *4*, 206–212. [CrossRef]
72. Niefind, K.; Guerra, B.; Ermakowa, I.; Issinger, O.G. Crystal Structure of Human Protein Kinase CK2: Insights into Basic Properties of the CK2 Holoenzyme. *EMBO J.* **2001**, *20*, 5320–5331. [CrossRef] [PubMed]
73. Meggio, F.; Marin, O.; Pinna, L.A. Substrate Specificity of Protein Kinase CK2. *Cell. Mol. Biol. Res.* **1994**, *40*, 401–409. [PubMed]
74. Chitalia, V.C.; Munawar, A.H. A Painful Lesson from the COVID-19 Pandemic: The Need for Broad-Spectrum, Host-Directed Antivirals. *J. Transl. Med.* **2020**, *18*, 390. [CrossRef] [PubMed]

Disclaimer/Publisher's Note: The statements, opinions and data contained in all publications are solely those of the individual author(s) and contributor(s) and not of MDPI and/or the editor(s). MDPI and/or the editor(s) disclaim responsibility for any injury to people or property resulting from any ideas, methods, instructions or products referred to in the content.

2. ROLE OF CK2 IN CONTROLLING ER-PHAGY

I contributed to the research work of Dr. Settembre's group (Telethon Institute of Genetics and Medicine, Italy), that demonstrated that FAM34C cannot bind LC3B when phosphorylated by CK2. During starvation, mTORC1 inhibition limits FAM134C phosphorylation by CK2, hence promoting receptor activation and ER-phagy. Although ER-phagy deregulation has not been implicated in human diseases yet, preliminary evidence suggests that deregulation of FAM134C-mediated ER-phagy might contribute to the ER pathology and lipid alterations observed in diseases associated with mTORC1 hyperactivity. In particular, my work demonstrated that: 1) CK2 phosphorylates the ER-phagy receptor FAM34C on the S435, S436 and T440 sites; 2) mTORC1 phosphorylates the β subunit of CK2; 3) this affects the ability of CK2 to recognize some of its substrates. The results of this investigation were published under the title "Phosphorylation of FAM134C by CK2 controls starvation-induced ER-phagy" in the journal *Science Advances* (Di Lorenzo et al., 2022).

CELL BIOLOGY

Phosphorylation of FAM134C by CK2 controls starvation-induced ER-phagy

Giorgia Di Lorenzo[1]†, Francescopaolo Iavarone[1]†, Marianna Maddaluno[1], Ana Belén Plata-Gómez[2], Simone Aureli[3], Camila Paz Quezada Meza[4], Laura Cinque[1,5], Alessandro Palma[1], Alessio Reggio[1], Carmine Cirillo[1], Francesca Sacco[6], Alexandra Stolz[7,8], Gennaro Napolitano[1,9], Oriano Marin[4], Lorenzo A. Pinna[4,10], Maria Ruzzene[4,10], Vittorio Limongelli[3,11], Alejo Efeyan[2], Paolo Grumati[1,5]*, Carmine Settembre[1,5]*

Copyright © 2022 The Authors, some rights reserved; exclusive licensee American Association for the Advancement of Science. No claim to original U.S. Government Works. Distributed under a Creative Commons Attribution License 4.0 (CC BY).

Selective degradation of the endoplasmic reticulum (ER) via autophagy (ER-phagy) is initiated by ER-phagy receptors, which facilitate the incorporation of ER fragments into autophagosomes. FAM134 reticulon family proteins (FAM134A, FAM134B, and FAM134C) are ER-phagy receptors with structural similarities and nonredundant functions. Whether they respond differentially to the stimulation of ER-phagy is unknown. Here, we describe an activation mechanism unique to FAM134C during starvation. In fed conditions, FAM134C is phosphorylated by casein kinase 2 (CK2) at critical residues flanking the LIR domain. Phosphorylation of these residues negatively affects binding affinity to the autophagy proteins LC3. During starvation, mTORC1 inhibition limits FAM134C phosphorylation by CK2, hence promoting receptor activation and ER-phagy. Using a novel tool to study ER-phagy in vivo and FAM134C knockout mice, we demonstrated the physiological relevance of FAM134C phosphorylation during starvation-induced ER-phagy in liver lipid metabolism. These data provide a mechanistic insight into ER-phagy regulation and an example of autophagy selectivity during starvation.

INTRODUCTION

(Macro)autophagy begins with the sequestration of cytosolic substrates in autophagic vesicles that subsequently fuse with lysosomes where cargo degradation occurs (*1*). Nutrient starvation represents the most potent physiological inducer of autophagy. Starvation-induced autophagy is mainly controlled by mechanistic target of rapamycin complex 1 (mTORC1) that phosphorylates members of the autophagy initiation complex ULK1 and ATG13 and the transcription factors TFEB and TFE3 (*2*–*6*). The mechanisms controlling autophagy substrate capture during starvation-induced autophagy are not well defined, and this type of autophagy is considered a bulk process.

The selection of substrates during autophagy can be mediated by autophagy receptors, which are able to bind cytosolic cargoes facilitating their sequestration into forming autophagosomes. Autophagy receptors associate with the LC3 and GABARAP proteins on autophagic membranes through the LC3-interating region (LIR) and GABARAP-interacting motif, respectively (*7*, *8*). Selective autophagy cargo includes the endoplasmic reticulum (ER) (ER-phagy), mitochondria (mitophagy), lipid droplets (lipophagy), and several other cellular components.

ER-phagy is emerging as a critical quality control mechanism to preserve ER homeostasis (*9*–*14*). FAM134B was described as the first mammalian autophagy receptor that controls the degradation of the ER (*15*), and its activity can be modulated at both transcriptional and posttranslational levels (*16*–*19*). Subsequently, additional ER membrane proteins have been characterized as ER-phagy receptors (TEX264, SEC62, RTN3L, CCPG1, and ATL3) (*20*–*25*). Recently, we further expanded this knowledge by characterizing the two FAM134B paralogs, FAM134A and FAM134C (*26*). FAM134 proteins represent the first ER-phagy receptor family. Despite the strong homology in the LIR region and the presence of a reticulon homology domain in all of them, the FAM134 family members have several unique characteristics. For example, FAM134B overexpression is sufficient to promote ER-phagy (*17*), while FAM134A and FAM134C appear to be inactive in steady-state conditions (*26*). Whether functional changes in the structure and/or the interactome profiles of FAM134A and FAM134C are needed for their activation is currently unknown.

In this study, we identified a mechanism of FAM134C activation that contributes to ER-phagy induction during starvation. FAM134C activation is controlled by casein kinase 2 (CK2)–dependent phosphorylation at critical and unique residues that are proximal to the LIR motif. This phosphorylation event modulates the interaction between FAM134C and LC3 proteins, and it is modulated during starvation in an mTORC1-dependent manner. We showed the physiological relevance of FAM134C phosphorylation in vivo and, using in vivo tools to study ER-phagy, an altered FAM134C mediated activation of ER-phagy in mice with aberrant mTORC1 signaling.

RESULTS

Regulation of FAM134 proteins by starvation and mTORC1 inhibition

To study the response of the FAM134 proteins to starvation and mTOR inhibition, we used U2OS cells that express doxycycline-inducible

[1]Telethon Institute of Genetics and Medicine (TIGEM), Pozzuoli, Italy. [2]Metabolism and Cell Signaling Laboratory, Spanish National Cancer Research Centre (CNIO), Madrid, Spain. [3]Università della Svizzera italiana (USI), Faculty of Biomedical Sciences, Euler Institute, Lugano, Switzerland. [4]Department of Biomedical Sciences, University of Padova, Padova, Italy. [5]Department of Clinical Medicine and Surgery, Federico II University, Naples, Italy. [6]Department of Biology, University of Rome "Tor Vergata", Rome, Italy. [7]Institute of Biochemistry II, Faculty of Medicine, Goethe University, Frankfurt am Main, Germany. [8]Buchmann Institute for Molecular Life Sciences (BMLS), Goethe University, Frankfurt am Main, Germany. [9]Department of Translational Medicine, Federico II University, Naples, Italy. [10]CNR Neuroscience Institute, Padova, Italy. [11]Department of Pharmacy, Federico II University, Naples, Italy.
*Corresponding author. Email: p.grumati@tigem.it (P.G.); settembre@tigem.it (C.S.)
†These authors contributed equally to this work.

hemagglutinin (HA)-FAM134A, HA-FAM134B, and HA-FAM134C at comparable levels (fig. S1A). We analyzed FAM134 lysosomal flux before and after treatment with the mTOR inhibitor Torin1 and in the presence of bafilomycin A1 (BafA1), an inhibitor of lysosomal degradation. The addition of BafA1 to cells for 4 hours resulted in a massive accumulation of FAM134B, but not of FAM134A and FAM134C, within LAMP1-positive vesicles, thus indicating that FAM134B lysosomal flux was higher compared to the other family members (Fig. 1, A and B), consistent with previous observations (*26*).

The addition of Torin1 stimulated FAM134C and FAM134A lysosomal puncta formation, with FAM134C showing a more robust response (Fig. 1, A and B). Conversely, Torin1 did not further increase FAM134B lysosomal puncta number, in the presence and absence of BafA1 (Fig. 1, A and B).

Next, we generated human embryonic kidney (HEK) 293 cells stably expressing FAM134 proteins tagged with red fluorescent protein–enhanced green fluorescent protein (RFP-EGFP) to measure FAM134 delivery to lysosomes in response to a time course of Torin1 treatment by fluorescence-activated cell sorting (FACS) analysis (Fig. 1C). The acidic environment inside the lysosome efficiently quenches the fluorescent signal of EGFP but not of RFP, and the fluorescent shift can be measured by FACS. We observed that FAM134C was the most responsive to Torin1 administration, showing about 20-fold increased acidification upon 6 hours of Torin1 administration. Differently from what we observed in U2OS cells, Torin1 enhanced FAM134B lysosomal delivery in HEK293 cells, although at much lower levels compared to FAM134C.

To assess the relative contributions of the FAM134 proteins during Torin1-induced ER-phagy, we generated RCS cells lacking either *Fam134a*, *Fam134b*, *Fam134c*, or all three combined (*Fam134*^{TKO}) (fig. S1B) and expressing the mKeima reporter fused to the ER membrane protein RAMP4. The mKeima protein is unaffected by lysosomal proteases, and the appearance of a proteolytically cleaved mKeima from RAMP4 can be used to measure lysosomal delivery of RAMP4-decorated ER fragments (*20*, *27*). We observed that *Fam134c*^{KO} and *Fam134*^{TKO} showed a significant stronger impairment of Torin1-induced ER-phagy compared with the other genotypes, as measured by the levels of processed mKeima (Fig. 1, D and E). Similarly, FACS analysis in Torin1-treated control and Fam134 knockout (KO) cells expressing the fluorescent ER-phagy reporter SS-RFP-GFP-KDEL demonstrated reduction of ER-phagy flux in all *Fam134* KO cells, with *Fam134c*^{KO} and *Fam134*^{TKO} having the strongest effects (Fig. 1F). To gain insights into the functional relevance of these observations, we performed full proteome mass spectrometry (MS) analysis on U2OS and RCS cells that overexpress and lack FAM134 proteins, respectively. In both U2OS and RCS control cells, Torin1 treatment significantly down-regulates several ER proteins in an ER-phagy–dependent fashion, because this effect was blunted in *Atg7*^{KO} and *Fam134*^{TKO} cells (Fig. 1, G and H; fig. S2; and table S5). We found that the overexpression of HA-FAM134C increased the number of ER proteins down-regulated by Torin1 stimulation to a higher extent compared with HA-FAM134B or HA-FAM134A overexpression (Fig. 1G and table S4). Furthermore, *Fam134c*^{KO} caused the strongest inhibition of Torin1-induced ER protein degradation compared with *Fam134b* and *Fam134a* deletions (Fig. 1H, fig. S2, and table S5). Collectively, gain- and loss-of-function experiments performed in different cell types and using diverse approaches uncovered an unexpected prominent role of FAM134C, over other family members, during mTORC1-dependent starvation-induced ER-phagy. These data prompted us to search for a possible mechanism of FAM134C activation during starvation and mTORC1 inhibition.

FAM134C phosphorylation at critical residues controls its activation during starvation

The lysosomal delivery of HA-FAM134C was potently induced in response to serum, amino acids, or their combined deprivation [Hanks' balanced salt solution (HBSS) medium] in U2OS cells (fig. S3A). Phosphoproteomic analysis comparing starved (HBSS) with nutrient- and insulin-rich medium (full medium) U2OS cells expressing HA-FAM134C identified specific residues located in the C terminus of FAM134C (S285, S335, S435, S436, and T440) significantly phosphorylated in full versus starved medium conditions (Fig. 2A). The analysis of a published phosphoproteome dataset of starved versus insulin-stimulated Hepa-1-6 cell lines (*28*) confirmed that endogenous FAM134C was significantly more phosphorylated at S436 and T440 in insulin-stimulated conditions (fig. S3B). The S435, S436, and T440 residues are in the cytosolic C-terminal region of the protein in proximity (−12, −11, and −7, respectively) of the LIR sequence that binds to LC3/GABARAP proteins (starting at F447). To elucidate the role played by these residues, we investigated the binding mode between FAM134C and LC3B. As no experimental structure was available, we first generated a homology model of the FAM134C binding interface encompassing the residues P434 to P460 (FAM134C_P434-P460 hereafter) (Fig. 2B and fig. S4, A to I). Molecular docking simulations and parallel-tempering molecular dynamics (PT-MD) calculations of the FAM134C/LC3B complex were performed to identify the interprotein contacts that stabilize the heterodimer structure. These methods are widely used to study molecular binding systems (*29*, *30*). The PT-MD calculations showed that all the residues S435, S436, and T440 engage in H-bond interactions with LC3B. FAM134C's T440 and S435 form H-bonds with the backbone oxygens of LC3B V46 and L71, respectively, while FAM134C's S435 engages in two H-bonds, one with the backbone oxygen of LC3B N74 and the other with the Q77 side chain (Fig. 2B). The full list of the FAM134C_P434-P460/LC3B interactions is reported in table S6. The obtained structure of the FAM134C_P434-P460/LC3B binding complex highlights the role played by S435, S436, and T440 in the formation and stability of the heterodimer, prompting us to further investigate the impact of the phosphorylation of these amino acids. To this end, we computed the electrostatic map of LC3B through the "Adaptive Poisson-Boltzmann Solver" software (*31*). Here, it can be noted that the region of LC3B interacting with FAM134C's S435, S436, and T440 is relatively neutral in terms of charge, suggesting that phosphorylation of the indicated residues, increasing the local electron density, might lead to a less favorable interaction with LC3B. We also investigated how single and triple mutations S435D, S436D, and T440D in FAM134C affect the binding affinity to LC3B. The substitution of serine and threonine residues with aspartate allows assessing the result of charge modification in FAM134C, mimicking the effect of phosphorylation at these sites. Our results show that both the triple mutant (3D) and the single mutants S435D and S436D strongly decrease the FAM134C binding score to LC3B, while such effect is less pronounced in the T440D mutant (see fig. S4, J to L). On the other hand, the triple mutant resulting from the substitution of S435, S436, and T440 with alanine (3A), instead of aspartate, has a binding score like that of the

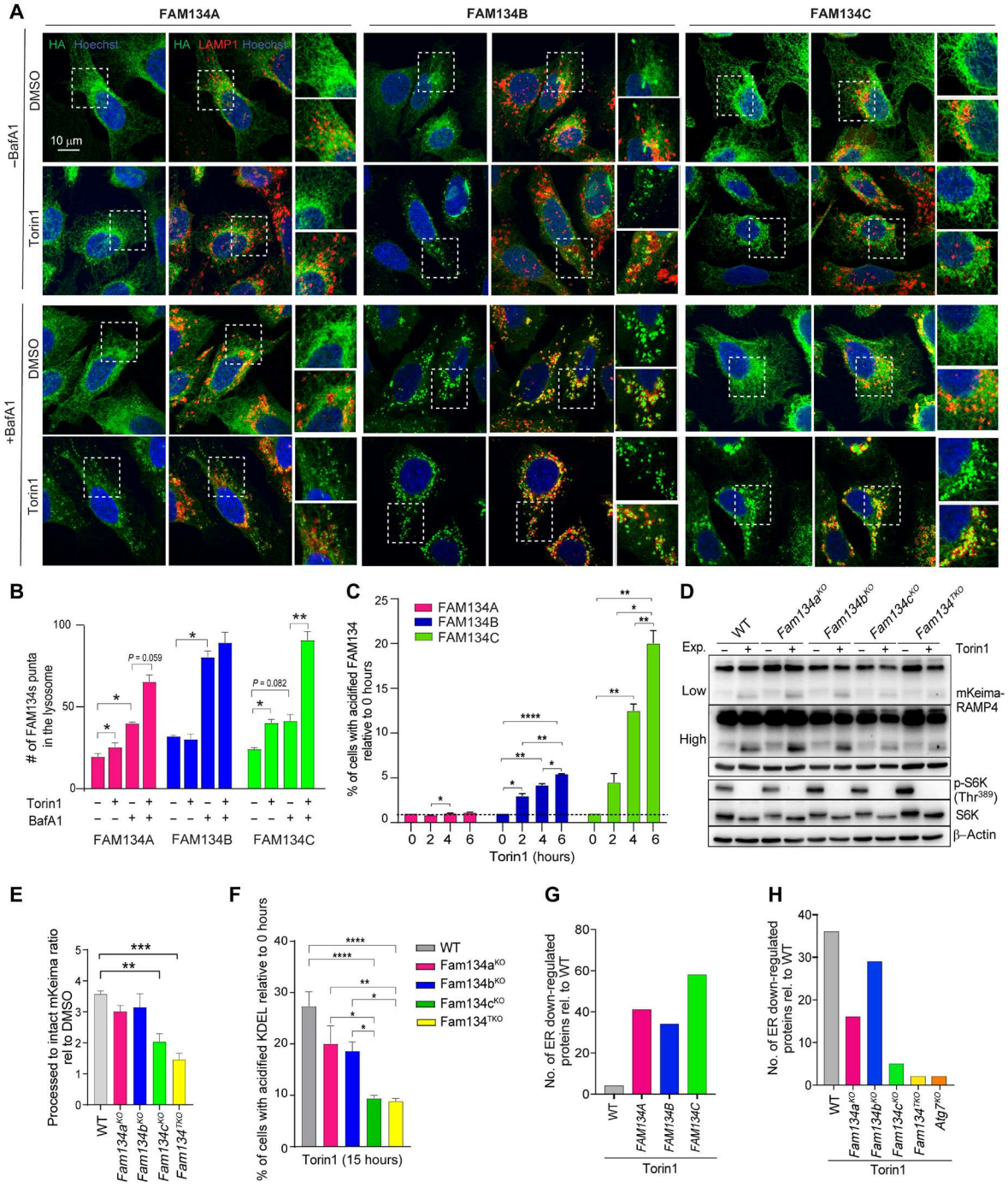

Fig. 1. Regulation of FAM134 protein by mTORC1 inhibition. (**A**) Representative images of immunofluorescence staining for HA, LAMP1, and nuclei in HA-FAM134s–expressing U2OS cells cultured with BafA1 (200 nM; 4 hours) and/or Torin1 (150 nM; 8 hours), where indicated. Scale bar, 10 μm. (**B**) Quantification of HA puncta into LAMP1-positive vesicles. Mean ± SEM. $N = 3$ biological replicates. $n = 15$ cells per experiment. Two-way analysis of variance (ANOVA) and Tukey's multiple comparison test: $^{*}P < 0.05$ and $^{**}P < 0.005$. (**C**) Fluorescence-activated cell sorting (FACS) analysis in human embryonic kidney (HEK) 293T cells expressing ssRFP-GFP-FAM134s. Torin1 (150 nM) was added for the indicated time points. Quantification of red fluorescence shift relative to untreated (0 hours). Mean ± SEM. $N = 4$ biological replicates. Two-way ANOVA and Tukey's multiple comparison test: $^{****}P < 0.0001$, $^{**}P < 0.005$, and $^{*}P < 0.05$. (**D**) Representative Western blot analysis in RCS cells expressing mKeima-RAMP4 treated with Torin1 (150 nM; 15 hours). β-Actin was used as a loading control. (**E**) Quantification of mKeima/mKeima-Ramp4 ratio relative to dimethyl sulfoxide (DMSO)–treated cells. Mean ± SEM. $N = 4$ biological replicates. One-way ANOVA and Tukey's multiple comparison test: $^{**}P < 0.005$ and $^{***}P < 0.0005$. (**F**) FACS analysis in RCS cells expressing ssRFP-GFP-KDEL treated with Torin1 (150 nM; 15 hours). Quantification of red fluorescence shift relative to untreated. Mean ± SEM. $N = 6$ biological replicates. One-way ANOVA and Tukey's multiple comparison test: $^{****}P < 0.0001$, $^{**}P < 0.005$, and $^{*}P < 0.05$. (**G** and **H**) Proteome of U2OS (G) and RCS cells (H) untreated or treated with Torin1 (150 nM; 12 hours). Bar graphs show the number of ER proteins down-regulated by Torin1 (150 nM; 12 hours) in control [wild type (WT)] and HA-FAM134–overexpressing U2OS cells (G) and in RCS with indicated genotypes (H). $N = 3$ biological replicates. Adjusted P value < 0.05

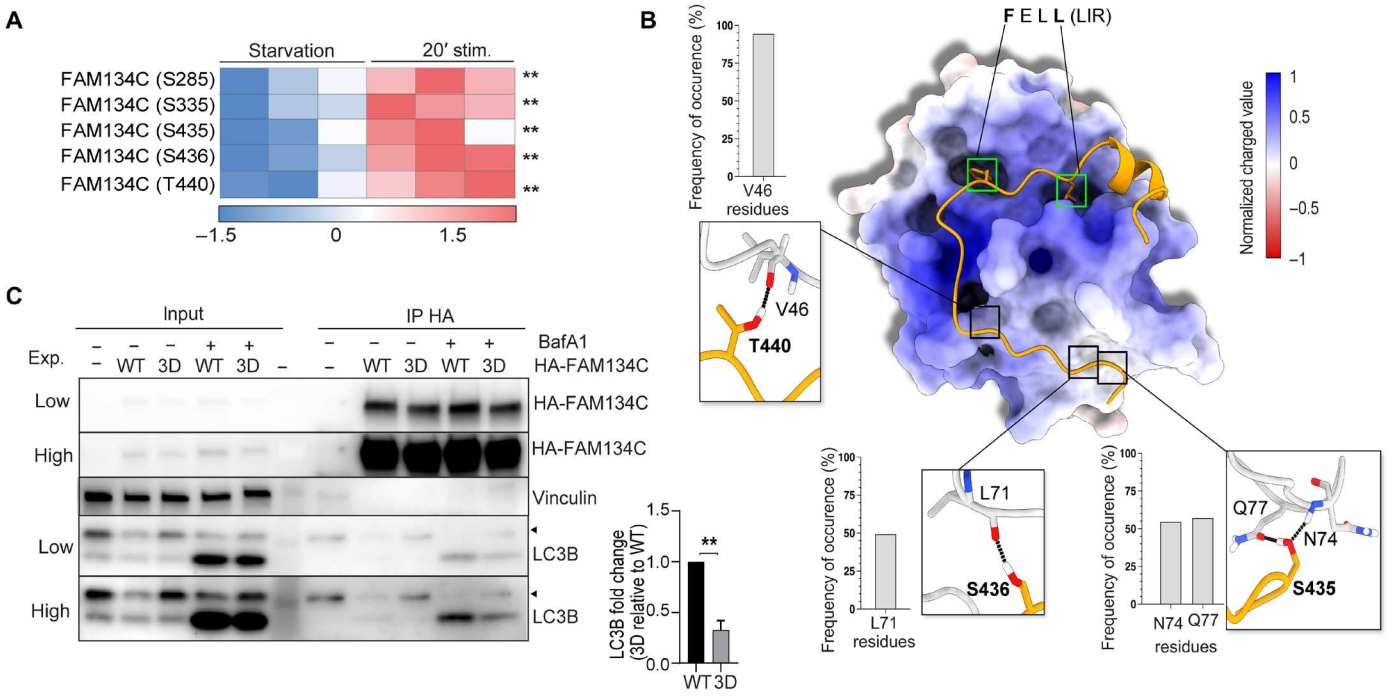

Fig. 2. Phosphorylation of FAM134C controls its affinity for LC3B. (**A**) Heatmap of the phosphorylation levels of FAM134C at indicated residues in U2OS cells cultured in starved (HBSS medium) versus stimulated (amino acids + 100 nM insulin) medium. Heatmap is color-coded according to the intensity level of the phosphorylated site. $N = 3$ biological replicates. FDR: $^{**}P < 0.005$. (**B**) Structural analysis of the FAM134C_P434-P460/LC3B complex. Projection of the electrostatic potential map of LC3B onto the structure of the centroid associated with the most populated cluster family. The insets display the interactions established by Ser^{435}, Ser^{436}, and Thr^{440} of FAM134C with LC3B and their frequency of occurrence in the PT-MD principle conformational state. LC3B was represented through its solvent-accessible surface, colored according to the local electrostatic potential map values following the color gradient on the right side. FAM134C_P434-P460 was represented in ribbon and colored in orange. Green boxes highlight the first (F) and the fourth (L) amino acids of the FAM134C LIR domain. (**C**) Western blot analysis showing immunoprecipitation (IP) experiment of HA-FAM134C-WT and HA-FAM134C-3D overexpressed in U2OS cells. Low and high refers to different exposures of the membrane. BafA1 (200 nM) was supplied where indicated. Arrowheads indicate a nonspecific band. On the right, bar graph shows quantification of LC3B binding of FAM134C-3D relative to WT in the presence of BafA1. Mean ± SEM. $N = 3$ biological replicates. Student's paired t test: $^{**}P < 0.005$.

wild type (WT). These results support the model that phosphorylation at S435, S436, and, at a less extent, T440 could affect the FAM134C binding to LC3B. To experimentally prove the functional role of FAM134C phosphorylation, we mutagenized S435, S436, and T440 residues into alanine [phosphomutant (3A)] or aspartic acid [phosphomimetic (3D)], and consistent with the in silico analysis, coimmunoprecipitation (co-IP) experiments showed a reduced interaction of 3D-FAM134C compared to FAM134C WT with endogenous LC3B (Fig. 2C). In unstimulated conditions, 3D-Myc-FAM134C showed a reticular localization like WT-Myc-FAM134C. However, unlike WT-Myc-FAM134C, the 3D-Myc-FAM134C protein was relocalized significantly less in LAMP1-positive vesicles in the presence of Torin1 and BafA1 (Fig. 3, A and B). Conversely, we observed that 3A-Myc-FAM134C formed multiple LAMP1-positive puncta even in the absence of Torin1 (Fig. 3, A and B). Similar data were obtained analyzing colocalization of WT-, 3A-, and 3D-Myc-FAM134C proteins with the autophagosome marker LC3 (fig. S5). These data suggest that phosphorylation of FAM134C at S435, S436, and T440 controls its activation during ER-phagy by regulating FAM134C affinity for LC3B. To corroborate these results, we reconstituted mouse embryonic fibroblast (MEF) *Fam134c*^{KO} with WT-, 3D-, and 3A-Myc-FAM134C proteins (fig. S6). MEF *Fam134c*^{KO} had no ER-phagy defects in basal conditions but showed impaired mTOR-dependent activation of ER-phagy (Fig. 3, C and D), which was rescued by reintroducing WT- or 3A-Myc-FAM134C but not 3D-Myc-FAM134C protein (Fig. 3, E and F).

CK2 phosphorylates and controls lysosomal delivery of FAM134C

The FAM134C region containing residues S435, S436, and T440 shows the consensus binding sequence for protein kinase CK2, a constitutively active serine/threonine kinase whose holoenzyme is composed of two catalytic subunits (α and α^{I}) and a dimer of regulatory β subunits (*32*, *33*). We analyzed an IP-MS experiment on phospho-Ser/Thr peptides using a CK2 substrate antibody (S*/T*D/EXD/E) to identify CK2 substrates and observed that S435, S436, and T440, as well as S258, T283, S288, S313, and S320, in FAM134C, are bona fide CK2 phosphorylation sites (PhosphoSitePlus database) (Fig. 4A) (*34*). Consistently, a commercially available phospho-CK2 substrate antibody detected immunoprecipitated FAM134C. Moreover, this detection was blunted by preincubating cells with the CK2 inhibitor CX4945 (Fig. 4, B and C). IP-MS of the FAM134 proteins demonstrated that FAM134C, but not FAM134A or FAM134B, interacts with CK2 α, α^{I}, and β subunits (Fig. 4D and table S7). To formally demonstrate that FAM134C is a bona fide CK2 substrate, we generated WT and 3A mutant FAM134C fragments, encompassing the C-terminal cytosolic region of FAM134C ($FAM134C^{250–466}$), where the phosphorylation occurs. An in vitro kinase assay showed

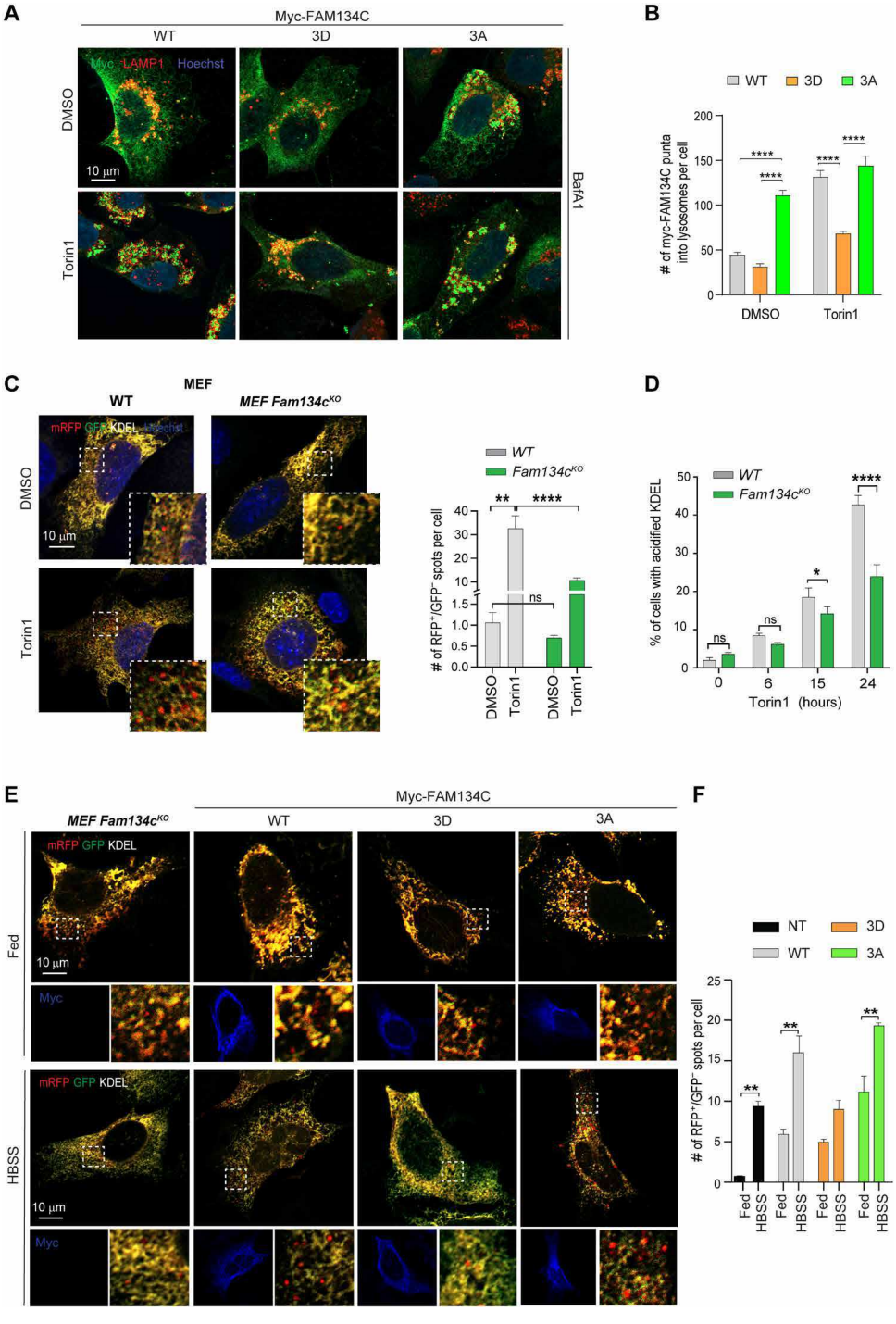

Fig. 3. FAM134C activity is regulated by phosphorylation. (**A**) Representative immunofluorescence staining of Myc, LAMP1, and nuclei in U2OS cells transfected with WT-, 3D-, and 3A-Myc-FAM134C. Cells were treated for 2 hours with BafA1 (100 nM), and where indicated, Torin1 (250 nM) was added for 6 hours. Scale bar, 10 µm. (**B**) Quantification of Myc-FAM134C lysosomal puncta per cell. Bar graph shows mean ± SEM. $N = 3$ biological replicates. $n = 15$ cells per experiment. Two-way ANOVA and Tukey's multiple comparison test: ****$P < 0.0001$. (**C**) Representative immunofluorescence staining for RFP, GFP, and nuclei in WT and *Fam134c*^{KO} MEF cells, stably expressing the ER-phagy reporter ssRFP-GFP-KDEL, after Torin1 treatment (150 nM; 24 hours). Scale bar, 10 µm. Quantification shows the number of red-only positive puncta (ssRFP$^+$) per cell. Mean ± SEM. $N = 3$ biological replicates. $n = 15$ cells per experiment. Two-way ANOVA and Sidak's and Tukey's multiple comparison test: ***$P < 0.0005$ and **$P < 0.005$. ns, not significant. (**D**) Quantification of red fluorescent shift performed by FACS analysis in WT and *Fam134c*^{KO} MEF cells, stably expressing ssRFP-GFP-KDEL, treated with Torin1 (150 nM) or DMSO at the indicated time points. $N = 3$ biological replicates. Two-way ANOVA and Sidak's and Tukey's multiple comparison test: ****$P < 0.0001$ and *$P < 0.05$. (**E**) Representative images of *Fam134c*^{KO} MEFs cells expressing ssRFP-GFP-KDEL and transfected with WT, 3D, or 3A mutant FAM134C proteins. Cells were kept in complete medium or starved for 8 hours in HBSS. Scale bars, 10 µm. (**F**) Quantification of red-only puncta (RFP$^+$/GFP$^-$) average per cell. Bar graph shows mean ± SEM. $N = 3$ biological replicates. $n = 15$ cells per experiment. Two-way ANOVA and Tukey's multiple comparison test: **$P < 0.005$ and *$P < 0.05$.

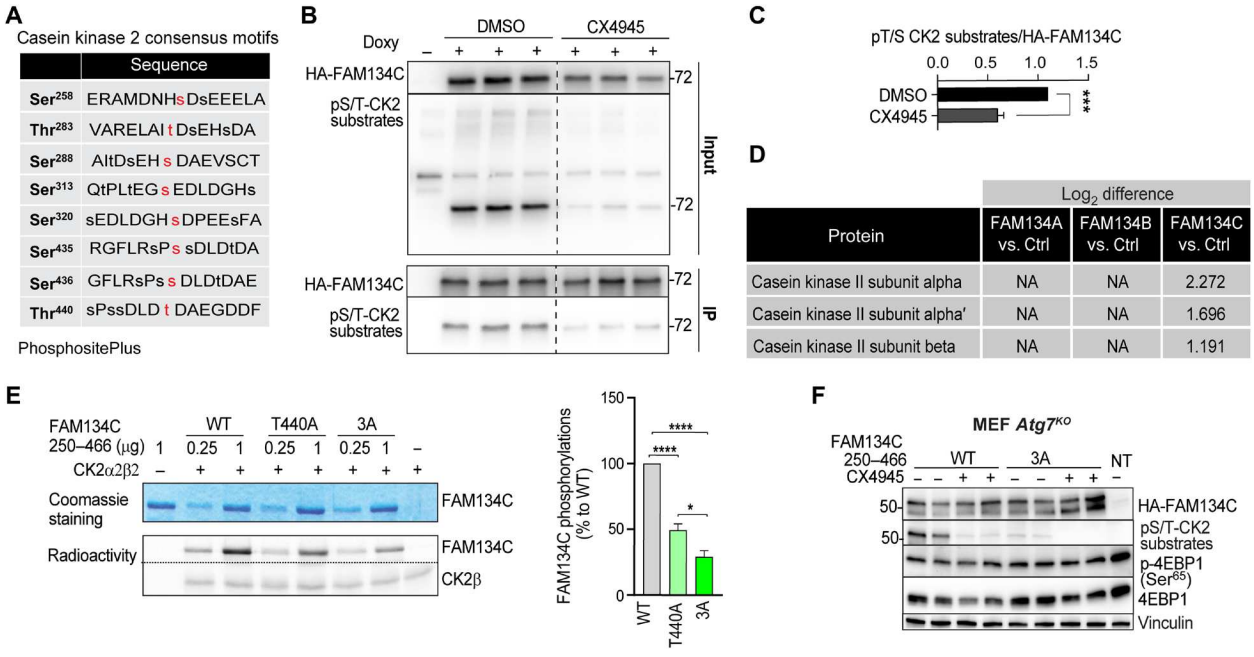

Fig. 4. CK2 phosphorylates FAM134C. (**A**) List of putative residues with CK2 consensus at the C terminus of FAM134C (data obtained from the PhosphositePlus website). (**B**) U2OS cells expressing doxycycline-inducible HA-tagged FAM134C were subjected to IP. Inputs and immunoprecipitates were analyzed by immunoblotting using the indicated antibodies. (**C**) Bar graph shows quantification of phosphorylated/total HA-FAM134C ratio relative to (B). Mean ± SEM. $N = 3$ biological replicates. Student's paired t test: ***$P < 0.0005$. CX4945: CK2 inhibitor (4 μM; 6 hours) and BafA1 (200 nM; 6 hours). (**D**) CK2 α and β subunit interaction with FAM134 proteins based on IP-MS interactome experiment from U2OS FLAG-HA-FAM134A, FLAG-HA-FAM134B, and FLAG-HA-FAM134C doxycycline-inducible cells. NA, not detected. Numeric values represent $\log_2$ difference. (**E**) In vitro CK2 phosphorylation radioactive assay. C-terminal FAM134C WT and phosphomutant (T440A and 3A) peptides and CK2β (control substrate) were incubated with CK2α in the presence of radioactive adenosine triphosphate (ATP). Substrate phosphorylation was detected by autoradiography. Equal amounts of proteins were verified by Coomassie staining. On the bottom, relative quantitation of the bands is performed by analysis with the CyclonePlus Storage Phosphor System (PerkinElmer); the unit amounts of each peptide are indicated, and activity is reported as % of that measured with 5 units of CK2α. Mean ± SEM. $N = 3$ biological replicates. One-way ANOVA and Tukey's multiple comparison test: ****$P < 0.0001$ and *$P < 0.05$. (**F**) Western blot analysis of CK2-dependent phosphorylation of WT- and 3A-HA-FAM134C$^{250–466}$ peptides transfected in *Atg7*^{KO} MEFs untreated or treated with the CK2 inhibitor CX4945 (4 μM; 6 hours). Vinculin was used as loading control. NT, not transfected.

that CK2 phosphorylates WT-FAM134C$^{250–466}$ and that the phosphorylation efficiency was significantly reduced using the 3A-FAM134C$^{250–466}$ variant (Fig. 4E). The residual phosphorylation observed incubating the 3A-FAM134C$^{250–466}$ mutant with CK2 is consistent with the presence of additional CK2 sites in the FAM134C$^{250–466}$ peptide (Fig. 4A). When transfected in cells, WT-FAM134C$^{250–466}$, but not the 3A-FAM134C$^{250–466}$ mutant, is recognized by the phospho-CK2 substrate antibody (Fig. 4F). This detection was abrogated by CX4945 pretreatment (Fig. 4F). Consistent with a phosphorylation-dependent mechanism of FAM134C regulation, the pharmacological inhibition of CK2 enhanced full-length FAM134C binding efficiency with endogenous LC3B (Fig. 5A) and promoted WT- but not 3D-Myc-FAM134C lysosomal localization and degradation (rescued by BafA1) (Fig. 5, B and C). Similar data were obtained using a different pharmacological inhibitor of CK2 (SGC-CK2-1) (Fig. 5B). Notably, CK2 inhibition had no effect on FAM134A and FAM134B delivery to lysosomes (fig. S7A). Together, these data suggest that FAM134C is a bona fide CK2 substrate and that CK2 controls FAM134C, but not FAM134A and FAM134B, activity.

CK2 inhibition failed to induce ER-phagy in U2OS cells expressing the ER-phagy reporter SS-RFP-GFP-KDEL. The Protein Atlas database (www.proteinatlas.org) indicates that *FAM134C* is highly expressed in pancreatic endocrine cells, collecting duct cells and alveolar cells. We confirmed these data comparing FAM134C transcript and protein levels between A549 (alveolar cells) and U2OS cell lines. Moreover, we tested ER-phagy in A549, stably expressing the ER-phagy reporter RFP-GFP-KDEL, and found that CK2 inhibition promoted ER-phagy in A549, but not in U2OS, cells (fig. S7, B to D). These data suggest that CK2 controls ER-phagy flux in cells expressing high levels of endogenous FAM134C.

mTORC1 inhibition promotes FAM134C activation via CK2 regulation

Because starvation conditions induced FAM134C dephosphorylation at residues that are phosphorylated by CK2 (Figs. 2A and 4A and fig. S3B), we investigated whether FAM134C phosphorylation at S435, S436, and T440 was also modulated by mTOR inhibition. To prevent autophagy-mediated degradation of FAM134C upon Torin1 administration, we analyzed phosphorylation levels of WT-FAM134C$^{250–466}$ and 3A-FAM134C$^{250–466}$ fragments in RCS cells treated with BafA1 and in MEFs lacking the autophagy protein Atg7. We found that the phosphorylation levels of the WT-FAM134C$^{250–466}$ peptide, but not of the 3A-FAM134C$^{250–466}$ peptide, were significantly reduced by Torin1 treatment in both cell lines (Fig. 6A and fig. S8A), supporting the model that FAM134C phosphorylation can be modulated by mTOR inhibition.

We tested whether CK2 activity was influenced by starvation and mTOR inhibition. CK2 kinase assay on recombinant CK2 incubated

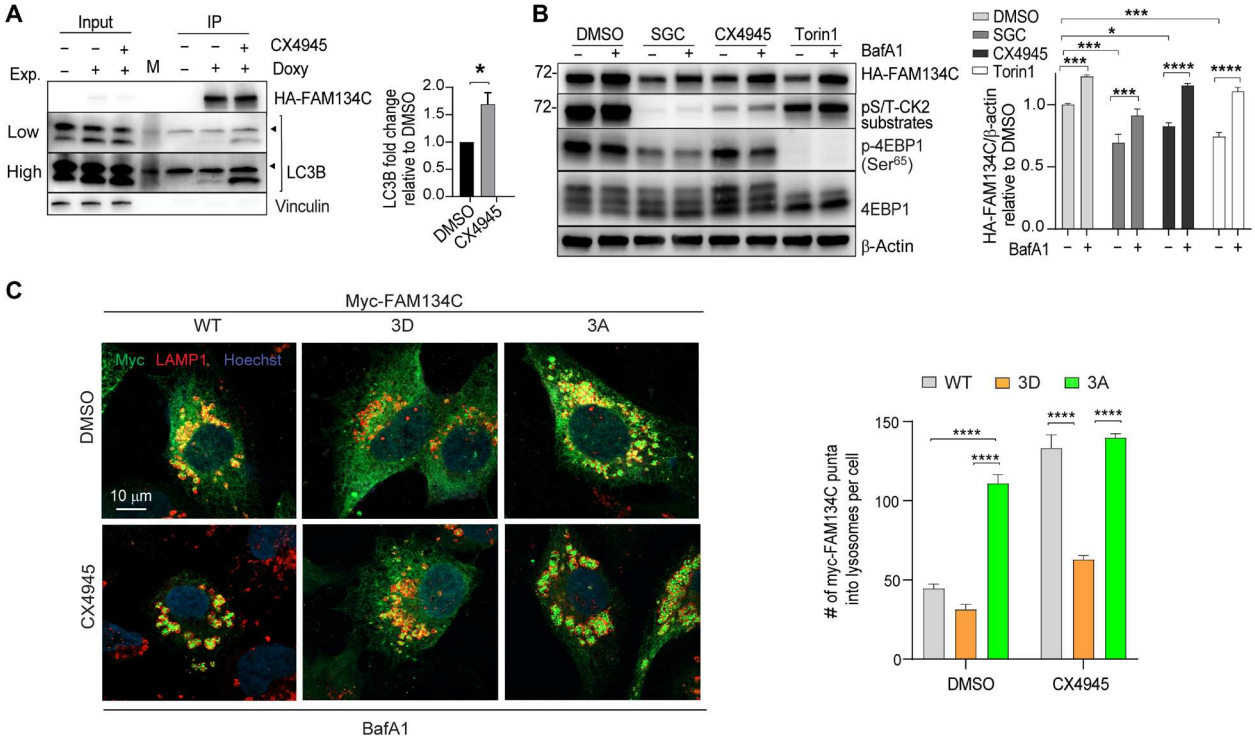

Fig. 5. Regulation of FAM134C by CK2. (**A**) Representative Western blot analysis of IP experiments of doxycycline-inducible HA-FAM134C treated with CX4945 was indicated (4 μM; 4 hours). Vinculin was used as loading control for input. Arrowheads indicate a nonspecific band. On the right, the bar graph shows quantification of immunoprecipitated LC3B relative to untreated samples. Mean ± SEM. $N = 3$ biological replicates. Student's paired t test: $^{*}P < 0.05$. (**B**) Representative Western blot analysis of HA-FAM134C in U2OS cells overexpressing doxycycline-inducible HA-FAM134C treated with DMSO, Torin1 (250 nM; 6 hours), CK2 inhibitor CX4945 (4 μM; 6 hours), or CK2 inhibitor SGC-CK2-1 (50 nM; 6 hours) in the absence or presence of BafA1 (100 nM). β-Actin was used as a loading control. Bar graph shows quantification of HA-FAM134C/β-actin ratio relative to DMSO-treated samples. Mean ± SEM. $N = 3$ biological replicates. Sidak's and Tukey's multiple comparison test: $^{****}P < 0.0001$, $^{***}P < 0.0005$, and $^{*}P < 0.05$. (**C**) Representative immunofluorescence staining of Myc (green), LAMP1 (red), and nuclei (blue) in U2OS cells transiently transfected with Myc-FAM134C-WT, Myc-FAM134C-3D, and Myc-FAM134C-3A. Cells were pretreated for 2 hours with BafA1 (100 nM), and then DMSO or CK2 inhibitor CX4945 (4 μM) was added for 6 hours. Scale bar, 10 μm. On the right, bar graph shows quantification of Myc-FAM134C in LAMP1-positive vesicles. Mean ± SEM. $N = 3$ biological replicates. $n = 15$ cells per experiment. Two-way ANOVA and Tukey's multiple comparison test: $^{****}P < 0.0001$.

with different concentrations of Torin1 demonstrated that CK2 is not directly inhibited by Torin1 (fig. S8B). In yeast, starvation and mTORC1 inhibition were reported to modulate the affinity of CK2 for its substrates through the phosphorylation of the CK2 regulatory subunit β1 at Ser^{111} (*35*). We found that the level of CK2β phosphorylation at Ser^{209}, which is located in close proximity to the positive regulatory region domain of CK2β (*33*), was significantly reduced by both HBSS and Torin1 treatments (Fig. 6, B and C). Ser^{209} CK2β has a proline in +1 position, having a sequence that is compatible with the sites phosphorylated by mTOR. In vitro peptide phosphorylation assay using a commercial truncated form of mTOR kinase demonstrated that mTOR can phosphorylate a peptide reproducing the sequence of human CK2β [203–215] including Ser^{209} in a concentration- and time-dependent manner (Fig. 6, D and E) at levels that are similar to the known mTORC1 substrate Thr^{389} of S6K (fig. S8C). The overlay of literature-derived CK2 substrates obtained from PhosphoSitePlus (*34*) with our phosphoproteomic dataset reveals that the phosphorylation levels of 18 bona fide CK2 substrates were significantly different in stimulated versus starved conditions (fig. S8D). Torin1 treatment reduced the phosphorylation of AKT Ser^{129} (*36*) and CDC37 Ser^{13} (*37*), two well-established reporters of CK2 activity (Fig. 6F). In MEFs where mTORC1 and mTORC2 activity can be inhibited via tamoxifen-inducible deletion of Raptor or Rictor subunits, respectively (*Rptor/Rictor*-indKO MEFs) (*38*), we observed reduced phosphorylation levels of AKT Ser^{129} and CDC37 Ser^{13} in *Rptor*-indKO, but not in *Rictor*-indKO, MEFs (Fig. 6G). Furthermore, probing the phospho-CK2 substrate antibody on total cell lysates, we observed that deletion of *Rptor*, but not *Rictor*, altered the CK2 phosphorylation pattern (Fig. 6G). Although we cannot exclude that other cellular elements might interpose between mTORC1 and CK2 in vivo, collectively, these data suggest that CK2 activity on a subset of substrates can be modulated during starvation by mTORC1, providing a possible explanation for the mTORC1-mediated regulation of FAM134C during starvation.

FAM134C degradation during starvation is controlled by mTOR in vivo

To investigate the physiological relevance of our findings, we generated adeno-associated virus (AAV) serotype 2/9 expressing the ER-phagy reporter ss-RFP-GFP-KDEL. AAV2/9-ssRFP-GFP-KDEL was systemically administered to WT C57B6 mice, and after 4 weeks, liver samples were isolated from 24-hour starved and ad libitum–fed mice. Starvation significantly increased the number of red-only puncta of infected WT hepatocytes compared with fed mice (Fig. 7A), suggesting that this tool can be used in vivo to monitor ER-phagy activation. Next, we infected mice with a liver-specific

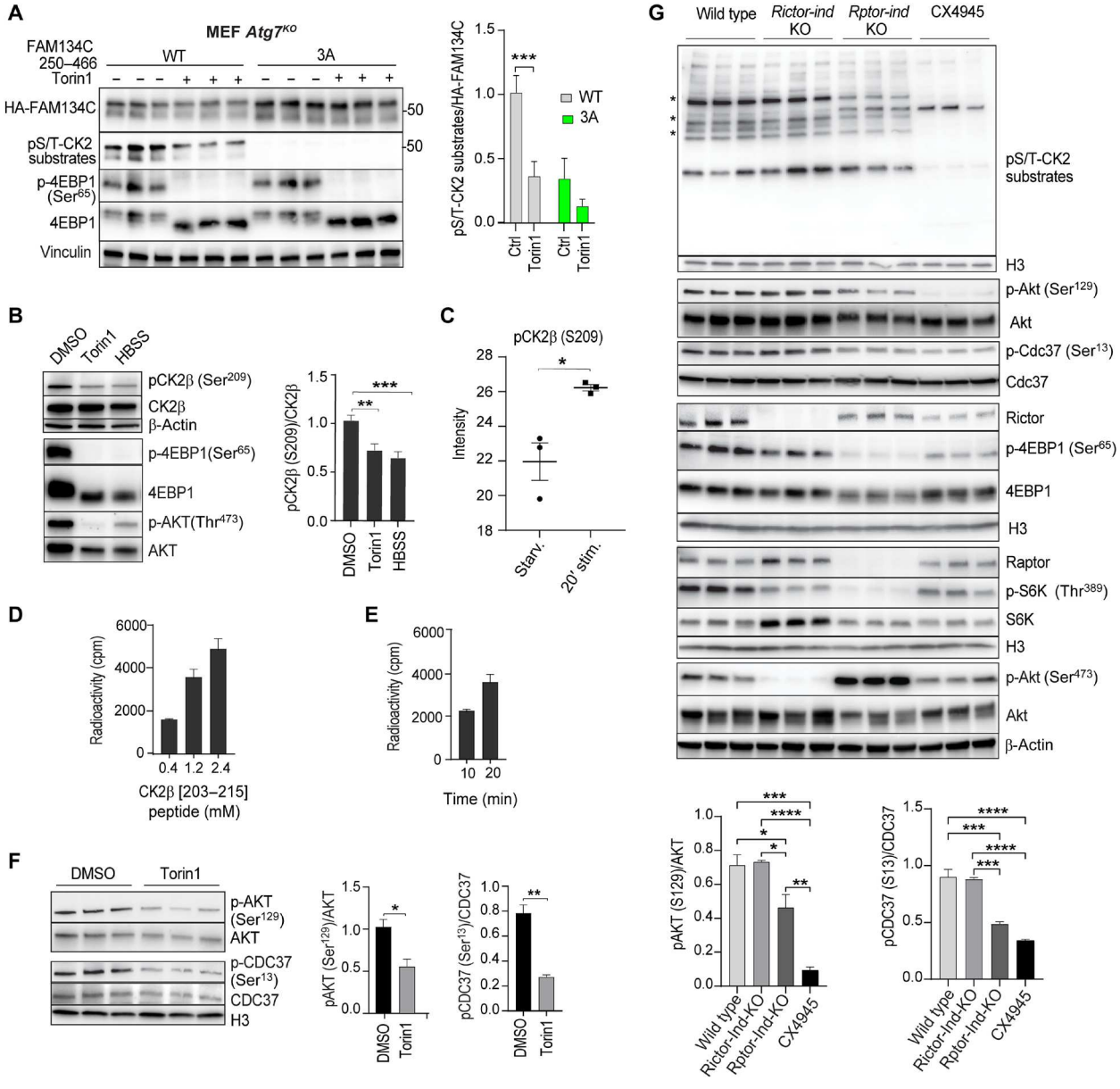

Fig. 6. CK2-dependent phosphorylation of FAM134C is modulated by mTORC1. (**A**) Western blot analysis of *Atg7*^{KO} MEF cells transfected with WT- or 3A-HA-FAM134C$^{250–466}$ peptides and treated with Torin1 (1 μM; 6 hours). (**B**) Western blot analysis of U2OS cells transfected with GFP-CK2β plasmid treated with DMSO, Torin1 (1 μM), or HBSS (4 hours). Vinculin (A) or β-actin (B) was used as loading controls. Quantification (A and B) of phosphorylated/total protein ratio. $N = 6$ (A) and $N = 4$ (B) biological replicates. Mean ± SEM. Two-way ANOVA and Sidak's multiple comparison test: $^{**}P < 0.005$ and $^{***}P < 0.0005$. (**C**) Phosphorylation analysis of CK2β in U2OS cells. $N = 3$ biological replicates. Student's paired *t* test: $^{*}P < 0.05$. (**D** and **E**) Radioactive phosphorylation assays using (D) mTOR (200 ng; 20 min) and CK2β [203–215] peptide at the indicated concentrations and (E) mTOR (200 ng) and CK2β [203–215] peptide (1.2 mM) for the indicated times. Mean ± SEM. $N = 2$. (**F**) Western blot analysis of MEF cells treated with DMSO or Torin1 (1 μM; 6 hours). $N = 3$ biological replicates. H3 histone was used as loading control. Bar graphs show quantifications (mean ± SEM) of phosphorylated AKT and CDC37/total protein ratio. Student's paired *t* test: $^{*}P < 0.05$ and $^{**}P < 0.005$ (**G**) Western blot analysis of WT, tamoxifen-inducible Raptor KO (*Rptor-indKO*), or Rictor KO (*Rictor-indKO*) MEFs. WT MEFs were treated with CX4945 (4 μM; 6 hours) as control. Asterisk (*) denotes bands changing intensity. $N = 3$ biological replicates. Bar graphs show quantifications (mean ± SEM) of phosphorylated AKT and CDC37/total protein ratio. Two-way ANOVA and Sidak's multiple comparison test: $^{*}P < 0.05$, $^{**}P < 0.005$, $^{***}P < 0.0005$, and $^{****}P < 0.0001$.

Tsc1 KO (Li-*Tsc1*^{KO}) and with a guanosine triphosphate (GTP)–bound constitutively active form of *RagA* (*RagA*^{GTP}); both models showed constitutive mTORC1 signaling even under fasting conditions (fig. S9, A and B) (*39*). Li-*Tsc1*^{KO} and *RagA*^{GTP} hepatocytes showed a significantly reduced number of red-only puncta compared to WT, suggesting defective starvation-induced ER-phagy (Fig. 7A). WT mice infected with AAV2/9-ssRFP-GFP-KDEL treated with the mTOR inhibitor (WYE-132) for 24 hours showed a significant increase of red-only puncta compared with vehicle-treated mice (Fig. 7B). These gain- and loss-of-function data demonstrate that ER-phagy is primarily regulated by mTORC1 in liver during starvation.

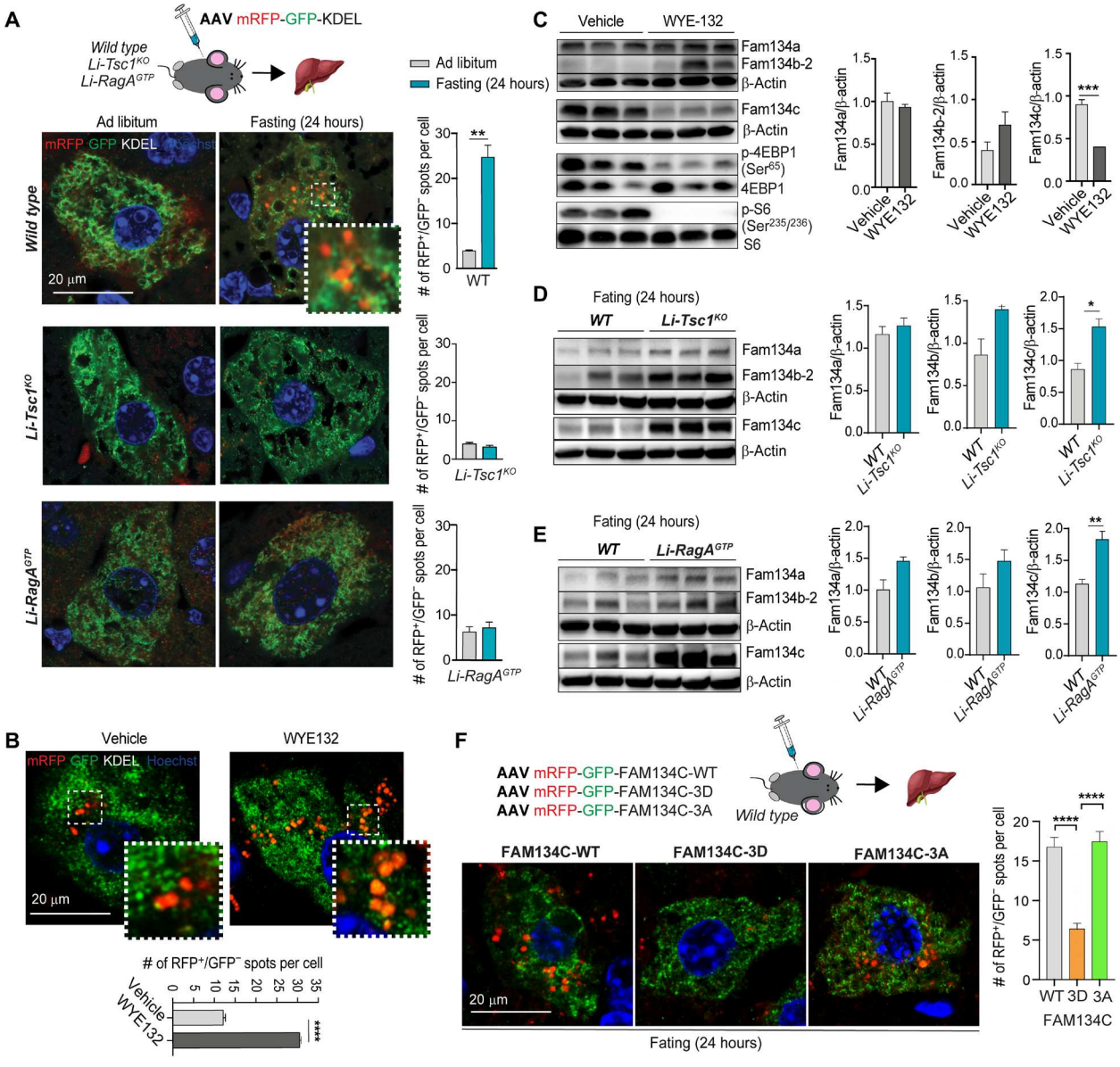

Fig. 7. Starvation and mTOR inhibition regulate Fam134c degradation in vivo. (**A**) Representative immunofluorescence staining of RFP, GFP, and nuclei in liver sections isolated from WT, *Li-Tsc1*^{KO}, and *Li-RagA*^{GTP} mice injected with AAV ssRFP-GFP-KDEL kept with food at libitum or fasted for 24 hours. Scale bar, 20 µm. Quantification shows red-only positive puncta (RFP^{+}) number per cell. Mean ± SEM. $N = 3$ biological replicates. $n = 15$ cells per experiment. Student's paired t test: $^{**}P < 0.005$. (**B**) Representative immunofluorescence staining of RFP, GFP, and nuclei in liver from WT mice injected with AAV ssRFP-GFP-KDEL and treated with WYE-132 (mTOR inhibitor) or vehicle for 24 hours. Scale bar, 20 µm. Quantification of red-only puncta (RFP^{+}/GFP^{-}) average per cell. Mean ± SEM. $N = 3$ biological replicates. $n = 15$ cells per experiment. Student's paired t test: $^{****}P < 0.0001$. (**C**) Western blot analysis of liver extracts from WT mice treated with WYE-132 (mTOR inhibitor) or vehicle for 24 hours. β-Actin was used as a loading control. $N = 3$ biological replicates. Student's paired t test: $^{***}P < 0.0005$. (**D** and **E**) Western blot analysis of liver samples isolated from WT, *Li-Tsc1*^{KO} (D), or *Li-RagA*^{GTP} (E) mice fasted for 24 hours. β-Actin was used as a loading control. $N = 3$ biological replicates. Student's paired t test: $^{*}P < 0.05$ and $^{**}P < 0.005$. (**F**) Representative immunofluorescence staining of RFP, GFP, and nuclei in liver from WT mice injected with AAV mRFP-GFP-FAM134C-WT, mRFP-GFP-FAM134C-3D, or mRFP-GFP-FAM134C-3A and fasted for 24 hours. Scale bar, 20 µm. On the right, quantification shows red-only puncta (RFP^{+}/GFP^{-}) average per cell. Mean ± SEM. $n = 50$ cells. One-way ANOVA and Tukey's multiple comparison test: $^{****}P < 0.0001$.

Consistent with a role of FAM134C during starvation-induced ER-phagy, liver samples isolated from starved and WYE-132–treated mice showed complete degradation of Fam134c, but not of Fam134a (Fig. 7C and fig. S9C). Fam134b-2 levels were instead increased in WYE-132–treated or starved animals (Fig. 7C and fig. S9C), consistent with a transcriptional induction of *Fam134b-2* during starvation in liver (*16*). Furthermore, Fam134c, but not the other Fam134s, accumulated in liver samples isolated from starved Li-*Tsc1*^{KO} and *RagA*^{GTP} mice compared to controls (Fig. 7, D and E). These data provide physiological relevance to the model by which Fam134c activity is controlled by mTORC1 levels.

To study whether Fam134c degradation is dependent on phosphorylation in vivo, we generated AAV2/9 viruses expressing WT-FAM134C, 3D-FAM134C, and 3A-FAM134C proteins fused

with the RFP-GFP tandem reporter. Infected mice were analyzed after 24 hours of fasting, and we observed the appearance of numerous red-only dots in the hepatocytes infected with RFP-GFP-FAM134C-WT and RFP-GFP-FAM134C-3A but not with RFP-GFP-FAM134C-3D proteins (Fig. 7F). These data also suggest that in vivo dephosphorylation is needed for FAM134C activation.

Deletion of FAM134C, but not of FAM134B, impairs liver lipid metabolism upon mTOR inhibition

Next, we analyzed ER-phagy in mice lacking the *Retreg3* gene, which encodes Fam134c (*Retreg3*$^{-/-}$). Control and *Retreg3*$^{-/-}$ mice were infected with AAV2/9-ss-RFP-GFP-KDEL and then kept with food ad libitum or starved for 24 hours before sacrifice. We observed robust ER-phagy induction upon starvation in control mice, but not in *Retreg3*$^{-/-}$ mice (Fig. 8A), demonstrating the importance of Fam134c during starvation-induced ER-phagy in vivo. Proteomic analysis performed in *Fam134c*^{KO}, but not *Fam134b*^{KO}, cells showed impaired degradation of enzymes involved in lipid biosynthesis upon Torin1 treatment (fig. S2). As mTORC1 is a critical regulator of liver lipid metabolism particularly during starvation (*3*), we analyzed lipid content in liver sections of WT, *Retreg3*$^{-/-}$, and *Retreg1*$^{-/-}$ (encoding for Fam134b) mice treated with vehicle or mTOR inhibitor WYE-132 for 24 hours (Fig. 8, B and C). Untreated mice showed no alteration in lipid contents, independently of genotype. As expected, the pharmacological inhibition of mTOR significantly increased lipid content in the liver of WT, *Retreg3*$^{-/-}$, and *Retreg1*$^{-/-}$ mice; however, *Retreg3*$^{-/-}$ accumulated significantly higher levels of lipids compared to WT and *Retreg1*$^{-/-}$ mice, suggesting that FAM134C-mediated ER-phagy is important for liver lipid metabolism during starvation and mTOR inhibition (Fig. 8C).

DISCUSSION

In this work, we characterized a novel mechanism of FAM134C activation in response to starvation and mTORC1 inhibition. We propose that, during starvation, the inhibition of mTORC1 facilitates the capture of ER fragments within forming autophagosomes by enhancing the interaction between LC3/GABARAP proteins and FAM134C (Fig. 8D).

In vivo, we observed that FAM134C is quickly and very efficiently degraded in liver samples isolated from fasting and WYE-132–treated animals. Conversely, FAM134B showed an opposite response, a marked increase upon starvation and mTORC1 inhibition. One possibility is that FAM134C is involved in the initial step of ER-phagy and is regulated by a phosphorylation-dependent mechanism, whereas FAM134B accounts for a later, transcriptionally regulated, ER-phagy response to starvation. Furthermore, we demonstrated that *Fam134c* deletion in vivo affected mTOR-mediated regulation of liver lipid metabolism, a phenotype that was not evident in mice lacking *Fam134b*, demonstrating that FAM134 proteins have physiologically different roles during starvation-induced ER-phagy.

Mechanistically, we found that FAM134C binding to LC3B in response to the fed/fasting transition is regulated by CK2-mediated phosphorylation of three residues (S435, S436, and T440) located in proximity but not adjacent to the FAM134C LIR domain (F447-L450). This regulation is specific to FAM134C, because both FAM134A and FAM134B lack correspondent CK2 phosphosites; hence, their activity is not influenced by CK2. Notably, CK2 inhibition promotes ER-phagy in lung alveolar cells that express high levels of FAM134C, but not in U2OS cell line where FAM134C levels are low, suggesting that the relative expression of autophagy receptors might drive substrate specificity during autophagy.

CK2 was previously implicated in the regulation of mitophagy via phosphorylation of FUNDC1 (*40*), and also in this case, phosphorylation negatively modulates the avidity of the receptor for mATG8s. Therefore, in both cases, CK2 has the peculiar ability to negatively modulate the affinity of the autophagy receptors for mATG8s. Conversely, CK2-mediated phosphorylation of the ER-phagy receptor TEX264 at residues located in positions −1, −2, and −4 upstream the LIR domain was recently shown to enhance its binding to LC3/GABARAP proteins, hence promoting ER-phagy (*41*). The differential effects of this phosphorylation can be explained by the proximity of the phosphorylated residue to the LIR domain. The residues phosphorylated by CK2 in FAM134C interact with a region of LC3B that has a relatively neutral charge; thus, phosphorylation, by significantly increasing the local electron density, might lead to a less favorable interaction with LC3B. Conversely, the LIR domain binds an electron-poor (positively charged) LC3B region; therefore, phosphorylation of residues immediately adjacent to the LIR sequence might favor binding strength, as observed for TEX264, OPT, NIX, and BNIP3 (*41*–*44*).

CK2 is a constitutively active kinase, which is regulated at the substrate level (*33*, *45*). In yeast, CK2 substrate affinity can be influenced by mTORC1 via its effector kinase Kns1 (*35*). In mammalian cells, phosphorylation of eIF2β and Pdx1 substrates by CK2 depends on both mTORC1 and insulin signaling, respectively (*46*, *47*). In this work, we demonstrated that FAM134C is a newly identified CK2 substrate that is regulated in an mTORC1-dependent fashion.

ER-phagy deregulation has not been implicated in human diseases yet. However, we showed that impaired ER-phagy was associated with aberrant accumulation of FAM134C in liver samples isolated from mice with hyperactive mTORC1, suggesting that deregulation of FAM134C-mediated ER-phagy might contribute to the ER pathology and lipid alterations observed in diseases associated with mTORC1 hyperactivity (*48*).

Last, our work defines a mechanism of autophagy substrate selectivity that is operated during starvation-induced autophagy, providing a link between metabolic and quality control autophagy. The cross-talk between bulk and selective autophagy is still largely unexplored (*49*). The identification of new principles governing autophagy cargo selectivity holds potential implications for the treatment of many human diseases (*50*, *51*).

MATERIALS AND METHODS

Cell culture

U2OS TRex cells were provided by S. Blacklow (Brigham and Women's Hospital and Harvard Medical School). The RCS cell line was a Swarm chondrosarcoma chondrocyte line. *Rptor/Rictor*-inducible KO MEFs were provided by M. N. Hall. MEF *Atg7*^{KO} cells were a gift from M. Komatsu and N. Mizushima. *Fam134c*^{KO} MEFs were provided by C. Hübner (Jena University). HEK293T cells were purchased from the American Type Culture Collection.

Cells were maintained at 37°C with 5% CO_2 in Dulbecco's modified Eagle's medium (DMEM) and supplemented with 10% fetal bovine serum (FBS) and 1% penicillin and streptomycin. Complete starvation was performed in HBSS (Euroclone, ECB4006L), serum

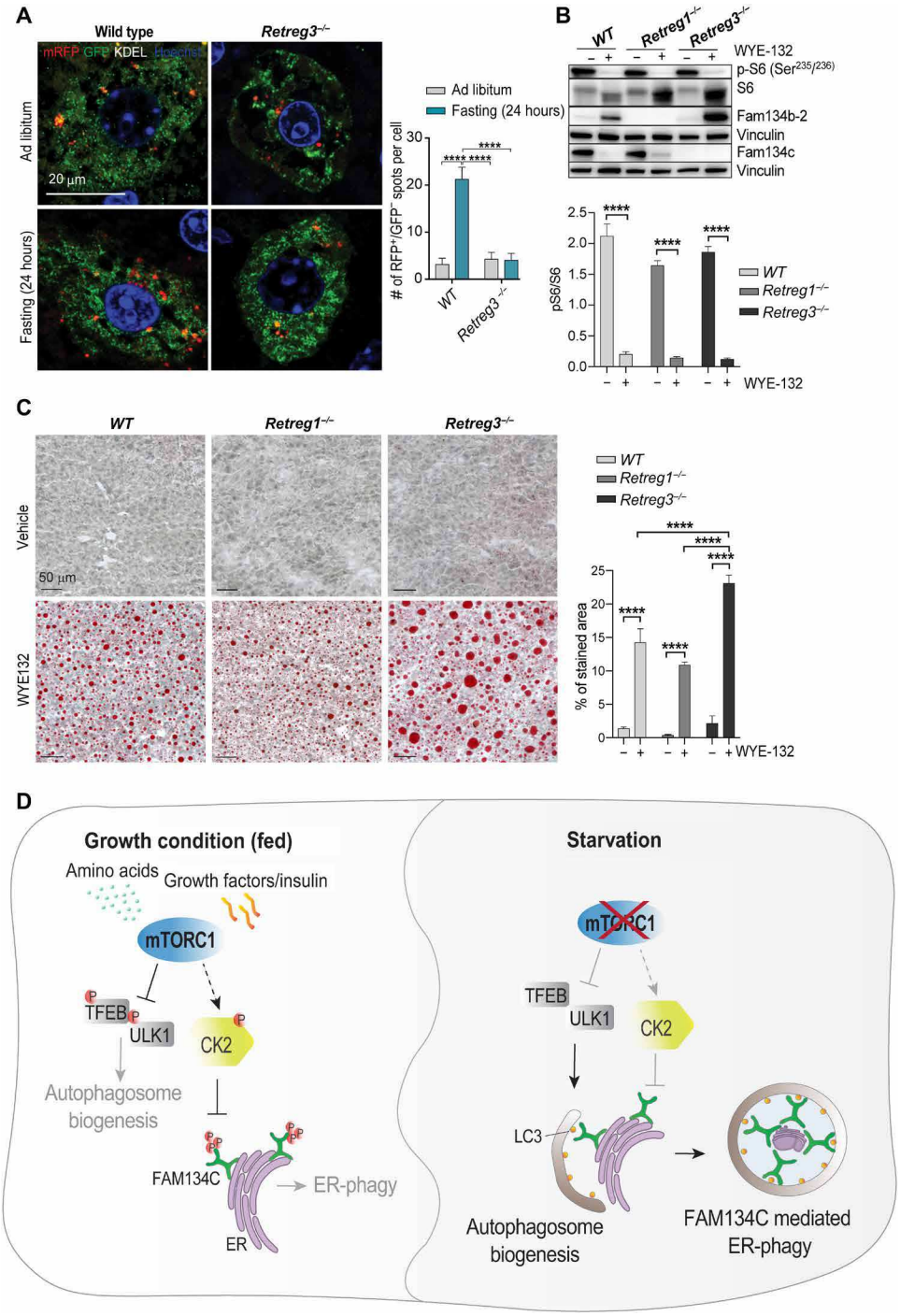

Fig. 8. Loss of Fam134c in mouse impairs lipid metabolism in liver upon mTOR inhibition. (**A**) Representative immunofluorescence staining of RFP (red), GFP (green), and nuclei (blue) in liver from WT and *Retreg3*$^{-/-}$ mouse after ad libitum feeding or 24 hours of fasting. Scale bar, 20 μm. Quantification shows red-only positive puncta (RFP^{+}) number per cell relative to ad libitum condition. Mean ± SEM. $N = 3$ biological replicates. $n = 15$ cells per experiment. Two-way ANOVA and Tukey's multiple comparison test: ****$P < 0.0001$. (**B**) Representative Western blot analysis of indicated proteins in liver from WT, *Retreg1*$^{-/-}$, and *Retreg3*$^{-/-}$ mice treated with WYE-132 (mTOR inhibitor) or vehicle for 24 hours. Vinculin was used as a loading control. On the bottom, quantification shows phosphorylated/total protein ratio. Mean ± SEM. $N = 5$ biological replicates. Two-way ANOVA and Tukey's multiple comparison test: ****$P < 0.0001$. (**C**) Representative images of Oil Red O staining in WT, *Retreg1*$^{-/-}$, and *Retreg3*$^{-/-}$ mouse liver sections. Mice were treated with WYE-132 (mTOR inhibitor) or vehicle for 24 hours. On the right, quantification of red area was reported as percentage (%) of total area. Mean ± SEM. $N = 5$ biological replicates. Two-way ANOVA and Tukey's multiple comparison test: ****$P < 0.0001$. (**D**) Proposed model of FAM134C activation during starvation. The inhibition of mTORC1 concomitantly induces autophagosome biogenesis and reduction of FAM134C phosphorylation that favors autophagy of FAM134C-decorated ER fragments.

starvation was performed in DMEM (Euroclone, ECM0728), and amino acid starvation was performed in amino acid–free RPMI (US Biological, R9010-01) supplemented with 10% dialyzed FBS (Invitrogen, Thermo Fisher Scientific). Cells were reverse-transfected with Lipofectamine LTX and Plus reagent according to the manufacturer's instructions. Plasmids are listed in table S8. Stable cell lines were generated using retroviral or lentiviral virus generated in HEK293T cells. For retrovirus, 1.3 μg of MSCV-N-Flag-HA-IRES-PURO-FAM134s and PCMVneo-mKeima-RAMP4 (table S8) vectors with the packaging plasmid viral Gag-Pol (0.95 μg) and the envelope plasmid VSV-G (0.75 μg) was transfected in a p60 dish. The medium containing lenti- or retroviral particles was spun down to eliminate dead cells. For retroviral infection, cells were spun down with retroviral suspension containing polybrene (8 μg/ml) for 90 min at 2300 rpm, followed by a medium change after 6 hours or overnight incubation. For lentivirus, 3.3 μg of plasmids pcW57-ssRFP-GFP-KDEL or pcW57-ssRFP-GFP-FAM134s (table S8) with pPAX2 packaging plasmid (2.7 μg) and pMD2.G envelope plasmid (1 μg) was cotransfected in HEK293T cells using a six-well plate. For lentivirus infection, cells were incubated with lentiviral suspension containing with polybrene (8 μg/ml; Merck, #TR-1003-G) for 24 hours. Confluent infected cell lines were then selected with the respective antibiotics.

Generation of CRISPR clones

To deplete the genes of interest, we applied the clustered regularly interspaced short palindromic repeats (CRISPR)–CRISPR-associated protein 9 (Cas9) technology. The all-in-one vector (Sigma-Aldrich) contains specific single-guide RNA (sgRNA) under the control of a U6 promoter, a recombinant form of Cas9 protein under the control of the cytomegalovirus (CMV) promoter, and an eGFP reporter gene under the control of the SV40 promoter. RCS cells were transfected with 5 μg of all-in-one vector containing one of the following sgRNA: Atg7 sgRNA sequence: CGCTGAGGTTCACCATCCT; Fam134a sgRNA sequence: CCCCCTGAAGAACCGCACT; Fam134b sgRNA sequence: TGAGCTCTGTGGGTAAGCCAAGG; and Fam134c sgRNA sequence: CGGGCACGCTGAGCAACCG (–).

After transfection, single-cell sorting for the eGFP fluorescence was performed by FACS using BD FACSAria III. To identify the specific mutations, confluent cells were then subjected to polymerase chain reaction (PCR) analysis followed by Sanger sequencing. Selected clones were then validated by Western blotting analysis of the protein of interest.

Chemicals

BafA1 (Euroclone, #BK54645S) was used at 100 or 200 nM for the indicated time. Torin1 (Euroclone, #BK14379S) was used at 150 nM, 250 nM, or 1 μM at different time points. CK2 inhibitor CX4945 (Selleckchem, #S2248) was used at 4 μM for 6 hours. The CK2 inhibitor SGC-CK2-1 (Tocris, #7450) was used at 50 nM for 6 hours. the mTOR inhibitor WYE-125132 (Selleckchem, #PZ0321) was used for in vivo experiments at 10 mg/kg and injected three times every 8 hours. Doxycycline (Sigma-Aldrich, #D9891) was used at 4 μg/ml and added 24 hours before the experiments. Tamoxifen (Sigma-Aldrich, #H6278) was used at 1 μM for 72 hours.

Cloning procedures and DNA mutagenesis

To generate HA- and Myc-FAM134s plasmids, FAM134s and FAM134C mutants were cloned into pDONR223 vector (Invitrogen) using the BP Clonase Reaction Kit (Invitrogen, #11789020) and further recombined, through the LR Clonase Reaction Kit (Invitrogen, #11791020), into the GATEWAY destination vectors iTAP MSCV-N-FLAG-HA IRES-PURO or Myc-pcDNA3.1 (table S8). Myc-pcDNA3.1 GATEWAY destination vector was generated from a standard Myc-pcDNA3.1 (table S8), where the GATEWAY features (attR1-CAT/CmR-ccdB-attR2) were inset in the multiple cloning site.

For the generation of pcW57-ssRFP-GFP-FAM134s, the eGFP sequence was cleaved out from pcW57-ssRFP-GFP-KDEL (table S8) and amplified, while FAM134s sequences were amplified from Myc-FAM134s pcDNA3.1 (table S8). The In-Fusion Multiple-Insert Cloning procedure, using the In-Fusion HD Cloning Kit (Takara, # 639649), was applied to clone the two inserts into the linearized pcW57-ssRFP vector.

The C-terminal FAM134C WT and mutants were generated by amplification of the 250– to 466–amino acid sequence into the GATEWAY destination vector iTAP MSCV-N-FLAG-HA IRES-PURO or pGEX-4T1-GST (table S8). To purify C-terminal FAM134C and FAM134C mutant proteins, GST-FAM134C vectors were generated, cloning the cDNAs into the GATEWAY destination vectors pGEX-4T1 (table S8). For the generation of the retrovirus pCMVneo-mKeima-Ramp4, the Ramp4 sequence was amplified from TetOn-mCherry-eGFP-RAMP4 vector (table S8) fused at the N terminus with mKeima and inserted into pCMVneo using the In-Fusion HD Cloning Kit (Takara, # 639649) according to the manufacturer's instructions.

To generate the AAV, the construct mRFP-GFP-KDEL or mRFP-GFP-FAM134C-WT or mRFP-GFP-FAM134C-3D was amplified from the respective vectors (table S8). The pTigem plasmid (table S8) containing the inverted terminal repeats of AAV2, the kanamycin resistance sequences, and the CMV promoter was linearized, and inserts were cloned using the In-Fusion HD Cloning Kit.

For FAM134C mutagenesis, primers were designed using the QuikChange Primer Design tool (Agilent). cDNA mutations were generated via PCR site-directed mutagenesis using QuikChange II mutagenesis kit (Agilent), according to the manufacturer's protocol. Transformation was performed in DH5α Competent Cells (Invitrogen).

Immunoblotting of total cell lysates

Cells were washed twice with phosphate-buffered saline (PBS) and then scraped in radioimmunoprecipitation assay (RIPA) lysis buffer [20 mM tris (pH 8.0), 150 mM NaCl, 0.1% SDS, 1% NP-40, and 0.5% sodium deoxycholate] supplemented with PhosSTOP and EDTA-free protease inhibitor tablets with 1× final concentration (Roche). Cell lysates were incubated on ice for 20 min; then, the soluble fraction was isolated by centrifugation at 15,000 rpm for 20 min at 4°C. Protein concentration was measured using the colorimetric bicinchoninic acid (BCA) protein assay kit (Pierce Chemical Co.). Protein extracts (25 to 50 μg) were separated by SDS–polyacrylamide gel electrophoresis (SDS-PAGE) and transferred onto polyvinylidene difluoride (Merck Millipore) or nitrocellulose membrane (PerkinElmer). Primary antibodies used are listed in table S9. Horseradish peroxidase–conjugated goat anti-mouse or anti-rabbit immunoglobulin G antibody was used at 1:2000 (Vector Laboratories). Signal detection was performed using ECL Star Enhanced Chemiluminescent Substrate (Euroclone) according to the manufacturer's protocol. The Western blotting images were acquired using the ChemiDoc-lt imaging system (UVP).

Coimmunoprecipitation

HEK293T cells were cotransfected with pMSCVneo-GFP-LC3 plasmid together with 3D-Myc-FAM134C or 3A-Myc-FAM134C. After 24 hours of transfection, cells were incubated for 8 hours with BafA1 (100 nM), harvested, and lysed in RIPA buffer containing protease and phosphatase inhibitor cocktails. Lysates were centrifuged at 14,800 rpm for 20 min and quantified, and 500 μg was incubated overnight at 4°C with 10 μl of anti-Myc agarose bead slurry (Diagnostic Brokers Associated, yta-100). Beads were then washed three times in RIPA buffer, resuspended in Laemmli buffer, and boiled. The 50% of the immunoprecipitated fraction was loaded on SDS-PAGE, and Western blotting analysis was performed using the anti-GFP and anti-Myc antibodies.

Stable cell lines for FAM134s were induced with doxycycline (1 μg/ml) for 24 hours. U2OS cells expressing FAM134s were harvested in 50 mM tris-HCl (pH 8.0), 120 mM NaCl, 1% (v/v) NP-40, and complete protease inhibitor cocktail in a confluent 15-cm-diameter petri dish. Lysates were cleared by centrifugation at 10,000*g* for 10 min and incubated overnight at 4°C with monoclonal anti–HA-agarose antibody (Thermo Fisher Scientific, #26181), previously conjugated to Protein G Sepharose beads (Thermo Fisher Scientific, #15918014). Beads were then washed three times in 0.1% (v/v) NP-40. Proteins were eluted by boiling in Laemmli buffer and loaded on SDS-PAGE for Western blot analysis or processed for MS analysis.

Immunofluorescence

Cells were fixed for 15 min in 4% paraformaldehyde (PFA) in PBS and permeabilized for 20 min in blocking buffer [0.05% (w/v) saponin, 0.5% (w/v) bovine serum albumin (BSA), 50 mM NH_4Cl, and 0.02% NaN_3 in PBS]. Cells were incubated overnight in a humid chamber with primary antibodies (table S9), washed three times in PBS, and incubated for 1 hour at room temperature with the secondary (Alexa Fluor–labeled) antibodies. After three washes in PBS, cells were incubated for 20 min with Hoechst 33342 (1 μg/ml) and finally mounted in Mowiol. Anti-mouse or anti-rabbit Alexa Fluor–labeled antibody (1:1000; Thermo Fisher Scientific) was used. All confocal experiments were acquired with an LSM 880 confocal microscope (Carl Zeiss) equipped with a 63× or 100× objective and using a slice thickness of 0.5 μm. All the quantifications were performed using ImageJ plugins.

ER-phagy assays: ssRFP-GFP-KDEL and mKeima-RAMP4

Fam134c^{KO} MEF and *Fam134*^{KOs} RCS cell lines were infected with lentivirus pCW57-CMV-ssRFP-GFP-KDEL to generate ER-phagy reporter-inducible cell lines. The expression of the plasmid was induced with doxycycline (4 μg/ml; 24 hours), and starvations or Torin1 treatment was applied at different time points, as indicated. Cells were either collected in PBS and the fluorescence was analyzed with BD FACSAria III or fixed in 4% PFA for 15 min to quantify the number of red-only puncta after image acquisition. For FACS analysis, 10,000 fluorescent events (both red and green) were collected and red fluorescent shift was analyzed by applying a specific threshold based on the untreated samples.

Protein expression and purification from bacteria

FAM134C (250 to 466) was cloned into pGEX6P1 and expressed as glutathione *S*-transferase (GST) fusion proteins in *Escherichia coli* BL21 DE3. Cells were lysed by sonication in lysis buffer [20 mM tris-HCl (pH 7.5), 10 mM EDTA (pH 8), 5 mM EGTA, 150 nM NaCl, and 1% Triton X-100], and the lysate was cleared by centrifugation. The expressed protein was purified by 20 nM glutathione (GSH) in 10 mM tris (pH 8), 1 mM dithiothreitol, 1 mM EDTA, and 300 nM NaCl with final pH 8.

In vitro phosphorylation assays

To perform the FAM134C phosphorylation assay, different amounts of WT or mutant recombinant FAM134C C-terminal proteins were incubated with recombinant tetrameric CK2 (7 ng) for 20 min at 30°C in a total volume of 20 μl of radioactive phosphorylation buffer containing 50 mM tris-HCl (pH 7.5), 10 mM $MgCl_2$, 0.1 M NaCl, and 10 μM [γ-^{33}P]adenosine triphosphate (ATP) (Hartmann Analytic) at 5000 counts per minute (cpm)/pmol. Reactions were stopped by adding Laemmli buffer. Proteins were resolved onto 11% SDS-PAGE, stained with Coomassie blue, and analyzed by digital autoradiography (CyclonePlus Storage Phosphor System, PerkinElmer) to detect and quantify radioactive bands.

For CK2 kinase assay, CK2 activity was measured toward the model peptide substrate RRRADDSDDDDD (0.1 mM), as elsewhere described (*52*). For the mTOR kinase assays, the RRR-QAASNFKSPVKTIR peptide corresponding to CK2β human sequence [203–215] and the control peptide RRR-NQVFLGFTYVAP, corresponding to p70 S6 kinase human sequence [382–393], were synthetized using a multiple peptides synthesizer (SyroII, MultiSynTech GmbH) (the three additional arginine residues at the N terminus allow peptide binding to phosphocellulose paper upon kinase assays). Recombinant truncated mTOR (1362–end, Millipore) was incubated at 30°C in a total volume of 25 μl of a radioactive phosphorylation mixture containing 50 mM Hepes (pH 7.5), 1 mM EGTA, 3 mM $MnCl_2$, and 100 μM [γ-^{33}P]ATP (Hartmann Analytic) at 3000 cpm/pmol. Reactions were stopped by sample absorption on phosphocellulose papers. Papers were washed three times with 75 mM phosphoric acid and counted in a scintillation counter (PerkinElmer).

MS proteomics and phosphoproteomics

For the proteomic experiment, cells were plated into six-well plates and incubated for 1 hour in complete DMEM the following day. Afterward, cells were washed twice with PBS and then incubated for 20 min in RIPA lysis buffer [20 mM tris (pH 8.0), 150 mM NaCl, 0.1% SDS, 1% NP-40, and 0.5% sodium deoxycholate] supplemented with PhosSTOP and EDTA-free protease inhibitor tablets. Cell lysates were then centrifuged at 15,000 rpm for 20 min at 4°C. The soluble fraction was collected, and protein concentration was measured using the colorimetric BCA protein assay kit (Pierce Chemical Co., Boston, MA, USA). Protein extracts (50 μg) were then processed for MS analysis.

For phosphorylation analysis, HA-FAM134C U2OS stable cell lines were induced with doxycycline (4 μg/ml) for 24 hours. Cells were starved for 5 hours (HBSS containing 200 nM BafA1) and stimulated for 20 min with complete DMEM supplemented with 1× essential (Invitrogen, #11130051) and nonessential amino acids (Invitrogen, #11140050), 1× glutamine (Invitrogen, #25030081), and 100 nM insulin (Merck, #I9278). Cells were washed twice with PBS, scraped, and incubated for 20 min with RIPA lysis buffer supplemented with PhosSTOP and EDTA-free protease inhibitor tablets.

All the experiments were performed in a labeling-free setting. For full proteomes in FAM134-overexpressing cells and IP-MS interactomes, proteins were precipitated in acetone and then reduced and alkylated in a solution of 6 M guanidine-HCl, 5 mM tris(2-carboxyethyl)phosphine (TCEP), and 20 mM chloroacetamide.

Peptides were obtained by digesting proteins with LysC (Wako) for 3 hours at 37°C and with the endopeptidase sequencing-grade trypsin (Promega) overnight at 37°C. Collected peptide mixtures were concentrated and desalted using the Stop and Go Extraction (STAGE) technique (*53*). For full proteomes in RCS cells, peptides were obtained using the iST Kit from PreOmics. For phosphoproteomes, U2OS cells were lysed [2% SDS, 50 mM tris-HCl (pH 8), 150 mM NaCl, 10 mM TCEP, and 40 mM chloracetamide], heated at 95°C for 10 min, and sonicated with Sonics Vibra-Cell (1-s ON/1-s OFF pulse for 30 s using 30% amplitude). The equivalent of 1 mg of protein lysate was precipitated by methanol/chloroform using four volumes of ice-cold methanol, one volume of chloroform, and three volumes of water. The mixture was centrifuged at 20,000*g* for 30 min, the upper aqueous phase was removed, and three volumes of ice-cold methanol were added. Proteins were pelleted by centrifugation and washed twice with one volume of ice-cold methanol and air-dried. The resulting protein pellet was resuspended in 8 M urea with 10 mM 4-(2-hydroxyethyl)-1-piperazinepropanesulfonic acid (EPPS) (pH 8.2). For digestion, 300 µg of proteins was diluted to 1 M urea and incubated 1:50 (w/w) ratio with LysC (Wako Chemicals) for 3 hours and 1:100 (w/w) ratio with sequencing-grade trypsin (Promega) overnight. The reaction was acidified using trifluoroacetic acid (TFA) (0.5%) and purified using Sep-Pak tC18 (Waters, 50 mg) according to the manufacturer's protocol. Phosphopeptides were enriched using Titansphere Phos-TiO beads (GL Sciences Inc.) according to the manufacturer's protocol. Phosphopeptides were cleaned up by C8 stage tip and fractionated using C18 stage tips. After washing (80% acetonitrile) and after an equilibration step with 0.1% TFA, peptides were loaded on C18 stage tips in 0.1% TFA solution and washed twice with 0.1% TFA in water. Samples were vacuum-dried for liquid chromatography (LC)–MS measurements.

Instruments for LC-MS/MS analysis consisted of NanoLC 1200 coupled via a nanoelectrospray ionization source to the quadrupole-based Q Exactive HF benchtop mass spectrometer. Peptide separation was carried out according to their hydrophobicity on a homemade chromatographic column, 75-µm inside diameter, 8-µm tip, bed-packed with Reprosil-PUR (C18-AQ), 1.9-µm particle size, 120-Å pore size, using a binary buffer system consisting of solution A (0.1% formic acid) and solution B (80% acetonitrile and 0.1% formic acid). Runs of 120 min after loading were used for proteome samples, with a constant flow rate of 300 nl/min. After sample loading, run started at 5% buffer B for 5 min, followed by a series of linear gradients, from 5 to 30% B in 90 min, then a 10-min step to reach 50% and a 5-min step to reach 95%. This last step was maintained for 10 min. Q Exactive HF settings are as follows: MS spectra were acquired using 3E6 as an AGC target, a maximal injection time of 20 ms, and a 120,000 resolution at 200 mass/charge ratio (m/z). The mass spectrometer was operated in a data-dependent Top20 mode with subsequent acquisition of higher-energy collisional dissociation fragmentation MS/MS spectra of the top 20 most intense peaks. Resolution, for MS/MS spectra, was set to 15,000 at 200 m/z, AGC target to 1E5, maximum injection time to 20 ms, and the isolation window to 1.6 Th. The intensity threshold was set at 2.0 E4 and dynamic exclusion at 30 s.

Data analysis

All experiments were performed in at least three independent biological replicates. For MS, all acquired raw files were processed using MaxQuant (1.6.2.10) and using the implemented Andromeda search engine. For protein assignment, spectra were correlated with the UniProt Homo Sapiens and Rattus Norvegicus database (v. 2019) including a list of common contaminants. Searches were performed with tryptic specifications and default settings for mass tolerances for MS and MS/MS spectra. Carbamidomethyl at cysteine residues was set as a fixed modification, while oxidations at methionine, acetylation at the N terminus, and phosphorylation STY (in the case of phosphoproteomes) were defined as variable modifications. The minimal peptide length was set to seven amino acids, and the false discovery rate (FDR) for proteins and peptide spectrum matches to 1%. The match-between-run feature with a time window of 0.7 min was used. For further analysis, the Perseus software (1.6.2.3) was used and first filtered for contaminants and reverse entries as well as proteins that were only identified by a modified peptide. For full proteomes and IP interactomes, the label-free quantification ratios were logarithmized, grouped, and filtered for minimum valid number (minimum of three in at least one group). Missing values have been replaced by random numbers that are drawn from a normal distribution.

Data obtained for the total proteome analysis in U2OS and RCS cells are reported in tables S1 and S2, respectively. For ER proteome analysis, ER proteins were downloaded from the Subcellular Location section of The Human Protein Atlas database (www.proteinatlas.org/about/download). Data were filtered to keep only ER and ribosomal proteins (table S3). In Fig. 1H (proteome analysis in RCS), the proteins found to be significantly modulated by Torin1 treatment in control cells were used for downstream analyses in cells with the different genotypes (table S5). For phosphoproteomes, intensity values were filtered for the sites that have localization probability of >0.75. After this, the values were logarithmized, grouped, and filtered for minimum valid number (minimum of three in at least one group). Last, the intensities were normalized by subtracting the median intensity of each sample. Significantly regulated proteins between conditions were determined by Student's t test using FDR < 0.05 as threshold. Data are available via ProteomeXchange with identifier PXD030451 (username: reviewer_pxd030451@ebi.ac.uk; password: KoKm7mWD).

MD simulations

The three-dimensional (3D) structure of LC3B (PDB ID 6LAN) was obtained from the Research Collaboratory for Structural Bioinformatics Protein Data Bank (RCSB PDB) (*54*). The side chains of residues D48, E62, and S90 were not univocally resolved, allowing us to choose by visual inspection the side chain conformations B, A, and A for these three residues, respectively. The first nine residues, belonging to CCDC50, were removed to obtain the LC3 WT. The 3D structure of FAM134C_P434-P460 was built by means of the MODELLER suite using the FAM134B structure with PDB ID 7BRQ as template. The starting 3D structure of the complex formed by FAM134C_P434-P460 and LC3B was obtained by using the molecular docking program HADDOCK 2.4 (*55*). In the docking calculation, we defined the active residues a priori, i.e., F447 and L450 for FAM134C_P434-P460 and I23, F52, and I66 for LC3B. To select the best binding pose, we measured the distance between FAM134C's L438 and LC3b's L71, a hydrophobic interaction predicted to be crucial for the binding mechanism. The binding complex obtained from docking was then solvated using a box of TIP3P water model and a salinity of 0.15 M NaCl. The N terminus and C terminus of FAM134C_P434-P460 were capped with an acetyl and a methyl amino-protecting group, respectively. The Amber ff99sb-ildn force field was used (*56*) for the MD calculations that were run using the GROMACS

2020.5 engine. Each simulation box underwent a thermalization cycle with smoothly decreasing restraints on heavy atoms to gently equilibrate the structure. In detail, we used the following protocol: Heating the system from 100 to 300 K by increasing the temperature by 50 K each step composed of 1 ns of canonical ensemble (NVT) simulation followed by 1 ns of isothermal–isobaric (NPT) ensemble simulation. During the thermalization, the V-rescale thermostat was used, whereas the Langevin dynamics temperature control scheme was used in the production runs. Periodic boundary conditions were applied, and the particle mesh Ewald method was used to treat long-range electrostatic interactions (*57*). For short-range interactions, a cutoff distance of 1.0 nm was applied. The pressure was fixed at a reference value equal to 1 bar by means of the Parrinello-Rahman barostat (*58*).

Parallel-tempering MD

We used 70 independent replicas of 500 ns of the FAM134C_P434-P460/LC3b system. Each replica was simulated at a different temperature to cover the temperature range from 300 to 450 K. The temperature of each replica was defined using the formula reported by Prakash *et al.* (*59*). Positional restraints were applied on the secondary structure Cαs of LC3B and on D445-P460's Cαs of FAM134C_P434-P460. For the production phase, we used the same protocol previously reported for the MD simulations.

FAM134C_P434-P460/LC3b binding interface evaluation

The protein-protein interactions established by the residues at the FAM134C_P434-P460/LC3B's interface were assessed by calculating their frequency of occurrence using the PLOT NA routine of Drug Discovery Tool (*60*) and displayed as histograms. We set a distance cutoff value of 4 Å to define two interacting residues.

Animal housing

All mice in this study were housed under specific pathogen–free conditions, at 22°C, and with 12-hour dark/12-hour light cycles (light cycle from 8:00 a.m. to 8:00 p.m.). Mice were fed with a standard chow diet and were of pure C57BL/6 background. All mice were observed weekly by trained personnel. All studies on mice were conducted in strict accordance with the Institutional Guidelines for animal research and approved by the Italian Ministry of Health, Department of Public Health, Animal Health, Nutrition, and Food Safety in accordance to the law on animal experimentation (D.Lgs. 26/2014). Furthermore, all animal treatments were reviewed and approved in advance by the Ethics Committee at the Telethon Institute of Genetics and Medicine (TIGEM) Institute (Pozzuoli, Italy) or according to protocols approved by the Centro Nacional de Investigaciones Oncológicas (CNIO)-Instituto de Salud Carlos III Ethics Committee for Research and Animal Welfare (CEIyBA) at the CNIO (Madrid, Spain).

All mice used were maintained in a C57BL/6 strain background. To minimize variability, mice belonging to the same litter were grouped on the basis of their genotype.

Animal procedures

For fasting experiments, mice were separated in clean cages without access to food from 8a.m. to 8a.m. the following day. For the experiments with the mTOR inhibitor WYE-125132, mice were starved from 6 p.m. to 1 p.m. the following day and then injected intraperitoneally with WYE-125132 or vehicle (10 mg/kg) [30% PEG400 (polyethylene glycol, molecular weight 400), 0.5% Tween 80, and 5% propylene glycol] and refed with chow 1 hour after the injections. Vehicle or WYE-125132 was injected three times, every 8 hours, for a total treatment of 24 hours.

For Western blotting, 25 mg of liver was homogenized in 1 ml of RIPA buffer containing protease and phosphatase inhibitor cocktails using a Tissue Lyser II homogenizer (QIAGEN) and left on a rotating wheel overnight at 4°C. Then, pellets were discarded by spinning down for 30 min at maximum speed, and BCA assay was performed on supernatants to determine protein concentration.

Immunostaining of RFP and GFP was performed on 10-μm-thick formalin-fixed and paraffin-embedded liver sections. Sections were permeabilized in 3% (w/v) BSA, 0.3% Triton X-100 in PBS for 20 min and then incubated with 10% goat serum in PBS for 1 hour. Primary antibodies were incubated overnight at 4°C. Sections were washed three times with 0.1% BSA in PBS and then incubated for 1 hour with secondary antibodies Alexa Fluor–conjugated and 4′,6-diamidino-2-phenylindole (DAPI). Sections were mounted in Mowiol mounting medium and analyzed using a superresolution confocal LSM 880 microscope (Carl Zeiss).

For Oil Red O staining, tissues were embedded in O.C.T. (optimal cutting temperature) compound and cut into 10-μm sections, fixed in formalin, and stained following the IHC World protocol. To quantify the Oil Red O–positive area, images were processed through the threshold tool of the ImageJ software to segment out and measure the staining areas as percentage of total area.

Generation of *Retreg3* KO mice

Mice carrying *Retreg3* KO were generated using the European Conditional Mouse Mutagenesis/KnockOut Mouse Project (EUCOMM/KOMP)-CSD "Knockout-First" ES cell resource at MRC Harwell Institute. The targeting cassette of the transgenic *Retreg3* allele contains a promotorless β-galactosidase and neomycin resistance genes flanked by [LoxP-flippase (FLP) recognition target] and LoxP sites flanking exon 2 of the *Retreg3* gene. Excision of exon 2 was achieved by crossing the transgenic mice carrying the transgenic cassette with germline Cre-expressing mice.

Genotyping strategy consists of a three-primer PCR setup by designing a mutant reverse primer (5mut-R1, GAACTTCGGAATAGGAACTTCG) that sits in the 5′ FRT site and a forward primer (Fam134c-5arm-WTF, GGCATTAATATACACAATAGCACAA) to give a mutant-specific band [119 base pairs (bp)] when the cassette is present, or a WT band (269 bp) when the cassette is not present and a reverse primer (Fam134c-Crit-WTR, GGCACGTGGATTTCTGAGTT) sitting in exon 2 is used. When the cassette is present, the product between Fam134c-5arm-WTF and Fam134c-Crit-WTR is too large to be amplified under standard PCR conditions.

Mice with constitutive nutrient and growth factor signaling in liver, $Li\text{-}TSC1^{KO}$ and $Li\text{-}RagA^{GTP}$, were achieved by breeding $TSC1^{flox/flox}$ mice and $RagA^{GTP/flox}$ mice with Albumin-Cre transgenic mice, as described in (*39*).

AAV vector production and injection

AAV2/9 vectors were produced by InnovaVector (www.innovavector.eu/) by triple transfection of HEK293 cells with (i) mRFP-GFP-KDEL, mRFP-GFP-Fam134c-WT, mRFP-GFP-Fam134c-3D, or mRFP-GFP-Fam134c-3A; (ii) pTigem Helper, which supplies the adenoviral genes for replication; and (iii) pTigem Rep/Cap, which contains the gene sequence for the replication protein (rep) of AAV2 and for the capsid (cap)

proteins of the selected serotype. AAV2/9 vectors were then purified by two rounds of $CsCl_2$ gradients. Physical titers of the viral preparations (genome copies per milliliter) were determined by real-time PCR quantification using TaqMan (Applied Biosystems) and dot-blot analysis. The final titer of each preparation was calculated as the average between the PCR quantification and dot-blot results.

For the AAV injections, following anesthesia with isoflurane, 1×10^{12} viral particles in 100 µl of PBS were injected into the retro-orbital venous plexus of 8-week-old mice with a 27-gauge syringe. Mice were euthanized 4 weeks after the injection.

Statistical analysis

All statistical data were calculated using GraphPad Prism 7 except for proteomic and phosphoproteomic data that were calculated by Perseus. Data comparisons were performed using Student's *t* test or analysis of variance (ANOVA) (one-way or two-way) with Sidak's and/or Tukey's multiple comparison test. P values of <0.05 were considered significant. All experiments were repeated at least three times. The exact sample size for each experiment is reported as N in the caption of each figure. Results are presented as the mean ± SEM.

SUPPLEMENTARY MATERIALS

Supplementary material for this article is available at https://science.org/doi/10.1126/sciadv.abo1215

View/request a protocol for this paper from *Bio-protocol*.

REFERENCES AND NOTES

1. N. Mizushima, Autophagy in protein and organelle turnover. *Cold Spring Harb. Symp. Quant. Biol.* **76**, 397–402 (2011).
2. Y. C. Kim, K.-L. Guan, mTOR: A pharmacologic target for autophagy regulation. *J. Clin. Invest.* **125**, 25–32 (2015).
3. G. Y. Liu, D. M. Sabatini, mTOR at the nexus of nutrition, growth, ageing and disease. *Nat. Rev. Mol. Cell Biol.* **21**, 183–203 (2020).
4. N. Hosokawa, T. Hara, T. Kaizuka, C. Kishi, A. Takamura, Y. Miura, S. Iemura, T. Natsume, K. Takehana, N. Yamada, J.-L. Guan, N. Oshiro, N. Mizushima, Nutrient-dependent mTORC1 association with the ULK1-Atg13-FIP200 complex required for autophagy. *Mol. Biol. Cell* **20**, 1981–1991 (2009).
5. I. G. Ganley, D. H. Lam, J. Wang, X. Ding, S. Chen, X. Jiang, ULK1.ATG13.FIP200 complex mediates mTOR signaling and is essential for autophagy. *J. Biol. Chem.* **284**, 12297–12305 (2009).
6. C. Di Malta, L. Cinque, C. Settembre, Transcriptional regulation of autophagy: Mechanisms and diseases. *Front. Cell Dev. Biol.* **7**, 114 (2019).
7. V. Kirkin, V. V. Rogov, A diversity of selective autophagy receptors determines the specificity of the autophagy pathway. *Mol. Cell* **76**, 268–285 (2019).
8. A. Gubas, I. Dikic, A guide to the regulation of selective autophagy receptors. *FEBS J.* **289**, 75–89 (2022).
9. A. Forrester, C. De Leonibus, P. Grumati, E. Fasana, M. Piemontese, L. Staiano, I. Fregno, A. Raimondi, A. Marazza, G. Bruno, M. Iavazzo, D. Intartaglia, M. Seczynska, E. van Anken, I. Conte, M. A. De Matteis, I. Dikic, M. Molinari, C. Settembre, A selective ER-phagy exerts procollagen quality control via a Calnexin-FAM134B complex. *EMBO J.* **38**, e99847 (2019).
10. I. Fregno, E. Fasana, T. J. Bergmann, A. Raimondi, M. Loi, T. Soldà, C. Galli, R. D'Antuono, D. Morone, A. Danieli, P. Paganetti, E. van Anken, M. Molinari, ER-to-lysosome-associated degradation of proteasome-resistant ATZ polymers occurs via receptor-mediated vesicular transport. *EMBO J.* **37**, e99259 (2018).
11. S. Parashar, R. Chidambaram, S. Chen, C. R. Liem, E. Griffis, G. G. Lambert, N. C. Shaner, M. Wortham, J. C. Hay, S. Ferro-Novick, Endoplasmic reticulum tubules limit the size of misfolded protein condensates. *eLife* **10**, e71642 (2021).
12. S. Ferro-Novick, F. Reggiori, J. L. Brodsky, ER-Phagy, ER homeostasis, and ER quality control: Implications for disease. *Trends Biochem. Sci.* **46**, 630–639 (2021).
13. M. Stephani, L. Picchianti, A. Gajic, R. Beveridge, E. Skarwan, V. Sanchez de Medina Hernandez, A. Mohseni, M. Clavel, Y. Zeng, C. Naumann, M. Matuszkiewicz, E. Turco, C. Loefke, B. Li, G. Dürnberger, M. Schutzbier, H. T. Chen, A. Abdrakhmanov, A. Savova, K.-S. Chia, A. Djamei, I. Schaffner, S. Abel, L. Jiang, K. Mechtler, F. Ikeda, S. Martens, T. Clausen, Y. Dagdas, A cross-kingdom conserved ER-phagy receptor maintains endoplasmic reticulum homeostasis during stress. *eLife* **9**, e58396 (2020).
14. M. Molinari, ER-phagy responses in yeast, plants, and mammalian cells and their crosstalk with UPR and ERAD. *Dev. Cell* **56**, 949–966 (2021).
15. A. Khaminets, T. Heinrich, M. Mari, P. Grumati, A. K. Huebner, M. Akutsu, L. Liebmann, A. Stolz, S. Nietzsche, N. Koch, M. Mauthe, I. Katona, B. Qualmann, J. Weis, F. Reggiori, I. Kurth, C. A. Hübner, I. Dikic, Regulation of endoplasmic reticulum turnover by selective autophagy. *Nature* **522**, 354–358 (2015).
16. S. Kohno, Y. Shiozaki, A. L. Keenan, S. Miyazaki-Anzai, M. Miyazaki, An N-terminal-truncated isoform of FAM134B (FAM134B-2) regulates starvation-induced hepatic selective ER-phagy. *Life Sci. Alliance* **2**, e201900340 (2019).
17. L. Cinque, C. De Leonibus, M. Iavazzo, N. Krahmer, D. Intartaglia, F. G. Salierno, R. De Cegli, C. Di Malta, M. Svelto, C. Lanzara, M. Maddaluno, L. G. Wanderlingh, A. K. Huebner, M. Cesana, F. Bonn, E. Polishchuk, C. A. Hübner, I. Conte, I. Dikic, M. Mann, A. Ballabio, F. Sacco, P. Grumati, C. Settembre, MiT/TFE factors control ER-phagy via transcriptional regulation of FAM134B. *EMBO J.* **39**, e105696 (2020).
18. X. Jiang, X. Wang, X. Ding, M. Du, B. Li, X. Weng, J. Zhang, L. Li, R. Tian, Q. Zhu, S. Chen, L. Wang, W. Liu, L. Fang, D. Neculai, Q. Sun, FAM134B oligomerization drives endoplasmic reticulum membrane scission for ER-phagy. *EMBO J.* **39**, e102608 (2020).
19. F. Iavarone, G. Di Lorenzo, C. Settembre, Regulatory events controlling ER-phagy. *Curr. Opin. Cell Biol.* **76**, 102084 (2022).
20. H. An, A. Ordureau, J. A. Paulo, C. J. Shoemaker, V. Denic, J. W. Harper, TEX264 is an endoplasmic reticulum-resident ATG8-interacting protein critical for ER remodeling during nutrient stress. *Mol. Cell* **74**, 891–908.e10 (2019).
21. H. Chino, T. Hatta, T. Natsume, N. Mizushima, Intrinsically disordered protein TEX264 mediates ER-phagy. *Mol. Cell* **74**, 909–921.e6 (2019).
22. F. Fumagalli, J. Noack, T. J. Bergmann, E. Cebollero, G. B. Pisoni, E. Fasana, I. Fregno, C. Galli, M. Loi, T. Soldà, R. D'Antuono, A. Raimondi, M. Jung, A. Melnyk, S. Schorr, A. Schreiber, L. Simonelli, L. Varani, C. Wilson-Zbinden, O. Zerbe, K. Hofmann, M. Peter, M. Quadroni, R. Zimmermann, M. Molinari, Translocon component Sec62 acts in endoplasmic reticulum turnover during stress recovery. *Nat. Cell Biol.* **18**, 1173–1184 (2016).
23. P. Grumati, G. Morozzi, S. Hölper, M. Mari, M.-L. I. Harwardt, R. Yan, S. Müller, F. Reggiori, M. Heilemann, I. Dikic, Full length RTN3 regulates turnover of tubular endoplasmic reticulum via selective autophagy. *eLife* **6**, e25555 (2017).
24. M. D. Smith, M. E. Harley, A. J. Kemp, J. Wills, M. Lee, M. Arends, A. von Kriegsheim, C. Behrends, S. Wilkinson, CCPG1 is a non-canonical autophagy cargo receptor essential for ER-Phagy and pancreatic ER proteostasis. *Dev. Cell* **44**, 217–232.e11 (2018).
25. Q. Chen, Y. Xiao, P. Chai, P. Zheng, J. Teng, J. Chen, ATL3 is a tubular ER-phagy receptor for GABARAP-mediated selective autophagy. *Curr. Biol.* **29**, 846–855.e6 (2019).
26. A. Reggio, V. Buonomo, R. Berkane, R. M. Bhaskara, M. Tellechea, I. Peluso, E. Polishchuk, G. Di Lorenzo, C. Cirillo, M. Esposito, A. Hussain, A. K. Huebner, C. A. Hübner, C. Settembre, G. Hummer, P. Grumati, A. Stolz, Role of FAM134 paralogues in endoplasmic reticulum remodeling, ER-phagy, and collagen quality control. *EMBO Rep.* **22**, e52289 (2021).
27. N. Sun, D. Malide, J. Liu, I. I. Rovira, C. A. Combs, T. Finkel, A fluorescence-based imaging method to measure in vitro and in vivo mitophagy using mt-Keima. *Nat. Protoc.* **12**, 1576–1587 (2017).
28. S. J. Humphrey, S. B. Azimifar, M. Mann, High-throughput phosphoproteomics reveals in vivo insulin signaling dynamics. *Nat. Biotechnol.* **33**, 990–995 (2015).
29. S. Raniolo, V. Limongelli, Ligand binding free-energy calculations with funnel metadynamics. *Nat. Protoc.* **15**, 2837–2866 (2020).
30. E. Nuti, F. Casalini, S. I. Avramova, S. Santamaria, M. Fabbi, S. Ferrini, L. Marinelli, V. La Pietra, V. Limongelli, E. Novellino, G. Cercignani, E. Orlandini, S. Nencetti, A. Rossello, Potent arylsulfonamide inhibitors of tumor necrosis factor-α converting enzyme able to reduce activated leukocyte cell adhesion molecule shedding in cancer cell models. *J. Med. Chem.* **53**, 2622–2635 (2010).
31. E. Jurrus, D. Engel, K. Star, K. Monson, J. Brandi, L. E. Felberg, D. H. Brookes, L. Wilson, J. Chen, K. Liles, M. Chun, P. Li, D. W. Gohara, T. Dolinsky, R. Konecny, D. R. Koes, J. E. Nielsen, T. Head-Gordon, W. Geng, R. Krasny, G.-W. Wei, M. J. Holst, J. A. McCammon, N. A. Baker, Improvements to the APBS biomolecular solvation software suite. *Protein Sci.* **27**, 112–128 (2018).
32. A. Venerando, M. Ruzzene, L. A. Pinna, Casein kinase: The triple meaning of a misnomer. *Biochem. J.* **460**, 141–156 (2014).
33. S. E. Roffey, D. W. Litchfield, CK2 regulation: Perspectives in 2021. *Biomedicine* **9**, 1361 (2021).
34. P. V. Hornbeck, B. Zhang, B. Murray, J. M. Kornhauser, V. Latham, E. Skrzypek, PhosphoSitePlus, 2014: Mutations, PTMs and recalibrations. *Nucleic Acids Res.* **43**, D512–D520 (2015).
35. M. E. Sanchez-Casalongue, J. Lee, A. Diamond, S. Shuldiner, R. D. Moir, I. M. Willis, Differential phosphorylation of a regulatory subunit of protein kinase CK2 by target of rapamycin complex 1 signaling and the Cdc-like kinase Kns1. *J. Biol. Chem.* **290**, 7221–7233 (2015).

36. G. Di Maira, M. Salvi, G. Arrigoni, O. Marin, S. Sarno, F. Brustolon, L. A. Pinna, M. Ruzzene, Protein kinase CK2 phosphorylates and upregulates Akt/PKB. *Cell Death Differ.* **12**, 668–677 (2005).
37. Y. Miyata, E. Nishida, CK2 controls multiple protein kinases by phosphorylating a kinase-targeting molecular chaperone, Cdc37. *Mol. Cell. Biol.* **24**, 4065–4074 (2004).
38. N. Cybulski, V. Zinzalla, M. N. Hall, Inducible raptor and rictor knockout mouse embryonic fibroblasts. *Methods Mol. Biol.* **821**, 267–278 (2012).
39. C. de la Calle Arregui, A. B. Plata-Gómez, N. Deleyto-Seldas, F. García, A. Ortega-Molina, J. Abril-Garrido, E. Rodriguez, I. Nemazanyy, L. Tribouillard, A. de Martino, E. Caleiras, R. Campos-Olivas, F. Mulero, M. Laplante, J. Muñoz, M. Pende, G. Sabio, D. M. Sabatini, A. Efeyan, Limited survival and impaired hepatic fasting metabolism in mice with constitutive Rag GTPase signaling. *Nat. Commun.* **12**, 3660 (2021).
40. G. Chen, Z. Han, D. Feng, Y. Chen, L. Chen, H. Wu, L. Huang, C. Zhou, X. Cai, C. Fu, L. Duan, X. Wang, L. Liu, X. Liu, Y. Shen, Y. Zhu, Q. Chen, A regulatory signaling loop comprising the PGAM5 phosphatase and CK2 controls receptor-mediated mitophagy. *Mol. Cell* **54**, 362–377 (2014).
41. H. Chino, A. Yamasaki, K. L. Ode, H. R. Ueda, N. N. Noda, N. Mizushima, Phosphorylation by casein kinase 2 enhances the interaction between ER-phagy receptor TEX264 and ATG8 proteins. *EMBO Rep.* **23**, e54801 (2022).
42. V. V. Rogov, H. Suzuki, E. Fiskin, P. Wild, A. Kniss, A. Rozenknop, R. Kato, M. Kawasaki, D. G. McEwan, F. Löhr, P. Güntert, I. Dikic, S. Wakatsuki, V. Dötsch, Structural basis for phosphorylation-triggered autophagic clearance of Salmonella. *Biochem. J.* **454**, 459–466 (2013).
43. V. V. Rogov, H. Suzuki, M. Marinković, V. Lang, R. Kato, M. Kawasaki, M. Buljubašić, M. Šprung, N. Rogova, S. Wakatsuki, A. Hamacher-Brady, V. Dötsch, I. Dikic, N. R. Brady, I. Novak, Phosphorylation of the mitochondrial autophagy receptor Nix enhances its interaction with LC3 proteins. *Sci. Rep.* **7**, 1131 (2017).
44. L. P. Poole, A. Bock-Hughes, D. E. Berardi, K. F. Macleod, ULK1 promotes mitophagy via phosphorylation and stabilization of BNIP3. *Sci. Rep.* **11**, 20526 (2021).
45. C. Borgo, C. D'Amore, L. Cesaro, S. Sarno, L. A. Pinna, M. Ruzzene, M. Salvi, How can a traffic light properly work if it is always green? The paradox of CK2 signaling. *Crit. Rev. Biochem. Mol. Biol.* **56**, 321–359 (2021).
46. V. Gandin, L. Masvidal, M. Cargnello, L. Gyenis, S. McLaughlan, Y. Cai, C. Tenkerian, M. Morita, P. Balanathan, O. Jean-Jean, V. Stambolic, M. Trost, L. Furic, L. Larose, A. E. Koromilas, K. Asano, D. Litchfield, O. Larsson, I. Topisirovic, mTORC1 and CK2 coordinate ternary and eIF4F complex assembly. *Nat. Commun.* **7**, 11127 (2016).
47. R. Meng, C. Götz, M. Montenarh, The role of protein kinase CK2 in the regulation of the insulin production of pancreatic islets. *Biochem. Biophys. Res. Commun.* **401**, 203–206 (2010).
48. Y. J. Kang, M.-K. Lu, K.-L. Guan, The TSC1 and TSC2 tumor suppressors are required for proper ER stress response and protect cells from ER stress-induced apoptosis. *Cell Death Differ.* **18**, 133–144 (2011).
49. V. Deretic, G. Kroemer, Autophagy in metabolism and quality control: Opposing, complementary or interlinked functions? *Autophagy* **18**, 283–292 (2021).
50. I. Dikic, Z. Elazar, Mechanism and medical implications of mammalian autophagy. *Nat. Rev. Mol. Cell Biol.* **19**, 349–364 (2018).
51. N. Mizushima, B. Levine, Autophagy in human diseases. *N. Engl. J. Med.* **383**, 1564–1576 (2020).
52. A. Dalle Vedove, F. Zonta, E. Zanforlin, N. Demitri, G. Ribaudo, G. Cazzanelli, A. Ongaro, S. Sarno, G. Zagotto, R. Battistutta, M. Ruzzene, G. Lolli, A novel class of selective CK2 inhibitors targeting its open hinge conformation. *Eur. J. Med. Chem.* **195**, 112267 (2020).
53. J. Rappsilber, Y. Ishihama, M. Mann, Stop and go extraction tips for matrix-assisted laser desorption/ionization, nanoelectrospray, and LC/MS sample pretreatment in proteomics. *Anal. Chem.* **75**, 663–670 (2003).
54. P. Hou, K. Yang, P. Jia, L. Liu, Y. Lin, Z. Li, J. Li, S. Chen, S. Guo, J. Pan, J. Wu, H. Peng, W. Zeng, C. Li, Y. Liu, D. Guo, A novel selective autophagy receptor, CCDC50, delivers K63 polyubiquitination-activated RIG-I/MDA5 for degradation during viral infection. *Cell Res.* **31**, 62–79 (2021).
55. G. C. P. van Zundert, J. P. G. L. M. Rodrigues, M. Trellet, C. Schmitz, P. L. Kastritis, E. Karaca, A. S. J. Melquiond, M. van Dijk, S. J. de Vries, A. M. J. J. Bonvin, The HADDOCK2.2 Web Server: User-friendly integrative modeling of biomolecular complexes. *J. Mol. Biol.* **428**, 720–725 (2016).
56. K. Lindorff-Larsen, S. Piana, K. Palmo, P. Maragakis, J. L. Klepeis, R. O. Dror, D. E. Shaw, Improved side-chain torsion potentials for the Amber ff99SB protein force field. *Proteins* **78**, 1950–1958 (2010).
57. H. G. Petersen, Accuracy and efficiency of the particle mesh Ewald method. *J. Chem. Phys.* **103**, 3668–3679 (1995).
58. M. Parrinello, A. Rahman, Polymorphic transitions in single crystals: A new molecular dynamics method. *J. Appl. Phys.* **52**, 7182–7190 (1981).
59. M. K. Prakash, A. Barducci, M. Parrinello, Replica temperatures for uniform exchange and efficient roundtrip times in explicit solvent parallel tempering simulations. *J. Chem. Theory Comput.* **7**, 2025–2027 (2011).
60. S. Aureli, D. Di Marino, S. Raniolo, V. Limongelli, DDT—Drug Discovery Tool: A fast and intuitive graphics user interface for docking and molecular dynamics analysis. *Bioinformatics* **35**, 5328–5330 (2019).

Acknowledgments: We thank G. Diez Roux and P. Ashley-Norman for critical reading of the manuscript. We thank the microscopy, MS, advanced histopathology, and FACS facilities at TIGEM Institute. We thank E. Nusco for helping us with AAV injections. **Funding:** This work was supported by European Research Council (ERC) (714551), Telethon intramural grants, and Associazione Italiana per la Ricerca sul Cancro (AIRC) (IG 2015 Id 17717) (to C.S.) and Telethon Foundation (TMPGCBX16TT), AFM Telethon (Trampoline Grant), and AIRC (MFAG-2020-24856) (to P.G.). G.D.L. is a recipient of AIRC fellowship "Francesco Alicino" (25407). V.L. acknowledges funding from the ERC (101001784), the Italian MIUR-PRIN 2017 (2017FJZZRC), and the Swiss National Supercomputing Center (CSCS) (project ID u8). The work of A.S. was supported by the German Research Foundation DFG (SFB1177/2 and WO210/20-2) and the Dr. Rolf M. Schwiete Stiftung (13/2017). A.E. is supported by the RETOS projects Programme of Spanish Ministry of Science, Innovation and Universities, Spanish State Research Agency (grants SAF2015-67538-R and PID2019-104012RB-I00), and the ERC (638891). A.B.P.-G. is a recipient of Ph.D. fellowship from MICIU/AEI (BES-2017-081381). A.R. is a recipient of Umberto Veronesi Foundation postdoctoral fellowship. **Author contributions:** G.D.L. and F.I. performed most of the experiments. F.I. and A.B.P.-G. performed in vivo experiments. M.M. performed mutagenesis experiments. S.A. and V.L. performed LC3-FAM134C binding analysis. C.P.Q.M. performed in vitro phosphorylation assays. L.C. analyzed CK2 substrate phosphorylation. F.S., A.P., C.C., and A.S. analyzed proteomic data. G.N. provided critical suggestions. A.R. performed proteomic experiments. A.E. supervised in vivo experiments. M.R., L.A.P., and O.M. supervised CK2 experiments. C.S. designed the study. P.G. and C.S. conceived and supervised the experiments. C.S., P.G., V.L., and M.R. wrote the paper. G.D.L. and F.I. prepared the figures. All the authors read the manuscript. **Competing interests:** The authors declare that they have no competing interests. **Data and materials availability:** All data needed to evaluate the conclusions in the paper are present in the paper and/or the Supplementary Materials.

Submitted 14 January 2022
Accepted 20 July 2022
Published 31 August 2022
10.1126/sciadv.abo1215

3. ROLE OF CK2 IN THE GLYCOLYTIC PHENOTYPE OF TUMOR CELLS

I contributed to a related project carried by our group that had as main objective the study of the role of CK2 in tumor metabolic rewiring, one of the hallmarks of cancer. By CK2 targeting of tumor cells, this work showed a functional role of CK2, especially for CK2α, in the higher glycolytic rate of tumor cells. In particular, my work helped to demonstrate that HIF-1 amount, and consequent hexokinase-2 (HK2) and lactate dehydrogenase (LDH) levels, were lower in CK2 knockout clones compared to wild type cells in U2OS and SKNBE cells. The results of this investigation were published under the title “Contribution of the CK2 Catalytic Isoforms α and α' to the Glycolytic Phenotype of Tumor Cells” in the journal *Cells* (Zonta et al., 2021).

cells

MDPI

Article

Contribution of the CK2 Catalytic Isoforms α and α′ to the Glycolytic Phenotype of Tumor Cells

Francesca Zonta [1,2], Christian Borgo [1], Camila Paz Quezada Meza [1,2], Ionica Masgras [2], Andrea Rasola [1], Mauro Salvi [1], Lorenzo A. Pinna [1,2] and Maria Ruzzene [1,2,*]

[1] Department of Biomedical Sciences, University of Padova, 35131 Padova, Italy; francesca.zonta@unipd.it (F.Z.); christian.borgo@unipd.it (C.B.); camilapaz.quezadameza@studenti.unipd.it (C.P.Q.M.); andrea.rasola@unipd.it (A.R.); mauro.salvi@unipd.it (M.S.); lorenzo.pinna@unipd.it (L.A.P.)
[2] CNR Neuroscience Institute, 35131 Padova, Italy; ionica.masgras@unipd.it
* Correspondence: maria.ruzzene@unipd.it; Tel.: +39-049-8276112

Abstract: CK2 is a Ser/Thr protein kinase overexpressed in many cancers. It is usually present in cells as a tetrameric enzyme, composed of two catalytic (α or α′) and two regulatory (β) subunits, but it is active also in its monomeric form, and the specific role of the different isoforms is largely unknown. CK2 phosphorylates several substrates related to the uncontrolled proliferation, motility, and survival of cancer cells. As a consequence, tumor cells are addicted to CK2, relying on its activity more than healthy cells for their life, and exploiting it for developing multiple oncological hallmarks. However, little is known about CK2 contribution to the metabolic rewiring of cancer cells. With this study we aimed at shedding some light on it, especially focusing on the CK2 role in the glycolytic onco-phenotype. By analyzing neuroblastoma and osteosarcoma cell lines depleted of either one (α) or the other (α′) CK2 catalytic subunit, we also aimed at disclosing possible pro-tumor functions which are specific of a CK2 isoform. Our results suggest that both CK2 α and α′ contribute to cell proliferation, survival and tumorigenicity. The analyzed metabolic features disclosed a role of CK2 in tumor metabolism, and suggest prominent functions for CK2 α isoform. Results were also confirmed by CK2 pharmacological inhibition. Overall, our study provides new information on the mechanism of cancer cells addiction to CK2 and on its isoform-specific functions, with fundamental implications for improving future therapeutic strategies based on CK2 targeting.

Keywords: CK2; casein kinase 2; isoforms; cancer metabolism

check for updates

Citation: Zonta, F.; Borgo, C.; Quezada Meza, C.P.; Masgras, I.; Rasola, A.; Salvi, M.; Pinna, L.A.; Ruzzene, M. Contribution of the CK2 Catalytic Isoforms α and α′ to the Glycolytic Phenotype of Tumor Cells. *Cells* **2021**, *10*, 181. https://doi.org/10.3390/cells10010181

Received: 28 November 2020
Accepted: 15 January 2021
Published: 18 January 2021

Publisher's Note: MDPI stays neutral with regard to jurisdictional claims in published maps and institutional affiliations.

Copyright: © 2021 by the authors. Licensee MDPI, Basel, Switzerland. This article is an open access article distributed under the terms and conditions of the Creative Commons Attribution (CC BY) license (https://creativecommons.org/licenses/by/4.0/).

1. Introduction

The rewiring of metabolism is a hallmark of cancer, and the shift in ATP generation from oxidative phosphorylation to glycolysis and the production of lactate even under oxygen-rich conditions (aerobic glycolysis) is a major metabolic feature of many cancer cells [1].

CK2 (previously known as casein kinase 2) is a Ser/Thr protein kinase, ubiquitously expressed, but particularly abundant in cancer cells [2–4]. It phosphorylates a huge number of proteins, and is involved in several cellular processes, with a major role in supporting cell proliferation and survival [5,6]. It is usually present in cells as a constitutively active tetrameric enzyme, composed of two catalytic (α or α′) and two regulatory (β) subunits [7]. Catalytic subunits are active even in the absence of the β subunit, but the relevance of the monomeric form in cells has not been proved, yet. However, several evidences support a possible pro-tumor function of the isolated catalytic subunits [8,9]. The two isoforms α and α′ are very similar in structure and often considered overlapping in functions; however, also isoform-specific functions have been described [10,11] and a possible differential role in tumors has been hypothesized [12]. CK2 involvement in cancer has been known since many years, and has been described as a "lateral action", where, by phosphorylating crucial

substrates, it potentiates signaling related to most cancer hallmarks. However, CK2 importance in cancer metabolism is less documented, even though its functions in hormonal regulation of carbohydrate metabolism have been described [13]. Zhang and colleagues [14] observed that glucose uptake and lactate secretion were lower in bladder cancer cell lines where CK2α expression was knocked down. Consistently, they found that a number of glycolysis-related genes were less expressed in these cells, or in w.t. bladder cancer cells treated with the CK2 inhibitor CX-4945, and they interpreted this as a consequence of the CK2-dependent reduction of S473 Akt phosphorylation. This paper only refers to CK2α isoform. Yang et al. [15] reported about the modulation of pyruvate kinase M isoforms by CK2. They found that, in colon cancer cells overexpressing CK2α, the constitutively active PKM1 was downregulated through a proteasome-dependent mechanism, while the level of PKM2 (whose induction contributes to the Warburg effect) was unchanged, but it was more localized in the nucleus, where it promotes a higher expression of LDHA.

Another study [16], by an isotope tracer metabolite analysis, showed that glucose is more important than glutamine in sustaining the tumor phenotype of CK2α-overexpressing cells, where ROS levels were found to decrease.

The CK2 implication in cancer energetics can be also inferred by its regulatory role on Akt and its effectors mTORC1 and β-catenin [17,18], ultimately affecting the modulation of key metabolic targets, as recently described [19]. Moreover, CK2 plays a role in adipocyte metabolism [20], and its possible implication in cancer aberrant lipid metabolism has been hypothesized [21].

These observations prompted us to investigate more in depth how metabolic features of tumor cells depend on CK2, especially focusing on the specific functions of the individual catalytic isoforms. To this aim, we exploited the CRISPR-Cas9 technology to turn off the expression of either α or α′ CK2 catalytic subunits in SK-N-BE (human neuroblastoma) and U2OS (human osteosarcoma) cells, giving rise to clones hereinafter denoted as KOα and KOα′, and we analyzed how this impacted on cellular and metabolic features.

2. Materials and Methods

2.1. Antibodies and Chemicals

Anti-CK2α/α′ (MCA3031Z) was purchased from Bio-Rad (Hercules, CA, USA), anti-CK2 β (ab76025) and anti-pSer129 Akt (ab133458) from Abcam, anti-total Akt (clone H-136), anti-Hk2 (clone 1A7) and anti-total LDH (clone H-160) from Santa Cruz Biotechnologies (Dallas, TX, USA), anti-β actin (A2228) and anti-tubulin (T5168) from Sigma; anti-Hif-1α (127309) from GeneTex.

The CK2 inhibitor CX-4945 (5-[(3-Chlorophenyl)amino]-benzo[c]-2,6-naphthyridine-8-carboxylic) was purchased from MedChemExpress and the chemical inducer of hypoxia DMOG (dimethyloxallyl glycine) was from Sigma. Inhibitors solutions at different concentrations were prepared in 100% DMSO (Sigma, St. Louis, MO, USA).

2.2. Cell Culture

For this study, we used the human neuroblastoma cell line SK-N-BE (synonyms SK-N-BE(2)), and the human osteosarcoma cell line U2OS.

All cells (wild type, w.t. and KO clones, see below) were grown in Dulbecco's Modified Eagle Medium (D-MEM, Sigma) containing 5 mM glucose, supplemented with 10% (*v/v*) fetal bovine serum (FBS) and PSG (1% penicillin and streptomycin and 2 mM L-Glutamine) (Sigma). Cells were maintained at 37 °C in a humidified atmosphere of 95% air and 5% CO_2.

2.3. Generation of CK2-Knockout Cells by CRISPR-Cas9 Editing Tool

All-in-one plasmids expressing Cas9–Dasher green fluorescent protein (GFP) and the single guide RNA (sgRNA) guide (CMV-Cas9-2A-GFP, Cas9-ElecD) to target the specific CK2 subunits were purchased from ATUM (Newark, CA, USA). The sgRNA guide sequences targeting CK2 in SK-N-BE are: 5′-CCTGGATTATTGTCACAGCA-3′ (clone 1) and 5′-TTACATGTATGAGATTCTGA-3′ (clone 2) for CK2α (*Csnk2a1*), 5′-GGGTCTACGCCGAGGTGAAC-3′

(clone 1) and TTAATATCACCAACAATGAG (clone 2) (clone 2) for CK2α′ (*Csnk2a2*). The sgRNA guide sequences targeting CK2 in U2OS are: 5′-CCTGGATTATTGTCACAGCA-3′ (clone 1) and 5′-TTACATGTATGAGATTCTGA-3′ (clone 2) for CK2α (*Csnk2a1*), 5′-GGGTCTACGCCG AGGTGAAC-3′ (clone 1) and 5′-AACTGGTTCGAAAACTTGGT-3′ (clone 2) for CK2α′ (*Csnk2a2*).

Individual CK2 subunit knockout was performed as previously detailed [22]. Briefly, cells were co-transfected with 1 μg of sgRNA plasmid and Lipofectamine 3000 (Thermo Fisher Scientific, Waltham, MA, USA) according to the manufacturer's instructions. At 48 h post-transfection GFP-positive cells were sorted in 96-well plates using fluorescence-activated cell sorting with a FACSAria II Cell Sorter (BD BioSciences, Franklin Lakes, NJ, USA). Sorted cells were expanded to obtain individual clones, which were selected by immunoblotting in order to verify the complete absence of target protein expression.

As a control, we also produced a monoclonal w.t. line, whose phenotype largely overlapped that of the w.t. cells used throughout the study. To this purpose, cells have been transfected with an GFP vector and GFP-positive cells were sorted in 96-well plates by FACS and expanded to obtain individual clones.

2.4. Cell Treatments and Lysis

Cells were cultured in dishes up to 70–80% confluence, then treated at the indicated time and concentration conditions with the chemical compounds (CX-4945 or DMOG), or with solvent in the case of control cells. Non-toxic concentrations were applied, ensuring viability level was >70%, as assessed by the MTT (3-(4,5-dimethylthiazol-2-yl)-3,5-diphenyltriazolium bromide) method [23]. At different time points, cells were harvested, centrifuged and washed with PBS. Cells were lysed with a buffer containing 0.5% (*v/v*) Triton X-100, as elsewhere described [24] and subjected to the Bradford quantification assay before SDS-PAGE separation and western blot analysis.

2.5. Western Blotting Analysis and Titration of the CK2 Antibody Reactivity

Equal amounts of proteins (10–20 μg) from cell lysates were resolved by 7.5%, 11%, or 15% SDS-PAGE and transferred to Immobilon-P membranes (Merck-Millipore, Burlington, MA, USA) using the Lightning Blotter Transfer System (Perkin Elmer, Waltham, MA, USA). Dried membranes were then washed in TTBS buffer (50 mM Tris-HCl pH 7.5, 50 mM NaCl, 0.1% Tween-20), and incubated with the indicated antibodies. Membranes were then incubated with secondary HRP-conjugated antibody (Perkin Elmer) for 30 min and bands were detected by a chemiluminescence solution composed by 50 mM Tris, pH 9.35, 0.02% (v/v) H_2O_2 and 50% (v/v) luminol solution plus 30% (*w/v*) BSA, with an enhanced chemiluminescent detection system (Thermo Fisher Scientific). Immunostained bands were quantified using a 4000 mm Pro Kodak Image Station, followed by analysis with Carestream Molecular Imaging software. β-actin or α-tubulin were used as a loading control.

For the titration of the CK2 antibody reactivity, recombinant human CK2 subunits were analyzed. They were produced, purified and kindly donated by Stefania Sarno, Padova [25]. Purified proteins, dialyzed against 25 mM Tris-HCl pH 7.5 and 50% glycerol, were stored at −20 °C, before loading on SDS-PAGE. Gels were either stained by Colloidal Coomassie Blue or transferred to Immobilon-P membranes and analyzed by Western blotting with the anti-CK2α/α′ antibody.

2.6. Cell Growth Assay

The growth of viable cells was monitored by a Trypan blue exclusion assay. SK-N-BE (5×10^4) or U2OS (2×10^3) cells were seeded in triplicate in 6-well/plates. Cells were allowed to attach for 5 h, then t = 0 was considered, and the number of viable cells was monitored every 24 h up to 96 h. To this purpose, cells were washed, treated with 0.05% trypsin solution, centrifuged, resuspended in a 0.13% Trypan blue solution and counted in an hematocytometer, excluding stained (dead) cells. Unstained (viable) cells were counted in triplicate for each time point.

2.7. Spheroid Formation Assay

Cells were seeded in quadruplicates at 1×10^3 cells/well in 200 µL of culture medium supplemented with 5% (v/v) FBS, in a 96-well plate with round bottom wells precoated with 50 µL of 1% agar in culture medium [26]. Images were taken every 24 h for 7–8 days, by using a Leica DMI4000 automated inverted microscope equipped with a Leica DFC300 FX camera (2.5× objective, magnification-changer 1.6).

2.8. Clonogenic Survival Assays

Cells were plated at 250 (SK-N-BE) or 100 (U2OS) cells/well in 6-well plates, in full growth medium. Media were replaced by fresh culture medium every 4 days. After 15 days, cells were washed with PBS, fixed with methanol and stained with 0.5% crystal violet. Digital images of cell colonies were obtained using a scanning device (Epson Perfection V700 Photo). Quantification of the clonogenic assay was performed with the ImageJ plugin "ColonyArea" [27] to determine the area covered by colonies in the well and the colony intensity percentage.

2.9. Wound-Healing Assays

Wound-healing assays were performed by creating identical wound areas into the cell monolayer using Ibidi culture-inserts (Ibidi GmbH, Cat. no. 80209). Cells were seeded in triplicate in complete culture medium on each side of the Ibidi culture-insert, into a 24-well plate, at proper cell densities (1.5×10^6 SK-N-BE cells/mL and 5.5×10^4 U2OS cells/mL). After 24 h, cells reached confluence, and the culture-inserts were removed in order to form a cell-free gap into the cell monolayer. Each well was washed once with PBS to remove cell debris and immediately refilled with fresh D-MEM medium supplemented with 5% (v/v) FBS and 2mM L-glutamine. The wound images were captured at this time (t = 0) and at the indicated time points (24–48 h for SK-N-BE, 2–4–8 h for U2OS) using a Leica DMI4000 automated inverted microscope equipped with a Leica DFC300 FX camera (2.5× objective, magnification-changer 1.6). Images of in vitro scratch wound healing assays were analyzed with a plugin of ImageJ software (1.52t version) adapted from [28] and relative cell migration of each cell line was measured.

2.10. Extracellular Lactate Concentration Analysis

Extracellular lactate concentration was measured using an L-Lactate Assay Kit (Promega, Madison, WI, USA), following the manufacturer's instructions. Briefly, cells were seeded in a 96-well plate at the proper cell density (2×10^4 SK-N-BE or 8×10^3 U2OS w.t. and KO cells) in D-MEM supplemented with 1% (v/v) dialyzed FBS (Thermo Fischer Scientific); medium was collected at various time point and stored at −20 °C until analysis. The lactate concentration in each sample was detected by an enzymatic assay, which results in a luminescent product, proportional to the lactate present. Signals were detected with a luminometer plate reader (Tecan M200 Infinite Pro Microplate Reader) and expressed as average relative light units. A standard curve was built with known amounts of lactate, to identify the linear range; samples of cell culture medium were diluted 1 to 20 folds, to ensure reading within the linear range.

2.11. Seahorse Glycolysis Stress Test

Cellular glycolytic phenotype was analyzed by the extracellular flux analyzer Seahorse (Agilent, Santa Clara, CA, USA) (XF Analyzer for SK-N-BE cells, or XFe Analyzer for U2OS cells), performing glycolytic stress tests and following the extracellular acidification rate (ECAR) in real time, as previously reported [29]. Briefly, cells were seeded in a Seahorse 24-well assay plate in D-MEM, with 10% (v/v) FBS, 5 mM glucose and 2 mM L-Glutamine, at cell densities determined in order to have 80% confluence after 24 h (7×10^4 SK-N-BE cells/well, and 2×10^4 U2OS cells/well). After 24 h, cells were washed and medium was replaced with prewarmed running medium (D-MEM without phenol red supplemented with 1 mM sodium pyruvate, 30 mM sodium chloride and 2 mM L-Glutamine,

pH 7.4, and incubated in a non-CO_2 incubator at 37 °C for 60 min. ECAR were recorded in basal conditions (in the absence of glucose) and following sequential injections of 10 mM Glucose, 1 μg/mL oligomycin (mitochondrial ATP synthase inhibitor; this concentration completely abolished ATP synthase activity, as judged by the evaluation of the Oxygen Consumption Rate (OCR), not shown), 100 mM 2-DG (2-deoxyglucose, hexokinase 2 inhibitor). Glucose addition induces the glycolytic pathway, thus highlighting the "glycolytic response". The subsequent injection of oligomycin, which blocks the mitochondrial ATP production, allows to estimate the maximal glycolysis. Lastly, administration of 2-DG measures the non-glycolytic ECAR. The "glycolytic capacity" and the "glycolytic reserve" were obtained by subtracting to the maximal glycolytic rate the residual non-glycolytic ECAR and the glycolytic response, respectively. Cells were lysed post-measurement and protein content, measured by the Bradford method, was used as a normalization value. Quantification of the different glycolytic parameters was performed with different Agilent software. XF software, which is associated to the XF analyzer and was used for SK-N-BE cells (Figure 8A,C), calculates the AUC (Area Under Curves) for each phase. In the case of SK-N-BE treatments with CX-4945 (Figure 8C), since the length of the phases was different, three points were chosen for each phase (points 1–3 for basal glycolysis; 5–7 for the response to glucose addition; 13–15 for the maximal glycolysis; 18–20 for non-glycolytic acidification). The software Wave, associated to XFe Analyzer which was used for U2OS cells (Figure 8B), for each phase considers the last point before further addition (point 3 for basal glycolysis; 6 for the response to glucose addition; 9 for the maximal glycolysis; 11 for non-glycolytic acidification), thus reports data as mpH/min.

2.12. Cell Viability Assay

Cell viability was detected by means of MTT reagent: cells (10^5 cells/100 μL) were incubated for 24 h or 48 h in a 96-well plate in D-MEM supplemented with 1% (*v*/*v*) FBS, in the presence of the indicated compounds, or of DMSO vehicle, (1%, *v*/*v*) for control cells. 1 h before the end of the incubation, 10 μL of MTT solution (5 mg/mL in PBS) were added to each well. Incubations were stopped by addition of 20 μL of lysis solution at pH 4.7, as described elsewhere [23]. Plates were read for OD at λ590 nm, in a Titertek Multiskan Plus plate reader (Flow Laboratories, Puteaux, France). IC_{50} (concentrations inducing 50% of cell death) values were calculated with Prism 7 software (GraphPad Software, San Diego, CA, USA).

For the combined treatments, the CalcuSyn (version 2.11; Biosoft, Cambridge, GB) median effect model was used to calculate the combination index values (CI), where synergy, additivity, and antagonism are defined by CI < 1, CI = 1 or CI > 1, respectively, according to the Chou-Talalay method [30].

2.13. Statistical Analysis

The number of experiments is indicated in each figure legend. Quantification refers to experiments with the different KO clones of each subunit in a certain cell lines, unless differently specified. Statistical significance was evaluated by One-way Anova analysis using GraphPad Prism 7 program, setting (*) $p < 0.05$, (**) $p < 0.01$, (***) $p < 0.001$, (****) $p < 0.0001$.

3. Results

3.1. CK2 Profile in w.t. Cell Lines and KO Clones

For our study, we used SK-N-BE (neuroblastoma) and U2OS (osteosarcoma) tumor cells. For both lines, different KO clones of each subunit were obtained throughout this investigation (see Section 2), and they were variably used for performing experiments. Unless differently specified, the results shown for a certain KO clone were reproducible with the other clone of the same subunit (while, for quantifications, all data from experiments with different clones were considered). In some analysis, the two KO clones of the same subunit displayed different behaviors (suggesting possible effects due to compensating events,

and/or not directly ascribable to the CK2 subunit deletion); in those cases, the results obtained with both clones are shown.

SK-N-BE and U2OS cells express significant amount of both α and α′. The relative percentage of the catalytic isoforms is around 70% α and 30% α′ in SKNBE, and 45% α and 55% α′ in U2OS, as assessed by using an antibody which recognizes with the same efficacy the two subunits (Figure 1A). Therefore, these two lines provide a model for two different conditions as far as the most abundant isoform is concerned. Applying the CRISPR-Cas9 technology, we produced cells of both lines that do not express either α (KOα) or α′ (KOα′) (Figure 1B). The expression of the regulatory β subunit of CK2 was roughly unchanged in KOα′ clones, while it was reduced in KOα clones, as already observed in other cell lines [31]. The CK2 cellular activity, measured through the level of the endogenous substrate pSer129 Akt [17], was reduced in the KO clones compared to w.t. cells, and the effect was more evident in KOα for SKNBE, and in KOα′ in U2OS, consistent with the proportion of the catalytic isoform suppressed (Figure 1B).

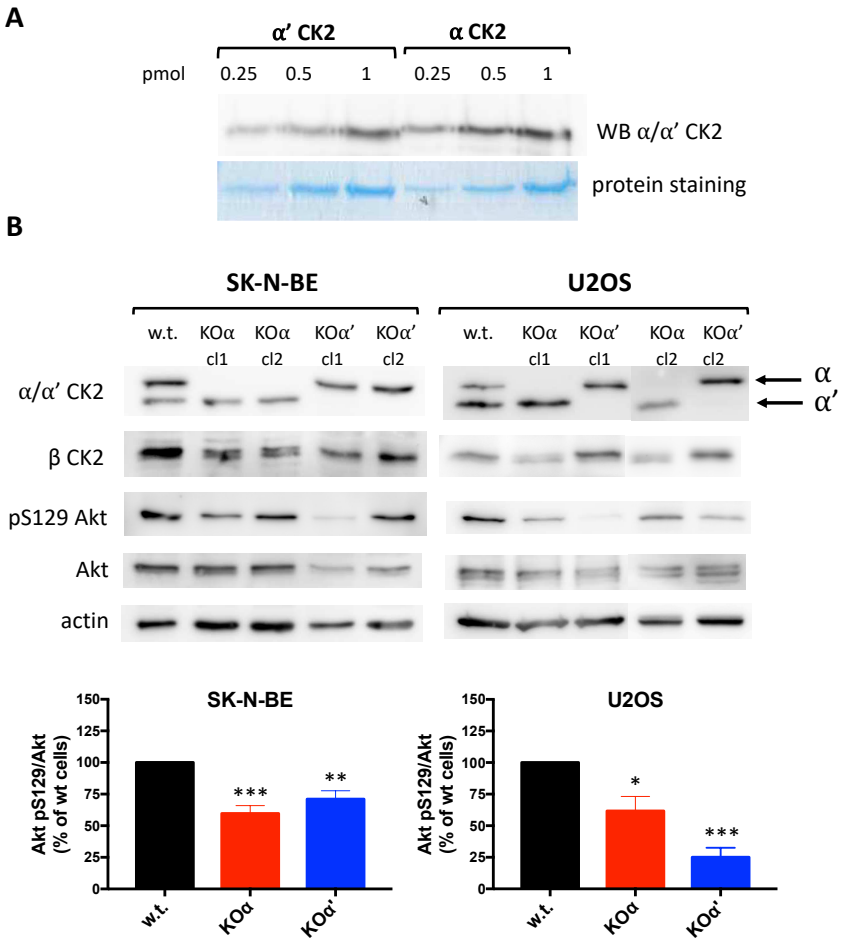

Figure 1. CK2 expression and activity in SK-N-BE and U2OS cells. (**A**) Titration of the antibody reactivity towards CK2 catalytic subunits. The indicated amounts of recombinant CK2 catalytic subunits (myc-α′ or α) were loaded on SDS-PAGE, and either blotted for the WB (western blot) analysis or stained by Colloidal Coomassie Blue; (**B**) CK2 expression and activity in w.t. and KO clones of the cells used for this study. 10 μg proteins from cell lysates were analyzed by WB with the indicated antibodies. The last two right lanes belong to an independent experiment. As a reporter of CK2 endogenous activity, pS129 Akt signal has been quantified, normalized to total Akt signal, and reported in the bar graph as % of w.t. cells. At least three independent experiments were performed; representative western blots are shown, while quantification in the bar graphs reports the mean values ± SEM of all experiments and of the two clones of the same KO. Statistical significance refers to w.t. cells. (*) $p < 0.05$, (**) $p < 0.01$, (***) $p < 0.001$

3.2. Deletion of an Individual CK2 Catalytic Subunit Reduces 3D Growth, Clonogenic Potential, and Motility

First we wanted to assess if the knockout of CK2 α or α′ affects the proliferation rate of SK-N-BE and U2OS tumor cells grown in monolayer.

In SK-N-BE neuroblastoma cells, both α and α′ KO displayed a slower proliferation compared to w.t. cells (Figure 2). Results were less clear for the U2OS osteosarcoma model: the U2OS KOα′ cells were more proliferative than the w.t. cells, while KOα were quite similar to w.t. (Figure 2).

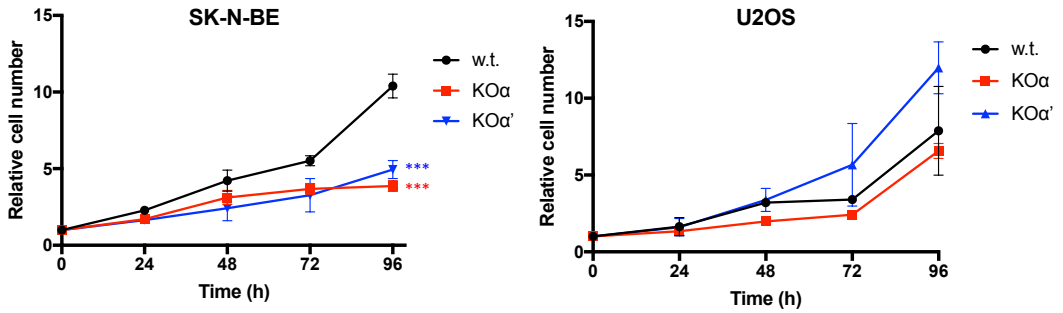

Figure 2. Proliferation curves of w.t. and KO clones of SK-N-BE and U2OS cells. The cell number was evaluated every 24 h, by means of Trypan blue exclusion assay (see methods for details). Experiments were performed in triplicates; at least three independent experiments were performed. The curve for each KO reports the means values ± SEM obtained with the different clones of the same KO. Significance calculated at 96 h refers to w.t. cells. (***) $p < 0.001$

To better understand the proliferative phenotypes, we decided to perform spheroid formation assays, since the growth in soft agar more closely recapitulates the actual growth of a tumor mass. We found that the 3D growth of SK-N-BE KO for either α or α′ was reduced compared to w.t. (Figure 3A), while it was quite similar for w.t. and KO clones of U2OS cells (Figure 3B).

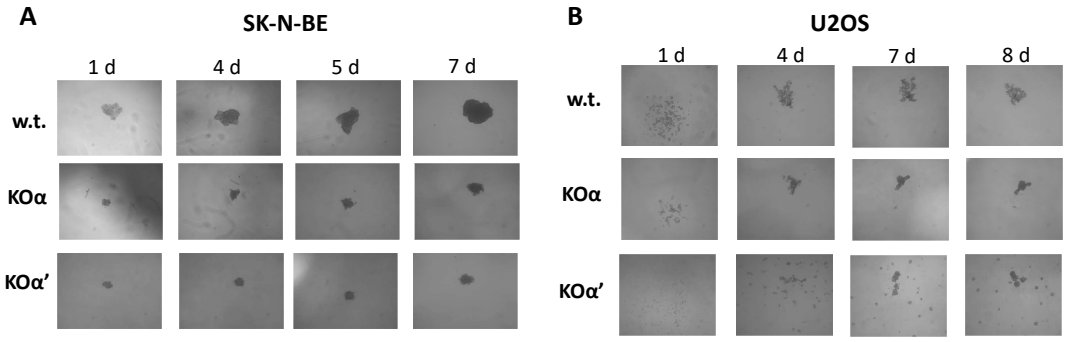

Figure 3. Spheroid formation potential of w.t. and KO clones of (**A**) SK-N-BE cells, and (**B**) U2OS cells were seeded in a 96-well plate precoated with 50 µL of 1% agar (see Section 2). Inverted microscope images taken at the indicated times (d = days) are shown. At least two separate experiments were performed, in quadruplicates. Representative images (SK-N-BE KOα clone 1, KOα′ clone 1; U2OS KOα clone 2, KOα′ clone 1) are shown.

To further investigate the importance of the CK2 subunits on the growth potential of tumor cells, we performed clonogenic assays; this approach provides more information, assuming that the number of colonies measures the cell survival, while the colony diameter mainly depends on the proliferation rate [32]. The clonogenic potential of both α and α′ KO of SK-N-BE was lower than that of w.t. cells (Figure 4A). Similarly, the KOα U2OS cells displayed a much lower number of colonies and smaller colonies compared to w.t. cells (Figure 4B). The clonogenic potential of two different KOα′ U2OS clones was instead quite different, although for both of them the colony size and number were reduced compared to w.t. cells (Figure 4B). Additionally, considering the higher proliferating rate of U2OS

KOα′ cells (Figure 2), for the time being we cannot conclude that in these cells α′ strongly contribute to the proliferation and survival, which are instead profoundly hampered by the deletion of α.

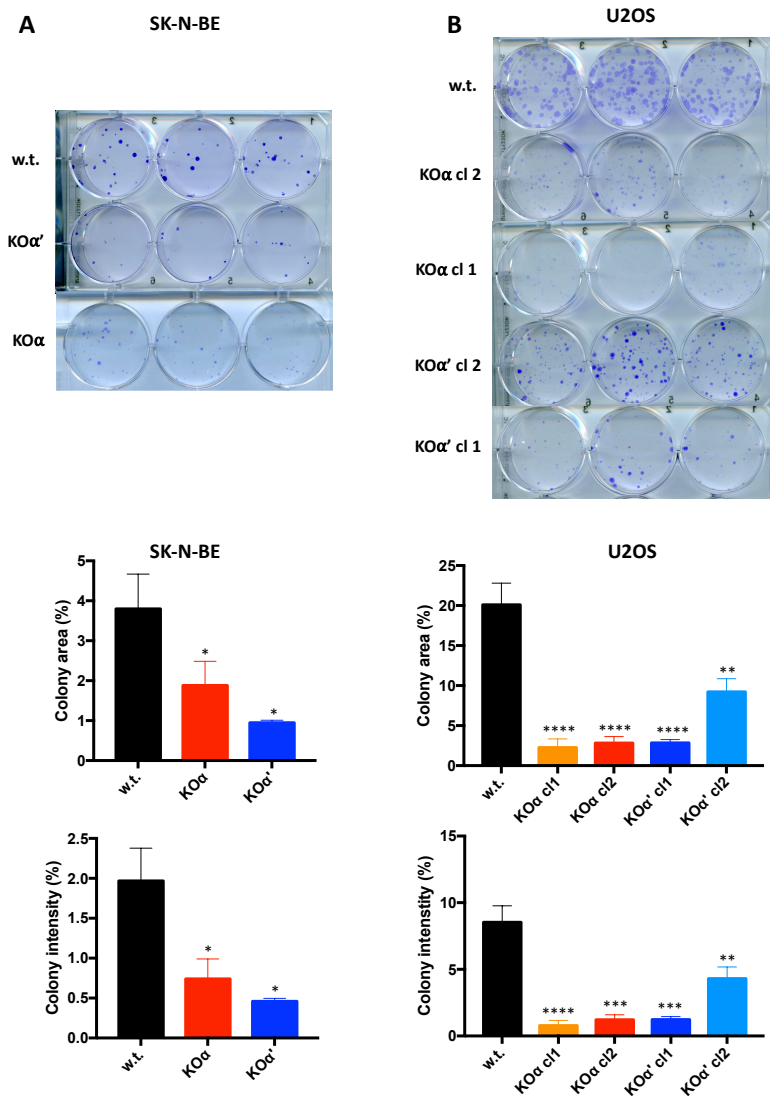

Figure 4. Clonogenic potential of w.t. and KO clones. (**A**) 250 SK-N-BE cells/well (w.t. or KOα clone 1, or KOα′ clone 1), or (**B**) 100 U2OS cells/well (w.t. or clones as indicated) were plated, then grown for 15 days. Colonies were stained with Crystal violet, and images were taken by a scanner device at day 15. At least two separate experiments in triplicate were performed; three representative images are shown for each clone. The bar graphs on the bottom show the quantification of the area covered by colonies (upper graph) and the colony intensity percentage (lower graph), which is related to the number of cells in a colony (mean values ± SEM). Significance refers to w.t. cells. (*) $p < 0.05$, (**) $p < 0.01$, (***) $p < 0.001$, (****) $p < 0.0001$.

In conclusion, our experiments highlight a lower proliferation and survival potential of all the SK-N-BE KO clones and of the U2OS KOα clones, compared to their w.t. counterpart.

We then evaluated the migration of cells deprived of one of the CK2 catalytic subunits by performing wound healing experiments. We noticed a slower migration of SK-N-BE w.t. compared to U2OS w.t. cells, thus the duration of the experiments was necessarily different for the two cell lines. In SK-N-BE cells, a significant closure of the gap area was observed after 48 h for w.t. cells, while in KOα′, and especially KOα cells, the closure was slower (Figure 5A). In U2OS cells, the almost complete closure was reached after 8 h for w.t.

cells, while at that time the wound was still open in KO clones, especially in α′ KO cells (Figure 5B). These results suggest that both α and α′ contribute to the migration, with a more marked effect of α deletion in SK-N-BE and α′ in U2OS cells, consistent with the relative expression of each catalytic subunit in the two cell lines.

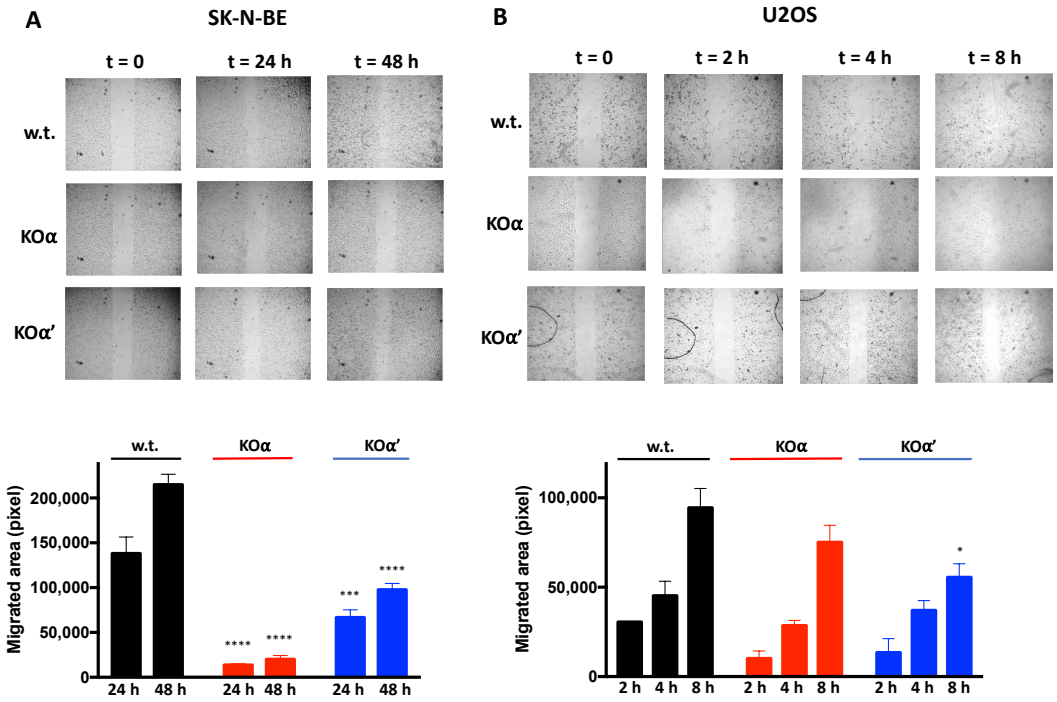

Figure 5. Migration of w.t. and KO clones of (**A**) SK-N-BE (KOα clone 1, KOα′ clone 1) and (**B**) U2OS (KOα clone 1, KOα′ clone 2) cells. Cell migration was assessed by wound-healing assay. Images were taken at the indicated times after the removal of the insert (t = 0). The experiments were performed three times. Representative images are shown. The bar graphs on the bottom show the quantification of the migrated areas of at least 2 different experiments, each one performed in triplicates (see Section 2 for details). Significance refers to the corresponding time in w.t. cells. (*) $p < 0.05$, (***) $p < 0.001$, (****) $p < 0.0001$.

3.3. Effect of CK2 Targeting on Hypoxic Response and Glycolysis Enzymes

It has been reported that the inhibition of CK2 reduces stability and/or activity of HIF-1α, one of the hypoxia sensor subunits of HIF-1 [33–35]. HIF-1 is a transcription factor of special relevance in the metabolic rewiring of cancer cells, as it mediates cellular adaptation to hypoxic stress by upregulating several downstream targets, among which hexokinase-2 (HK2) and lactate dehydrogenase-A (LDH-A) [36], that increase glucose utilization and boost aerobic glycolysis [37]. Therefore, we decided to evaluate HIF-1α levels in our model cells.

As found in other cells [33–35], HIF-1α was reduced in response to treatment with the CK2 inhibitor CX-4945, provided that the treatment lasted enough (48h, Figure 6A). In SK-N-BE and U2OS cells, HIF-1α level was hardly detectable under normoxic conditions, but it was significantly increased by cell treatment with Dimethyloxallyl Glycine (DMOG) which induces chemical hypoxia [38] (Figure 6B,C). We observed that in both cell lines, in normoxia and especially upon hypoxia induction, the HIF-1α level was significantly lower in KOα, but not in KOα′ cells, compared to w.t. cells (Figure 6B,C). Moreover, the amount of HK2 and LDH-A induced by treatment of U2OS cells with DMOG was also lower in KOα cells, while was not significantly affected in KOα′. Similarly, in SK-N-BE the induction of HK2 by DMOG was reduced in KOα (compared to w.t. cells) much more than in KOα′ cells; in our hands, LDH-A was not induced in w.t. SK-N-BE cells by DMOG treatment, thus preventing any comparison with the KO clones (not shown).

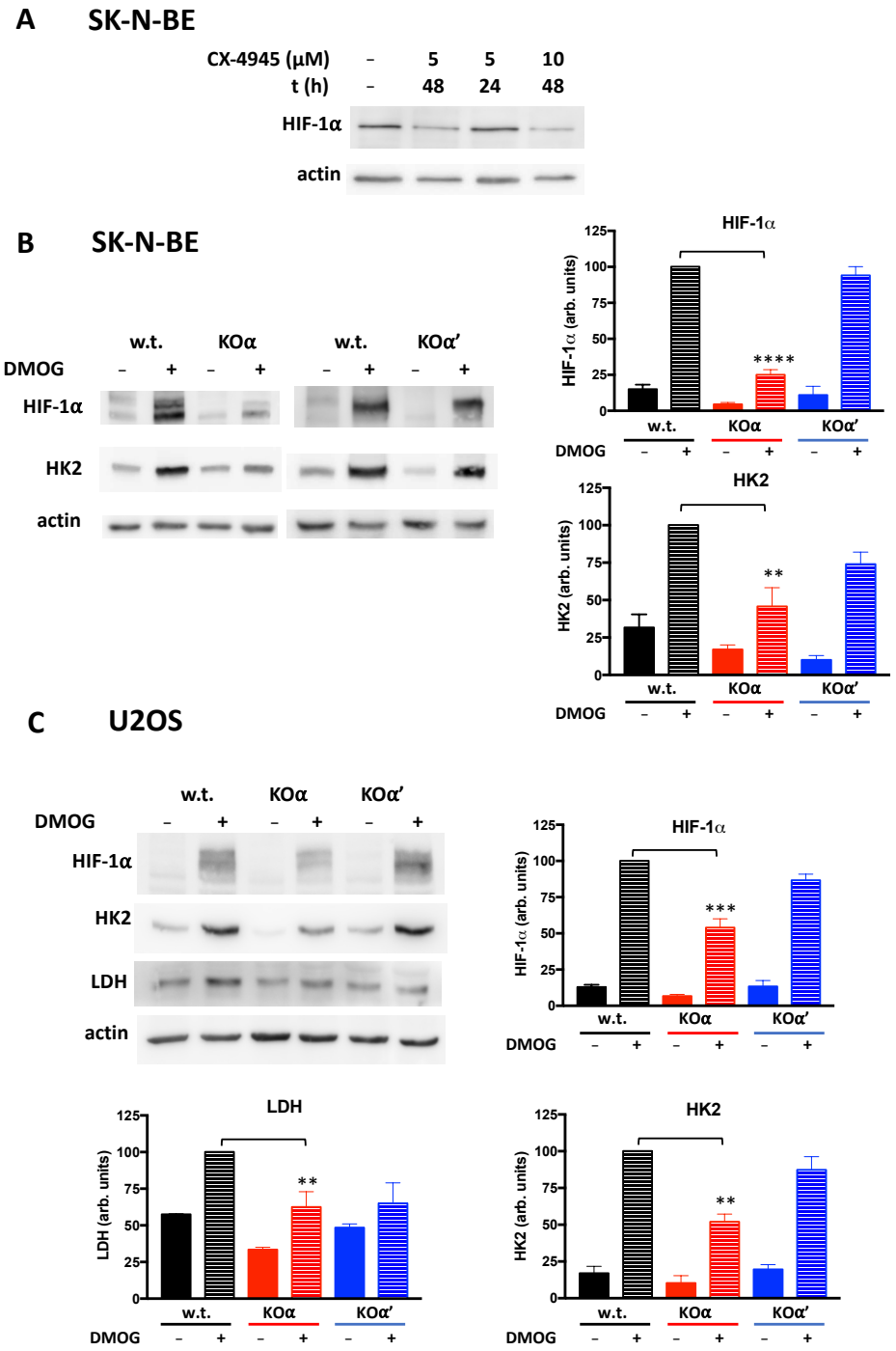

Figure 6. HIF-1α levels in w.t. and KO clones of SK-N-BE and U2OS cells. (**A**) w.t. SK-N-BE cells were treated with CX-4945 at the indicated time and concentration conditions. 30 μg proteins from lysates were analyzed by WB for the HIF-1α levels. Actin was used as loading control. (**B**) SK-N-BE cells (w.t or KOα clone 1, or KOα' clone 1) or (**C**) U2OS cells (w.t or KOα clone 1 or KOα' clone 2) were treated, where indicate (+), with 2mM dimethyloxallyl glycine (DMOG) for 20 h. 30 μg proteins from cell lysates were analyzed by WB for the indicated proteins. Actin was used as loading control. At least three independent experiments (also with different clones) were performed. Representative WB are shown. The bar graphs report quantification of HIF-1α, HK2 and LDH, as normalized mean values ± SEM of all experiments, in arbitrary units, obtained by analyses with Kodak 1D Image software. Significance refers to the corresponding condition in w.t. cells. (**) $p < 0.01$, (***) $p < 0.001$, (****) $p < 0.0001$.

The results described so far suggest that in tumor cells the glucose metabolism might be regulated by a single CK2 catalytic subunit. We therefore extended our study by characterizing the glycolytic phenotype of our KO clones.

3.4. Extracellular Lactate Production

The results shown in Figure 6 prompted us to evaluate the extracellular lactate production, as an indication of the glycolytic flux. We found that the lactate production was significantly lower in KOα clones compared to the respective w.t. cells, for both SK-N-BE and U2OS lines (Figure 7A). The deletion of α′ was instead less effective in affecting lactate secretion. As previously reported in bladder cancer cells [14], we have also found that pharmacological CK2 inhibition by CX-4945 cell treatment was able to reduce lactate production in a dose-dependent manner; consistently with a major role of CK2 α isoform, the KOα cells were less sensitive to CX-4945 treatment (Figure 7B).

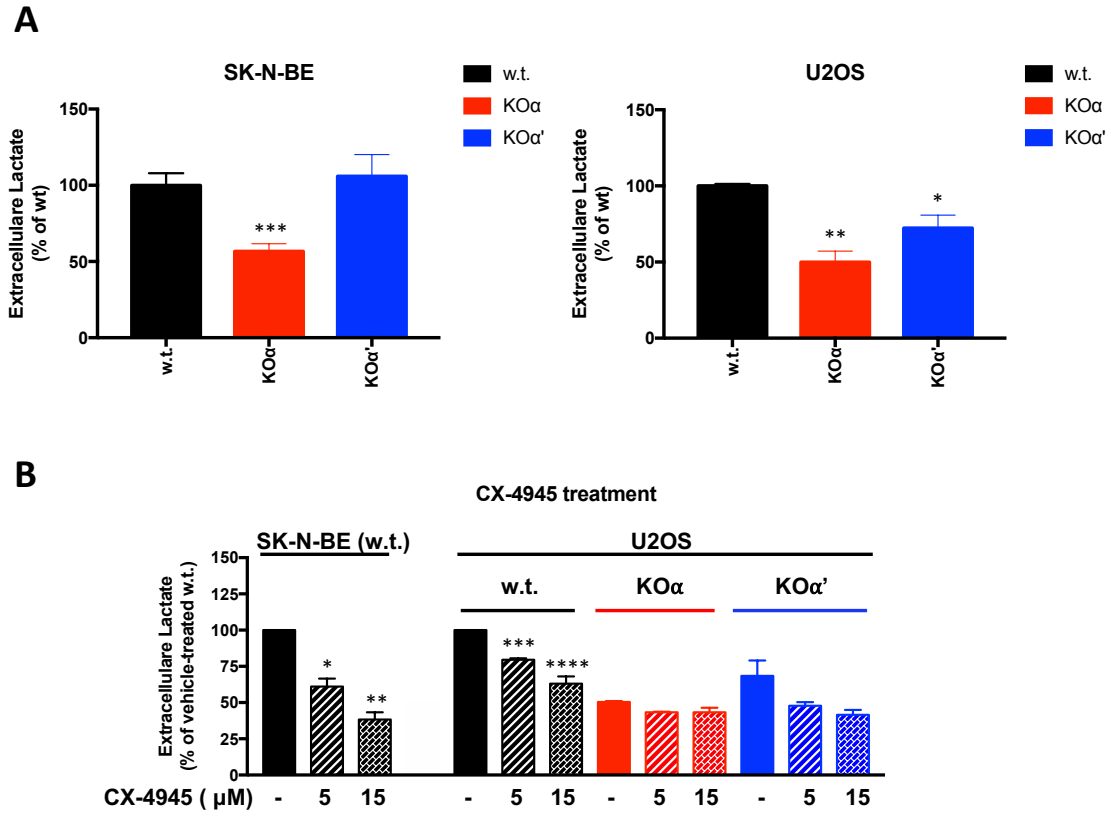

Figure 7. Lactate production in response to CK2 knock out or pharmacological inhibition. (**A**) The extracellular lactate secreted in the culture medium in 8 h by the indicated cells was analyzed by means of a luminescence assay. Values for each KO are the means ± SEM obtained with the different clones of the same KO. At least three independent experiments were performed, in duplicate. Significance refers to w.t. cells (**B**) Cells were analyzed for the extracellular lactate secreted in the culture medium in 6 h, in the absence or in the presence of the indicated concentrations of CX-4945. Three independent experiments were performed, in duplicate. Results (means ± SEM) are reported as % compared to the respective w.t. cells, in the absence of CX-4945. Significance refers to untreated control. (*) $p < 0.05$, (**) $p < 0.01$, (***) $p < 0.001$, (****) $p < 0.0001$.

These results suggest that CK2 signaling intervenes in the metabolic shift of tumor cell to glycolysis, with a more marked function of the α isoform.

3.5. Analysis of the Extracellular Acidification Rate

To better define the metabolic phenotype of our tumor cells, we exploited the Seahorse metabolic analyzer and performed glycolysis stress test experiments which allow to follow in real time the extra-cellular acidification rate (ECAR) caused by glycolytic activ-

ity. We found that both the glycolytic response (measured as the ECAR increase caused by glucose administration), and the maximal glycolytic capacity (assessed by inhibiting oxidative phosphorylation in the presence of glucose) were lower in SK-N-BE KO clones of either α or α′, with the strongest effect observed in KOα cells (Figure 8A). Similarly, in U2OS cells a general less glycolytic phenotype of KO clones compared to w.t. cells was observed (Figure 8B); in this case, however, there were important differences between clones. The glycolytic capacity and reserve were significantly reduced in both the two KOα clones (with also basal glycolysis and glycolytic response reduced in one of them). Instead, one of the KOα′ clones was quite similar to the w.t. cells, while the other significantly differed from them, therefore, we cannot unambiguously evaluate the real importance of this subunit in this kind of analysis. In general, we can conclude that for both SK-N-BE and U2OS cells, CK2 α seems to contribute more than CK2α′ to the glycolytic profile. As shown in Figure 8C, the Seahorse experiments performed with cells treated with the CK2 inhibitor CX-4945 demonstrated that also CK2 chemical targeting reduces the acidification rate due to glucose metabolism.

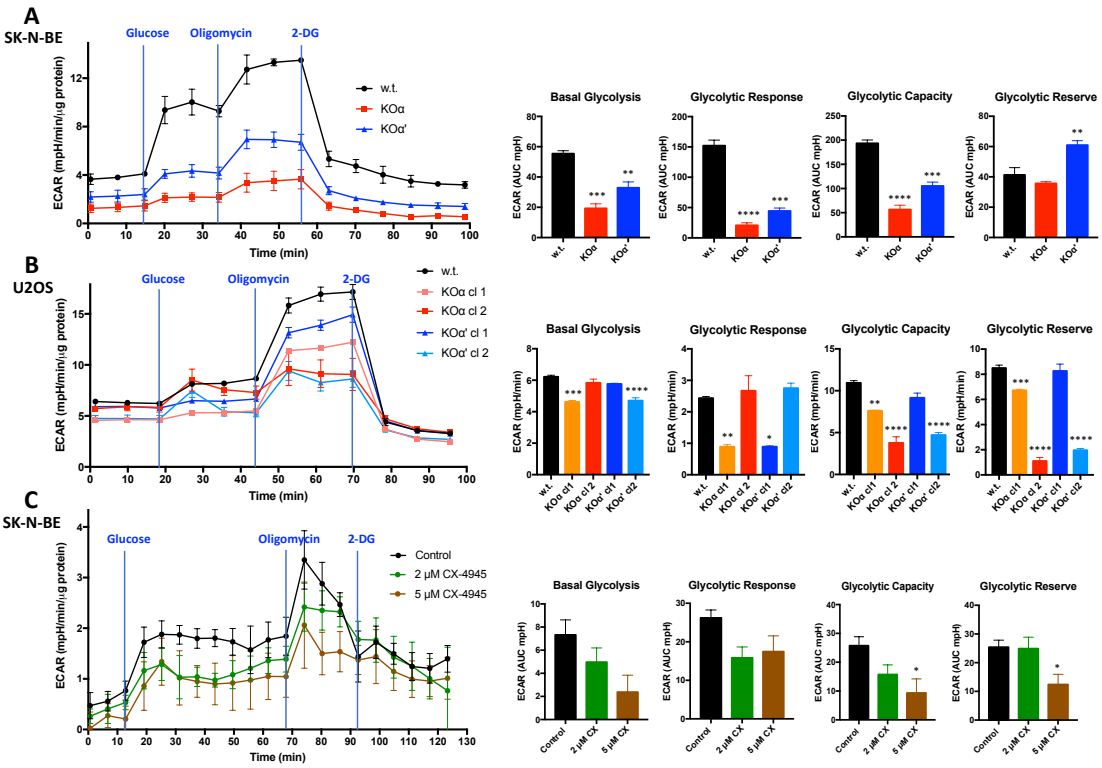

Figure 8. Seahorse glycolytic stress test of w.t. and KO clones of SK-N-BE and U2OS cells. The glycolysis stress tests were performed using a Seahorse extracellular flux analyzer. ECAR (extracellular acidification rate) was monitored following the indicated additions and normalized to protein concentrations. Each experiment was performed at least in quadruplicate. Values are expressed as the mean ± SEM. At least two independent experiments were performed; representative profiles are shown. (**A**) SK-N-BE cells glycolytic stress test profile (left) (KOα clone 1, KOα′ clone 2) and quantification of the experiment (right), performed with the XF software. ECAR values are expressed in AUC (Area Under Curves) units, quantifying the area of the curves corresponding to the different phases of the experiment (see Section 2). Significance refers to w.t. cells; (**B**) U2OS cells glycolytic stress test profile (left) (w.t. cells or the indicated clones) and quantification of the experiment (right), performed with the Wave software. ECAR values are expressed in mpH/min, as detected at the last measure point of each phase of the experiment (see Section 2). Significance refers to w.t. cells; (**C**) SK-N-BE cells glycolytic stress test profile, upon treatment with vehicle (control) or the indicated concentration of CX-4945 for 5 h before running the Seahorse experiment (left). Quantification of the experiment is shown on the right, performed with the XF software. ECAR values are expressed in AUC (Area Under Curves) units, quantifying the area of the curves under three points of each phases of the experiment (see Section 2). Significance refers to vehicle-treated control cells. (*) $p < 0.05$, (**) $p < 0.01$, and (***) $p < 0.001$, (****) $p < 0.0001$.

4. Discussion

In this work, we analyze the effect of CK2 targeting on the metabolic phenotype of cancer cells, by means of model cell lines and selective deletion of a single CK2 catalytic subunit.

Although the role of CK2 in the metabolic rewiring of cancer cells has been partly anticipated [14–16], our study is the first direct comparison of the specific contribution of each subunit. We found strong evidences supporting the CK2 involvement in the glycolytic phenotype of tumor cells, and suggesting a general more pronounced effect of α than α′ on this typical metabolic rewiring. This was evident, for example, on HIF-1α amount and activation, and consequent HK2 and LDH levels (Figure 6), on lactate production (Figure 7), on Seahorse glycolytic profile (Figure 8) (although with some variance among different clones, whose explanation will require further investigation). On these features, for both cell lines we observed a stronger divergence of KOα than KOα′ from w.t. cells. In the case of KOα′ U2OS cells, the lactate production was even equal to that measured in w.t. cells (Figure 7A). This is in partial discrepancy with the Seahorse experiments of Figure 8A (where one KOα′ clone is less glycolytic than w.t. cells). However, it has to be reasoned that the lactate assay provides a picture of a static situation at a certain time, while the Seahorse experiment is a real-time analysis, ideally measuring the acidification rate due not only to lactate production. In any case, both approaches support a major role for CK2α.

Our observations on the isoform-specific effects do not seem to depend on the amount of residual CK2 catalytic activity, which is different in the two cell lines (see Figure 1), and, instead, correlates with the migration potential (Figure 5). In contrast, specific functions of α respect to α′ appear to play a role in the regulation of metabolic rewiring. CK2 isoform-specific substrates/partners/functions have been already reported [11,31,39–41]; further studies will be necessary to assess their effective implication in cancer cell metabolism and to identify novel targets and mechanisms that might be implicated. However, it is also important to notice that, as previously observed in other cell lines [31], the KOα clones display a reduction of the β CK2 regulatory subunit, which is not (or only marginally) appreciable in KOα′ cells (Figure 1). Therefore, it is likely that KOα cells have a lower cellular amount of the tetrameric CK2 holoenzyme. This observation further complicates the interpretation of our data, since it has been shown that knocking out β is detrimental to the phosphorylation of a number of CK2 targets but not of others [42]. In fact, monomeric and tetrameric CK2 display different activity towards a panel of selected substrates [7]. We cannot exclude, therefore, that the more evident effects observed in KOα cells are due to the lower amount of tetrameric CK2. In discriminating between the importance of CK2α and tetrameric CK2, an advantage would potentially derive from the establishment of KOβ cells; however, for the time being, any attempt to produce tumor cell devoid of β has failed (unpublished results). Implicitly, this suggests that the tetrameric form of CK2 is essential for cancer cell survival.

Several inhibitors are available for CK2 (with two of them, CX-4945 [43] and CIGB-300 [44] already at a clinical level). Tumor cells have been widely documented to respond to CK2 inhibitors, alone or in combination with conventional drugs (as reviewed in [45]). Concerning the cell lines used in this work, Figure S1A shows that SK-N-BE cells are sensitive to the CK2 inhibitors CX-4945, TDB (Tetra-bromo-deoxyribofuranosyl-benzimidazole) [46] and K137 (*N*′-(4,5,6,7-tetrabromo-1Hbenzimidazol-2-yl)propane-1,3-diamine, also known as 2b) [47,48], with IC50 in the μM range (see Figure S1A). As for U2OS cells, we have already published that CX-4945 reduces their viability, with an IC_{50} around 4 μM [23]. Interestingly, we have also preliminary evidence suggesting that the combined treatment with a CK2 inhibitor (CX-4945) and a metabolic inhibitor (2-DG) produces synergistic effects on U2OS cell viability (Figure S1B), allowing to reduce the effective doses of each drug. The calculated combination index of 0.37 supports a synergistic effect. These results give a particular significance to the work presented here, in the perspective of future therapeutic strategies based on CK2 targeting.

Most CK2 inhibitors are equally effective towards the different CK2 forms, but attempts have been done to develop strategies/compounds able to discriminate between them, either tetrameric vs monomeric [49], or α vs α′ [50]. The knowledge of the mechanism(s) underlying the contribution of each CK2 form to cancer metabolic phenotype is crucial for the choice of the correct inhibition strategy for therapeutic applications.

Apart from the α/α′ issue, our results unequivocally support the CK2 implication in the metabolic glycolytic phenotype of different tumor cells, and suggest that CK2 inhibition may hamper the energy supply strategies of cancer cells, thus offering further opportunities of therapeutic plans.

Supplementary Materials: The following are available online at https://www.mdpi.com/2073-4409/10/1/181/s1, Figure S1: Effect of CK2 inhibitors on cell viability.

Author Contributions: Conceptualization, M.R.; data curation, F.Z., M.R.; methodology, F.Z., C.B, M.S., I.M., A.R.; investigation, F.Z., C.B., C.P.Q.M., I.M.; writing—original draft preparation, M.R.; writing—review and editing, M.R., L.A.P., C.B., A.R.; supervision, M.R., M.S., A.R.; project administration, M.R.; funding acquisition, L.A.P., M.R., M.S., A.R., I.M. All authors have read and agreed to the published version of the manuscript.

Funding: This work was supported by Associazione Italiana per la Ricerca sul Cancro (AIRC), grant IG 18756 to L.A.P. and grant IG 2017/20749 to A.R., AFM-Telethon, grant 22974 to M.R., Fondazione per la Ricerca sulla Fibrosi Cistica (grants FFC#12/2017 and FFC#11/2019 adopted by Delegazione FFC di Fabriano Ancona con la Delegazione FFC di Umbertide Città di Castello) to M.S., Children's Tumor Foundation (YIA grant 2016-01-010 to I.M.)

Institutional Review Board Statement: Not applicable.

Informed Consent Statement: Not applicable.

Data Availability Statement: Data presented in this study are contained within this article and the supplementary materials, or available upon request to the corresponding author.

Acknowledgments: We are grateful to Stefania Sarno (University of Padova) who kindly provided the CK2 subunits used for the antibody standardization shown in Figure 1.

Conflicts of Interest: The authors declare no conflict of interest.

References

1. Hanahan, D.; Weinberg, R.A. Hallmarks of Cancer: The Next Generation. *Cell* **2011**, *144*, 646–674. [CrossRef] [PubMed]
2. Ruzzene, M.; Pinna, L.A. Addiction to protein kinase CK2: A common denominator of diverse cancer cells? *Biochim. Biophys. Acta Proteins Proteom.* **2010**, *1804*, 499–504. [CrossRef] [PubMed]
3. Ortega, C.E.; Seidner, Y.; Dominguez, I. Mining CK2 in Cancer. *PLoS ONE* **2014**, *9*, e115609. [CrossRef]
4. Chua, M.M.J.; Lee, M.; Dominguez, I. Cancer-type dependent expression of CK2 transcripts. *PLoS ONE* **2017**, *12*, e0188854. [CrossRef]
5. Litchfield, D.W. Protein kinase CK2: Structure, regulation and role in cellular decisions of life and death. *Biochem. J.* **2003**, *369*, 1–15. [CrossRef] [PubMed]
6. Ahmad, K.A.; Wang, G.; Unger, G.; Slaton, J.; Ahmed, K. Protein Kinase CK2—A Key Suppressor of Apoptosis. *Adv. Enzyme Regul.* **2008**, *48*, 179–187. [CrossRef]
7. Pinna, L.A. Protein kinase CK2: A challenge to canons. *J. Cell Sci.* **2002**, *115*, 3873–3878. [CrossRef]
8. Filhol, O.; Giacosa, S.; Wallez, Y.; Cochet, C. Protein kinase CK2 in breast cancer: The CK2β regulatory subunit takes center stage in epithelial plasticity. *Cell. Mol. Life Sci.* **2015**, *72*, 3305–3322. [CrossRef]
9. Deshiere, A.; Duchemin-Pelletier, E.; Spreux, E.; Ciais, D.; Combes, F.; Vandenbrouck, Y.; Couté, Y.; Mikaelian, I.; Giusiano, S.; Charpin, C.; et al. Unbalanced expression of CK2 kinase subunits is sufficient to drive epithelial-to-mesenchymal transition by Snail1 induction. *Oncogene* **2013**, *32*, 1373–1383. [CrossRef]
10. Litchfield, D.W.; Bosc, D.G.; Canton, D.A.; Saulnier, R.B.; Vilk, G.; Zhang, C. Functional specialization of CK2 isoforms and characterization of isoform-specific binding partners. *Mol. Cell. Biochem.* **2001**, *227*, 21–29. [CrossRef]
11. Turowec, J.P.; Vilk, G.; Gabriel, M.; Litchfield, D.W. Characterizing the convergence of protein kinase CK2 and caspase-3 reveals isoform-specific phosphorylation of caspase-3 by CK2α′: Implications for pathological roles of CK2 in promoting cancer cell survival. *Oncotarget* **2013**, *4*, 560–571. [CrossRef] [PubMed]

12. Villamañan, L.; Alcaraz, E.; Pinna, L.A.; Ruzzene, M.; Itarte, E.; Arús, C.; Plana, M.; Candiota, A.P. Up-Regulation of the Alpha Prime Subunit of Protein Kinase CK2 as a Marker of Fast Proliferation in GL261 Cultured Cells. *Pathol. Oncol. Res.* **2019**, *25*, 1659–1663. [CrossRef] [PubMed]
13. Al Quobaili, F.; Montenarh, M. CK2 and the regulation of the carbohydrate metabolism. *Metab. Clin. Exp.* **2012**, *61*, 1512–1517. [CrossRef] [PubMed]
14. Zhang, X.; Yang, X.; Yang, C.; Li, P.; Yuan, W.; Deng, X.; Cheng, Y.; Li, P.; Yang, H.; Tao, J.; et al. Targeting protein kinase CK2 suppresses bladder cancer cell survival via the glucose metabolic pathway. *Oncotarget* **2016**, *7*, 87361–87372. [CrossRef] [PubMed]
15. Yang, K.M.; Kim, K. Protein Kinase CK2 Modulation of Pyruvate Kinase M Isoforms Augments the Warburg Effect in Cancer Cells. *J. Cell. Biochem.* **2018**, *119*, 8501–8510. [CrossRef]
16. Im, D.-K.; Cheong, H.; Lee, J.S.; Oh, M.-K.; Yang, K.M. Protein kinase CK2-dependent aerobic glycolysis-induced lactate dehydrogenase A enhances the migration and invasion of cancer cells. *Sci. Rep.* **2019**, *9*, 5337. [CrossRef]
17. Di Maira, G.; Salvi, M.; Arrigoni, G.; Marin, O.; Sarno, S.; Brustolon, F.; Pinna, L.A.; Ruzzene, M. Protein kinase CK2 phosphorylates and upregulates Akt/PKB. *Cell Death Differ.* **2005**, *12*, 668–677. [CrossRef]
18. Ponce, D.P.; Yefi, R.; Cabello, P.; Maturana, J.L.; Niechi, I.; Silva, E.; Galindo, M.; Antonelli, M.; Marcelain, K.; Armisén, R.; et al. CK2 functionally interacts with AKT/PKB to promote the β-catenin-dependent expression of survivin and enhance cell survival. *Mol. Cell. Biochem.* **2011**, *356*, 127–132. [CrossRef]
19. Silva-Pavez, E.; Tapia, J.C. Protein Kinase CK2 in Cancer Energetics. *Front. Oncol.* **2020**, *10*, 893. [CrossRef]
20. Borgo, C.; Milan, G.; Favaretto, F.; Stasi, F.; Fabris, R.; Salizzato, V.; Cesaro, L.; Belligoli, A.; Arianna, D.-D.; Foletto, M.; et al. CK2 modulates adipocyte insulin-signaling and is up-regulated in human obesity. *Sci. Rep.* **2017**, *7*, 1–15. [CrossRef]
21. Guerra, B.; Issinger, O.-G. Role of Protein Kinase CK2 in Aberrant Lipid Metabolism in Cancer. *Pharmaceuticals* **2020**, *13*, 292. [CrossRef] [PubMed]
22. Borgo, C.; Franchin, C.; Scalco, S.; Bosello-Travain, V.; Donella-Deana, A.; Arrigoni, G.; Salvi, M.; Pinna, L.A. Generation and Quantitative Proteomics Analysis of CK2$\alpha/\alpha'(-/-)$ Cells. *Sci. Rep.* **2017**, *7*, 42409. [CrossRef] [PubMed]
23. Zanin, S.; Borgo, C.; Girardi, C.; O'Brien, S.E.; Miyata, Y.; Pinna, L.A.; Donella-Deana, A.; Ruzzene, M. Effects of the CK2 Inhibitors CX-4945 and CX-5011 on Drug-Resistant Cells. *PLoS ONE* **2012**, *7*, e49193. [CrossRef] [PubMed]
24. Ottaviani, D.; Marin, O.; Arrigoni, G.; Franchin, C.; Vilardell, J.; Sandre, M.; Li, W.; Parfitt, D.A.; Pinna, L.A.; E Cheetham, M.; et al. Protein kinase CK2 modulates HSJ1 function through phosphorylation of the UIM2 domain. *Hum. Mol. Genet.* **2017**, *26*, 611–623. [CrossRef] [PubMed]
25. Sarno, S.; Ruzzene, M.; Frascella, P.; Pagano, M.A.; Meggio, F.; Zambon, A.; Mazzorana, M.; Di Maira, G.; Lucchini, V.; Pinna, L.A. Development and exploitation of CK2 inhibitors. *Mol. Cell. Biochem.* **2005**, *274*, 69–76. [CrossRef] [PubMed]
26. Pampaloni, F.; Richa, R.; Ansari, N.; Stelzer, E.H.K. Live Spheroid Formation Recorded with Light Sheet-Based Fluorescence Microscopy. *Adv. Struct. Saf. Stud.* **2014**, *1251*, 43–57. [CrossRef]
27. Guzmán, C.; Bagga, M.; Kaur, A.; Westermarck, J.; Abankwa, D. ColonyArea: An ImageJ Plugin to Automatically Quantify Colony Formation in Clonogenic Assays. *PLoS ONE* **2014**, *9*, e92444. [CrossRef]
28. Venter, C.; Niesler, C.U. Rapid quantification of cellular proliferation and migration using ImageJ. *Biotechniques* **2019**, *66*, 99–102. [CrossRef]
29. Masgras, I.; Ciscato, F.; Brunati, A.M.; Tibaldi, E.; Indraccolo, S.; Curtarello, M.; Chiara, F.; Cannino, G.; Papaleo, E.; Lambrughi, M.; et al. Absence of Neurofibromin Induces an Oncogenic Metabolic Switch via Mitochondrial ERK-Mediated Phosphorylation of the Chaperone TRAP1. *Cell Rep.* **2017**, *18*, 659–672. [CrossRef]
30. Chou, T.-C. Drug Combination Studies and Their Synergy Quantification Using the Chou-Talalay Method. *Cancer Res.* **2010**, *70*, 440–446. [CrossRef]
31. Salizzato, V.; Zanin, S.; Borgo, C.; Lidron, E.; Salvi, M.; Rizzuto, R.; Pallafacchina, G.; Donella-Deana, A. Protein kinase CK2 subunits exert specific and coordinated functions in skeletal muscle differentiation and fusogenic activity. *FASEB J.* **2019**, *33*, 10648–10667. [CrossRef] [PubMed]
32. Lucido, C.T.; Miskimins, W.K.; Vermeer, P.D. Propranolol Promotes Glucose Dependence and Synergizes with Dichloroacetate for Anti-Cancer Activity in HNSCC. *Cancers* **2018**, *10*, 476. [CrossRef] [PubMed]
33. Mottet, D.; Ruys, S.P.D.; Demazy, C.; Raes, M.; Michiels, C. Role for casein kinase 2 in the regulation of HIF-1 activity. *Int. J. Cancer* **2005**, *117*, 764–774. [CrossRef] [PubMed]
34. Guerra, B.; Rasmussen, T.D.L.; Schnitzler, A.; Jensen, H.H.; Boldyreff, B.S.; Miyata, Y.; Marcussen, N.; Niefind, K.; Issinger, O.-G. Protein kinase CK2 inhibition is associated with the destabilization of HIF-1α in human cancer cells. *Cancer Lett.* **2015**, *356*, 751–761. [CrossRef]
35. Ampofo, E.; Kietzmann, T.; Zimmer, A.; Jakupovic, M.; Montenarh, M.; Götz, C. Phosphorylation of the von Hippel–Lindau protein (VHL) by protein kinase CK2 reduces its protein stability and affects p53 and HIF-1α mediated transcription. *Int. J. Biochem. Cell Biol.* **2010**, *42*, 1729–1735. [CrossRef]
36. Luo, W.; Hu, H.; Chang, R.; Zhong, J.; Knabel, M.; O'Meally, R.; Cole, R.N.; Pandey, A.; Semenza, G.L. Pyruvate Kinase M2 Is a PHD3-Stimulated Coactivator for Hypoxia-Inducible Factor 1. *Cell* **2011**, *145*, 732–744. [CrossRef]
37. Lee, P.; Chandel, N.S.; Simon, M.C. Cellular adaptation to hypoxia through hypoxia inducible factors and beyond. *Nat. Rev. Mol. Cell Biol.* **2020**, *21*, 268–283. [CrossRef]

38. Milkiewicz, M.; Pugh, C.W.; Egginton, S. Inhibition of endogenous HIF inactivation induces angiogenesis in ischaemic skeletal muscles of mice. *J. Physiol.* **2004**, *560*, 21–26. [CrossRef]
39. Bosc, D.G.; Graham, K.C.; Saulnier, R.B.; Zhang, C.; Prober, D.; Gietz, R.D.; Litchfield, D.W. Identification and Characterization of CKIP-1, a Novel Pleckstrin Homology Domain-containing Protein That Interacts with Protein Kinase CK2. *J. Biol. Chem.* **2000**, *275*, 14295–14306. [CrossRef]
40. Messenger, M.M.; Saulnier, R.B.; Gilchrist, A.D.; Diamond, P.; Gorbsky, G.J.; Litchfield, D.W. Interactions between Protein Kinase CK2 and Pin1. Evidence for Phosphorylation-Dependent Interactions. *J. Biol. Chem.* **2002**, *277*, 23054–23064. [CrossRef]
41. Lettieri, A.; Borgo, C.; Zanieri, L.; D'Amore, C.; Oleari, R.; Paganoni, A.; Pinna, L.A.; Cariboni, A.; Salvi, M. Protein Kinase CK2 Subunits Differentially Perturb the Adhesion and Migration of GN11 Cells: A Model of Immature Migrating Neurons. *Int. J. Mol. Sci.* **2019**, *20*, 5951. [CrossRef] [PubMed]
42. Franchin, C.; Borgo, C.; Cesaro, L.; Zaramella, S.; Vilardell, J.; Salvi, M.; Arrigoni, G.; Pinna, L.A. Re-evaluation of protein kinase CK2 pleiotropy: New insights provided by a phosphoproteomics analysis of CK2 knockout cells. *Cell. Mol. Life Sci.* **2018**, *75*, 2011–2026. [CrossRef] [PubMed]
43. Martins, L.R.; Lúcio, P.; Melão, A.; Antunes, I.; A Cardoso, B.; Stansfield, R.; Bertilaccio, M.T.S.; Ghia, P.; Drygin, D.; Silva, M.G.; et al. Activity of the clinical-stage CK2-specific inhibitor CX-4945 against chronic lymphocytic leukemia. *Leukemia* **2013**, *28*, 179–182. [CrossRef] [PubMed]
44. Perea, S.E.; Baladrón, I.; Valenzuelasilva, C.M.; Perera, Y. CIGB-300: A peptide-based drug that impairs the Protein Kinase CK2-mediated phosphorylation. *Semin. Oncol.* **2018**, *45*, 58–67. [CrossRef]
45. D'Amore, C.; Borgo, C.; Sarno, S.; Salvi, M. Role of CK2 inhibitor CX-4945 in anti-cancer combination therapy—Potential clinical relevance. *Cell. Oncol.* **2020**, *43*, 1003–1016. [CrossRef]
46. Cozza, G.; Girardi, C.; Ranchio, A.; Lolli, G.; Sarno, S.; Orzeszko, A.; Kazimierczuk, Z.; Battistutta, R.; Ruzzene, M.; Pinna, L.A. Cell-permeable dual inhibitors of protein kinases CK2 and PIM-1: Structural features and pharmacological potential. *Cell. Mol. Life Sci.* **2014**, *71*, 3173–3185. [CrossRef]
47. Schneider, C.C.; Kartarius, S.; Montenarh, M.; Orzeszko, A.; Kazimierczuk, Z. Modified tetrahalogenated benzimidazoles with CK2 inhibitory activity are active against human prostate cancer cells LNCaP in vitro. *Bioorganic Med. Chem.* **2012**, *20*, 4390–4396. [CrossRef]
48. Cozza, G.; Zanin, S.; Sarno, S.; Costa, E.; Girardi, C.; Ribaudo, G.; Salvi, M.; Zagotto, G.; Ruzzene, M.; Pinna, L.A. Design, validation and efficacy of bisubstrate inhibitors specifically affecting ecto-CK2 kinase activity. *Biochem. J.* **2015**, *471*, 415–430. [CrossRef]
49. Prudent, R.; Sautel, C.F.; Cochet, C. Structure-based discovery of small molecules targeting different surfaces of protein-kinase CK2. *Biochim. Biophys. Acta Proteins Proteom.* **2010**, *1804*, 493–498. [CrossRef]
50. Bollacke, A.; Nienberg, C.; Le Borgne, M.; Jose, J. Toward selective CK2alpha and CK2alpha' inhibitors: Development of a novel whole-cell kinase assay by Autodisplay of catalytic CK2alpha'. *J. Pharm. Biomed. Anal.* **2016**, *121*, 253–260. [CrossRef]

REFERENCES

Abdul-Ghani, M., Suen, C., Jiang, B., Deng, Y., Weldrick, J. J., Putinski, C., Brunette, S., Fernando, P., Lee, T. T., Flynn, P., Leenen, F. H. H., Burgon, P. G., Stewart, D. J., & Megeney, L. A. (2017). Cardiotrophin 1 stimulates beneficial myogenic and vascular remodeling of the heart. *Cell Research*, *27*(10), 1195–1215. https://doi.org/10.1038/cr.2017.87

Aksenova, M. V., Burbaeva, G. S., Kandror, K. V., Kapkov, D. V., & Stepanov, A. S. (1991). The decreased level of casein kinase 2 in brain cortex of schizophrenic and Alzheimer's disease patients. *FEBS Letters*, *279*(1), 55–57. https://doi.org/10.1016/0014-5793(91)80249-3

Allende, J. E., & Allende, C. C. (1995). Protein kinases. 4. Protein kinase CK2: An enzyme with multiple substrates and a puzzling regulation. *FASEB Journal: Official Publication of the Federation of American Societies for Experimental Biology*, *9*(5), 313–323. https://doi.org/10.1096/fasebj.9.5.7896000

Amarante-Mendes, G. P., Rana, A., Datoguia, T. S., Hamerschlak, N., & Brumatti, G. (2022). BCR-ABL1 Tyrosine Kinase Complex Signaling Transduction: Challenges to Overcome Resistance in Chronic Myeloid Leukemia. *Pharmaceutics*, *14*(1), Article 1. https://doi.org/10.3390/pharmaceutics14010215

Ardito, F., Giuliani, M., Perrone, D., Troiano, G., & Muzio, L. L. (2017). The crucial role of protein phosphorylation in cell signaling and its use as targeted therapy (Review). *International Journal of Molecular Medicine*, *40*(2), 271–280. https://doi.org/10.3892/ijmm.2017.3036

Arter, C., Trask, L., Ward, S., Yeoh, S., & Bayliss, R. (2022). Structural features of the protein kinase domain and targeted binding by small-molecule inhibitors. *The Journal of Biological Chemistry*, *298*(8), 102247. https://doi.org/10.1016/j.jbc.2022.102247

Asif, M., Kaygusuz, E., Shinawi, M., Nickelsen, A., Hsieh, T.-C., Wagle, P., Budde, B. S., Hochscherf, J., Abdullah, U., Höning, S., Nienberg, C., Lindenblatt, D., Noegel, A. A., Altmüller, J., Thiele, H., Motameny, S., Fleischer, N., Segal, I., Pais, L., … Hussain, M. S. (2022). De novo variants of CSNK2B cause a new intellectual disability-craniodigital syndrome by disrupting the canonical Wnt signaling pathway. *Human Genetics and Genomics Advances*, *3*(3), 100111. https://doi.org/10.1016/j.xhgg.2022.100111

Atkinson, E. L., Iegre, J., Brear, P. D., Zhabina, E. A., Hyvönen, M., & Spring, D. R. (2021). Downfalls of Chemical Probes Acting at the Kinase ATP-Site: CK2 as a Case Study. *Molecules*, *26*(7), 1977. https://doi.org/10.3390/molecules26071977

Atwal, R. S., Desmond, C. R., Caron, N., Maiuri, T., Xia, J., Sipione, S., & Truant, R. (2011). Kinase inhibitors modulate huntingtin cell localization and toxicity. *Nature Chemical Biology*, *7*(7), 453–460. https://doi.org/10.1038/nchembio.582

Bajorek, M., Caly, L., Tran, K. C., Maertens, G. N., Tripp, R. A., Bacharach, E., Teng, M. N., Ghildyal, R., & Jans, D. A. (2014). The Thr205 Phosphorylation Site within Respiratory Syncytial Virus Matrix (M) Protein Modulates M Oligomerization and Virus Production. *Journal of Virology*, *88*(11), 6380–6393. https://doi.org/10.1128/jvi.03856-13

Ballardin, D., Cruz-Gamero, J. M., Bienvenu, T., & Rebholz, H. (2022). Comparing Two Neurodevelopmental Disorders Linked to CK2: Okur-Chung Neurodevelopmental Syndrome and Poirier-Bienvenu Neurodevelopmental Syndrome—Two Sides of the Same Coin? *Frontiers in Molecular Biosciences*, *9*. https://www.frontiersin.org/articles/10.3389/fmolb.2022.850559

Bartley, C. M., O'Keefe, R. A., Blice-Baum, A., Mihailescu, M.-R., Gong, X., Miyares, L., Karaca, E., & Bordey, A. (2016). Mammalian FMRP S499 Is Phosphorylated by CK2 and Promotes Secondary Phosphorylation of FMRP. *eNeuro*, *3*(6), ENEURO.0092-16.2016. https://doi.org/10.1523/ENEURO.0092-16.2016

Basta, H. A., Bacot-Davis, V. R., Ciomperlik, J. J., & Palmenberg, A. C. (2014). Encephalomyocarditis virus leader is phosphorylated by CK2 and syk as a requirement for

subsequent phosphorylation of cellular nucleoporins. *Journal of Virology*, *88*(4), 2219–2226. https://doi.org/10.1128/JVI.03150-13

Benini, M., Fortuni, S., Condò, I., Alfedi, G., Malisan, F., Toschi, N., Serio, D., Massaro, D. S., Arcuri, G., Testi, R., & Rufini, A. (2017). E3 Ligase RNF126 Directly Ubiquitinates Frataxin, Promoting Its Degradation: Identification of a Potential Therapeutic Target for Friedreich Ataxia. *Cell Reports*, *18*(8), 2007–2017. https://doi.org/10.1016/j.celrep.2017.01.079

Bitirim, C. V., Tuncay, E., & Turan, B. (2018). Demonstration of subcellular migration of CK2α localization from nucleus to sarco(endo)plasmic reticulum in mammalian cardiomyocytes under hyperglycemia. *Molecular and Cellular Biochemistry*, *443*(1–2), 25–36. https://doi.org/10.1007/s11010-017-3207-6

Bodenbach, L., Fauss, J., Robitzki, A., Krehan, A., Lorenz, P., Lozeman, F. J., & Pyerin, W. (1994). Recombinant human casein kinase II. *European Journal of Biochemistry*, *220*(1), 263–273. https://doi.org/10.1111/j.1432-1033.1994.tb18622.x

Boldyreff, B., Meggio, F., Pinna, L. A., & Issinger, O. G. (1994). Protein kinase CK2 structure-function relationship: Effects of the beta subunit on reconstitution and activity. *Cellular & Molecular Biology Research*, *40*(5–6), 391–399.

Bonanni, P., Baggio, M., Duma, G. M., Negrin, S., Danieli, A., & Giorda, R. (2021). Developmental and epilepsy spectrum of Poirier-Bienvenu neurodevelopmental syndrome: Description of a new case study and review of the available literature. *Seizure*, *93*, 133–139. https://doi.org/10.1016/j.seizure.2021.10.019

Borgo, C., Cesaro, L., Salizzato, V., Ruzzene, M., Massimino, M. L., Pinna, L. A., & Donella-Deana, A. (2013). Aberrant signalling by protein kinase CK2 in imatinib-resistant chronic myeloid leukaemia cells: Biochemical evidence and therapeutic perspectives. *Molecular Oncology*, *7*(6), 1103–1115. https://doi.org/10.1016/j.molonc.2013.08.006

Borgo, C., D'Amore, C., Cesaro, L., Sarno, S., Pinna, L. A., Ruzzene, M., & Salvi, M. (2021b). How can a traffic light properly work if it is always green? The paradox of CK2 signaling. *Critical Reviews in Biochemistry and Molecular Biology*, *56*(4), 321–359. https://doi.org/10.1080/10409238.2021.1908951

Borgo, C., D'Amore, C., Sarno, S., Salvi, M., & Ruzzene, M. (2021a). Protein kinase CK2: A potential therapeutic target for diverse human diseases. *Signal Transduction and Targeted Therapy*, *6*(1), 183. https://doi.org/10.1038/s41392-021-00567-7

Borgo, C., Franchin, C., Cesaro, L., Zaramella, S., Arrigoni, G., Salvi, M., & Pinna, L. A. (2019). A proteomics analysis of CK2β(-/-) C2C12 cells provides novel insights into the biological functions of the non-catalytic β subunit. *The FEBS Journal*, *286*(8), 1561–1575. https://doi.org/10.1111/febs.14799

Borgo, C., Milan, G., Favaretto, F., Stasi, F., Fabris, R., Salizzato, V., Cesaro, L., Belligoli, A., Sanna, M., Foletto, M., Prevedello, L., Vindigni, V., Bardini, R., Donella-Deana, A., & Vettor, R. (2017). CK2 modulates adipocyte insulin-signaling and is up-regulated in human obesity. *Scientific Reports*, *7*(1), 17569. https://doi.org/10.1038/s41598-017-17809-w

Borgo, C., & Ruzzene, M. (2021). Protein kinase CK2 inhibition as a pharmacological strategy. *Advances in Protein Chemistry and Structural Biology*, *124*, 23–46. https://doi.org/10.1016/bs.apcsb.2020.09.003

Bouhaddou, M., Memon, D., Meyer, B., White, K. M., Rezelj, V. V., Correa Marrero, M., Polacco, B. J., Melnyk, J. E., Ulferts, S., Kaake, R. M., Batra, J., Richards, A. L., Stevenson, E., Gordon, D. E., Rojc, A., Obernier, K., Fabius, J. M., Soucheray, M., Miorin, L., … Krogan, N. J. (2020). The Global Phosphorylation Landscape of SARS-CoV-2 Infection. *Cell*, *182*(3), 685-712.e19. https://doi.org/10.1016/j.cell.2020.06.034

Bradeen, H. A., Eide, C. A., O'Hare, T., Johnson, K. J., Willis, S. G., Lee, F. Y., Druker, B. J., & Deininger, M. W. (2006). Comparison of imatinib mesylate, dasatinib (BMS-354825), and nilotinib (AMN107) in an N-ethyl-N-nitrosourea (ENU)-based mutagenesis screen: High efficacy of drug combinations. *Blood*, *108*(7), 2332–2338. https://doi.org/10.1182/blood-2006-02-004580

Bradley, J. L., Blake, J. C., Chamberlain, S., Thomas, P. K., Cooper, J. M., & Schapira, A. H. (2000). Clinical, biochemical and molecular genetic correlations in Friedreich's ataxia. *Human Molecular Genetics*, *9*(2), 275–282. https://doi.org/10.1093/hmg/9.2.275

Branford, S., Rudzki, Z., Walsh, S., Parkinson, I., Grigg, A., Szer, J., Taylor, K., Herrmann, R., Seymour, J. F., Arthur, C., Joske, D., Lynch, K., & Hughes, T. (2003). Detection of BCR-ABL mutations in patients with CML treated with imatinib is virtually always accompanied by clinical resistance, and mutations in the ATP phosphate-binding loop (P-loop) are associated with a poor prognosis. *Blood*, *102*(1), 276–283. https://doi.org/10.1182/blood-2002-09-2896

Buchou, T., Vernet, M., Blond, O., Jensen, H. H., Pointu, H., Olsen, B. B., Cochet, C., Issinger, O.-G., & Boldyreff, B. (2003). Disruption of the Regulatory β Subunit of Protein Kinase CK2 in Mice Leads to a Cell-Autonomous Defect and Early Embryonic Lethality. *Molecular and Cellular Biology*, *23*(3), 908–915. https://doi.org/10.1128/MCB.23.3.908-915.2003

Burnett, G., & Kennedy, E. P. (1954). THE ENZYMATIC PHOSPHORYLATION OF PROTEINS. *Journal of Biological Chemistry*, *211*(2), 969–980. https://doi.org/10.1016/S0021-9258(18)71184-8

Campuzano, V., Montermini, L., Lutz, Y., Cova, L., Hindelang, C., Jiralerspong, S., Trottier, Y., Kish, S. J., Faucheux, B., Trouillas, P., Authier, F. J., Dürr, A., Mandel, J. L., Vescovi, A., Pandolfo, M., & Koenig, M. (1997). Frataxin is reduced in Friedreich ataxia patients and is associated with mitochondrial membranes. *Human Molecular Genetics*, *6*(11), 1771–1780. https://doi.org/10.1093/hmg/6.11.1771

Campuzano, V., Montermini, L., Moltò, M. D., Pianese, L., Cossée, M., Cavalcanti, F., Monros, E., Rodius, F., Duclos, F., Monticelli, A., Zara, F., Cañizares, J., Koutnikova, H., Bidichandani, S. I., Gellera, C., Brice, A., Trouillas, P., De Michele, G., Filla, A., … Pandolfo, M. (1996). Friedreich's Ataxia: Autosomal Recessive Disease Caused by an Intronic GAA Triplet Repeat Expansion. *Science*, *271*(5254), 1423–1427. https://doi.org/10.1126/science.271.5254.1423

Canton, D. A., Zhang, C., & Litchfield, D. W. (2001). Assembly of protein kinase CK2: Investigation of complex formation between catalytic and regulatory subunits using a zinc-finger-deficient mutant of CK2beta. *Biochemical Journal*, *358*(Pt 1), 87–94.

Castello, J., LeFrancois, B., Flajolet, M., Greengard, P., Friedman, E., & Rebholz, H. (2018). CK2 regulates 5-HT4 receptor signaling and modulates depressive-like behavior. *Molecular Psychiatry*, *23*(4), 872–882. https://doi.org/10.1038/mp.2017.240

Castillo, M. A., Ghose, S., Tamminga, C. A., & Ulery-Reynolds, P. G. (2010). Deficits in syntaxin 1 phosphorylation in schizophrenia prefrontal cortex. *Biological Psychiatry*, *67*(3), 208–216. https://doi.org/10.1016/j.biopsych.2009.07.029

Castro, I. H., Pignataro, M. F., Sewell, K. E., Espeche, L. D., Herrera, M. G., Noguera, M. E., Dain, L., Nadra, A. D., Aran, M., Smal, C., Gallo, M., & Santos, J. (2019). Frataxin Structure and Function. In J. R. Harris & J. Marles-Wright (Eds.), *Macromolecular Protein Complexes II: Structure and Function* (pp. 393–438). Springer International Publishing. https://doi.org/10.1007/978-3-030-28151-9_13

Cesaro, L., Zuliani, A. M., Bosello Travain, V., & Salvi, M. (2023). Exploring Protein Kinase CK2 Substrate Recognition and the Dynamic Response of Substrate Phosphorylation to Kinase Modulation. *Kinases and Phosphatases*, *1*(4), Article 4. https://doi.org/10.3390/kinasesphosphatases1040015

Chai, S. K., Nichols, G. L., & Rothman, P. (1997). Constitutive activation of JAKs and STATs in BCR-Abl-expressing cell lines and peripheral blood cells derived from leukemic patients. *Journal of Immunology (Baltimore, Md.: 1950)*, *159*(10), 4720–4728.

Chantalat, L., Leroy, D., Filhol, O., Nueda, A., Benitez, M. J., Chambaz, E. M., Cochet, C., & Dideberg, O. (1999). Crystal structure of the human protein kinase CK2 regulatory subunit reveals its zinc finger-mediated dimerization. *The EMBO Journal*, *18*(11), 2930–2940. https://doi.org/10.1093/emboj/18.11.2930

Chatterjee, B., & Thakur, S. S. (2022). SARS-CoV-2 Infection Triggers Phosphorylation: Potential Target for Anti-COVID-19 Therapeutics. *Frontiers in Immunology*, *13*. https://www.frontiersin.org/articles/10.3389/fimmu.2022.829474

Chen, H., Gill, A., Dove, B. K., Emmett, S. R., Kemp, C. F., Ritchie, M. A., Dee, M., & Hiscox, J. A. (2005). Mass spectroscopic characterization of the coronavirus infectious bronchitis virus nucleoprotein and elucidation of the role of phosphorylation in RNA binding by using surface plasmon resonance. *Journal of Virology*, *79*(2), 1164–1179. https://doi.org/10.1128/JVI.79.2.1164-1179.2005

Chen, M., Li, D., Krebs, E. G., & Cooper, J. A. (1997). The casein kinase II beta subunit binds to Mos and inhibits Mos activity. *Molecular and Cellular Biology*, *17*(4), 1904–1912. https://doi.org/10.1128/MCB.17.4.1904

Cherubini, F., Serio, D., Guccini, I., Fortuni, S., Arcuri, G., Condò, I., Rufini, A., Moiz, S., Camerini, S., Crescenzi, M., Testi, R., & Malisan, F. (2015). Src inhibitors modulate frataxin protein levels. *Human Molecular Genetics*, *24*(15), 4296–4305. https://doi.org/10.1093/hmg/ddv162

Chong, R., Swiss, R., Briones, G., Stone, K. L., Gulcicek, E. E., & Agaisse, H. (2009). Regulatory mimicry in Listeria monocytogenes actin-based motility. *Cell Host & Microbe*, *6*(3), 268–278. https://doi.org/10.1016/j.chom.2009.08.006

Chu, S., Li, L., Singh, H., & Bhatia, R. (2007). BCR-tyrosine 177 plays an essential role in Ras and Akt activation and in human hematopoietic progenitor transformation in chronic myelogenous leukemia. *Cancer Research*, *67*(14), 7045–7053. https://doi.org/10.1158/0008-5472.CAN-06-4312

Chua, M. M. J., Ortega, C. E., Sheikh, A., Lee, M., Abdul-Rassoul, H., Hartshorn, K. L., & Dominguez, I. (2017). CK2 in Cancer: Cellular and Biochemical Mechanisms and Potential Therapeutic Target. *Pharmaceuticals*, *10*(1), 18. https://doi.org/10.3390/ph10010018

Clarke, C. J., & Holyoake, T. L. (2017). Preclinical approaches in chronic myeloid leukemia: From cells to systems. *Experimental Hematology*, *47*, 13–23. https://doi.org/10.1016/j.exphem.2016.11.005

Cole, P. A., Shen, K., Qiao, Y., & Wang, D. (2003). Protein tyrosine kinases Src and Csk: A tail's tale. *Current Opinion in Chemical Biology*, *7*(5), 580–585. https://doi.org/10.1016/j.cbpa.2003.08.009

Condò, I., Ventura, N., Malisan, F., Rufini, A., Tomassini, B., & Testi, R. (2007). In vivo maturation of human frataxin. *Human Molecular Genetics*, *16*(13), 1534–1540. https://doi.org/10.1093/hmg/ddm102

Copland, M., Hamilton, A., Elrick, L. J., Baird, J. W., Allan, E. K., Jordanides, N., Barow, M., Mountford, J. C., & Holyoake, T. L. (2006). Dasatinib (BMS-354825) targets an earlier progenitor population than imatinib in primary CML but does not eliminate the quiescent fraction. *Blood*, *107*(11), 4532–4539. https://doi.org/10.1182/blood-2005-07-2947

Corben, L. A., Tai, G., Wilson, C., Collins, V., Churchyard, A. J., & Delatycki, M. B. (2010). A comparison of three measures of upper limb function in Friedreich ataxia. *Journal of Neurology*, *257*(4), 518–523. https://doi.org/10.1007/s00415-009-5352-7

Cortes, J. E., Kim, D.-W., Pinilla-Ibarz, J., le Coutre, P. D., Paquette, R., Chuah, C., Nicolini, F. E., Apperley, J. F., Khoury, H. J., Talpaz, M., DeAngelo, D. J., Abruzzese, E., Rea, D., Baccarani, M., Müller, M. C., Gambacorti-Passerini, C., Lustgarten, S., Rivera, V. M., Haluska, F. G., … Kantarjian, H. M. (2018). Ponatinib efficacy and safety in Philadelphia chromosome-positive leukemia: Final 5-year results of the phase 2 PACE trial. *Blood*, *132*(4), 393–404. https://doi.org/10.1182/blood-2016-09-739086

Costabile, T., Capretti, V., Abate, F., Liguori, A., Paciello, F., Pane, C., De Rosa, A., Peluso, S., De Michele, G., Filla, A., & Saccà, F. (2018). Emotion Recognition and Psychological Comorbidity in Friedreich's Ataxia. *Cerebellum (London, England)*, *17*(3), 336–345. https://doi.org/10.1007/s12311-018-0918-5

Cozza, G., Girardi, C., Ranchio, A., Lolli, G., Sarno, S., Orzeszko, A., Kazimierczuk, Z., Battistutta, R., Ruzzene, M., & Pinna, L. A. (2014). Cell-permeable dual inhibitors of protein kinases CK2 and PIM-1: Structural features and pharmacological potential. *Cellular and Molecular Life Sciences*, *71*(16), 3173–3185. https://doi.org/10.1007/s00018-013-1552-5

Cozza, G., Pinna, L. A., & Moro, S. (2013). Kinase CK2 inhibition: An update. *Current Medicinal Chemistry*, *20*(5), 671–693. https://doi.org/10.2174/092986713804999312

Cozza, G., Zanin, S., Sarno, S., Costa, E., Girardi, C., Ribaudo, G., Salvi, M., Zagotto, G., Ruzzene, M., & Pinna, L. A. (2015). Design, validation and efficacy of bisubstrate inhibitors specifically affecting ecto-CK2 kinase activity. *The Biochemical Journal*, *471*(3), 415–430. https://doi.org/10.1042/BJ20141127

CSNK2A1 Foundation – understanding Okur-Chung neurodevelopmental syndrome. (n.d.). Retrieved December 28, 2023, from https://www.csnk2a1foundation.org/

Cubuk, J., Alston, J. J., Incicco, J. J., Singh, S., Stuchell-Brereton, M. D., Ward, M. D., Zimmerman, M. I., Vithani, N., Griffith, D., Wagoner, J. A., Bowman, G. R., Hall, K. B., Soranno, A., & Holehouse, A. S. (2021). The SARS-CoV-2 nucleocapsid protein is dynamic, disordered, and phase separates with RNA. *Nature Communications*, *12*(1), Article 1. https://doi.org/10.1038/s41467-021-21953-3

Dal Pero, F., Di Maira, G., Marin, O., Bortoletto, G., Pinna, L. A., Alberti, A., Ruzzene, M., & Gerotto, M. (2007). Heterogeneity of CK2 phosphorylation sites in the NS5A protein of different hepatitis C virus genotypes. *Journal of Hepatology*, *47*(6), 768–776. https://doi.org/10.1016/j.jhep.2007.07.020

Daley, G. Q., Van Etten, R. A., & Baltimore, D. (1990). Induction of chronic myelogenous leukemia in mice by the P210bcr/abl gene of the Philadelphia chromosome. *Science (New York, N.Y.)*, *247*(4944), 824–830. https://doi.org/10.1126/science.2406902

Damuni, Z., & Reed, L. J. (1988). Purification and properties of a protamine kinase and a type II casein kinase from bovine kidney mitochondria. *Archives of Biochemistry and Biophysics*, *262*(2), 574–584. https://doi.org/10.1016/0003-9861(88)90408-0

Davidson, A. D., Williamson, M. K., Lewis, S., Shoemark, D., Carroll, M. W., Heesom, K. J., Zambon, M., Ellis, J., Lewis, P. A., Hiscox, J. A., & Matthews, D. A. (2020). Characterisation of the transcriptome and proteome of SARS-CoV-2 reveals a cell passage induced in-frame deletion of the furin-like cleavage site from the spike glycoprotein. *Genome Medicine*, *12*(1), 68. https://doi.org/10.1186/s13073-020-00763-0

Davis, K. A., Morelli, M., & Patton, J. T. (2017). Rotavirus NSP1 Requires Casein Kinase II-Mediated Phosphorylation for Hijacking of Cullin-RING Ligases. *mBio*, *8*(4), e01213-17. https://doi.org/10.1128/mBio.01213-17

de Gooijer, M. C., Guillén Navarro, M., Bernards, R., Wurdinger, T., & van Tellingen, O. (2018). An Experimenter's Guide to Glioblastoma Invasion Pathways. *Trends in Molecular Medicine*, *24*(9), 763–780. https://doi.org/10.1016/j.molmed.2018.07.003

de Jong, R., ten Hoeve, J., Heisterkamp, N., & Groffen, J. (1997). Tyrosine 207 in CRKL is the BCR/ABL phosphorylation site. *Oncogene*, *14*(5), 507–513. https://doi.org/10.1038/sj.onc.1200885

de Oliveira, P. S. L., Ferraz, F. A. N., Pena, D. A., Pramio, D. T., Morais, F. A., & Schechtman, D. (2016). Revisiting protein kinase–substrate interactions: Toward therapeutic development. *Science Signaling*, *9*(420), re3–re3. https://doi.org/10.1126/scisignal.aad4016

Deguchi, Y., Kimura, S., Ashihara, E., Niwa, T., Hodohara, K., Fujiyama, Y., & Maekawa, T. (2008). Comparison of imatinib, dasatinib, nilotinib and INNO-406 in imatinib-resistant cell lines. *Leukemia Research*, *32*(6), 980–983. https://doi.org/10.1016/j.leukres.2007.11.008

Delatycki, M. B., Camakaris, J., Brooks, H., Evans-Whipp, T., Thorburn, D. R., Williamson, R., & Forrest, S. M. (1999). Direct evidence that mitochondrial iron accumulation occurs in Friedreich ataxia. *Annals of Neurology*, *45*(5), 673–675.

Delorme, V., Cayla, X., Faure, G., Garcia, A., & Tardieux, I. (2003). Actin dynamics is controlled by a casein kinase II and phosphatase 2C interplay on Toxoplasma gondii Toxofilin. *Molecular Biology of the Cell*, *14*(5), 1900–1912. https://doi.org/10.1091/mbc.e02-08-0462

Deshiere, A., Duchemin-Pelletier, E., Spreux, E., Ciais, D., Combes, F., Vandenbrouck, Y., Couté, Y., Mikaelian, I., Giusiano, S., Charpin, C., Cochet, C., & Filhol, O. (2013). Unbalanced expression of CK2 kinase subunits is sufficient to drive epithelial-to-mesenchymal transition by Snail1 induction. *Oncogene*, *32*(11), Article 11. https://doi.org/10.1038/onc.2012.165

Di Lorenzo, G., Iavarone, F., Maddaluno, M., Plata-Gómez, A. B., Aureli, S., Quezada Meza, C. P., Cinque, L., Palma, A., Reggio, A., Cirillo, C., Sacco, F., Stolz, A., Napolitano, G., Marin,

O., Pinna, L. A., Ruzzene, M., Limongelli, V., Efeyan, A., Grumati, P., & Settembre, C. (2022). Phosphorylation of FAM134C by CK2 controls starvation-induced ER-phagy. *Science Advances*, *8*(35), eabo1215. https://doi.org/10.1126/sciadv.abo1215

Di Maira, G., Brustolon, F., Bertacchini, J., Tosoni, K., Marmiroli, S., Pinna, L. A., & Ruzzene, M. (2007). Pharmacological inhibition of protein kinase CK2 reverts the multidrug resistance phenotype of a CEM cell line characterized by high CK2 level. *Oncogene*, *26*(48), 6915–6926. https://doi.org/10.1038/sj.onc.1210495

Di Maira, G., Brustolon, F., Pinna, L. A., & Ruzzene, M. (2009). Dephosphorylation and inactivation of Akt/PKB is counteracted by protein kinase CK2 in HEK 293T cells. *Cellular and Molecular Life Sciences: CMLS*, *66*(20), 3363–3373. https://doi.org/10.1007/s00018-009-0108-1

Di Maira, G., Gentilini, A., Pastore, M., Caligiuri, A., Piombanti, B., Raggi, C., Rovida, E., Lewinska, M., Andersen, J. B., Borgo, C., Salvi, M., Ottaviani, D., Ruzzene, M., & Marra, F. (2019). The protein kinase CK2 contributes to the malignant phenotype of cholangiocarcinoma cells. *Oncogenesis*, *8*(11), 61. https://doi.org/10.1038/s41389-019-0171-x

Di Maira, G., Salvi, M., Arrigoni, G., Marin, O., Sarno, S., Brustolon, F., Pinna, L. A., & Ruzzene, M. (2005). Protein kinase CK2 phosphorylates and upregulates Akt/PKB. *Cell Death and Differentiation*, *12*(6), 668–677. https://doi.org/10.1038/sj.cdd.4401604

Di Stazio, M., Zanus, C., Faletra, F., Pesaresi, A., Ziccardi, I., Morgan, A., Girotto, G., Costa, P., Carrozzi, M., d'Adamo, A. P., & Musante, L. (2023). Haploinsufficiency as a Foreground Pathomechanism of Poirer-Bienvenu Syndrome and Novel Insights Underlying the Phenotypic Continuum of CSNK2B-Associated Disorders. *Genes*, *14*(2), 250. https://doi.org/10.3390/genes14020250

Doliba, N. M., Liu, Q., Li, C., Chen, P., Liu, C., Naji, A., & Matschinsky, F. M. (2017). Inhibition of cholinergic potentiation of insulin secretion from pancreatic islets by chronic elevation of glucose and fatty acids: Protection by casein kinase 2 inhibitor. *Molecular Metabolism*, *6*(10), 1240–1253. https://doi.org/10.1016/j.molmet.2017.07.017

Dominguez, I., Degano, I. R., Chea, K., Cha, J., Toselli, P., & Seldin, D. C. (2011). CK2α is essential for embryonic morphogenesis. *Molecular and Cellular Biochemistry*, *356*(1), 209–216. https://doi.org/10.1007/s11010-011-0961-8

Donato, N. J., Wu, J. Y., Stapley, J., Gallick, G., Lin, H., Arlinghaus, R., & Talpaz, M. (2003). BCR-ABL independence and LYN kinase overexpression in chronic myelogenous leukemia cells selected for resistance to STI571. *Blood*, *101*(2), 690–698. https://doi.org/10.1182/blood.V101.2.690

Donella-Deana, A., Cesaro, L., Ruzzene, M., Brunati, A. M., Marin, O., & Pinna, L. A. (1998). Spontaneous autophosphorylation of Lyn tyrosine kinase at both its activation segment and C-terminal tail confers altered substrate specificity. *Biochemistry*, *37*(5), 1438–1446. https://doi.org/10.1021/bi971332s

DONELLA-DEANA, A., CESARO, L., SARNO, S., RUZZENE, M., BRUNATI, A. M., MARIN, O., VILK, G., DOHERTY-KIRBY, A., LAJOIE, G., LITCHFIELD, D. W., & PINNA, L. A. (2003). Tyrosine phosphorylation of protein kinase CK2 by Src-related tyrosine kinases correlates with increased catalytic activity. *Biochemical Journal*, *372*(3), 841–849. https://doi.org/10.1042/bj20021905

Drosten, C., Günther, S., Preiser, W., van der Werf, S., Brodt, H.-R., Becker, S., Rabenau, H., Panning, M., Kolesnikova, L., Fouchier, R. A. M., Berger, A., Burguière, A.-M., Cinatl, J., Eickmann, M., Escriou, N., Grywna, K., Kramme, S., Manuguerra, J.-C., Müller, S., … Doerr, H. W. (2003). Identification of a novel coronavirus in patients with severe acute respiratory syndrome. *The New England Journal of Medicine*, *348*(20), 1967–1976. https://doi.org/10.1056/NEJMoa030747

Druker, B. J., Talpaz, M., Resta, D. J., Peng, B., Buchdunger, E., Ford, J. M., Lydon, N. B., Kantarjian, H., Capdeville, R., Ohno-Jones, S., & Sawyers, C. L. (2001). Efficacy and safety of a specific inhibitor of the BCR-ABL tyrosine kinase in chronic myeloid leukemia. *The New*

England Journal of Medicine, *344*(14), 1031–1037. https://doi.org/10.1056/NEJM200104053441401

Drygin, D., Ho, C. B., Omori, M., Bliesath, J., Proffitt, C., Rice, R., Siddiqui-Jain, A., O'Brien, S., Padgett, C., Lim, J. K. C., Anderes, K., Rice, W. G., & Ryckman, D. (2011). Protein kinase CK2 modulates IL-6 expression in inflammatory breast cancer. *Biochemical and Biophysical Research Communications*, *415*(1), 163–167. https://doi.org/10.1016/j.bbrc.2011.10.046

Duong-Ly, K. C., & Peterson, J. R. (2013). The Human Kinome and Kinase Inhibition. *Current Protocols in Pharmacology*, *60*(1), 2.9.1-2.9.14. https://doi.org/10.1002/0471141755.ph0209s60

Eddy, S. F., Guo, S., Demicco, E. G., Romieu-Mourez, R., Landesman-Bollag, E., Seldin, D. C., & Sonenshein, G. E. (2005). Inducible IkappaB kinase/IkappaB kinase epsilon expression is induced by CK2 and promotes aberrant nuclear factor-kappaB activation in breast cancer cells. *Cancer Research*, *65*(24), 11375–11383. https://doi.org/10.1158/0008-5472.CAN-05-1602

Efficace, F., Baccarani, M., Breccia, M., Alimena, G., Rosti, G., Cottone, F., Deliliers, G. L., Baratè, C., Rossi, A. R., Fioritoni, G., Luciano, L., Turri, D., Martino, B., Di Raimondo, F., Dabusti, M., Bergamaschi, M., Leoni, P., Simula, M. P., Levato, L., … GIMEMA. (2011). Health-related quality of life in chronic myeloid leukemia patients receiving long-term therapy with imatinib compared with the general population. *Blood*, *118*(17), 4554–4560. https://doi.org/10.1182/blood-2011-04-347575

Eide, C. A., & O'Hare, T. (2015). Chronic Myeloid Leukemia: Advances in Understanding Disease Biology and Mechanisms of Resistance to Tyrosine Kinase Inhibitors. *Current Hematologic Malignancy Reports*, *10*(2), 158–166. https://doi.org/10.1007/s11899-015-0248-3

Eigentler, A., Nachbauer, W., Donnemiller, E., Poewe, W., Gasser, R. W., & Boesch, S. (2014). Low bone mineral density in Friedreich ataxia. *Cerebellum (London, England)*, *13*(5), 549–557. https://doi.org/10.1007/s12311-014-0568-1

Ellis, J. J., & Kobe, B. (2013). Protein Phosphorylation. In G. C. K. Roberts (Ed.), *Encyclopedia of Biophysics* (pp. 2037–2040). Springer. https://doi.org/10.1007/978-3-642-16712-6_184

Endicott, J. A., Noble, M. E. M., & Johnson, L. N. (2012). The structural basis for control of eukaryotic protein kinases. *Annual Review of Biochemistry*, *81*, 587–613. https://doi.org/10.1146/annurev-biochem-052410-090317

Ernst, M. E., Baugh, E. H., Thomas, A., Bier, L., Lippa, N., Stong, N., Mulhern, M. S., Kushary, S., Akman, C. I., Heinzen, E. L., Yeh, R., Bi, W., Hanchard, N. A., Burrage, L. C., Leduc, M. S., Chong, J. S. C., Bend, R., Lyons, M. J., Lee, J. A., … Aggarwal, V. (2021). CSNK2B: A broad spectrum of neurodevelopmental disability and epilepsy severity. *Epilepsia*, *62*(7), e103–e109. https://doi.org/10.1111/epi.16931

Fabbian, S., Giachin, G., Bellanda, M., Borgo, C., Ruzzene, M., Spuri, G., Campofelice, A., Veneziano, L., Bonchio, M., Carraro, M., & Battistutta, R. (2022). Mechanism of CK2 Inhibition by a Ruthenium-Based Polyoxometalate. *Frontiers in Molecular Biosciences*, *9*. https://www.frontiersin.org/articles/10.3389/fmolb.2022.906390

Fan, M. M. Y., Zhang, H., Hayden, M. R., Pelech, S. L., & Raymond, L. A. (2008). Protective up-regulation of CK2 by mutant huntingtin in cells co-expressing NMDA receptors. *Journal of Neurochemistry*, *104*(3), 790–805. https://doi.org/10.1111/j.1471-4159.2007.05016.x

Fang, S., Xu, L., Huang, M., Qisheng Li, F., & Liu, D. X. (2013). Identification of two ATR-dependent phosphorylation sites on coronavirus nucleocapsid protein with nonessential functions in viral replication and infectivity in cultured cells. *Virology*, *444*(1–2), 225–232. https://doi.org/10.1016/j.virol.2013.06.014

Faraj, S. E., Roman, E. A., Aran, M., Gallo, M., & Santos, J. (2014). The alteration of the C-terminal region of human frataxin distorts its structural dynamics and function. *The FEBS Journal*, *281*(15), 3397–3419. https://doi.org/10.1111/febs.12869

Fatoki, T. H., Ibraheem, O., Ogunyemi, I. O., Akinmoladun, A. C., Ugboko, H. U., Adeseko, C. J., Awofisayo, O. A., Olusegun, S. J., & Enibukun, J. M. (2021). Network analysis, sequence and structure dynamics of key proteins of coronavirus and human host, and molecular docking of

selected phytochemicals of nine medicinal plants. *Journal of Biomolecular Structure and Dynamics*, *39*(16), 6195–6217. https://doi.org/10.1080/07391102.2020.1794971

Faust, M., Schuster, N., & Montenarh, M. (1999). Specific binding of protein kinase CK2 catalytic subunits to tubulin. *FEBS Letters*, *462*(1), 51–56. https://doi.org/10.1016/S0014-5793(99)01492-1

Filhol, O., & Cochet, C. (2009). Protein Kinase CK2 in Health and Disease. *Cellular and Molecular Life Sciences*, *66*(11), 1830–1839. https://doi.org/10.1007/s00018-009-9151-1

Filhol, O., Giacosa, S., Wallez, Y., & Cochet, C. (2015). Protein kinase CK2 in breast cancer: The CK2β regulatory subunit takes center stage in epithelial plasticity. *Cellular and Molecular Life Sciences: CMLS*, *72*(17), 3305–3322. https://doi.org/10.1007/s00018-015-1929-8

Filla, A., De Michele, G., Cavalcanti, F., Pianese, L., Monticelli, A., Campanella, G., & Cocozza, S. (1996). The relationship between trinucleotide (GAA) repeat length and clinical features in Friedreich ataxia. *American Journal of Human Genetics*, *59*(3), 554–560.

Firnau, M.-B., & Brieger, A. (2022). CK2 and the Hallmarks of Cancer. *Biomedicines*, *10*(8), Article 8. https://doi.org/10.3390/biomedicines10081987

Firzlaff, J. M., Galloway, D. A., Eisenman, R. N., & Lüscher, B. (1989). The E7 protein of human papillomavirus type 16 is phosphorylated by casein kinase II. *The New Biologist*, *1*(1), 44–53.

Fischer, E. H., & Krebs, E. G. (1955). CONVERSION OF PHOSPHORYLASE b TO PHOSPHORYLASE a IN MUSCLE EXTRACTS. *Journal of Biological Chemistry*, *216*(1), 121–132. https://doi.org/10.1016/S0021-9258(19)52289-X

Foka, P., Dimitriadis, A., Kyratzopoulou, E., Giannimaras, D. A., Sarno, S., Simos, G., Georgopoulou, U., & Mamalaki, A. (2014). A complex signaling network involving protein kinase CK2 is required for hepatitis C virus core protein-mediated modulation of the iron-regulatory hepcidin gene expression. *Cellular and Molecular Life Sciences: CMLS*, *71*(21), 4243–4258. https://doi.org/10.1007/s00018-014-1621-4

French, A. C., Luscher, B., & Litchfield, D. W. (2007). Development of a Stabilized Form of the Regulatory CK2β Subunit That Inhibits Cell Proliferation *. *Journal of Biological Chemistry*, *282*(40), 29667–29677. https://doi.org/10.1074/jbc.M706457200

Gadzicki, D., von Neuhoff, N., Steinemann, D., Just, M., Büsche, G., Kreipe, H., Wilkens, L., & Schlegelberger, B. (2005). BCR-ABL gene amplification and overexpression in a patient with chronic myeloid leukemia treated with imatinib. *Cancer Genetics and Cytogenetics*, *159*(2), 164–167. https://doi.org/10.1016/j.cancergencyto.2004.09.021

Gao, Z., Lee, P., Stafford, J. M., von Schimmelmann, M., Schaefer, A., & Reinberg, D. (2014). An AUTS2-Polycomb complex activates gene expression in the CNS. *Nature*, *516*(7531), 349–354. https://doi.org/10.1038/nature13921

Gibson, S. A., & Benveniste, E. N. (2018). Protein Kinase CK2: An Emerging Regulator of Immunity. *Trends in Immunology*, *39*(2), 82–85. https://doi.org/10.1016/j.it.2017.12.002

Glover, C. V. (1986). A filamentous form of Drosophila casein kinase II. *Journal of Biological Chemistry*, *261*(30), 14349–14354. https://doi.org/10.1016/S0021-9258(18)67025-5

Gomes, A. M., Soares, M. V. D., Ribeiro, P., Caldas, J., Póvoa, V., Martins, L. R., Melão, A., Serra-Caetano, A., de Sousa, A. B., Lacerda, J. F., & Barata, J. T. (2014). Adult B-cell acute lymphoblastic leukemia cells display decreased PTEN activity and constitutive hyperactivation of PI3K/Akt pathway despite high PTEN protein levels. *Haematologica*, *99*(6), 1062–1068. https://doi.org/10.3324/haematol.2013.096438

Gordon, D. E., Hiatt, J., Bouhaddou, M., Rezelj, V. V., Ulferts, S., Braberg, H., Jureka, A. S., Obernier, K., Guo, J. Z., Batra, J., Kaake, R. M., Weckstein, A. R., Owens, T. W., Gupta, M., Pourmal, S., Titus, E. W., Cakir, M., Soucheray, M., McGregor, M., … Krogan, N. J. (2020b). Comparative host-coronavirus protein interaction networks reveal pan-viral disease mechanisms. *Science*, *370*(6521), eabe9403. https://doi.org/10.1126/science.abe9403

Gordon, D. E., Jang, G. M., Bouhaddou, M., Xu, J., Obernier, K., White, K. M., O'Meara, M. J., Rezelj, V. V., Guo, J. Z., Swaney, D. L., Tummino, T. A., Hüttenhain, R., Kaake, R. M., Richards, A. L., Tutuncuoglu, B., Foussard, H., Batra, J., Haas, K., Modak, M., … Krogan, N.

J. (2020a). A SARS-CoV-2 protein interaction map reveals targets for drug repurposing. *Nature*, *583*(7816), 459–468. https://doi.org/10.1038/s41586-020-2286-9

Gorre, M. E., Mohammed, M., Ellwood, K., Hsu, N., Paquette, R., Rao, P. N., & Sawyers, C. L. (2001). Clinical Resistance to STI-571 Cancer Therapy Caused by BCR-ABL Gene Mutation or Amplification. *Science*, *293*(5531), 876–880. https://doi.org/10.1126/science.1062538

Gowda, C., Song, C., Kapadia, M., Payne, J. L., Hu, T., Ding, Y., & Dovat, S. (2017). Regulation of cellular proliferation in acute lymphoblastic leukemia by Casein Kinase II (CK2) and Ikaros. *Advances in Biological Regulation*, *63*, 71–80. https://doi.org/10.1016/j.jbior.2016.09.003

Graham, K. C., & Litchfield, D. W. (2000). The regulatory beta subunit of protein kinase CK2 mediates formation of tetrameric CK2 complexes. *The Journal of Biological Chemistry*, *275*(7), 5003–5010. https://doi.org/10.1074/jbc.275.7.5003

Gray, G. K., McFarland, B. C., Rowse, A. L., Gibson, S. A., & Benveniste, E. N. (2014). Therapeutic CK2 inhibition attenuates diverse prosurvival signaling cascades and decreases cell viability in human breast cancer cells. *Oncotarget*, *5*(15), 6484–6496. https://doi.org/10.18632/oncotarget.2248

Guo, L., Wang, Q., Weng, L., Hauser, L. A., Strawser, C. J., Mesaros, C., Lynch, D. R., & Blair, I. A. (2018). Characterization of a new N-terminally acetylated extra-mitochondrial isoform of frataxin in human erythrocytes. *Scientific Reports*, *8*(1), 17043. https://doi.org/10.1038/s41598-018-35346-y

Haddad, F. G., Issa, G. C., Jabbour, E., & Yilmaz, M. (2022). Ponatinib for the treatment of adult patients with resistant or intolerant Chronic-Phase Chronic Myeloid Leukemia. *Expert Opinion on Pharmacotherapy*, *23*(7), 751–758. https://doi.org/10.1080/14656566.2022.2064742

Hanahan, D. (2022). Hallmarks of Cancer: New Dimensions. *Cancer Discovery*, *12*(1), 31–46. https://doi.org/10.1158/2159-8290.CD-21-1059

Hantschel, O., & Superti-Furga, G. (2004). Regulation of the c-Abl and Bcr–Abl tyrosine kinases. *Nature Reviews Molecular Cell Biology*, *5*(1), Article 1. https://doi.org/10.1038/nrm1280

Harding, I. H., Lynch, D. R., Koeppen, A. H., & Pandolfo, M. (2020). Central Nervous System Therapeutic Targets in Friedreich Ataxia. *Human Gene Therapy*, *31*(23–24), 1226–1236. https://doi.org/10.1089/hum.2020.264

Hathaway, G. M., & Traugh, J. A. (1979). Cyclic nucleotide-independent protein kinases from rabbit reticulocytes. Purification of casein kinases. *The Journal of Biological Chemistry*, *254*(3), 762–768.

Hathaway, G. M., & Traugh, J. A. (1982). Casein Kinases—Multipotential Protein Kinases. In B. L. Horecker & E. R. Stadtman (Eds.), *Current Topics in Cellular Regulation* (Vol. 21, pp. 101–127). Academic Press. https://doi.org/10.1016/B978-0-12-152821-8.50009-8

Hayat, R., Manzoor, M., & Hussain, A. (2022). Wnt signaling pathway: A comprehensive review. *Cell Biology International*, *46*(6), 863–877. https://doi.org/10.1002/cbin.11797

He, B., Wang, Q., Liu, X., Lu, Z., Han, J., Pan, C., Carter, B. Z., Liu, Q., Xu, N., & Zhou, H. (2020). A novel HDAC inhibitor chidamide combined with imatinib synergistically targets tyrosine kinase inhibitor resistant chronic myeloid leukemia cells. *Biomedicine & Pharmacotherapy = Biomedecine & Pharmacotherapie*, *129*, 110390. https://doi.org/10.1016/j.biopha.2020.110390

He, H., Tan, M., Pamarthy, D., Wang, G., Ahmed, K., & Sun, Y. (2007). CK2 phosphorylation of SAG at Thr10 regulates SAG stability, but not its E3 ligase activity. *Molecular and Cellular Biochemistry*, *295*(1), 179–188. https://doi.org/10.1007/s11010-006-9287-3

He, Y., Zhou, Y., Wu, H., Kou, Z., Liu, S., & Jiang, S. (2004). Mapping of antigenic sites on the nucleocapsid protein of the severe acute respiratory syndrome coronavirus. *Journal of Clinical Microbiology*, *42*(11), 5309–5314. https://doi.org/10.1128/JCM.42.11.5309-5314.2004

Hériché, J. K., & Chambaz, E. M. (1998). Protein kinase CK2alpha is a target for the Abl and Bcr-Abl tyrosine kinases. *Oncogene*, *17*(1), 13–18. https://doi.org/10.1038/sj.onc.1201900

Hériché, J. K., Lebrin, F., Rabilloud, T., Leroy, D., Chambaz, E. M., & Goldberg, Y. (1997). Regulation of protein phosphatase 2A by direct interaction with casein kinase 2alpha. *Science (New York, N.Y.)*, *276*(5314), 952–955. https://doi.org/10.1126/science.276.5314.952

Holecek, M., Muthny, T., Kovarik, M., & Sispera, L. (2006). Proteasome inhibitor MG-132 enhances whole-body protein turnover in rat. *Biochemical and Biophysical Research Communications*, *345*(1), 38–42. https://doi.org/10.1016/j.bbrc.2006.04.053

Houshmand, M., Blanco, T. M., Circosta, P., Yazdi, N., Kazemi, A., Saglio, G., & Zarif, M. N. (2019). Bone marrow microenvironment: The guardian of leukemia stem cells. *World Journal of Stem Cells*, *11*(8), 476–490. https://doi.org/10.4252/wjsc.v11.i8.476

Hu, W.-T., Li, H.-C., Lee, S.-K., Ma, H.-C., Yang, C.-H., Chen, H.-L., & Lo, S.-Y. (2013). Both core and F proteins of hepatitis C virus could enhance cell proliferation in transgenic mice. *Biochemical and Biophysical Research Communications*, *435*(1), 147–152. https://doi.org/10.1016/j.bbrc.2013.04.059

Huang, J., Chen, Z., Li, J., Chen, Q., Li, J., Gong, W., Huang, J., Liu, P., & Huang, H. (2017). Protein kinase CK2α catalytic subunit ameliorates diabetic renal inflammatory fibrosis via NF-κB signaling pathway. *Biochemical Pharmacology*, *132*, 102–117. https://doi.org/10.1016/j.bcp.2017.02.016

Hui, E. K.-W., & Nayak, D. P. (2002). Role of G protein and protein kinase signalling in influenza virus budding in MDCK cells. *The Journal of General Virology*, *83*(Pt 12), 3055–3066. https://doi.org/10.1099/0022-1317-83-12-3055

Humphrey, S. J., James, D. E., & Mann, M. (2015). Protein Phosphorylation: A Major Switch Mechanism for Metabolic Regulation. *Trends in Endocrinology & Metabolism*, *26*(12), 676–687. https://doi.org/10.1016/j.tem.2015.09.013

Hunter, T. (2007). The age of crosstalk: Phosphorylation, ubiquitination, and beyond. *Molecular Cell*, *28*(5), 730–738. https://doi.org/10.1016/j.molcel.2007.11.019

Hyer, M. L., Milhollen, M. A., Ciavarri, J., Fleming, P., Traore, T., Sappal, D., Huck, J., Shi, J., Gavin, J., Brownell, J., Yang, Y., Stringer, B., Griffin, R., Bruzzese, F., Soucy, T., Duffy, J., Rabino, C., Riceberg, J., Hoar, K., … Bence, N. F. (2018). A small-molecule inhibitor of the ubiquitin activating enzyme for cancer treatment. *Nature Medicine*, *24*(2), 186–193. https://doi.org/10.1038/nm.4474

Indelicato, E., Nachbauer, W., Eigentler, A., Amprosi, M., Matteucci Gothe, R., Giunti, P., Mariotti, C., Arpa, J., Durr, A., Klopstock, T., Schöls, L., Giordano, I., Bürk, K., Pandolfo, M., Didszdun, C., Schulz, J. B., Boesch, S., & EFACTS (European Friedreich's Ataxia Consortium for Translational Studies). (2020). Onset features and time to diagnosis in Friedreich's Ataxia. *Orphanet Journal of Rare Diseases*, *15*(1), 198. https://doi.org/10.1186/s13023-020-01475-9

Jabbour, E., & Kantarjian, H. (2018). Chronic myeloid leukemia: 2018 update on diagnosis, therapy and monitoring. *American Journal of Hematology*, *93*(3), 442–459. https://doi.org/10.1002/ajh.25011

Jang, H.-J., Woo, Y.-M., Naka, K., Park, J.-H., Han, H.-J., Kim, H.-J., Kim, S.-H., Ahn, J.-S., Kim, T., Kimura, S., Zarabi, S., Lipton, J. H., Minden, M. D., Jung, C.-W., Kim, H.-J., Kim, J.-W., & Kim, D. D. H. (2021). Statins Enhance the Molecular Response in Chronic Myeloid Leukemia when Combined with Tyrosine Kinase Inhibitors. *Cancers*, *13*(21), 5543. https://doi.org/10.3390/cancers13215543

Ji, H., Wang, J., Nika, H., Hawke, D., Keezer, S., Ge, Q., Fang, B., Fang, X., Fang, D., Litchfield, D. W., Aldape, K., & Lu, Z. (2009). EGF-Induced ERK Activation Promotes CK2-Mediated Disassociation of α-Catenin from β-Catenin and Transactivation of β-Catenin. *Molecular Cell*, *36*(4), 547–559. https://doi.org/10.1016/j.molcel.2009.09.034

Jia, H., Liu, Y., Xia, R., Tong, C., Yue, T., Jiang, J., & Jia, J. (2010). Casein kinase 2 promotes Hedgehog signaling by regulating both smoothened and Cubitus interruptus. *The Journal of Biological Chemistry*, *285*(48), 37218–37226. https://doi.org/10.1074/jbc.M110.174565

Jia, Z.-M., Ai, X., Teng, J.-F., Wang, Y.-P., Wang, B.-J., & Zhang, X. (2016). P21 and CK2 interaction-mediated HDAC2 phosphorylation modulates KLF4 acetylation to regulate bladder cancer cell proliferation. *Tumour Biology: The Journal of the International Society for Oncodevelopmental Biology and Medicine*, *37*(6), 8293–8304. https://doi.org/10.1007/s13277-015-4618-1

Jiang, C., Ma, Z., Zhang, G., Yang, X., Du, Q., & Wang, W. (2019). CSNK2A1 Promotes Gastric Cancer Invasion Through the PI3K-Akt-mTOR Signaling Pathway. *Cancer Management and Research*, *11*, 10135–10143. https://doi.org/10.2147/CMAR.S222620

Jiralerspong, S., Liu, Y., Montermini, L., Stifani, S., & Pandolfo, M. (1997). Frataxin shows developmentally regulated tissue-specific expression in the mouse embryo. *Neurobiology of Disease*, *4*(2), 103–113. https://doi.org/10.1006/nbdi.1997.0139

Johnson, D. E., O'Keefe, R. A., & Grandis, J. R. (2018). Targeting the IL-6/JAK/STAT3 signalling axis in cancer. *Nature Reviews. Clinical Oncology*, *15*(4), 234–248. https://doi.org/10.1038/nrclinonc.2018.8

Johnson, L. N., & Lewis, R. J. (2001). Structural Basis for Control by Phosphorylation. *Chemical Reviews*, *101*(8), 2209–2242. https://doi.org/10.1021/cr000225s

Kajiwara, Y., Buxbaum, J. D., & Grice, D. E. (2009). SLITRK1 Binds 14-3-3 and Regulates Neurite Outgrowth in a Phosphorylation-Dependent Manner. *Biological Psychiatry*, *66*(10), 918–925. https://doi.org/10.1016/j.biopsych.2009.05.033

Kanev, G. K., Graaf, C. de, Esch, I. J. P. de, Leurs, R., Würdinger, T., Westerman, B. A., & Kooistra, A. J. (2019). The Landscape of Atypical and Eukaryotic Protein Kinases. *Trends in Pharmacological Sciences*, *40*(11), 818–832. https://doi.org/10.1016/j.tips.2019.09.002

Kantarjian, H. M., Jabbour, E., Deininger, M., Abruzzese, E., Apperley, J., Cortes, J., Chuah, C., DeAngelo, D. J., DiPersio, J., Hochhaus, A., Lipton, J., Nicolini, F. E., Pinilla-Ibarz, J., Rea, D., Rosti, G., Rousselot, P., Shah, N. P., Talpaz, M., Srivastava, S., … Mauro, M. (2022). Ponatinib after failure of second-generation tyrosine kinase inhibitor in resistant chronic-phase chronic myeloid leukemia. *American Journal of Hematology*, *97*(11), 1419–1426. https://doi.org/10.1002/ajh.26686

Kim, H.-R., Kim, K., Lee, K.-H., Kim, S. J., & Kim, J. (2008). Inhibition of casein kinase 2 enhances the death ligand- and natural kiler cell-induced hepatocellular carcinoma cell death. *Clinical and Experimental Immunology*, *152*(2), 336–344. https://doi.org/10.1111/j.1365-2249.2008.03622.x

Kim, Y. S., Lee, J. H., Park, J. W., & Bae, Y. S. (2001). Regulation of protein kinase CKII by direct interaction with the C-terminal region of p47(phox). *Biochemical and Biophysical Research Communications*, *286*(1), 87–93. https://doi.org/10.1006/bbrc.2001.5362

Klein, S., Meng, R., Montenarh, M., & Götz, C. (2017). The Phosphorylation of PDX-1 by Protein Kinase CK2 Is Crucial for Its Stability. *Pharmaceuticals*, *10*(1), Article 1. https://doi.org/10.3390/ph10010002

Koch, C. A., Agyei, R., Galicia, S., Metalnikov, P., O'Donnell, P., Starostine, A., Weinfeld, M., & Durocher, D. (2004). Xrcc4 physically links DNA end processing by polynucleotide kinase to DNA ligation by DNA ligase IV. *The EMBO Journal*, *23*(19), 3874–3885. https://doi.org/10.1038/sj.emboj.7600375

Koeppen, A. H. (2011). Friedreich's ataxia: Pathology, pathogenesis, and molecular genetics. *Journal of the Neurological Sciences*, *303*(1–2), 1–12. https://doi.org/10.1016/j.jns.2011.01.010

Koeppen, A. H., Ramirez, R. L., Becker, A. B., Bjork, S. T., Levi, S., Santambrogio, P., Parsons, P. J., Kruger, P. C., Yang, K. X., Feustel, P. J., & Mazurkiewicz, J. E. (2015). The pathogenesis of cardiomyopathy in Friedreich ataxia. *PloS One*, *10*(3), e0116396. https://doi.org/10.1371/journal.pone.0116396

Koffa, M. D., Kean, J., Zachos, G., Rice, S. A., & Clements, J. B. (2003). CK2 protein kinase is stimulated and redistributed by functional herpes simplex virus ICP27 protein. *Journal of Virology*, *77*(7), 4315–4325. https://doi.org/10.1128/jvi.77.7.4315-4325.2003

Kopecky-Bromberg, S. A., Martínez-Sobrido, L., Frieman, M., Baric, R. A., & Palese, P. (2007). Severe acute respiratory syndrome coronavirus open reading frame (ORF) 3b, ORF 6, and nucleocapsid proteins function as interferon antagonists. *Journal of Virology*, *81*(2), 548–557. https://doi.org/10.1128/JVI.01782-06

Kornev, A. P., Haste, N. M., Taylor, S. S., & Eyck, L. F. T. (2006). Surface comparison of active and inactive protein kinases identifies a conserved activation mechanism. *Proceedings of the*

National Academy of Sciences of the United States of America, *103*(47), 17783–17788. https://doi.org/10.1073/pnas.0607656103

Koutnikova, H., Campuzano, V., & Koenig, M. (1998). Maturation of wild-type and mutated frataxin by the mitochondrial processing peptidase. *Human Molecular Genetics*, *7*(9), 1485–1489. https://doi.org/10.1093/hmg/7.9.1485

Krek, W., Maridor, G., & Nigg, E. A. (1992). Casein kinase II is a predominantly nuclear enzyme. *The Journal of Cell Biology*, *116*(1), 43–55. https://doi.org/10.1083/jcb.116.1.43

Kuwahara, H., Nishizaki, M., & Kanazawa, H. (2008). Nuclear localization signal and phosphorylation of Serine350 specify intracellular localization of DRAK2. *Journal of Biochemistry*, *143*(3), 349–358. https://doi.org/10.1093/jb/mvm236

Kwon, J., Zhang, J., Mok, B., & Han, C. (2022). CK2-Mediated Phosphorylation Upregulates the Stability of USP13 and Promotes Ovarian Cancer Cell Proliferation. *Cancers*, *15*(1), 200. https://doi.org/10.3390/cancers15010200

Laboratorio Elea Phoenix S.A. (2015). *Randomised, Blind and Placebo-controlled Trial for the CIGB-300 Perilesional Application in Two Dose Levels in the Recurrent and Non Recurrent Genital Condyloma* (Clinical Trial Registration NCT01639638). clinicaltrials.gov. https://clinicaltrials.gov/study/NCT01639638

Laboratorio Elea Phoenix S.A. (2016). *Open Clinical Trial, Uncontrolled in Patients Bearing Squamous Cell Carcinoma or Adenocarcinoma of the Cervix Stage IIA and IIB FIGO Classification Treated With Radiotherapy External Endocavitary Brachytherapy + Concurrent Hemotherapy Weekly Systemic and Local Application of CIGB-300 Dose Escalation* (Clinical Trial Registration NCT01639625). clinicaltrials.gov. https://clinicaltrials.gov/study/NCT01639625

Lamarche, J. B., Côté, M., & Lemieux, B. (1980). The cardiomyopathy of Friedreich's ataxia morphological observations in 3 cases. *The Canadian Journal of Neurological Sciences. Le Journal Canadien Des Sciences Neurologiques*, *7*(4), 389–396. https://doi.org/10.1017/s0317167100022927

Lamers, M. M., & Haagmans, B. L. (2022). SARS-CoV-2 pathogenesis. *Nature Reviews Microbiology*, *20*(5), Article 5. https://doi.org/10.1038/s41579-022-00713-0

Landesman-Bollag, E., Channavajhala, P. L., Cardiff, R. D., & Seldin, D. C. (1998). P53 deficiency and misexpression of protein kinase CK2alpha collaborate in the development of thymic lymphomas in mice. *Oncogene*, *16*(23), 2965–2974. https://doi.org/10.1038/sj.onc.1201854

Laudet, B., Barette, C., Dulery, V., Renaudet, O., Dumy, P., Metz, A., Prudent, R., Deshiere, A., Dideberg, O., Filhol, O., & Cochet, C. (2007). Structure-based design of small peptide inhibitors of protein kinase CK2 subunit interaction. *The Biochemical Journal*, *408*(3), 363–373. https://doi.org/10.1042/BJ20070825

Lazaropoulos, M., Dong, Y., Clark, E., Greeley, N. R., Seyer, L. A., Brigatti, K. W., Christie, C., Perlman, S. L., Wilmot, G. R., Gomez, C. M., Mathews, K. D., Yoon, G., Zesiewicz, T., Hoyle, C., Subramony, S. H., Brocht, A. F., Farmer, J. M., Wilson, R. B., Deutsch, E. C., & Lynch, D. R. (2015). Frataxin levels in peripheral tissue in Friedreich ataxia. *Annals of Clinical and Translational Neurology*, *2*(8), 831–842. https://doi.org/10.1002/acn3.225

Lee, Y. S., Lee, D. Y., Yu, D. Y., Kim, S., & Lee, Y. C. (2014). Helicobacter pylori induces cell migration and invasion through casein kinase 2 in gastric epithelial cells. *Helicobacter*, *19*(6), 465–475. https://doi.org/10.1111/hel.12144

Lenzken, S. C., Stanga, S., Lanni, C., De Leonardis, F., Govoni, S., & Racchi, M. (2010). Recruitment of casein kinase 2 is involved in AbetaPP processing following cholinergic stimulation. *Journal of Alzheimer's Disease: JAD*, *20*(4), 1133–1141. https://doi.org/10.3233/JAD-2010-090232

Leroy, D., Filhol, O., Delcros, J. G., Pares, S., Chambaz, E. M., & Cochet, C. (1997a). Chemical Features of the Protein Kinase CK2 Polyamine Binding Site,. *Biochemistry*, *36*(6), 1242–1250. https://doi.org/10.1021/bi961949u

Leroy, D., Heriché, J.-K., Filhol, O., Chambaz, E. M., & Cochet, C. (1997b). Binding of Polyamines to an Autonomous Domain of the Regulatory Subunit of Protein Kinase CK2 Induces a

Conformational Change in the Holoenzyme: A PROPOSED ROLE FOR THE KINASE STIMULATION *. *Journal of Biological Chemistry*, *272*(33), 20820–20827. https://doi.org/10.1074/jbc.272.33.20820

Leroy, D., Schmid, N., Behr, J.-P., Filhol, O., Pares, S., Garin, J., Bourgarit, J.-J., Chambaz, E. M., & Cochet, C. (1995). Direct Identification of a Polyamine Binding Domain on the Regulatory Subunit of the Protein Kinase Casein Kinase 2 by Photoaffinity Labeling *. *Journal of Biological Chemistry*, *270*(29), 17400–17406. https://doi.org/10.1074/jbc.270.29.17400

Levene, P. A., & Alsberg, C. L. (1906). The Cleavage Products of Vitellin. *Journal of Biological Chemistry*, *2*(1), 127–133. https://doi.org/10.1016/S0021-9258(17)46054-6

Li, D., Zhou, B., Tian, X., Chen, X., Wang, Y., Hao, S., Zhang, C., & Hui, L. (2023). Genetic analysis and literature review of a Poirier-Bienvenu neurodevelopmental syndrome family line caused by a de novo frameshift variant in CSNK2B. *Molecular Genetics & Genomic Medicine*, e2327. https://doi.org/10.1002/mgg3.2327

Li, Q.-X. (2004). Comprehensive Assessment of Cell Growth Properties Using an Integrated and Nonsubjective Approach. *Preclinica*.

LITCHFIELD, D. W. (2003). Protein kinase CK2: Structure, regulation and role in cellular decisions of life and death. *Biochemical Journal*, *369*(1), 1–15. https://doi.org/10.1042/bj20021469

Llorens, F., Duarri, A., Sarró, E., Roher, N., Plana, M., & Itarte, E. (2006). The N-terminal domain of the human eIF2β subunit and the CK2 phosphorylation sites are required for its function. *Biochemical Journal*, *394*(Pt 1), 227–236. https://doi.org/10.1042/BJ20050605

Loizou, J. I., El-Khamisy, S. F., Zlatanou, A., Moore, D. J., Chan, D. W., Qin, J., Sarno, S., Meggio, F., Pinna, L. A., & Caldecott, K. W. (2004). The protein kinase CK2 facilitates repair of chromosomal DNA single-strand breaks. *Cell*, *117*(1), 17–28. https://doi.org/10.1016/s0092-8674(04)00206-5

Lolli, G., Cozza, G., Mazzorana, M., Tibaldi, E., Cesaro, L., Donella-Deana, A., Meggio, F., Venerando, A., Franchin, C., Sarno, S., Battistutta, R., & Pinna, L. A. (2012). Inhibition of Protein Kinase CK2 by Flavonoids and Tyrphostins. A Structural Insight. *Biochemistry*, *51*(31), 6097–6107. https://doi.org/10.1021/bi300531c

Lolli, G., Pinna, L. A., & Battistutta, R. (2012). Structural Determinants of Protein Kinase CK2 Regulation by Autoinhibitory Polymerization. *ACS Chemical Biology*, *7*(7), 1158–1163. https://doi.org/10.1021/cb300054n

Lolli, G., Ranchio, A., & Battistutta, R. (2014). Active form of the protein kinase CK2 α2β2 holoenzyme is a strong complex with symmetric architecture. *ACS Chemical Biology*, *9*(2), 366–371. https://doi.org/10.1021/cb400771y

Lupp, S., Götz, C., Khadouma, S., Horbach, T., Dimova, E. Y., Bohrer, A.-M., Kietzmann, T., & Montenarh, M. (2014). The upstream stimulatory factor USF1 is regulated by protein kinase CK2 phosphorylation. *Cellular Signalling*, *26*(12), 2809–2817. https://doi.org/10.1016/j.cellsig.2014.08.028

Lüscher, B., & Litchfield, D. W. (1994). Biosynthesis of casein kinase II in lymphoid cell lines. *European Journal of Biochemistry*, *220*(2), 521–526.

Lynch, D. R., Schadt, K., Kichula, E., McCormack, S., & Lin, K. Y. (2021). Friedreich Ataxia: Multidisciplinary Clinical Care. *Journal of Multidisciplinary Healthcare*, *14*, 1645–1658. https://doi.org/10.2147/JMDH.S292945

Majerciak, V., Pripuzova, N., Chan, C., Temkin, N., Specht, S. I., & Zheng, Z.-M. (2015). Stability of Structured Kaposi's Sarcoma-Associated Herpesvirus ORF57 Protein Is Regulated by Protein Phosphorylation and Homodimerization. *Journal of Virology*, *89*(6), 3256–3274. https://doi.org/10.1128/jvi.03721-14

Manni, S., Brancalion, A., Mandato, E., Tubi, L. Q., Colpo, A., Pizzi, M., Cappellesso, R., Zaffino, F., Di Maggio, S. A., Cabrelle, A., Marino, F., Zambello, R., Trentin, L., Adami, F., Gurrieri, C., Semenzato, G., & Piazza, F. (2013). Protein kinase CK2 inhibition down modulates the NF-κB and STAT3 survival pathways, enhances the cellular proteotoxic stress and synergistically

boosts the cytotoxic effect of bortezomib on multiple myeloma and mantle cell lymphoma cells. *PloS One*, *8*(9), e75280. https://doi.org/10.1371/journal.pone.0075280

Manning, G., Whyte, D. B., Martinez, R., Hunter, T., & Sudarsanam, S. (2002). The Protein Kinase Complement of the Human Genome. *Science*, *298*(5600), 1912–1934. https://doi.org/10.1126/science.1075762

Marin, O., Meggio, F., & Pinna, L. A. (1999a). Structural Features Underlying the Unusual Mode of Calmodulin Phosphorylation by Protein Kinase CK2: A Study with Synthetic Calmodulin Fragments. *Biochemical and Biophysical Research Communications*, *256*(2), 442–446. https://doi.org/10.1006/bbrc.1999.0348

Marin, O., Meggio, F., Sarno, S., Cesaro, L., Pagano, M. A., & Pinna, L. A. (1999b). Tyrosine versus serine/threonine phosphorylation by protein kinase casein kinase-2. A study with peptide substrates derived from immunophilin Fpr3. *The Journal of Biological Chemistry*, *274*(41), 29260–29265. https://doi.org/10.1074/jbc.274.41.29260

Marin, O., Meggio, F., Sarno, S., & Pinna, L. A. (1997). Physical dissection of the structural elements responsible for regulatory properties and intersubunit interactions of protein kinase CK2 beta-subunit. *Biochemistry*, *36*(23), 7192–7198. https://doi.org/10.1021/bi962885q

Marin, O., Sarno, S., Boschetti, M., Pagano, M. A., Meggio, F., Ciminale, V., D'Agostino, D. M., & Pinna, L. A. (2000). Unique features of HIV-1 Rev protein phosphorylation by protein kinase CK2 ('casein kinase-2'). *FEBS Letters*, *481*(1), 63–67. https://doi.org/10.1016/s0014-5793(00)01971-2

Martins, L. R., Lúcio, P., Silva, M. C., Anderes, K. L., Gameiro, P., Silva, M. G., & Barata, J. T. (2010). Targeting CK2 overexpression and hyperactivation as a novel therapeutic tool in chronic lymphocytic leukemia. *Blood*, *116*(15), 2724–2731. https://doi.org/10.1182/blood-2010-04-277947

Mascher, T., Helmann, J. D., & Unden, G. (2006). Stimulus perception in bacterial signal-transducing histidine kinases. *Microbiology and Molecular Biology Reviews: MMBR*, *70*(4), 910–938. https://doi.org/10.1128/MMBR.00020-06

McElhinny, J. A., Trushin, S. A., Bren, G. D., Chester, N., & Paya, C. V. (1996). Casein kinase II phosphorylates I kappa B alpha at S-283, S-289, S-293, and T-291 and is required for its degradation. *Molecular and Cellular Biology*, *16*(3), 899–906. https://doi.org/10.1128/MCB.16.3.899

McKeehan, W., & Hardesty, B. (1969). The mechanism of cycloheximide inhibition of protein synthesis in rabbit reticulocytes. *Biochemical and Biophysical Research Communications*, *36*(4), 625–630. https://doi.org/10.1016/0006-291X(69)90351-9

Meggio, F., Boldyreff, B., Issinger, O. G., & Pińna, L. A. (1994). Casein kinase 2 down-regulation and activation by polybasic peptides are mediated by acidic residues in the 55-64 region of the beta-subunit. A study with calmodulin as phosphorylatable substrate. *Biochemistry*, *33*(14), 4336–4342. https://doi.org/10.1021/bi00180a030

Meggio, F., Boldyreff, B., Marin, O., Marchiori, F., Perich, J. W., Issinger, O. G., & Pinna, L. A. (1992b). The effect of polylysine on casein-kinase-2 activity is influenced by both the structure of the protein/peptide substrates and the subunit composition of the enzyme. *European Journal of Biochemistry*, *205*(3), 939–945. https://doi.org/10.1111/j.1432-1033.1992.tb16860.x

Meggio, F., Boldyreff, B., Marin, O., Pinna, L. A., & Issinger, O. G. (1992a). Role of the beta subunit of casein kinase-2 on the stability and specificity of the recombinant reconstituted holoenzyme. *European Journal of Biochemistry*, *204*(1), 293–297. https://doi.org/10.1111/j.1432-1033.1992.tb16636.x

Meggio, F., D'Agostino, D. M., Ciminale, V., Chieco-Bianchi, L., & Pinna, L. A. (1996). Phosphorylation of HIV-1 Rev protein: Implication of protein kinase CK2 and pro-directed kinases. *Biochemical and Biophysical Research Communications*, *226*(2), 547–554. https://doi.org/10.1006/bbrc.1996.1392

Meggio, F., Donella Deana, A., Ruzzene, M., Brunati, A. M., Cesaro, L., Guerra, B., Meyer, T., Mett, H., Fabbro, D., & Furet, P. (1995). Different susceptibility of protein kinases to

staurosporine inhibition. Kinetic studies and molecular bases for the resistance of protein kinase CK2. *European Journal of Biochemistry*, *234*(1), 317–322. https://doi.org/10.1111/j.1432-1033.1995.317_c.x

Meggio, F., Marin, O., & Pinna, L. A. (1994). Substrate specificity of protein kinase CK2. *Cellular & Molecular Biology Research*, *40*(5–6), 401–409.

Meggio, F., & Pinna, L. A. (2003). One-thousand-and-one substrates of protein kinase CK2? *FASEB Journal: Official Publication of the Federation of American Societies for Experimental Biology*, *17*(3), 349–368. https://doi.org/10.1096/fj.02-0473rev

Meng, R., Al-Quobaili, F., Müller, I., Götz, C., Thiel, G., & Montenarh, M. (2010). CK2 phosphorylation of Pdx-1 regulates its transcription factor activity. *Cellular and Molecular Life Sciences: CMLS*, *67*(14), 2481–2489. https://doi.org/10.1007/s00018-010-0348-0

Messenger, M. M., Saulnier, R. B., Gilchrist, A. D., Diamond, P., Gorbsky, G. J., & Litchfield, D. W. (2002). Interactions between protein kinase CK2 and Pin1. Evidence for phosphorylation-dependent interactions. *The Journal of Biological Chemistry*, *277*(25), 23054–23064. https://doi.org/10.1074/jbc.M200111200

Mian, A. A., Haberbosch, I., Khamaisie, H., Agbarya, A., Pietsch, L., Eshel, E., Najib, D., Chiriches, C., Ottmann, O. G., Hantschel, O., Biondi, R. M., Ruthardt, M., & Mahajna, J. (2021). Crizotinib acts as ABL1 inhibitor combining ATP-binding with allosteric inhibition and is active against native BCR-ABL1 and its resistance and compound mutants BCR-ABL1T315I and BCR-ABL1T315I-E255K. *Annals of Hematology*, *100*(8), 2023–2029. https://doi.org/10.1007/s00277-020-04357-z

Miranda, C. J., Santos, M. M., Ohshima, K., Smith, J., Li, L., Bunting, M., Cossée, M., Koenig, M., Sequeiros, J., Kaplan, J., & Pandolfo, M. (2002). Frataxin knockin mouse. *FEBS Letters*, *512*(1–3), 291–297. https://doi.org/10.1016/s0014-5793(02)02251-2

Mishra, P., Seth, T., Mahapatra, M., & Saxena, R. (2013). Report of chronic myeloid leukemia in chronic phase from All India Institute of Medical Sciences, 1990-2010. *Indian Journal of Medical and Paediatric Oncology: Official Journal of Indian Society of Medical & Paediatric Oncology*, *34*(3), 159–163. https://doi.org/10.4103/0971-5851.123712

Mishra, S., Pertz, V., Zhang, B., Kaur, P., Shimada, H., Groffen, J., Kazimierczuk, Z., Pinna, L. A., & Heisterkamp, N. (2007). Treatment of P190 Bcr/Abl lymphoblastic leukemia cells with inhibitors of the serine/threonine kinase CK2. *Leukemia*, *21*(1), 178–180. https://doi.org/10.1038/sj.leu.2404460

Mitrovský, O., Myslivcová, D., Macháčková-Lopotová, T., Obr, A., Čermáková, K., Ransdorfová, Š., Březinová, J., Klamová, H., & Žáčková, M. (2023). Inhibition of casein kinase 2 induces cell death in tyrosine kinase inhibitor resistant chronic myelogenous leukemia cells. *PloS One*, *18*(5), e0284876. https://doi.org/10.1371/journal.pone.0284876

Montenarh, M. (2014). Protein Kinase CK2 and Angiogenesis. *Advances in Clinical and Experimental Medicine*, *23*(2), 153–158. https://doi.org/10.17219/acem/37040

Montenarh, M. (2016). Protein kinase CK2 in DNA damage and repair. *Translational Cancer Research*, *5*(1).

Montenarh, M., Grässer, F. A., & Götz, C. (2023). Protein Kinase CK2 and Epstein-Barr Virus. *Biomedicines*, *11*(2), 358. https://doi.org/10.3390/biomedicines11020358

Morita, K., & Sasaki, K. (2021). Current status and novel strategy of CML. *International Journal of Hematology*, *113*(5), 624–631. https://doi.org/10.1007/s12185-021-03127-5

Morotti, A., Panuzzo, C., Crivellaro, S., Carrà, G., Fava, C., Guerrasio, A., Pandolfi, P. P., & Saglio, G. (2015). BCR-ABL inactivates cytosolic PTEN through Casein Kinase II mediated tail phosphorylation. *Cell Cycle (Georgetown, Tex.)*, *14*(7), 973–979. https://doi.org/10.1080/15384101.2015.1006970

Mottram, P. M., Delatycki, M. B., Donelan, L., Gelman, J. S., Corben, L., & Peverill, R. E. (2011). Early changes in left ventricular long-axis function in Friedreich ataxia: Relation with the FXN gene mutation and cardiac structural change. *Journal of the American Society of Echocardiography: Official Publication of the American Society of Echocardiography*, *24*(7), 782–789. https://doi.org/10.1016/j.echo.2011.04.004

Muganda, P. M., Fischer, A., & Bernal, R. A. (1995). Identification of a casein kinase activity found elevated in human cytomegalovirus transformed cells. *Biochemical and Biophysical Research Communications*, *207*(2), 740–746. https://doi.org/10.1006/bbrc.1995.1249

Murtaza, I., Wang, H.-X., Feng, X., Alenina, N., Bader, M., Prabhakar, B. S., & Li, P.-F. (2008). Down-regulation of catalase and oxidative modification of protein kinase CK2 lead to the failure of apoptosis repressor with caspase recruitment domain to inhibit cardiomyocyte hypertrophy. *The Journal of Biological Chemistry*, *283*(10), 5996–6004. https://doi.org/10.1074/jbc.M706466200

Nair, R., Tolentino, J., & Hazlehurst, L. (2012). Role of STAT3 in Transformation and Drug Resistance in CML. *Frontiers in Oncology*, *2*. https://www.frontiersin.org/articles/10.3389/fonc.2012.00030

Nakashima, M., Tohyama, J., Nakagawa, E., Watanabe, Y., Siew, C. G., Kwong, C. S., Yamoto, K., Hiraide, T., Fukuda, T., Kaname, T., Nakabayashi, K., Hata, K., Ogata, T., Saitsu, H., & Matsumoto, N. (2019). Identification of de novo CSNK2A1 and CSNK2B variants in cases of global developmental delay with seizures. *Journal of Human Genetics*, *64*(4), Article 4. https://doi.org/10.1038/s10038-018-0559-z

Ng, K. P., Manjeri, A., Lee, K. L., Huang, W., Tan, S. Y., Chuah, C. T. H., Poellinger, L., & Ong, S. T. (2014). Physiologic hypoxia promotes maintenance of CML stem cells despite effective BCR-ABL1 inhibition. *Blood*, *123*(21), 3316–3326. https://doi.org/10.1182/blood-2013-07-511907

Nguyen, L. X. T., & Mitchell, B. S. (2013). Akt activation enhances ribosomal RNA synthesis through casein kinase II and TIF-IA. *Proceedings of the National Academy of Sciences*, *110*(51), 20681–20686. https://doi.org/10.1073/pnas.1313097110

Niefind, K., Guerra, B., Ermakowa, I., & Issinger, O.-G. (2001). Crystal structure of human protein kinase CK2: Insights into basic properties of the CK2 holoenzyme. *The EMBO Journal*, *20*(19), 5320–5331. https://doi.org/10.1093/emboj/20.19.5320

Niefind, K., Guerra, B., Pinna, L. A., Issinger, O. G., & Schomburg, D. (1998). Crystal structure of the catalytic subunit of protein kinase CK2 from Zea mays at 2.1 A resolution. *The EMBO Journal*, *17*(9), 2451–2462. https://doi.org/10.1093/emboj/17.9.2451

Nienberg, C., Retterath, A., Becher, K.-S., Saenger, T., Mootz, H. D., & Jose, J. (2016). Site-Specific Labeling of Protein Kinase CK2: Combining Surface Display and Click Chemistry for Drug Discovery Applications. *Pharmaceuticals*, *9*(3), Article 3. https://doi.org/10.3390/ph9030036

Nishi, H., Hashimoto, K., & Panchenko, A. R. (2011). Phosphorylation in protein-protein binding: Effect on stability and function. *Structure (London, England: 1993)*, *19*(12), 1807–1815. https://doi.org/10.1016/j.str.2011.09.021

Nitta, R. T., Bolin, S., Luo, E., Solow-Codero, D. E., Samghabadi, P., Purzner, T., Aujla, P. S., Nwagbo, G., Cho, Y.-J., & Li, G. (2019). Casein kinase 2 inhibition sensitizes medulloblastoma to temozolomide. *Oncogene*, *38*(42), 6867–6879. https://doi.org/10.1038/s41388-019-0927-y

O'Brien, K. A., Lemke, S. J., Cocke, K. S., Rao, R. N., & Beckmann, R. P. (1999). Casein kinase 2 binds to and phosphorylates BRCA1. *Biochemical and Biophysical Research Communications*, *260*(3), 658–664. https://doi.org/10.1006/bbrc.1999.0892

O'Hare, T., Eide, C. A., & Deininger, M. W. (2007). Bcr-Abl Kinase Domain Mutations and the Unsettled Problem of Bcr-AblT315I: Looking into the Future of Controlling Drug Resistance in Chronic Myeloid Leukemia. *Clinical Lymphoma and Myeloma*, *7*, S120–S130. https://doi.org/10.3816/CLM.2007.s.012

O'Hare, T., Shakespeare, W. C., Zhu, X., Eide, C. A., Rivera, V. M., Wang, F., Adrian, L. T., Zhou, T., Huang, W.-S., Xu, Q., Metcalf, C. A., Tyner, J. W., Loriaux, M. M., Corbin, A. S., Wardwell, S., Ning, Y., Keats, J. A., Wang, Y., Sundaramoorthi, R., … Clackson, T. (2009). AP24534, a Pan-BCR-ABL Inhibitor for Chronic Myeloid Leukemia, Potently Inhibits the T315I Mutant and Overcomes Mutation-Based Resistance. *Cancer Cell*, *16*(5), 401–412. https://doi.org/10.1016/j.ccr.2009.09.028

Ohtsuki, K., Maekawa, T., Harada, S., Karino, A., Morikawa, Y., & Ito, M. (1998). Biochemical characterization of HIV-1 Rev as a potent activator of casein kinase II in vitro. *FEBS Letters*, *428*(3), 235–240. https://doi.org/10.1016/s0014-5793(98)00538-9

Okochi, M., Walter, J., Koyama, A., Nakajo, S., Baba, M., Iwatsubo, T., Meijer, L., Kahle, P. J., & Haass, C. (2000). Constitutive phosphorylation of the Parkinson's disease associated alpha-synuclein. *The Journal of Biological Chemistry*, *275*(1), 390–397. https://doi.org/10.1074/jbc.275.1.390

Okur, V., Cho, M. T., Henderson, L., Retterer, K., Schneider, M., Sattler, S., Niyazov, D., Azage, M., Smith, S., Picker, J., Lincoln, S., Tarnopolsky, M., Brady, L., Bjornsson, H. T., Applegate, C., Dameron, A., Willaert, R., Baskin, B., Juusola, J., & Chung, W. K. (2016). De novo mutations in CSNK2A1 are associated with neurodevelopmental abnormalities and dysmorphic features. *Human Genetics*, *135*(7), 699–705. https://doi.org/10.1007/s00439-016-1661-y

ole-MoiYoi, O. K. (1995). Casein kinase II in theileriosis. *Science (New York, N.Y.)*, *267*(5199), 834–836. https://doi.org/10.1126/science.7846527

Orsini, A., Santangelo, A., Bravin, F., Bonuccelli, A., Peroni, D., Battini, R., Foiadelli, T., Bertini, V., Valetto, A., Iacomino, M., Nigro, V., Torella, A. L., Scala, M., Capra, V., Vari, M. S., Fetta, A., Di Pisa, V., Montanari, F., Epifanio, R., … Cordelli, D. M. (2022). Expanding Phenotype of Poirier–Bienvenu Syndrome: New Evidence from an Italian Multicentrical Cohort of Patients. *Genes*, *13*(2), Article 2. https://doi.org/10.3390/genes13020276

Oshima, T., Niwa, Y., Kuwata, K., Srivastava, A., Hyoda, T., Tsuchiya, Y., Kumagai, M., Tsuyuguchi, M., Tamaru, T., Sugiyama, A., Ono, N., Zolboot, N., Aikawa, Y., Oishi, S., Nonami, A., Arai, F., Hagihara, S., Yamaguchi, J., Tama, F., … Hirota, T. (2019). Cell-based screen identifies a new potent and highly selective CK2 inhibitor for modulation of circadian rhythms and cancer cell growth. *Science Advances*, *5*(1), eaau9060. https://doi.org/10.1126/sciadv.aau9060

Osman, A. E. G., & Deininger, M. W. (2021). Chronic Myeloid Leukemia: Modern therapies, current challenges and future directions. *Blood Reviews*, *49*, 100825. https://doi.org/10.1016/j.blre.2021.100825

Parhar, K., Morse, J., & Salh, B. (2007). The role of protein kinase CK2 in intestinal epithelial cell inflammatory signaling. *International Journal of Colorectal Disease*, *22*(6), 601–609. https://doi.org/10.1007/s00384-006-0193-7

Park, M. H. (2006). The post-translational synthesis of a polyamine-derived amino acid, hypusine, in the eukaryotic translation initiation factor 5A (eIF5A). *Journal of Biochemistry*, *139*(2), 161–169. https://doi.org/10.1093/jb/mvj034

Patel, A. B., O'Hare, T., & Deininger, M. W. (2017). Mechanisms of Resistance to ABL Kinase Inhibition in Chronic Myeloid Leukemia and the Development of Next Generation ABL Kinase Inhibitors. *Hematology/Oncology Clinics*, *31*(4), 589–612. https://doi.org/10.1016/j.hoc.2017.04.007

Patel, M., Isaacs, C. J., Seyer, L., Brigatti, K., Gelbard, S., Strawser, C., Foerster, D., Shinnick, J., Schadt, K., Yiu, E. M., Delatycki, M. B., Perlman, S., Wilmot, G. R., Zesiewicz, T., Mathews, K., Gomez, C. M., Yoon, G., Subramony, S. H., Brocht, A., … Lynch, D. R. (2016). Progression of Friedreich ataxia: Quantitative characterization over 5 years. *Annals of Clinical and Translational Neurology*, *3*(9), 684–694. https://doi.org/10.1002/acn3.332

Patterson, S. D., & Copland, M. (2023). The Bone Marrow Immune Microenvironment in CML: Treatment Responses, Treatment-Free Remission, and Therapeutic Vulnerabilities. *Current Hematologic Malignancy Reports*, *18*(2), 19–32. https://doi.org/10.1007/s11899-023-00688-6

Pediatric Brain Tumor Consortium. (2023). *PBTC-053: A Pediatric Brain Tumor Consortium Phase I/ II and Surgical Study of CX-4945 in Patients With Recurrent SHH Medulloblastoma* (Clinical Trial Registration NCT03904862). clinicaltrials.gov. https://clinicaltrials.gov/study/NCT03904862

Perea, S. E., Baladrón, I., Valenzuela, C., & Perera, Y. (2018). CIGB-300: A peptide-based drug that impairs the Protein Kinase CK2-mediated phosphorylation. *Seminars in Oncology*, *45*(1–2), 58–67. https://doi.org/10.1053/j.seminoncol.2018.04.006

Perea, S. E., Reyes, O., Baladron, I., Perera, Y., Farina, H., Gil, J., Rodriguez, A., Bacardi, D., Marcelo, J. L., Cosme, K., Cruz, M., Valenzuela, C., López-Saura, P. A., Puchades, Y., Serrano, J. M., Mendoza, O., Castellanos, L., Sanchez, A., Betancourt, L., … Acevedo, B. (2008). CIGB-300, a novel proapoptotic peptide that impairs the CK2 phosphorylation and exhibits anticancer properties both in vitro and in vivo. *Molecular and Cellular Biochemistry*, *316*(1), 163–167. https://doi.org/10.1007/s11010-008-9814-5

Pérez, G. V., Rosales, M., Ramón, A. C., Rodríguez-Ulloa, A., Besada, V., González, L. J., Aguilar, D., Vázquez-Blomquist, D., Falcón, V., Caballero, E., Carvalho, P. C., Caldeira, R. S., Yang, K., Perera, Y., & Perea, S. E. (2022). CIGB-300 Anticancer Peptide Differentially Interacts with CK2 Subunits and Regulates Specific Signaling Mediators in a Highly Sensitive Large Cell Lung Carcinoma Cell Model. *Biomedicines*, *11*(1), 43. https://doi.org/10.3390/biomedicines11010043

Phan-Dinh-Tuy, F., Henry, J., Boucheix, C., Perrot, J. Y., Rosenfeld, C., & Kahn, A. (1985). Protein kinases in human leukemic cells. *American Journal of Hematology*, *19*(3), 209–218. https://doi.org/10.1002/ajh.2830190302

Piazza, F. A., Ruzzene, M., Gurrieri, C., Montini, B., Bonanni, L., Chioetto, G., Di Maira, G., Barbon, F., Cabrelle, A., Zambello, R., Adami, F., Trentin, L., Pinna, L. A., & Semenzato, G. (2006). Multiple myeloma cell survival relies on high activity of protein kinase CK2. *Blood*, *108*(5), 1698–1707. https://doi.org/10.1182/blood-2005-11-013672

Pierre, F., Chua, P. C., O'Brien, S. E., Siddiqui-Jain, A., Bourbon, P., Haddach, M., Michaux, J., Nagasawa, J., Schwaebe, M. K., Stefan, E., Vialettes, A., Whitten, J. P., Chen, T. K., Darjania, L., Stansfield, R., Anderes, K., Bliesath, J., Drygin, D., Ho, C., … Ryckman, D. M. (2011). Discovery and SAR of 5-(3-Chlorophenylamino)benzo[c][2,6]naphthyridine-8-carboxylic Acid (CX-4945), the First Clinical Stage Inhibitor of Protein Kinase CK2 for the Treatment of Cancer. *Journal of Medicinal Chemistry*, *54*(2), 635–654. https://doi.org/10.1021/jm101251q

Pinna, L. A. (2002). Protein kinase CK2: A challenge to canons. *Journal of Cell Science*, *115*(20), 3873–3878. https://doi.org/10.1242/jcs.00074

Pinna, L. A., & Meggio, F. (1997). Protein kinase CK2 ("casein kinase-2") and its implication in cell division and proliferation. *Progress in Cell Cycle Research*, *3*, 77–97. https://doi.org/10.1007/978-1-4615-5371-7_7

Plotnikov, A., Chuderland, D., Karamansha, Y., Livnah, O., & Seger, R. (2019). Nuclear ERK Translocation is Mediated by Protein Kinase CK2 and Accelerated by Autophosphorylation. *Cellular Physiology and Biochemistry: International Journal of Experimental Cellular Physiology, Biochemistry, and Pharmacology*, *53*(2), 366–387. https://doi.org/10.33594/000000144

Poirier, K., Hubert, L., Viot, G., Rio, M., Billuart, P., Besmond, C., & Bienvenu, T. (2017). CSNK2B splice site mutations in patients cause intellectual disability with or without myoclonic epilepsy. *Human Mutation*, *38*(8), 932–941. https://doi.org/10.1002/humu.23270

Prudent, R., Moucadel, V., Laudet, B., Barette, C., Lafanechère, L., Hasenknopf, B., Li, J., Bareyt, S., Lacôte, E., Thorimbert, S., Malacria, M., Gouzerh, P., & Cochet, C. (2008). Identification of polyoxometalates as nanomolar noncompetitive inhibitors of protein kinase CK2. *Chemistry & Biology*, *15*(7), 683–692. https://doi.org/10.1016/j.chembiol.2008.05.018

Puttini, M., Coluccia, A. M. L., Boschelli, F., Cleris, L., Marchesi, E., Donella-Deana, A., Ahmed, S., Redaelli, S., Piazza, R., Magistroni, V., Andreoni, F., Scapozza, L., Formelli, F., & Gambacorti-Passerini, C. (2006). In vitro and in vivo activity of SKI-606, a novel Src-Abl inhibitor, against imatinib-resistant Bcr-Abl+ neoplastic cells. *Cancer Research*, *66*(23), 11314–11322. https://doi.org/10.1158/0008-5472.CAN-06-1199

Pyerin, W., & Ackermann, K. (2001). Transcriptional coordination of the genes encoding catalytic (CK2α) and regulatory (CK2β) subunits of human protein kinase CK2. *Molecular and Cellular Biochemistry*, *227*(1), 45–57. https://doi.org/10.1023/A:1013152621029

Quezada Meza, C. P., & Ruzzene, M. (2023). Protein Kinase CK2 and SARS-CoV-2: An Expected Interplay Story. *Kinases and Phosphatases*, *1*(2), Article 2. https://doi.org/10.3390/kinasesphosphatases1020009

Quotti Tubi, L., Gurrieri, C., Brancalion, A., Bonaldi, L., Bertorelle, R., Manni, S., Pavan, L., Lessi, F., Zambello, R., Trentin, L., Adami, F., Ruzzene, M., Pinna, L. A., Semenzato, G., & Piazza, F. (2013). Inhibition of protein kinase CK2 with the clinical-grade small ATP-competitive compound CX-4945 or by RNA interference unveils its role in acute myeloid leukemia cell survival, p53-dependent apoptosis and daunorubicin-induced cytotoxicity. *Journal of Hematology & Oncology*, *6*, 78. https://doi.org/10.1186/1756-8722-6-78

Rabalski, A. J., Gyenis, L., & Litchfield, D. W. (2016). Molecular Pathways: Emergence of Protein Kinase CK2 (CSNK2) as a Potential Target to Inhibit Survival and DNA Damage Response and Repair Pathways in Cancer Cells. *Clinical Cancer Research: An Official Journal of the American Association for Cancer Research*, *22*(12), 2840–2847. https://doi.org/10.1158/1078-0432.CCR-15-1314

Rabjerg, M., Guerra, B., Oliván-Viguera, A., Mikkelsen, M. L. N., Köhler, R., Issinger, O.-G., & Marcussen, N. (2017). Nuclear localization of the CK2α-subunit correlates with poor prognosis in clear cell renal cell carcinoma. *Oncotarget*, *8*(1), 1613–1627. https://doi.org/10.18632/oncotarget.13693

Radich, J. P., Deininger, M., Abboud, C. N., Altman, J. K., Berman, E., Bhatia, R., Bhatnagar, B., Curtin, P., DeAngelo, D. J., Gotlib, J., Hobbs, G., Jagasia, M., Kantarjian, H. M., Maness, L., Metheny, L., Moore, J. O., Pallera, A., Pancari, P., Patnaik, M., … Sundar, H. (2018). Chronic Myeloid Leukemia, Version 1.2019, NCCN Clinical Practice Guidelines in Oncology. *Journal of the National Comprehensive Cancer Network*, *16*(9), 1108–1135. https://doi.org/10.6004/jnccn.2018.0071

Raju, P., Shashikanth, N., Tsai, P.-Y., Pongkorpsakol, P., Chanez-Paredes, S., Steinhagen, P. R., Kuo, W.-T., Singh, G., Tsukita, S., & Turner, J. R. (2020). Inactivation of paracellular cation-selective claudin-2 channels attenuates immune-mediated experimental colitis in mice. *The Journal of Clinical Investigation*, *130*(10), 5197–5208. https://doi.org/10.1172/JCI138697

Ramazi, S., & Zahiri, J. (2021). Post-translational modifications in proteins: Resources, tools and prediction methods. *Database: The Journal of Biological Databases and Curation*, *2021*, baab012. https://doi.org/10.1093/database/baab012

Rance, G., Corben, L., Barker, E., Carew, P., Chisari, D., Rogers, M., Dowell, R., Jamaluddin, S., Bryson, R., & Delatycki, M. B. (2010). Auditory perception in individuals with Friedreich's ataxia. *Audiology & Neuro-Otology*, *15*(4), 229–240. https://doi.org/10.1159/000255341

Recknor, C. (2022). *A Phase II, Randomized and Controlled Investigator Initiated Trial Evaluating Safety, Pharmacokinetics and Clinical Benefit of Silmitasertib (CX-4945) in Outpatient Adult Subjects With Moderate Coronavirus Disease 2019 (COVID-19)* (Clinical Trial Registration NCT04663737). clinicaltrials.gov. https://clinicaltrials.gov/study/NCT04663737

Redaelli, S., Piazza, R., Rostagno, R., Magistroni, V., Perini, P., Marega, M., Gambacorti-Passerini, C., & Boschelli, F. (2009). Activity of bosutinib, dasatinib, and nilotinib against 18 imatinib-resistant BCR/ABL mutants. *Journal of Clinical Oncology: Official Journal of the American Society of Clinical Oncology*, *27*(3), 469–471. https://doi.org/10.1200/JCO.2008.19.8853

Reetz, K., Dogan, I., Costa, A. S., Dafotakis, M., Fedosov, K., Giunti, P., Parkinson, M. H., Sweeney, M. G., Mariotti, C., Panzeri, M., Nanetti, L., Arpa, J., Sanz-Gallego, I., Durr, A., Charles, P., Boesch, S., Nachbauer, W., Klopstock, T., Karin, I., … Schulz, J. B. (2015). Biological and clinical characteristics of the European Friedreich's Ataxia Consortium for Translational Studies (EFACTS) cohort: A cross-sectional analysis of baseline data. *The Lancet. Neurology*, *14*(2), 174–182. https://doi.org/10.1016/S1474-4422(14)70321-7

Remsing Rix, L. L., Rix, U., Colinge, J., Hantschel, O., Bennett, K. L., Stranzl, T., Müller, A., Baumgartner, C., Valent, P., Augustin, M., Till, J. H., & Superti-Furga, G. (2009). Global target profile of the kinase inhibitor bosutinib in primary chronic myeloid leukemia cells. *Leukemia*, *23*(3), Article 3. https://doi.org/10.1038/leu.2008.334

Research, C. for D. E. and. (2023). FDA approves first treatment for Friedreich's ataxia. *FDA*. https://www.fda.gov/drugs/news-events-human-drugs/fda-approves-first-treatment-friedreichs-ataxia

Rodriguez, F. A., Contreras, C., Bolanos-Garcia, V., & Allende, J. E. (2008). Protein kinase CK2 as an ectokinase: The role of the regulatory CK2β subunit. *Proceedings of the National Academy of Sciences*, *105*(15), 5693–5698. https://doi.org/10.1073/pnas.0802065105

Rossi, M., Ruiz de Azua, I., Barella, L. F., Sakamoto, W., Zhu, L., Cui, Y., Lu, H., Rebholz, H., Matschinsky, F. M., Doliba, N. M., Butcher, A. J., Tobin, A. B., & Wess, J. (2015). CK2 acts as a potent negative regulator of receptor-mediated insulin release in vitro and in vivo. *Proceedings of the National Academy of Sciences of the United States of America*, *112*(49), E6818-6824. https://doi.org/10.1073/pnas.1519430112

Rowley, J. D. (1973). Letter: A new consistent chromosomal abnormality in chronic myelogenous leukaemia identified by quinacrine fluorescence and Giemsa staining. *Nature*, *243*(5405), 290–293. https://doi.org/10.1038/243290a0

Rufini, A., Cavallo, F., Condò, I., Fortuni, S., De Martino, G., Incani, O., Di Venere, A., Benini, M., Massaro, D. S., Arcuri, G., Serio, D., Malisan, F., & Testi, R. (2015). Highly specific ubiquitin-competing molecules effectively promote frataxin accumulation and partially rescue the aconitase defect in Friedreich ataxia cells. *Neurobiology of Disease*, *75*, 91–99. https://doi.org/10.1016/j.nbd.2014.12.011

Rufini, A., Fortuni, S., Arcuri, G., Condò, I., Serio, D., Incani, O., Malisan, F., Ventura, N., & Testi, R. (2011). Preventing the ubiquitin-proteasome-dependent degradation of frataxin, the protein defective in Friedreich's ataxia. *Human Molecular Genetics*, *20*(7), 1253–1261. https://doi.org/10.1093/hmg/ddq566

Rummey, C., Flynn, J. M., Corben, L. A., Delatycki, M. B., Wilmot, G., Subramony, S. H., Bushara, K., Duquette, A., Gomez, C. M., Hoyle, J. C., Roxburgh, R., Seeberger, L., Yoon, G., Mathews, K. D., Zesiewicz, T., Perlman, S., & Lynch, D. R. (2021). Scoliosis in Friedreich's ataxia: Longitudinal characterization in a large heterogeneous cohort. *Annals of Clinical and Translational Neurology*, *8*(6), 1239–1250. https://doi.org/10.1002/acn3.51352

Ruzzene, M., & Pinna, L. A. (2010). Addiction to protein kinase CK2: A common denominator of diverse cancer cells? *Biochimica Et Biophysica Acta*, *1804*(3), 499–504. https://doi.org/10.1016/j.bbapap.2009.07.018

Sacco, F., Humphrey, S. J., Cox, J., Mischnik, M., Schulte, A., Klabunde, T., Schäfer, M., & Mann, M. (2016). Glucose-regulated and drug-perturbed phosphoproteome reveals molecular mechanisms controlling insulin secretion. *Nature Communications*, *7*, 13250. https://doi.org/10.1038/ncomms13250

Sagar, N. A., Tarafdar, S., Agarwal, S., Tarafdar, A., & Sharma, S. (2021). Polyamines: Functions, Metabolism, and Role in Human Disease Management. *Medical Sciences*, *9*(2), 44. https://doi.org/10.3390/medsci9020044

Salizzato, V., Borgo, C., Cesaro, L., Pinna, L. A., & Donella-Deana, A. (2016). Inhibition of protein kinase CK2 by CX-5011 counteracts imatinib-resistance preventing rpS6 phosphorylation in chronic myeloid leukaemia cells: New combined therapeutic strategies. *Oncotarget*, *7*(14), 18204–18218. https://doi.org/10.18632/oncotarget.7569

Salvi, M., Sarno, S., Cesaro, L., Nakamura, H., & Pinna, L. A. (2009). Extraordinary pleiotropy of protein kinase CK2 revealed by weblogo phosphoproteome analysis. *Biochimica Et Biophysica Acta*, *1793*(5), 847–859. https://doi.org/10.1016/j.bbamcr.2009.01.013

Salvi, M., Sarno, S., Marin, O., Meggio, F., Itarte, E., & Pinna, L. A. (2006). Discrimination between the activity of protein kinase CK2 holoenzyme and its catalytic subunits. *FEBS Letters*, *580*(16), 3948–3952. https://doi.org/10.1016/j.febslet.2006.06.031

Sarno, S., Vaglio, P., Marin, O., Meggio, F., Issinger, O. G., & Pinna, L. A. (1997). Basic residues in the 74-83 and 191-198 segments of protein kinase CK2 catalytic subunit are implicated in negative but not in positive regulation by the beta-subunit. *European Journal of Biochemistry*, *248*(2), 290–295. https://doi.org/10.1111/j.1432-1033.1997.00290.x

Sarrouilhe, D., & Baudry, M. (1996). Evidence of true protein kinase CKII activity in mitochondria and its spermine-mediated translocation to inner membrane. *Cellular and Molecular Biology (Noisy-Le-Grand, France)*, *42*(2), 189–197.

Saxena, A., Padmanabha, R., & Glover, C. V. (1987). Isolation and sequencing of cDNA clones encoding alpha and beta subunits of Drosophila melanogaster casein kinase II. *Molecular and Cellular Biology*, *7*(10), 3409–3417.

Schadt, K. A., Friedman, L. S., Regner, S. R., Mark, G. E., Lynch, D. R., & Lin, K. Y. (2012). Cross-sectional analysis of electrocardiograms in a large heterogeneous cohort of Friedreich ataxia subjects. *Journal of Child Neurology*, *27*(9), 1187–1192. https://doi.org/10.1177/0883073812448461

Schafranek, L., Nievergall, E., Powell, J. A., Hiwase, D. K., Leclercq, T., Hughes, T. P., & White, D. L. (2015). Sustained inhibition of STAT5, but not JAK2, is essential for TKI-induced cell death in chronic myeloid leukemia. *Leukemia*, *29*(1), Article 1. https://doi.org/10.1038/leu.2014.156

Schmucker, S., Argentini, M., Carelle-Calmels, N., Martelli, A., & Puccio, H. (2008). The in vivo mitochondrial two-step maturation of human frataxin. *Human Molecular Genetics*, *17*(22), 3521–3531. https://doi.org/10.1093/hmg/ddn244

Schwartz, E. I., Intine, R. V., & Maraia, R. J. (2004). CK2 is responsible for phosphorylation of human La protein serine-366 and can modulate rpL37 5'-terminal oligopyrimidine mRNA metabolism. *Molecular and Cellular Biology*, *24*(21), 9580–9591. https://doi.org/10.1128/MCB.24.21.9580-9591.2004

Schwartz, P. A., & Murray, B. W. (2011). Protein kinase biochemistry and drug discovery. *Bioorganic Chemistry*, *39*(5), 192–210. https://doi.org/10.1016/j.bioorg.2011.07.004

Seif, F., Khoshmirsafa, M., Aazami, H., Mohsenzadegan, M., Sedighi, G., & Bahar, M. (2017). The role of JAK-STAT signaling pathway and its regulators in the fate of T helper cells. *Cell Communication and Signaling: CCS*, *15*(1), 23. https://doi.org/10.1186/s12964-017-0177-y

Senhwa Biosciences, Inc. (2021). *A Phase I/II Study of CX-4945 in Combination With Gemcitabine and Cisplatin in the Frontline Treatment of Patients With Cholangiocarcinoma* (Clinical Trial Registration NCT02128282). clinicaltrials.gov. https://clinicaltrials.gov/study/NCT02128282

Senhwa Biosciences, Inc. (2023a). *A Dose Selection Phase 1 Study Evaluating the Safety and Tolerability of Silmitasertib* (Clinical Trial Registration NCT05817708). clinicaltrials.gov. https://clinicaltrials.gov/study/NCT05817708

Senhwa Biosciences, Inc. (2023b). *A Phase I, Multi-Center, Open-Label, Treatment Duration Increment, Expansion, Safety, and Pharmacodynamic Study of CX-4945 Administered Orally Twice Daily to Patients With Advanced Basal Cell Carcinoma* (Clinical Trial Registration NCT03897036). clinicaltrials.gov. https://clinicaltrials.gov/study/NCT03897036

Servas, C., Kiehlmeier, S., Hach, J., Gross, R., Götz, C., & Montenarh, M. (2017). The mammalian STE20-like kinase 1 (MST1) is a substrate for the apoptosis inhibiting protein kinase CK2. *Cellular Signalling*, *36*, 163–175. https://doi.org/10.1016/j.cellsig.2017.05.005

Seyer, L. A., Galetta, K., Wilson, J., Sakai, R., Perlman, S., Mathews, K., Wilmot, G. R., Gomez, C. M., Ravina, B., Zesiewicz, T., Bushara, K. O., Subramony, S. H., Ashizawa, T., Delatycki, M. B., Brocht, A., Balcer, L. J., & Lynch, D. R. (2013). Analysis of the visual system in Friedreich ataxia. *Journal of Neurology*, *260*(9), 2362–2369. https://doi.org/10.1007/s00415-013-6978-z

Shaath, H., & Alajez, N. M. (2020). Computational and Transcriptome Analyses Revealed Preferential Induction of Chemotaxis and Lipid Synthesis by SARS-CoV-2. *Biology*, *9*(9), Article 9. https://doi.org/10.3390/biology9090260

Shore, L. J., Soler, A. P., & Gilmour, S. K. (1997). Ornithine Decarboxylase Expression Leads to Translocation and Activation of Protein Kinase CK2 in Vivo *. *Journal of Biological Chemistry*, *272*(19), 12536–12543. https://doi.org/10.1074/jbc.272.19.12536

Shuai, K., Halpern, J., ten Hoeve, J., Rao, X., & Sawyers, C. L. (1996). Constitutive activation of STAT5 by the BCR-ABL oncogene in chronic myelogenous leukemia. *Oncogene*, *13*(2), 247–254.

Siddiqui-Jain, A., Drygin, D., Streiner, N., Chua, P., Pierre, F., O'Brien, S. E., Bliesath, J., Omori, M., Huser, N., Ho, C., Proffitt, C., Schwaebe, M. K., Ryckman, D. M., Rice, W. G., & Anderes, K. (2010). CX-4945, an orally bioavailable selective inhibitor of protein kinase CK2, inhibits prosurvival and angiogenic signaling and exhibits antitumor efficacy. *Cancer Research*, *70*(24), 10288–10298. https://doi.org/10.1158/0008-5472.CAN-10-1893

Silva, A., Jotta, P. Y., Silveira, A. B., Ribeiro, D., Brandalise, S. R., Yunes, J. A., & Barata, J. T. (2010). Regulation of PTEN by CK2 and Notch1 in primary T-cell acute lymphoblastic leukemia: Rationale for combined use of CK2- and gamma-secretase inhibitors. *Haematologica*, *95*(4), 674–678. https://doi.org/10.3324/haematol.2009.011999

Silva-Pavez, E., & Tapia, J. C. (2020). Protein Kinase CK2 in Cancer Energetics. *Frontiers in Oncology*, *10*. https://www.frontiersin.org/articles/10.3389/fonc.2020.00893

Simanovsky, M., Berlinsky, S., Sinai, P., Leiba, M., Nagler, A., & Galski, H. (2008). Phenotypic and gene expression diversity of malignant cells in human blast crisis chronic myeloid leukemia. *Differentiation*, *76*(8), 908–923. https://doi.org/10.1111/j.1432-0436.2008.00270.x

Singh, N. N., & Ramji, D. P. (2008). Protein kinase CK2, an important regulator of the inflammatory response? *Journal of Molecular Medicine (Berlin, Germany)*, *86*(8), 887–897. https://doi.org/10.1007/s00109-008-0352-0

Singh, P., Kumar, V., Gupta, S. K., Kumari, G., & Verma, M. (2021). Combating TKI resistance in CML by inhibiting the PI3K/Akt/mTOR pathway in combination with TKIs: A review. *Medical Oncology*, *38*(1), 10. https://doi.org/10.1007/s12032-021-01462-5

Sivachandran, N., Cao, J. Y., & Frappier, L. (2010). Epstein-Barr virus nuclear antigen 1 Hijacks the host kinase CK2 to disrupt PML nuclear bodies. *Journal of Virology*, *84*(21), 11113–11123. https://doi.org/10.1128/JVI.01183-10

Skjerpen, C. S., Nilsen, T., Wesche, J., & Olsnes, S. (2002). Binding of FGF-1 variants to protein kinase CK2 correlates with mitogenicity. *The EMBO Journal*, *21*(15), 4058–4069. https://doi.org/10.1093/emboj/cdf402

Song, D. H., Dominguez, I., Mizuno, J., Kaut, M., Mohr, S. C., & Seldin, D. C. (2003). CK2 phosphorylation of the armadillo repeat region of beta-catenin potentiates Wnt signaling. *The Journal of Biological Chemistry*, *278*(26), 24018–24025. https://doi.org/10.1074/jbc.M212260200

Soverini, S., Colarossi, S., Gnani, A., Rosti, G., Castagnetti, F., Poerio, A., Iacobucci, I., Amabile, M., Abruzzese, E., Orlandi, E., Radaelli, F., Ciccone, F., Tiribelli, M., di Lorenzo, R., Caracciolo, C., Izzo, B., Pane, F., Saglio, G., Baccarani, M., … on behalf of the GIMEMA Working Party on Chronic Myeloid Leukemia. (2006). Contribution of ABL Kinase Domain Mutations to Imatinib Resistance in Different Subsets of Philadelphia-Positive Patients: By the GIMEMA Working Party on Chronic Myeloid Leukemia. *Clinical Cancer Research*, *12*(24), 7374–7379. https://doi.org/10.1158/1078-0432.CCR-06-1516

Soverini, S., Mancini, M., Bavaro, L., Cavo, M., & Martinelli, G. (2018). Chronic myeloid leukemia: The paradigm of targeting oncogenic tyrosine kinase signaling and counteracting resistance for successful cancer therapy. *Molecular Cancer*, *17*, 49. https://doi.org/10.1186/s12943-018-0780-6

St-Denis, N. A., Derksen, D. R., & Litchfield, D. W. (2009). Evidence for Regulation of Mitotic Progression through Temporal Phosphorylation and Dephosphorylation of CK2α. *Molecular and Cellular Biology*, *29*(8), 2068–2081. https://doi.org/10.1128/MCB.01563-08

St-Denis, N. A., & Litchfield, D. W. (2009). Protein Kinase CK2 in Health and Disease. *Cellular and Molecular Life Sciences*, *66*(11), 1817–1829. https://doi.org/10.1007/s00018-009-9150-2

Steegmann, J. L., Baccarani, M., Breccia, M., Casado, L. F., García-Gutiérrez, V., Hochhaus, A., Kim, D.-W., Kim, T. D., Khoury, H. J., Le Coutre, P., Mayer, J., Milojkovic, D., Porkka, K., Rea, D., Rosti, G., Saussele, S., Hehlmann, R., & Clark, R. E. (2016). European LeukemiaNet recommendations for the management and avoidance of adverse events of treatment in

chronic myeloid leukaemia. *Leukemia*, *30*(8), 1648–1671. https://doi.org/10.1038/leu.2016.104

Strum, S. W., Gyenis, L., & Litchfield, D. W. (2022). CSNK2 in cancer: Pathophysiology and translational applications. *British Journal of Cancer*, *126*(7), Article 7. https://doi.org/10.1038/s41416-021-01616-2

Su, Y.-W., Huang, W.-Y., Lin, H.-C., Liao, P.-N., Lin, C.-Y., Lin, X.-Y., Huang, S.-H., Chen, Y.-T., & Wu, P.-S. (2023). Silmitasertib, a casein kinase 2 inhibitor, induces massive lipid droplet accumulation and nonapoptotic cell death in head and neck cancer cells. *Journal of Oral Pathology & Medicine: Official Publication of the International Association of Oral Pathologists and the American Academy of Oral Pathology*, *52*(3), 245–254. https://doi.org/10.1111/jop.13378

Surjit, M., Liu, B., Chow, V. T. K., & Lal, S. K. (2006). The nucleocapsid protein of severe acute respiratory syndrome-coronavirus inhibits the activity of cyclin-cyclin-dependent kinase complex and blocks S phase progression in mammalian cells. *The Journal of Biological Chemistry*, *281*(16), 10669–10681. https://doi.org/10.1074/jbc.M509233200

Tamaroff, J., DeDio, A., Wade, K., Wells, M., Park, C., Leavens, K., Rummey, C., Kelly, A., Lynch, D. R., & McCormack, S. E. (2022). Friedreich's Ataxia related Diabetes: Epidemiology and management practices. *Diabetes Research and Clinical Practice*, *186*, 109828. https://doi.org/10.1016/j.diabres.2022.109828

Taylor, S. S., Buechler, J. A., & Yonemoto, W. (1990). cAMP-DEPENDENT PROTEIN KINASE: FRAMEWORK FOR A DIVERSE FAMILY OF REGULATORY ENZYMES. *Annual Review of Biochemistry*, *59*(1), 971–1005. https://doi.org/10.1146/annurev.bi.59.070190.004543

Taylor, S. S., & Kornev, A. P. (2011). Protein kinases: Evolution of dynamic regulatory proteins. *Trends in Biochemical Sciences*, *36*(2), 65–77. https://doi.org/10.1016/j.tibs.2010.09.006

Tchernev, V. T., Mansfield, T. A., Giot, L., Kumar, A. M., Nandabalan, K., Li, Y., Mishra, V. S., Detter, J. C., Rothberg, J. M., Wallace, M. R., Southwick, F. S., & Kingsmore, S. F. (2002). The Chediak-Higashi protein interacts with SNARE complex and signal transduction proteins. *Molecular Medicine (Cambridge, Mass.)*, *8*(1), 56–64.

Torres, J., & Pulido, R. (2001). The tumor suppressor PTEN is phosphorylated by the protein kinase CK2 at its C terminus. Implications for PTEN stability to proteasome-mediated degradation. *The Journal of Biological Chemistry*, *276*(2), 993–998. https://doi.org/10.1074/jbc.M009134200

Trembley, J. H., Kren, B. T., Abedin, M. J., Shaughnessy, D. P., Li, Y., Dehm, S. M., & Ahmed, K. (2019). CK2 Pro-Survival Role in Prostate Cancer Is Mediated via Maintenance and Promotion of Androgen Receptor and NFκB p65 Expression. *Pharmaceuticals (Basel, Switzerland)*, *12*(2), 89. https://doi.org/10.3390/ph12020089

Trembley, J. H., Kren, B. T., Afzal, M., Scaria, G. A., Klein, M. A., & Ahmed, K. (2023). Protein kinase CK2—Diverse roles in cancer cell biology and therapeutic promise. *Molecular and Cellular Biochemistry*, *478*(4), 899–926. https://doi.org/10.1007/s11010-022-04558-2

Trivisano, M., Dominicis, A. D., Stregapede, F., Quintavalle, C., Micalizzi, A., Cappelletti, S., Dentici, M. L., Sinibaldi, L., Calabrese, C., Terracciano, A., Vigevano, F., Novelli, A., & Specchio, N. (2023). Refining of the electroclinical phenotype in familial and sporadic cases of CSNK2B-related Neurodevelopmental Syndrome. *Epilepsy & Behavior*, *147*, 109436. https://doi.org/10.1016/j.yebeh.2023.109436

Tugizov, S., Berline, J., Herrera, R., Penaranda, M. E., Nakagawa, M., & Palefsky, J. (2005). Inhibition of human papillomavirus type 16 E7 phosphorylation by the S100 MRP-8/14 protein complex. *Journal of Virology*, *79*(2), 1099–1112. https://doi.org/10.1128/JVI.79.2.1099-1112.2005

University Hospital, Grenoble. (2020). *Evaluation of a Promising New Combination of Protein Kinase Inhibitors on Organotypic Cultures of Human Renal Tumors* (Clinical Trial Registration NCT03571438). clinicaltrials.gov. https://clinicaltrials.gov/study/NCT03571438

University of Arizona. (2023). *Phase II, Randomized, Investigator Initiated Trial to Evaluate Safety and to Explore Clinical Benefit of Silmitasertib (CX-4945) in Patients With Severe Coronavirus*

Disease 2019 (COVID-19) (Clinical Trial Registration NCT04668209). clinicaltrials.gov. https://clinicaltrials.gov/study/NCT04668209

Unni, P., Friend, J., Weinberg, J., Okur, V., Hochscherf, J., & Dominguez, I. (2022). Predictive functional, statistical and structural analysis of CSNK2A1 and CSNK2B variants linked to neurodevelopmental diseases. *Frontiers in Molecular Biosciences*, *9*. https://www.frontiersin.org/articles/10.3389/fmolb.2022.851547

Valero, E., De Bonis, S., Filhol, O., Wade, R. H., Langowski, J., Chambaz, E. M., & Cochet, C. (1995). Quaternary structure of casein kinase 2. Characterization of multiple oligomeric states and relation with its catalytic activity. *The Journal of Biological Chemistry*, *270*(14), 8345–8352. https://doi.org/10.1074/jbc.270.14.8345

Venerando, A., Ruzzene, M., & Pinna, L. A. (2014). Casein kinase: The triple meaning of a misnomer. *Biochemical Journal*, *460*(2), 141–156. https://doi.org/10.1042/BJ20140178

Venkat, S., Tisdale, A. A., Schwarz, J. R., Alahmari, A. A., Maurer, H. C., Olive, K. P., Eng, K. H., & Feigin, M. E. (2020). Alternative polyadenylation drives oncogenic gene expression in pancreatic ductal adenocarcinoma. *Genome Research*, *30*(3), 347–360. https://doi.org/10.1101/gr.257550.119

Viht, K., Saaver, S., Vahter, J., Enkvist, E., Lavogina, D., Sinijärv, H., Raidaru, G., Guerra, B., Issinger, O.-G., & Uri, A. (2015). Acetoxymethyl Ester of Tetrabromobenzimidazole–Peptoid Conjugate for Inhibition of Protein Kinase CK2 in Living Cells. *Bioconjugate Chemistry*, *26*(12), 2324–2335. https://doi.org/10.1021/acs.bioconjchem.5b00383

V'kovski, P., Kratzel, A., Steiner, S., Stalder, H., & Thiel, V. (2021). Coronavirus biology and replication: Implications for SARS-CoV-2. *Nature Reviews. Microbiology*, *19*(3), 155–170. https://doi.org/10.1038/s41579-020-00468-6

Vogel, A. P., Brown, S. E., Folker, J. E., Corben, L. A., & Delatycki, M. B. (2014). Dysphagia and swallowing-related quality of life in Friedreich ataxia. *Journal of Neurology*, *261*(2), 392–399. https://doi.org/10.1007/s00415-013-7208-4

Wadey, K. S., Brown, B. A., Sala-Newby, G. B., Jayaraman, P.-S., Gaston, K., & George, S. J. (2017). Protein kinase CK2 inhibition suppresses neointima formation via a proline-rich homeodomain-dependent mechanism. *Vascular Pharmacology*, *99*, 34–44. https://doi.org/10.1016/j.vph.2017.09.004

Walsh, C. T., Garneau-Tsodikova, S., & Gatto, G. J. (2005). Protein posttranslational modifications: The chemistry of proteome diversifications. *Angewandte Chemie (International Ed. in English)*, *44*(45), 7342–7372. https://doi.org/10.1002/anie.200501023

Walsh, D. A., Perkins, J. P., & Krebs, E. G. (1968). An adenosine 3',5'-monophosphate-dependant protein kinase from rabbit skeletal muscle. *The Journal of Biological Chemistry*, *243*(13), 3763–3765.

Wang, D., Westerheide, S. D., Hanson, J. L., & Baldwin, A. S. (2000). Tumor necrosis factor alpha-induced phosphorylation of RelA/p65 on Ser529 is controlled by casein kinase II. *The Journal of Biological Chemistry*, *275*(42), 32592–32597. https://doi.org/10.1074/jbc.M001358200

Wang, G., Ahmad, K. A., & Ahmed, K. (2005). Modulation of death receptor-mediated apoptosis by CK2. *Molecular and Cellular Biochemistry*, *274*(1), 201–205. https://doi.org/10.1007/s11010-005-2952-0

Wells, C. I., Drewry, D. H., Pickett, J. E., Tjaden, A., Krämer, A., Müller, S., Gyenis, L., Menyhart, D., Litchfield, D. W., Knapp, S., & Axtman, A. D. (2021). Development of a potent and selective chemical probe for the pleiotropic kinase CK2. *Cell Chemical Biology*. https://doi.org/10.1016/j.chembiol.2020.12.013

Weng, L., Laboureur, L., Wang, Q., Guo, L., Xu, P., Gottlieb, L., Lynch, D. R., Mesaros, C., & Blair, I. A. (2020). Extra-mitochondrial mouse frataxin and its implications for mouse models of Friedreich's ataxia. *Scientific Reports*, *10*(1), 15788. https://doi.org/10.1038/s41598-020-72884-w

Weng, L.-P., Brown, J. L., & Eng, C. (2001). PTEN induces apoptosis and cell cycle arrest through phosphoinositol-3-kinase/Akt-dependent and -independent pathways. *Human Molecular Genetics*, *10*(3), 237–242. https://doi.org/10.1093/hmg/10.3.237

Willert, K., Brink, M., Wodarz, A., Varmus, H., & Nusse, R. (1997). Casein kinase 2 associates with and phosphorylates dishevelled. *The EMBO Journal*, *16*(11), 3089–3096. https://doi.org/10.1093/emboj/16.11.3089

Wingelhofer, B., Neubauer, H. A., Valent, P., Han, X., Constantinescu, S. N., Gunning, P. T., Müller, M., & Moriggl, R. (2018). Implications of STAT3 and STAT5 signaling on gene regulation and chromatin remodeling in hematopoietic cancer. *Leukemia*, *32*(8), 1713–1726. https://doi.org/10.1038/s41375-018-0117-x

Wirkner, U., Voss, H., Lichter, P., Ansorge, W., & Pyerin, W. (1995). Human protein kinase CK2 genes. *Journal of Cancer Research and Clinical Oncology*, *121*(1), A14–A14. https://doi.org/10.1007/BF02572021

Wong, A., Yang, J., Cavadini, P., Gellera, C., Lonnerdal, B., Taroni, F., & Cortopassi, G. (1999). The Friedreich's ataxia mutation confers cellular sensitivity to oxidant stress which is rescued by chelators of iron and calcium and inhibitors of apoptosis. *Human Molecular Genetics*, *8*(3), 425–430. https://doi.org/10.1093/hmg/8.3.425

Wu, J., Meng, F., Lu, H., Kong, L., Bornmann, W., Peng, Z., Talpaz, M., & Donato, N. J. (2008). Lyn regulates BCR-ABL and Gab2 tyrosine phosphorylation and c-Cbl protein stability in imatinib-resistant chronic myelogenous leukemia cells. *Blood*, *111*(7), 3821–3829. https://doi.org/10.1182/blood-2007-08-109330

Xia, H., Cao, Y., Dai, X., Marelja, Z., Zhou, D., Mo, R., Al-Mahdawi, S., Pook, M. A., Leimkühler, S., Rouault, T. A., & Li, K. (2012). Novel frataxin isoforms may contribute to the pathological mechanism of Friedreich ataxia. *PloS One*, *7*(10), e47847. https://doi.org/10.1371/journal.pone.0047847

Yamada, M., Katsuma, S., Adachi, T., Hirasawa, A., Shiojima, S., Kadowaki, T., Okuno, Y., Koshimizu, T., Fujii, S., Sekiya, Y., Miyamoto, Y., Tamura, M., Yumura, W., Nihei, H., Kobayashi, M., & Tsujimoto, G. (2005). Inhibition of protein kinase CK2 prevents the progression of glomerulonephritis. *Proceedings of the National Academy of Sciences of the United States of America*, *102*(21), 7736–7741. https://doi.org/10.1073/pnas.0409818102

Yamashita, T., Teramoto, S., & Kwak, S. (2016). Phosphorylated TDP-43 becomes resistant to cleavage by calpain: A regulatory role for phosphorylation in TDP-43 pathology of ALS/FTLD. *Neuroscience Research*, *107*, 63–69. https://doi.org/10.1016/j.neures.2015.12.006

Yan, W., Zheng, Y., Zeng, X., He, B., & Cheng, W. (2022). Structural biology of SARS-CoV-2: Open the door for novel therapies. *Signal Transduction and Targeted Therapy*, *7*(1), Article 1. https://doi.org/10.1038/s41392-022-00884-5

Yang, D., Wang, T., Ni, Y., Song, B., Ning, F., Hu, P., Luo, L., Wang, Y., & Ma, A. (2015). Apamin-Sensitive K+ Current Upregulation in Volume-Overload Heart Failure is Associated with the Decreased Interaction of CK2 with SK2. *The Journal of Membrane Biology*, *248*(6), 1181–1189. https://doi.org/10.1007/s00232-015-9839-0

Yang, Q., Zhang, Q., Yi, S., Qin, Z., Shen, F., Ou, S., Luo, J., & He, S. (2022). De Novo CSNK2B Mutations in Five Cases of Poirier-Bienvenu Neurodevelopmental Syndrome. *Frontiers in Neurology*, *13*, 811092. https://doi.org/10.3389/fneur.2022.811092

Yang, S., Wu, L., Liao, H., Lu, X., Zhang, X., Kuang, X., & Yang, L. (2021). Clinical and genetic analysis of six Chinese children with Poirier-Bienvenu neurodevelopmental syndrome caused by CSNK2B mutation. *Neurogenetics*, *22*(4), 323–332. https://doi.org/10.1007/s10048-021-00649-2

Yang, W., Gibson, S. A., Yan, Z., Wei, H., Tao, J., Sha, B., Qin, H., & Benveniste, E. N. (2020). Protein kinase 2 (CK2) controls CD4+ T cell effector function in the pathogenesis of colitis. *Mucosal Immunology*, *13*(5), 788–798. https://doi.org/10.1038/s41385-020-0258-x

Yde, C. W., Olsen, B. B., Meek, D., Watanabe, N., & Guerra, B. (2008). The regulatory β-subunit of protein kinase CK2 regulates cell-cycle progression at the onset of mitosis. *Oncogene*, *27*(37), Article 37. https://doi.org/10.1038/onc.2008.146

Ye, D., Wolff, N., Li, L., Zhang, S., & Ilaria, R. L., Jr. (2006). STAT5 signaling is required for the efficient induction and maintenance of CML in mice. *Blood*, *107*(12), 4917–4925. https://doi.org/10.1182/blood-2005-10-4110

Yoo, J.-Y., Choi, H.-K., Choi, K.-C., Park, S.-Y., Ota, I., Yook, J. I., Lee, Y.-H., Kim, K., & Yoon, H.-G. (2012). Nuclear hormone receptor corepressor promotes esophageal cancer cell invasion by transcriptional repression of interferon-γ-inducible protein 10 in a casein kinase 2-dependent manner. *Molecular Biology of the Cell*, *23*(15), 2943–2954. https://doi.org/10.1091/mbc.E11-11-0947

Yoon, J.-J., Lee, Y.-T., Chu, H., Son, S., & Kim, M. (2015). Phosphorylation of the nucleocapsid protein of Hantaan virus by casein kinase II. *Journal of Microbiology (Seoul, Korea)*, *53*(5), 343–347. https://doi.org/10.1007/s12275-015-5095-3

Zabriskie, M. S., Eide, C. A., Tantravahi, S. K., Vellore, N. A., Estrada, J., Nicolini, F. E., Khoury, H. J., Larson, R. A., Konopleva, M., Cortes, J. E., Kantarjian, H., Jabbour, E. J., Kornblau, S. M., Lipton, J. H., Rea, D., Stenke, L., Barbany, G., Lange, T., Hernández-Boluda, J.-C., … O'Hare, T. (2014). BCR-ABL1 Compound Mutations Combining Key Kinase Domain Positions Confer Clinical Resistance to Ponatinib in Ph Chromosome-Positive Leukemia. *Cancer Cell*, *26*(3), 428–442. https://doi.org/10.1016/j.ccr.2014.07.006

Zaki, A. M., van Boheemen, S., Bestebroer, T. M., Osterhaus, A. D. M. E., & Fouchier, R. A. M. (2012). Isolation of a novel coronavirus from a man with pneumonia in Saudi Arabia. *The New England Journal of Medicine*, *367*(19), 1814–1820. https://doi.org/10.1056/NEJMoa1211721

Zhang, C., Vilk, G., Canton, D. A., & Litchfield, D. W. (2002). Phosphorylation regulates the stability of the regulatory CK2beta subunit. *Oncogene*, *21*(23), 3754–3764. https://doi.org/10.1038/sj.onc.1205467

Zhang, H.-X., Jiang, S.-S., Zhang, X.-F., Zhou, Z.-Q., Pan, Q.-Z., Chen, C.-L., Zhao, J.-J., Tang, Y., Xia, J.-C., & Weng, D.-S. (2015). Protein kinase CK2α catalytic subunit is overexpressed and serves as an unfavorable prognostic marker in primary hepatocellular carcinoma. *Oncotarget*, *6*(33), 34800–34817. https://doi.org/10.18632/oncotarget.5470

Zhang, Q., Xia, Y., Wang, Y., Shentu, Y., Zeng, K., Mahaman, Y. A. R., Huang, F., Wu, M., Ke, D., Wang, Q., Zhang, B., Liu, R., Wang, J.-Z., Ye, K., & Wang, X. (2018). CK2 Phosphorylating I2PP2A/SET Mediates Tau Pathology and Cognitive Impairment. *Frontiers in Molecular Neuroscience*, *11*, 146. https://doi.org/10.3389/fnmol.2018.00146

Zhang, S., Long, H., Yang, Y.-L., Wang, Y., Hsieh, D., Li, W., Au, A., Stoppler, H. J., Xu, Z., Jablons, D. M., & You, L. (2013). Inhibition of CK2α down-regulates Notch1 signalling in lung cancer cells. *Journal of Cellular and Molecular Medicine*, *17*(7), 854–862. https://doi.org/10.1111/jcmm.12068

Zhang, S., Yang, Y.-L., Wang, Y., You, B., Dai, Y., Chan, G., Hsieh, D., Kim, I.-J., Fang, L. T., Au, A., Stoppler, H. J., Xu, Z., Jablons, D. M., & You, L. (2014). CK2α, over-expressed in human malignant pleural mesothelioma, regulates the Hedgehog signaling pathway in mesothelioma cells. *Journal of Experimental & Clinical Cancer Research: CR*, *33*(1), 93. https://doi.org/10.1186/s13046-014-0093-6

Zhao, J. J., Cheng, H., Jia, S., Wang, L., Gjoerup, O. V., Mikami, A., & Roberts, T. M. (2006). The p110alpha isoform of PI3K is essential for proper growth factor signaling and oncogenic transformation. *Proceedings of the National Academy of Sciences of the United States of America*, *103*(44), 16296–16300. https://doi.org/10.1073/pnas.0607899103

Zheng, Y., Qin, H., Frank, S. J., Deng, L., Litchfield, D. W., Tefferi, A., Pardanani, A., Lin, F.-T., Li, J., Sha, B., & Benveniste, E. N. (2011). A CK2-dependent mechanism for activation of the JAK-STAT signaling pathway. *Blood*, *118*(1), 156–166. https://doi.org/10.1182/blood-2010-01-266320

Zhou, B., Ritt, D. A., Morrison, D. K., Der, C. J., & Cox, A. D. (2016). Protein Kinase CK2α Maintains Extracellular Signal-regulated Kinase (ERK) Activity in a CK2α Kinase-independent Manner to Promote Resistance to Inhibitors of RAF and MEK but Not ERK in BRAF Mutant Melanoma. *The Journal of Biological Chemistry*, *291*(34), 17804–17815. https://doi.org/10.1074/jbc.M115.712885

Zhou, H., Zhu, P., Wang, J., Zhu, H., Ren, J., & Chen, Y. (2018). Pathogenesis of cardiac ischemia reperfusion injury is associated with CK2α-disturbed mitochondrial homeostasis via suppression of FUNDC1-related mitophagy. *Cell Death and Differentiation*, *25*(6), 1080–1093. https://doi.org/10.1038/s41418-018-0086-7

Zhu, N., Zhang, D., Wang, W., Li, X., Yang, B., Song, J., Zhao, X., Huang, B., Shi, W., Lu, R., Niu, P., Zhan, F., Ma, X., Wang, D., Xu, W., Wu, G., Gao, G. F., Tan, W., & China Novel Coronavirus Investigating and Research Team. (2020). A Novel Coronavirus from Patients with Pneumonia in China, 2019. *The New England Journal of Medicine*, *382*(8), 727–733. https://doi.org/10.1056/NEJMoa2001017

Zonta, F., Borgo, C., Quezada Meza, C. P., Masgras, I., Rasola, A., Salvi, M., Pinna, L. A., & Ruzzene, M. (2021). Contribution of the CK2 Catalytic Isoforms α and α' to the Glycolytic Phenotype of Tumor Cells. *Cells*, *10*(1), 181. https://doi.org/10.3390/cells10010181

ACKNOWLEDGMENTS

I am profoundly grateful to my P.I., Prof. Maria Ruzzene, for the guidance and the trust during these years.
I thank Dr. Christian Borgo for the guidance and his incredible patience.
I thank Prof. Lorenzo Pinna, Prof. Arianna Donella-Deana, Prof. Mauro Salvi, Prof. Stefania Sarno, Dr. Luca Cesaro, and all the former and current members of the Protein Phosphorylation Lab.
I thank Prof. Sandra Marmiroli and her group (University of Modena and Reggio Emilia, Italy) for their kindly receiving during mi visits to their lab, in particular Dr. Manuela Zavatti for the experimental support.
I also thank our collaborators, that helped to reach the achievements presented in this work: Prof. Oriano Marin (University of Padova, Italy), Prof. Giorgio Arrigoni (University of Padova, Italy), Prof. Malisan's group (University of Rome Tor Vergata, Italy), Andrea Venerando (University of Udine, Italy), Jong-Won Kim (Sungkyunkwan University, Korea) and Dennis Dong Hwan Kim (University Health Network, Canada).